OPTIMAL DESIGN AND DIAGNOSIS OF CONVENTIONAL AND UNCONVENTIONAL REACTORS

A Dissertation

by

SUNJEEV VENKATESWARAN

Submitted to the Graduate and Professional School of Texas A&M University
in partial fulfillment of the requirements for the degree of

DOCTOR OF PHILOSOPHY

Chair of Committee,	Costas Kravaris
Co-Chair of Committee,	Benjamin Wilhite
Committee Members,	Joseph Sang-II Kwon
	Goong Chen
Head of Department,	Arul Jayaraman

August 2021

Major Subject: Chemical Engineering

ABSTRACT

Demand for safer and more efficient chemical reactors has given rise to two kinds of research problems. One path has focused on finding new reactor designs that make reaction systems inherently safer compared to large conventional reactors and another direction has focused on building algorithms to make classical reactors (CSTR, Batch, Tubular) safer and more efficient. This dissertation is an attempt to tackle important problems in both directions. In the first part of this dissertation, design problems in two inherently safer and compact unconventional chemical reactors are studied namely, microreactors and heat exchangers. Using well established tools such as parametric sensitivity analysis, order of magnitude analysis and optimal control theory, the effect of solid phase axial heat conduction on isothermal operation and hotspot formation in microreactors, and the effect of catalyst distribution in thermal coupling in heat exchanger reactors is investigated. The second part of this dissertation focuses on making inherently unsafe conventional chemical reactors (such as CSTRs) safer and robust. To this end, an observer-based fault diagnosis scheme is developed for a general class of input affine nonlinear systems with and without measurement and process noises. Throughout the study, the fault diagnosis scheme is applied to chemical engineering examples including non-isothermal exothermic CSTRs.

DEDICATION

Dedicated to amma and appa (mom and dad)

ACKNOWLEDGEMENTS

First and foremost, I thank Prof. Kravaris. His enthusiasm for research and the care he takes in teaching are inspirational. Honestly, CHEN 631 was one of the best courses I have taken as a student and after it ended, I remember being so excited about working with him. He taught me so much over the past five years despite myself. I have learnt a lot from him, and I am sure there is much more to learn.

I would like to express my gratitude to Prof. Wilhite. When I met him in 2016, I was immediately intrigued by the research in microreactors and process intensification. I am lucky to have had him as the instructor for CHEN 624. In retrospect, the work on runaway/hotspot formation was born out of his teachings in the final part of the course. Without his insights and suggestions on a variety of chemical processes this thesis wouldn't have been possible.

I would like to thank Prof. Kwon and Prof. Chen for providing their time to serve on my Committee and always being available for any discussions related to my research.

I deeply appreciate and thank all my colleagues in Dr. Kravaris' (Joshiba, Mengxi, Nour, Dr. Ziyan, Dr. Zhaoyang and Dr. Chen) and Dr. Wilhite's (Dr. Srikanth and Dr. Naveen) group. I bounced so many ideas off them (especially Dr. Srikanth) even though most didn't make the thesis (thankfully!).

Thanks also go to many friends and colleagues in the chemical engineering department and the friends I met in College Station.

Last but not least, I would like to thank my parents for always being there for me. None of this would have been possible without their support.

CONTRIBUTORS AND FUNDING SOURCES

Contributors

This work was supported by a dissertation committee consisting of Professor Costas Kravaris, Professor Benjamin Wilhite, and Professor Joseph Sang-II Kwon of the Department of Chemical Engineering Department and Professor Goong Chen of the Department of Mathematics.

All work for the dissertation was completed by the student independently.

Funding sources

Graduate study was supported in part from the National Science Foundation through the grant CBET-1706201.

NOMENCLATURE

C_A fluid-phase reactant concentration, $mol.m^{-3}$

C_{A0} fluid-phase inlet reactant concentration, $mol.m^{-3}$

C_p fluid-phase heat capacity, $J.mol^{-1}.K^{-1}$

CP conduction parameter, reacting-fluid side, $\frac{k_w}{\rho C_p L v_0 \epsilon_{fw}}$

CP_1 conduction parameter, reacting-fluid side, $\frac{k_w}{\rho.C_p.L.v_0.\epsilon_{f_1 w}}$

CP_2 conduction parameter, coolant-fluid side, $\frac{k_w}{\rho.C_p.L.v_0.\epsilon_{f_2 w}}$

Fo solid-phase Fourier Number, $\frac{k_w}{(\rho C_p)_w.L.v_0}$

St_1 reacting fluid-to-solid wall Stanton Number, $\frac{h_1 \hat{a}_{f_1 s} L}{\rho C_p v_0}$

St_2 coolant fluid-to-solid wall Stanton Number, $\frac{h_2 \hat{a}_{f_2 s} L}{\rho C_p v_0}$

T_c coolant temperature, K

Da Damkohler Number, $k_0 e^{\left[\frac{Ea}{R.T_0}\right]} C_{A0} \frac{L}{v_0}$

E_a reaction activation energy, $J.mol^{-1}$

h_a heat-transfer coefficient for conductive losses to the ambient at z = 0, L.

h_1 reacting fluid-to-solid wall heat transfer coefficient

h_2 coolant fluid-to-Solid wall Heat transfer coefficient

ΔH_r heat of reaction

k_0 pre-exponential rate coefficient, s^{-1}

k_w solid-phase (wall) thermal conductivity,

L reactor axial length, m

R gas constant, $J.mol^{-1}.K^{-1}$

T fluid-phase temperature, K

T_c coolant temperature, K

T_a ambient temperature (at $z < 0$, $z > L$), K

T_0 fluid-phase inlet temperature, K

T_w wall temperature, K

u dimensionless fluid-phase reactant concentration, $\frac{C_A}{C_{A0}}$

v_0 fluid-phase superficial velocity

z axial position

B dimensionless heat of reaction

C reactant concentration, $mol.m^{-3}$

C_0 inlet reactant concentration, $mol.m^{-3}$

C_p heat capacity, $J.mol^{-1}.K^{-1}$

â channel surface area to volume ratio

ρ fluid-phase density

σ catalyst distribution

ϵ_{f2w} coolant fluid-to-solid phase (wall) volume ratio

ξ ratio of coolant- to reacting fluid heat transfer capacity to wall, $= \frac{h_1}{h_2}\frac{\hat{a}_{f_2s}}{\hat{a}_{f_1s}}\frac{\epsilon_{f_2w}}{\epsilon_{f_1w}}$

$\hat{a}_{f_1s}$ reacting fluid surface area-to-fluid phase volume ratio

$\hat{a}_{f_2 s}$	outer wall surface area-to-fluid phase volume ratio
$\epsilon_{f w}$	reacting fluid-to-solid phase (wall) volume ratio
γ	$\frac{E_a}{R.T_0}$

TABLE OF CONTENTS

Page

LIST OF FIGURES

Page

LIST OF TABLES

Page

1. INTRODUCTION

1.1. Conventional chemical reactors

Large stirred pots and empty tubes for chemical reactions are as old as the field of chemical engineering itself. Even now, 100 years after their emergence, conventional chemical reactors account for most of the chemical production in chemical industries[1-2]. The three most well-known chemical reactors include the continuous stirred tank reactor (CSTR), tubular reactor and batch reactor[2] and problems concerning their design and operation have been tackled since the 1950s.

1.1.1. Continuous stirred tank reactor (CSTR)

Continuous Stirred Tank Reactors (see Figure 1.1) are very commonly used for industrial processing. As the name suggests, these reactors are stirred tanks that are operated continuously. The CSTR is normally operated at steady state and is operated to be well mixed. As a result, spatial variations are neglected when modeling a CSTR. Since the temperature and concentration are identical everywhere within the reaction vessel, they are the same at the exit point as they are elsewhere in the tank. Thus, the temperature and concentration in the exit stream are modeled as being the same as those inside the reactor.

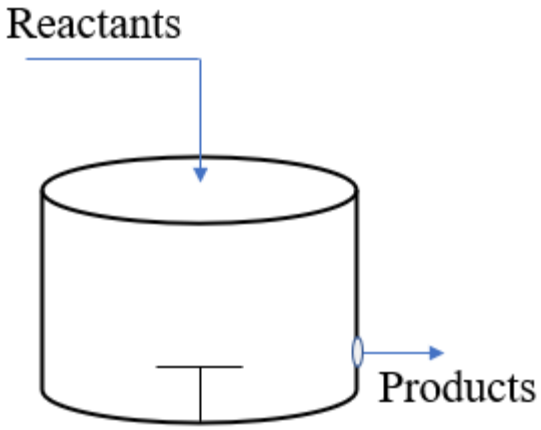

Figure 1.1 Continuous stirred tank reactor (CSTR).

1.1.2. Tubular reactor

Tubular reactors consist of a cylindrical pipe (see Figure 1.2) and, like the CSTR, normally operated at steady state**.** The reactants are continually consumed as they flow down the length of the reactor. In modeling the tubular reactor, we assume that the concentration varies continuously in the axial direction through the reactor. Consequently, the reaction rate, which is a function of concentration for all but zero-order reactions, will also vary axially.

Figure 1.2 Industrial tubular reactor.

1.1.3. Batch reactor

A batch reactor (see Figure 1.3) has neither inflow nor outflow of reactants or products while the reaction is being carried out. It typically, consists of a storage tank with an agitator and integral heating/cooling system. Generally, the reaction mixture is mixed perfectly so that there is no variation in the rate of reaction throughout the reactor volume. The advantages of the batch reactor lie with its versatility. A single vessel can carry out a sequence of different operations without the need to break containment. This is particularly useful when processing toxic or highly potent compounds.

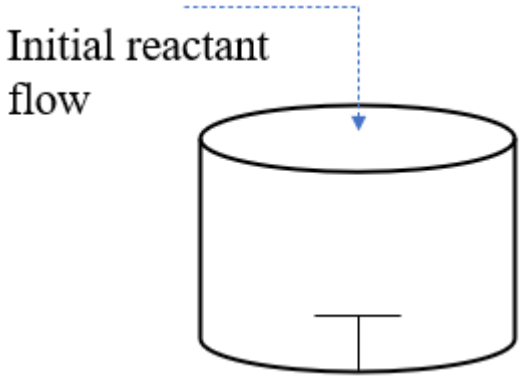

Figure 1.3 Batch reactor.

1.1.4. Challenges

The large sizes typically associated with conventional reactors give rise to different challenges that affects different aspects of chemical production; ranging from difficulties in novel process/ material screening to inefficiencies involved in day to day production [3]. These challenges can mainly be grouped into the following

I. Operational inefficiencies

- Conventional reactors have significant intraphase transport resistances. In such cases, diffusion of the reactants is generally the "rate determining step", and can cause significant reduction in reactor conversion and difficulties in studying intrinsic kinetics of novel reactions.
- High interphase transport resistances due to high surface area to volume ratios in conventional reactors restricting operation of the reactor at aggressive conditions (high temperature and/or pressure)

II. Scale up difficulties

- Chemical production in conventional reactors is a complex and cost intensive process requiring expensive lab scale and/ or pilot plant experiments before moving to large scale production.

III. Process safety

- Any fault or mishap can lead to disastrous consequences such as explosions because of their massive sizes and consequently large chemical hold up. A case in point is the T2 Laboratories reactor explosion[4] (2007, Jacksonville, Florida) that occurred due to cooling system failure and killed four people.

The foregoing challenges have given rise to two kinds of research problems. The first path, mainly tackled by reaction engineers, has focused on the construction of new chemical reactor designs that are inherently safer and compact compared to large conventional chemical reactors[3, 5-16]. These reactors are smaller and more compact

compared to classical reactors and, as we shall see, provide design challenges that were hitherto absent in their conventional counterparts.

In another direction, armed with systems and control theory, chemical engineers have come up with methods for ensuring widely used conventional chemical reactors operate in a safe and efficient manner. This has mainly taken the form of developing algorithms for fault diagnosis and subsequent fault tolerant control hereby making conventional rectors more resilient[17-26]. This dissertation is an attempt to solve important problems in both the paths and it will focus on methods for

a) Optimal design of a class of unconventional chemical reactors namely, microreactors and heat exchanger reactors (Sections 2,3, and 4)- This will make use of well-established tools such as sensitivity analysis, order-of magnitude analysis, and optimal control to derive fundamental insights to the design these unconventional reactors.
b) Fault detection and isolation in non-linear systems applied to conventional chemical reactors (Sections 5,6 and 7)- though the methods are developed for a general class of input affine systems, the main application will be highly exothermic non-isothermal chemical reactors that are inherently unsafe.

1.2. Unconventional reactors- microreactors

Microreactors are miniaturized reaction systems of sub-millimeter diameter such that intraphase transport resistances are alleviated while providing order-of-magnitude improvements in interphase transport rates relative to conventional systems[3, 10-11]. Because

of these unique advantages, combined with the potential for realizing modular and/or portable chemical processes, microreactors remain a focal point of research and development in process intensification[13-14, 27-29]. One of the first opportunities identified for microreactors was ability to safely perform hazardous chemistries, with emphasis on highly exothermic, fast reactions which traditionally pose significant runaway and explosion hazards[30-32]. For heat-transfer limited processes e.g., endothermic Fischer-Tropsch Synthesis, microreactors offer breakthroughs in both reaction rates and temperature uniformity[33-34] For both applications, high rates of transverse heat exchange between reacting fluid and coolant provide excellent temperature control.

The most common microreactor architecture is planar, in which a $1 \times n$ array of parallel microchannels are patterned into an individual plate of silicon, glass, ceramic or metal substrate[3, 10-11]. Scale-up of capacity is then realized via bonding multiple plates into a monolithic 'stack' which effectively consists of a large bundle of parallel channels embedded in single, continuous block of solid-phase substrate [13-14, 29] Heat addition or removal is readily introduced via alternating rows of reaction and coolant channel plates, while supply of reactant or coolant to individual channels is achieved via distribution manifolds which interface between the microchannel network and external plumbing [3, 10-11, 14]. The resulting microreactor is unique from traditional reactors in that the solid-phase volume, relative to that of either reacting fluid or coolant, is no longer negligible and therefore heat dispersion via solid-phase axial conduction must be accounted for [35-37]. Likewise, while sufficient external insulation may be readily provided to the microreactor block, as to ensure that convective and/or radiative heat losses to ambient are negligible,

solid-phase heat conduction may provide an additional pathway for heat removal via conduction from the microreactor block to external inlet/outlet manifolds ('packaging losses') [37-38].

1.2.1. Design challenge

The impact of solid-phase conduction and packaging losses depends heavily on whether the reaction is endothermic or exothermic. One of the goals of this thesis is to fundamentally investigate the differing roles of axial wall conduction on endothermic and exothermic microreactor design. The importance of solid-phase heat conduction on design criteria such as heat transfer efficiency, heat circulation, hotspot formation/ magnitude, ignition/extinction and runaway are well documented [16, 36-37, 39]

Endothermic reactions absorb energy from its surroundings resulting in a net increase in enthalpy. Highly endothermic reactions such as methane steam reforming are characterized by a steep temperature decrease (Figure 1.4) which results in low reactor conversion. Thus, the primary challenge in endothermic reactors is to maintain sufficiently high reaction rates[7-8, 40]. This can be done by having external heat inputs to counter the decrease in reactor temperature due to the reaction. However, care should be taken to not overheat the reactor as extreme temperatures could compromise catalyst and material stability. Therefore, the goal is to operate the reactor at a temperature that maintains high reaction rates while ensuring material stability and safety. But is it theoretically possible to operate a highly endothermic microreactor at a prespecified temperature? Microreactors do have a major advantage over their conventional counterparts in that the orders of magnitude in reduction in size offers massive improvements in heat fluxes. Therefore, the

amount of heat input available should not be a problem. However, as seen the reduced sizes of the internal substructures increase the proportion of solid-phase when compared to conventional reactors. The significant presence of solid components adds an additional layer of complexity to heat distribution in microreactors and engineers must consider this while designing heat inputs to an endothermic microreactor. Section 2 will focus on an attempt to systematically derive the heat inputs in highly endothermic microreactors using optimal control theory.

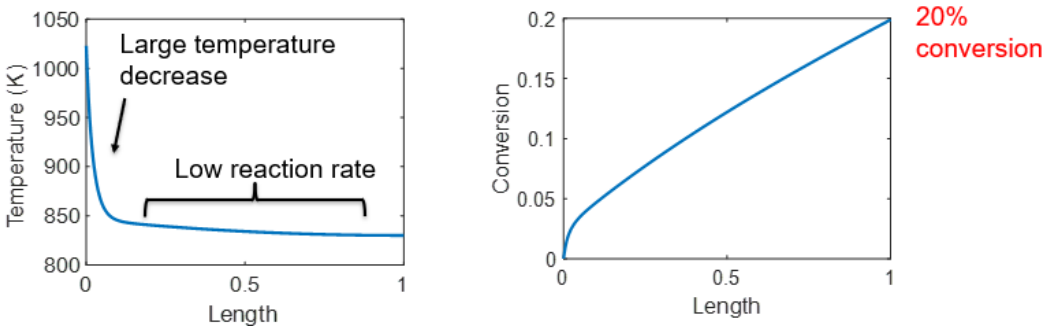

Figure 1.4 Endothermic reactor temperature and concentration profiles in the absence of heat inputs.

Exothermic reactions on other hand are fast and release large amounts of energy. This makes them susceptible to runaway and explosion hazards. Thanks to high rates of transverse heat exchange between the reacting fluid and the coolant, one of the first opportunities identified for microreactors was ability to safely perform hazardous chemistries, with emphasis on highly exothermic, fast reactions. However, as mentioned before solid-phase axial heat conduction brings out complexities in the heat distribution process. For example, it has been shown experimentally, that high thermal conductivity of

the solid-phase from which the device is fashioned (e.g., silicon, steel) axially disperses reaction heat for further prevention of localized hot-spots and/or runaway. Conversely, microreactors fashioned from low thermal conductivity materials (e.g., ceramics) have been explored for exploiting runaway in exothermic reactions to achieve breakthroughs in thermal efficiencies for regenerative combustors or heat-exchanger reactors [6, 12-13, 41-42]. Section 3 will be an attempt to obtain fundamental insights on the effect of axial wall conduction hotspot formation/runaway.

1.3. Unconventional reactors- heat exchanger reactors

Reactors integrating endothermic and exothermic reactions in a single vessel such that, the exothermic reaction acts as the heat source to drive the endothermic reaction continue to garner industrial interest for process intensification [15, 43-46]. This class of multi-functional intensified reactors make the process more energy efficient and compact, in turn enabling significant reduction in size, and operational and capital costs. Over the past 20 years, the search for efficient autothermal designs has been primarily focused upon the production of synthesis gas and/or hydrogen in an economical and scalable manner[43-45].

In the literature three archetypical autothermal reactor designs have been reported. Specifically, (a) reverse flow reactors[47-50], (b) directly coupled reactors,[40, 51-53] and (c) heat exchanger reactors[44-45, 54]. In the reverse flow reactor, the exothermic and endothermic reactions occur alternately within the same catalyst bed[47]; exothermic reaction providing heat to the bed in the first half of the cycle which is then consumed by subsequent endothermic reaction occurring in the second half of the cycle. In directly coupled reactors, both the exothermic and endothermic reactants are fed simultaneously to the same reactant

channel[52] such that the net reaction heat duty is null. The main drawback of these two reactor configurations is that there is no spatial separation of the two reacting flows. Thus, care must be taken to select catalysts which support both reactions and are stable in the presence of both reaction chemistries. Additionally, downstream separation may be required to decouple endothermic/ exothermic reaction products. These problems are addressed by the heat exchanger reactor configuration where exothermic and endothermic reactions occur in separate parallel reaction channels. Heat exchanger reactors offer additional operational flexibility as design parameters for each reaction channel (such as channel width, inlet concentration/ temperature, velocity etc.,) could be altered independently of the other reaction channel.

1.3.1. Design challenge

Effective thermal coupling in heat exchanger reactors remains a significant design challenge. Two commonly encountered extremes in thermal behavior are [43, 51, 54-58]

(i) Hotspot formation: occurs when heat generated in the combustion side cannot be consumed at the same rate, and temperature increases beyond acceptable limits, resulting in hot spots that can destroy catalyst coating and jeopardize structural integrity of the supporting material

(ii) Reactor quenching- the endothermic reaction rates are higher than combustion reaction rates, and consequently temperature drops, resulting in reactor extinction

Effective countercurrent coupling of exothermic and endothermic reactions and, equivalently, improving the match between respective heat generation and heat

consumption rates require modifications to the reactor design[43, 49, 59]. Modifications include using a distributed fuel feed along the reactor length (rather than feeding all the fuel flow at one end), multiple passes for better heat recovery and modifying the activity of the catalyst along the reactor length[56-57, 60]. Section 4 will focus on an attempt to systematically find the right catalyst activity profile along the length of the reactor using optimal control theory.

1.4. Nonlinear system fault diagnosis- applied to conventional chemical reactors

While unconventional reactors are a promising safer and efficient alternative to conventional reactors and have found niche applications in the pharmaceutical and specialty chemicals industry, widespread adoption is still lacking. This is because, as of now, heat exchanger reactors and microreactors are unable to match the production rate of conventional chemical reactors[11, 14]. Most of the chemical production is still done using conventional reactors[1] and one must also focus on operating these reactors in a safe and efficient manner while parallelly exploring new reactor designs.

Higher demand for safety and reliability has made fault diagnosis a major topic of research over the past three decades[61-63]. A fault is an unexpected/unpermitted major deviation in process variables from normal conditions[61]. Faults could arise due to several reasons, including mechanical failures, power failures, human errors, etc. Faults could lead to consequences ranging from off- spec product resulting in loss of profit, to potentially catastrophic explosions causing fatalities. These considerations provide a strong motivation for development of methods and strategies for quick fault diagnosis that would guide operators to bring the system back to normal operation[61].

Fault diagnosis techniques can be broadly grouped into two categories: hardware-redundancy-based fault diagnosis and analytical-redundancy-based fault diagnosis[61]. Hardware-redundancy-based techniques consist of a reconstruction of the system using identical hardware components parallel to the process[61]. This has been used in some safety-critical systems including aircrafts and nuclear power plants. However, while this technique certainly has its advantages in terms of reliability, it is limited by high costs, as constructing an identical redundant system for the sole purpose of fault diagnosis may not make economic sense in capital intensive industries[61]. Analytical redundancy on the other hand comprises of a virtual reconstruction of the system using a process model which is implemented in software form on a computer[61-66]. Analytical redundancy is achieved through known interdependence among the process variables provided by the model[61-63, 65-67]. The evolution of process variables of the virtual system will follow the outputs of the real system in the absence of faults and will show a measurable deviation in the presence of faults. The essence of analytical redundancy in fault diagnosis is checking consistency of the actual system behavior against the system model. Any inconsistency is measured in terms of residuals that deviate from zero only in the presence of a specific fault. Moreover, since accurate modeling of a real system is difficult and the effect of unknown disturbances or uncertainties could be corrupt the residual signal, it is important to carefully define the residual in a way that makes it unaffected by those disturbances. The central objective in model-based fault diagnosis is to develop a functional observer (also called residual generator) for each of the possible faults, in a way that the residual is unaffected by the other faults and unknown disturbances.

1.4.1. Functional observers

One of the most widely studied approaches in model-based fault detection and isolation (FDI) is the functional observer-based fault diagnosis approach. In control theory, a functional observer is an auxiliary system that is driven by the available system outputs and mirrors the dynamics of a physical process in order to estimate one or more functions of the system states [68-69]. Besides being of theoretical importance, the use of functional observers arises in many applications. For example, functional estimates are useful in feedback control system design because the control signal is often a linear combination of the states, and it is possible to utilize a functional observer to directly estimate the feedback control signal [68-70].

Over the past fifty years, considerable research has been carried out on estimating functions of the state vector for linear systems ever since Luenberger introduced the concept of functional observers in 1966 [69] and proved that it is feasible to construct a functional observer with number of states equal to observability index minus one. Subsequent research has focused on lower order functional observsers where necessary and sufficient conditions for their existence and stability have been derived [71-74], and parametric approaches to the design of lower order functional observers [75-76] and algorithms for solving the functional observer design conditions have also been developed [72-74, 77]. In a parallel direction, the problem of designing unknown input/ disturbance decoupled functional observers [78-80] and functional observers for systems with time delays [81-82] have also been tackled. In fact, strong connections between the design of functional observers for linear systems with unknown inputs and the design of delay-free functional

observers for time-delay systems have been established [75]. This implies that the design of linear functional observers for these systems can be done under the general framework of linear functional unknown input observers [75].

1.4.2. Functional observer-based fault diagnosis

The first functional observer-based FDI method for linear systems was proposed by Beard and Jones in the early 1970s [61, 83-84] which was a historic milestone in the area of fault diagnosis. Following this, many authors approached the fault diagnosis using a single or multiple Luenberger observers or Kalman filters[61-62, 65-66, 85-89]. In the late 70s the question of sensitivity of fault diagnosis schemes to modelling errors and unknown disturbances was raised which led to the development of FDI schemes that included disturbance decoupling conditions[65-67, 90-92]. In general, functional observer-based FDI methods for linear systems can be grouped into the following four categories[61, 63, 67] (i) Fault Detection Filter (ii) Diagnostic Observer (iii) Parity Space Approach (iv) Frequency Domain Approach. In the 90s interconnections between the amongst these methods were studied and equivalence between these methods has been established[61, 63-64, 93-94]. Thus parameters of the residual generator obtained using one approach can be transformed to derive the parameters of the residual generator for any other approach[61, 63, 93-94]. For a review of fault diagnosis for linear systems the reader is referred to excellent surveys by Frank and Ding[62, 67] and for more details on linear methods including the interconnections amongst different implementations the reader is referred to [61] .

1.4.3. Fault diagnosis in nonlinear systems

Many industrial systems, like chemical processes, exhibit strong nonlinearities which may render the application of linear methods ineffective. To design a reliable FDI system, explicit consideration of the nonlinear dynamics is needed for residual generation. Some fundamental results on the feasibility of disturbance decoupled fault detection and isolation have been derived in [95] using a differential geometric perspective, where the problem of fault detection was formulated in terms of the existence of an unobservability subspace and a quotient observable subsystem solely affected by the fault of interest. Following this, there have been studies dedicated to actuator fault detection and subsequent fault tolerant control in nonlinear systems including detection of a single fault[17-18] using a replica of the process model, and isolation amongst multiple faults[18-19] based on the assumption that each input in the system can directly affect only one state equation. There have also been approaches based on banks of high gain observers for generating residuals, with rigorously established convergence properties via Lyapunov methods, that have been shown to be applicable to the detection of a single sensor fault at a time[20] and at most two faults (sensor and/or actuator) in which case a potentially large number of observers are required to distinguish between the two faults[21-22]. In another work, linear matrix inequalities were used to prove convergence properties of a class of nonlinear state observers in Lipschitz nonlinear systems under full state observability from each one of the measurements, that was subsequently used for diagnosis of sensor faults occurring one at a time[96].

In another direction, there have been efforts seeking extensions of functional observer-based FDI methods to nonlinear systems in the spirit of linear systems methods [63, 97], and the challenges of building observer-based disturbance-decoupled residual generators became evident [98]. So far, concrete results have been restricted to special classes of nonlinear systems, including bilinear systems[99] and globally Lipschitz systems with triangular structure[95, 100]. In Section 5 a functional observer-based FDI for nonlinear systems will be presented from the point of view of exact observer error linearization[101]. The focus will be to build a robust functional observer fault diagnosis scheme to detect and isolate faults in the presence of uncertainties in non-linear processes. The main application considered throughout the section will be chemical processes involving, CSTRs, bioreactors and process network involving a CSTR and flash separator.

1.4.4. Discrete-time functional observers and fault diagnosis in the presence of noises

Measurements in industrial systems are often corrupted by noises. An FDI scheme developed without considering possible measurement errors will produce unnecessary false alarms rendering it useless. The final part of this dissertation will focus on building an FDI scheme that studies the sensitivity of the residuals to process and measurement noises by integrating statistical residual evaluation methods with model based FDI techniques. Although dynamical processes are continuous, measurements and the respective noises consist of sampled data and for this reason we will consider discrete-time systems as they are more amenable to analyzing the effect of noises. This would hinge on the development of functional observers for discrete- time non-linear systems.

For continuous-time nonlinear systems, functional observers for Lipschitz systems [102-103] and a class of nonlinear systems that can be decomposed as sum of Lipschitz and non-Lipschitz parts [75] (with the non-Lipschitz part considered as an unknown input/disturbance) have been developed. More recently, the problem of designing functional observers for estimating a single nonlinear functional has been tackled for general nonlinear systems from the point of view of observer error linearization [70] and the approach has been extended to a disturbance decoupled fault detection and isolation [104].

However, for discrete-time nonlinear systems results on functional observer design have been limited. Section 6 of this dissertation is an attempt to design functional observers for discrete-time nonlinear systems from the point of view of observer error linearization. These functional observers will then be used to diagnose faults in the presence of noises in Section 7.

2. ENDOTHERMIC MICROREACTORS- EFFECT OF SOLID PHASE CONDUCTION ON ISOTHERMAL OPERATION[*]

2.1. Introduction

In heat transfer limited processes such as the endothermic steam reforming of methane, the primary design challenge is to maintain sufficiently high temperatures and hence reaction rates via appropriate design of heating inputs[9]. Typically, highly endothermic reactions result in temperature profiles that show a large heat sink or "endotherm" at the inlet due to initially high reaction rates which may decrease the overall conversion of the reactor, introduce thermal stresses and/ or introduce coking risk. However excess heating can lead to catalyst sintering and material stability issues which may compromise the reactor lifetime [8, 29, 33]. Thus, the reactor temperature should be chosen carefully to maintain required conversion while ensuring catalyst/material stability. Following which, appropriate heat inputs should be given to maximize temperature uniformity along the reactor length at this temperature. The primary goal of this section is to obtain heat input profiles to minimize deviation from isothermal operation. To achieve this, a one-dimensional model is formulated which captures the primary transport effects in an archetypical catalytic wall micro-channel, and optimal control theory is applied to obtain the optimal heat inputs. Though the model is developed

[*] Parts of this section have been reprinted with permission from "Optimal heating profiles in tubular reactors with solid-phase axial wall conduction for isothermal operation". Venkateswaran, S., Wilhite, B., & Kravaris, C. (2019). *AIChE Journal*, *65*(11), e16742. Copyright 2019 Wiley.

with micro-reactors as the main application, it is applicable to even conventional tubular reactors with significant solid phase axial conduction.

The use of optimal control to maximize conversion and or minimize thermal excursions in tubular reactors neglecting solid-phase axial conduction have been studied previously[105-108]. Ko et al. [105] used optimal control to identify optimal heat transfer coefficient profiles which maximize yield for an elementary reversible exothermic reaction. Since the heat transfer coefficient appeared linearly in the model equations, the problem was singular and the input profile consists of regions where the input is maximum/minimum (bang-bang control) and regions where the input lies inside the feasible region (singular control). It was shown that in the optimal profiles, comprised an adiabatic subsection followed by a heat transfer coefficient profile inside the feasible input region. In optimal control terminology, this type of control is called "bang- singular". Smets et al. [106] obtained optimal coolant temperature profiles to optimize three different types of objective functions consisting of a combination of outlet conversion (terminal cost) and temperature deviation (running cost). They showed that for plug flow reactors, with objective functions including running costs, the optimal input is maximum-singular-minimum or bang-singular-bang and for objective functions with only terminal costs the optimal input is maximum-minimum. More recently, Logist et al. [108] conducted a similar analysis, extending to tubular reactors including axial dispersion and state variable constraints and observed that axial dispersion led to an increase in optimal objective function values. In this section it is shown that axial solid-phase conduction, being another form of heat redistribution, leads to higher optimal objective cost values.

While the magnitude of heat input is no longer a limitation in micro-reactors to endothermic reactor performance solid-phase axial heat conduction adds an additional layer of complexity. Previous numerical and experimental investigations showed that solid-phase conduction lowers the thermal efficiency of the reactor because a fraction of the heat input, instead of reaching the fluid phase, is conducted along the walls of the reactor resulting in conduction losses [16, 37]. Inspired by these results the present work aims to study the impact of solid-phase axial heat conduction and associated heat losses to packaging and plumbing for near-isothermal operation.

The organization of the section is as follows. The model is described in the next subsection and then optimal heat inputs in micro-reactors in the case when solid-phase axial wall conduction is negligible is discussed Following this, the case of significant axial conduction is considered. Then in the following subsection, the case when axial wall conduction is too high and the effect of CP on isothermal operability is covered. Finally, the work is summarized and concluded.

2.2. Model

In this subsection a model capturing the main transport phenomena in microreactors is presented. A one-dimensional steady state model is formulated to describe a single reacting fluid exchanging heat with the channel wall, which in turn is heated by an axially variable external heat source. As shown in Figure 2.1, the reactor consists of two parallel plates of finite length and thickness L and d_f, sandwiched by a wall of thickness d_w, and uniform thermal conductivity K_w. The fluid phase is assumed to follow plug flow with negligible radial or axial dispersion[109]. Radial and axial

dispersion are assumed to be negligible as $\frac{d_f}{L}, \frac{d_w}{L} \ll 1$ and Peclet numbers are >100 respectively for a typical miniaturized reactor [110-111]. Heat is absorbed within the fluid phase via homogeneous (or, pseudo homogeneous catalytic) reaction described by first order kinetics. For the case of a gas-solid catalytic reaction, the pseudo-homogeneous assumption (i.e catalyst effectiveness factor of ~ 1) is justified by catalyst dimensions of < 100μm typically reported for either packed or catalytic wall micro-reactors [5, 112]. Heat transport within the fluid phase occurs via combination of axial convection and transverse exchange with the solid wall. Heat transport within the solid phase occurs via combination of axial conduction and transverse exchange with an external heat source. Heat loss to plumbing and packaging, at both inlet and outlet of the wall, via solid phase conduction is described by assuming uniform external heat transfer coefficient h_a and packaging temperature T_a which is assumed to be equal to the inlet temperature T_0. The resulting steady state model can be written as follows

$$v_o \frac{dC_A}{dz} = -k_0 \, e^{\left[\frac{-E_a}{R\,T}\right]} C_A \tag{2.1}$$

$$v_0 \frac{dT}{dz} = \frac{-\Delta H_r}{\rho C_p} \, k_0 \, e^{\left[-\frac{E_a}{R\,T}\right]} C_A - \frac{h_1 \hat{a}_{f_1 s}}{\rho C_p} \, (T - T_w) \tag{2.2}$$

$$K_w \frac{d^2 T_w}{dz^2} = -\left[h \, \hat{a}_{f_1 s} \epsilon_{fw} \, (T - T_w) + \hat{a}_{f_2 s} \epsilon_{fw} q\right] \tag{2.3}$$

where ϵ_{fw} is the ratio of fluid channel volume to solid phase volume in the reactor. Initial conditions for fluid-phase concentration and temperature are

$$C_A(0) = C_{A0},\ T(0) = T_0 \tag{2.4}$$

and the boundary conditions for solid-phase temperature accounting for finite heat losses to adjacent plumbing, fittings are:

$$-k_w \frac{dT_w}{dz}(0) = h_{a0}\,(T_a - T_w)\,, \qquad -k_w \frac{dT_w}{dz}(L) = h_{aL}\,(T_w - T_a) \tag{2.5}$$

The model equations are converted to dimensionless form using the following transformations: $u = \frac{C_A}{C_{A0}}$, $\theta = \frac{T - T_0}{T_0}\,\gamma$, $\theta_w = \frac{T_w - T_0}{T_0}\,\gamma$ and the dimensionless input is: $\psi = \frac{q\,\gamma\,\hat{a}_{f_2 s}\,L}{\rho\,C_p\,v_0\,T_0}$. Furthermore, the dimensionless equations are cast as a system of first order ODEs to facilitate optimal control analysis

$$\frac{du}{ds} = -Da\, e^{\left[\frac{\theta}{1+\frac{\theta}{\gamma}}\right]} u = f_1 \tag{2.6}$$

$$\frac{d\theta}{ds} = B\,Da\, e^{\left[\frac{\theta}{1+\frac{\theta}{\gamma}}\right]} u - St\,(\theta - \theta_w) = f_2 \tag{2.7}$$

$$\frac{d\theta_w}{ds} = \theta_w' = f_3 \tag{2.8}$$

$$\frac{d\theta_w'}{ds} = -\left[\frac{St}{CP}(\theta - \theta_w) + \frac{\psi}{CP}\right] = f_4 \tag{2.9}$$

Dimensionless Boundary conditions

$$u(0) = u_0 = 1, \qquad \theta(0) = \theta_0 = 0 \tag{2.10}$$

$$-\frac{d\theta_w}{ds}(0) = Bi_0\,(\theta_a - \theta_w) \qquad -\frac{d\theta_w}{ds}(1) = Bi_1\,(\theta_w - \theta_a) \tag{2.11}$$

For simplicity and clarity of the present analysis, the packaging temperature is assumed to be equal to the inlet temperature $\theta_a = 0$ and identical heat transfer resistance

to end-losses via conduction to packaging/plumbing at either end of the reactor (i.e., Bi_o = Bi_1=Bi) is considered. The definitions of each dimensionless parameter and its physical significance are provided in Table 2.1.

Table 2.1 Dimensionless parameters and physical significance (Reprinted with permission from [113]).

Parameter	Expression	Physical Significance
Da	$k_0\, e^{\left[\frac{Ea}{R.T_0}\right]}\, C_{A0}\, \frac{L}{v_0}$	$\frac{\text{Reaction Rate}}{\text{Convective mass transport Rate}}$
B	$\frac{-\Delta H_r\, C_{A0}}{\rho C_p\, T_0}\, \gamma$	Dimensionless Adiabatic Temperature
St	$\frac{h\, \hat{a}_{f_1 s} L}{\rho C_p v_0}$	$\frac{\text{Convective heat transport rate to fluid}}{\text{Heat Capacity of fluid}}$
CP	$\frac{k_w}{\rho C_p\, L\, v_0\, \epsilon_{fw}}$	$\frac{\text{Conductive heat transfer rate}}{\text{Heat Capacity of fluid}}$
Bi	$\frac{h_a\, L}{k_w}$	$\frac{\text{Convective heat transfer rate to surroundings}}{\text{Conductive heat transfer rate}}$

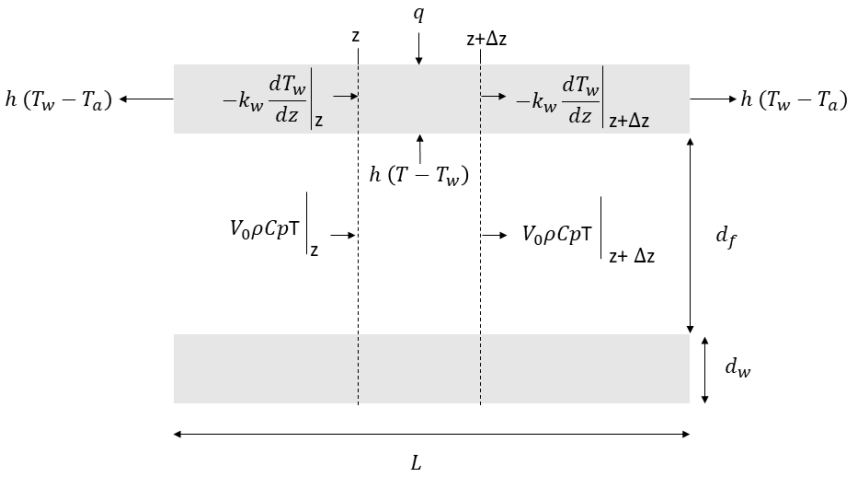

Figure 2.1 Schematic of 1-D model of a microreactor, in which a pseudo-homogeneous endothermic, first-order reaction is driven by an external heat source (Reprinted with permission from [113]).

In the simulations performed in this work, Methane steam reforming is the reaction considered. Cao et al. demonstrated the viability of using a 1st order kinetic model to describe MSR over a 10 wt % Rh/MgO/Al_2O_3 catalyst at 1023K and 4-20 atm [7]. Since this study is for a class of heat transfer limited gas-solid catalytic reaction, for the sake of obtaining generalized insight on heat transfer characteristics, a first order model is used.

$$\mathrm{R_{MSR}}\left(\frac{\mathrm{mol}}{\mathrm{m^3.h}}\right) = 2.21 * 10^{10} \exp\left(-\frac{93000}{\mathrm{RT}}\right) \mathrm{C_{CH4}} \frac{\mathrm{V_{cat}}}{\mathrm{V_f}} \qquad (2.12)$$

where $\mathrm{V_{cat}}$- is the volume of the catalyst and $\mathrm{V_f}$- is the volume of the fluid phase. The operating conditions are in[113] and the dimensionless parameters are as shown in Table 2.2 such that isothermal operation at this temperature would give a conversion $=1 - \mathrm{e}^{-\mathrm{Da}} =$

$1 - e^{-2.29} \sim 0.9$. The value of CP will be varied throughout the analysis to investigate the effect of wall conduction on near-isothermal operation

Table 2.2 Operating conditions (Reprinted with permission from [113]).

Dimensionless Parameters	Value
Da	2.29
γ	10.93
B	-10.44
St	40.74
Bi	0.001

2.3. The optimal control problem

As the aim of this section to obtain optimal heating rates for near-isothermal operation, the objective function of the optimal control problem is:

$$l = \int_0^1 \theta^2 \, ds \tag{2.13}$$

and the goal is to find an input $\psi \in \Psi$, where Ψ is the set of all admissible inputs:

$0 \leq \psi(s) \leq \psi_{max}$,

such that equation (2.13) is minimized, subject to the model equations (2.6-2.11). The Hamiltonian for this problem is defined as:

$$H = \lambda_1 f_1 + \lambda_2 f_2 + \lambda_3 f_3 + \lambda_4 f_4 + \theta^2 \tag{2.14}$$

where f_1, f_2, f_3, f_4 are the right hand sides of the model equations (2.6-2.9) and $\lambda_1, \lambda_2, \lambda_3, \lambda_4$ are the adjoint states. The minimum principle states that: $H(X^*, \lambda^*, \psi^*) \leq H(X^*, \lambda^*, \psi) \forall \psi \, \epsilon \Psi$, where $X = [u, \theta, \theta_w]$ is process state, where the superscript $*$ denotes the optimum value of the state/input. The adjoint state λ satisfies the following equations:

$$\frac{d\lambda_1}{ds} = -\lambda_1 f_{1_u} - \lambda_2 f_{2_u} \tag{2.15}$$

$$\frac{d\lambda_2}{ds} = -\lambda_1 f_{1_\theta} - \lambda_2 f_{2_\theta} - \lambda_4 f_{4\theta} \; - 2\theta \tag{2.16}$$

$$\frac{d\lambda_3}{ds} = -\lambda_2 f_{2_{\theta_w}} - \lambda_4 f_{4_{\theta_w}} \tag{2.17}$$

$$\frac{d\lambda_4}{ds} = -\lambda_3 \tag{2.18}$$

Along with the boundary condition:

$$\lambda_1(1) = \lambda_2(1) = 0 \tag{2.19}$$

$$\lambda_3(0) + Bi\lambda_4(0) = 0 \, , \lambda_3(1) - Bi\lambda_4(1) = 0 \tag{2.20}$$

where $f_{1u} = \frac{\partial f_1}{\partial u}, f_{1\theta} = \frac{\partial f_1}{\partial \theta}$ and so on, denote the partial derivatives of the right-hand sides of equations (2.6-2.9) with respect to the state variables.

In the optimal control problem under consideration equations (2.6-2.9) and equations (2.15-2.18), the input appears linearly in the Hamiltonian equation (2.14). The optimal control cannot be obtained in terms of the state and adjoint variables using the necessary condition $H_\psi = 0$. Such problems called termed singular and special techniques from singular optimal control theory are necessary[114]. In such cases, the optimal input is found by repeatedly differentiating $H_\psi = 0$ with respect to the independent variable, s,

until the input appears. For more information about optimal control and singular optimal control the reader is directed to standard texts on optimal control[114].

To analyze the behavior of the system when the input is unbounded, an alternative formulation of the optimal control problem which is a regularization of the original problem is considered. Here ψ is unbounded and the objective is to minimize the objective function:

$$l = \int_0^1 \theta^2 + \alpha\psi^2 ds \tag{2.21}$$

which now involves an additional input penalty. The weight coefficient $\alpha > 0$ is appropriately selected to adjust the magnitude of the input penalty. Applying standard first-variation principles[114] the optimal input profile is:

$$\psi = \frac{\lambda_4}{2\alpha CP^2} \tag{2.22}$$

The above expression along with the model equations (2.6-2.9) and adjoint equations (2.15-2.18) results in a two-point boundary value problem which is solved to obtain the optimum profiles. This formulation provides a facile way of numerically calculating the profiles when is α small, and thus allowing large heating rates, as an alternative to singular optimal control. However, for all other cases in this study the first formulation as it is practically easier to define the input bounds than the input penalty weights

2.4. Negligible axial heat conduction: CP→0

First, we consider the case of negligible axial wall conduction (i.e CP→0) as analyzing the behavior of the reactor under asymptotic limits of CP, provides useful insights on feasibility of perfect isothermality. For very low CP, the derivative in equation

(2.9) can be neglected and an algebraic equation is obtained, which when combined with equation (2.7) gives equation (2.24) and the reduced model may be written as:

$$\frac{du}{ds} = -Da\, e^{\left[\frac{\theta}{1+\frac{\theta}{\gamma}}\right]} u = g_1 \tag{2.23}$$

$$\frac{d\theta}{ds} = B\, Da\, e^{\left[\frac{\theta}{1+\frac{\theta}{\gamma}}\right]} u + \psi = g_2 \tag{2.24}$$

From equation (2.24) it immediately follows that isothermality would be feasible if the input ψ is

$$\psi = -B\, Da\, u \tag{2.25}$$

and if the input is unbounded, a perfectly isothermal reactor is possible.

2.4.1. Bounded inputs, CP→0

If $0 \leq \psi(s) \leq \psi_{max}$, then a perfectly isothermal reactor might not be possible. The optimal profiles in such cases will be found using optimal control theory formulated in the previous subsection but now with the simplified model, and the Hamiltonian defined accordingly. Here:

$$H(u, \theta, \lambda, \psi) = \theta^2 + \lambda_1 g_1 + \lambda_2 g_2 \tag{2.26}$$

and λ satisfies:

$$\frac{d\lambda_1}{ds} = -\lambda_1 g_{1_u} - \lambda_2 g_{2_u} \tag{2.27}$$

$$\frac{d\lambda_2}{ds} = -\lambda_1 g_{1_\theta} - \lambda_2 g_{2_\theta} - 2\theta \tag{2.28}$$

along with the terminal conditions (2.19). The input appears linearly in the Hamiltonian through g_2, therefore the optimal input is:

$$\psi = \begin{cases} \psi_{max}\,, & \lambda_2 < 0 \\ \psi_{sin} & \lambda_2 = 0 \\ 0 & \lambda_2 > 0 \end{cases} \tag{2.29}$$

When $\lambda_2 = 0$, the optimal input is singular, and, in this case, the input is obtained by solving the equations:

$$H_\psi = 0 \rightarrow \lambda_2 = 0$$

$$\frac{dH_\psi}{ds} = 0 \rightarrow \lambda_1 = -\frac{2\theta}{g_{1\theta}}$$

$$\frac{d^2H_\psi}{ds^2} = 0 \rightarrow \frac{d\theta}{ds} = 0$$

From the latter condition and equation (2.24) one immediately obtains the singular input:

$$\psi_{sin} = -B\ Da\ e^{\left[\frac{\theta}{1+\frac{\theta}{\gamma}}\right]}\ u \tag{2.30}$$

The above expression was also found in [106] in the context of a more general objective function. Furthermore, we can show that if the singular arc is the final portion of the optimal input, then $\theta = 0$ along the singular arc, since $\lambda_1(1) = -\frac{2\theta(1)}{g_{1\theta}} = 0$ implying $\theta = 0$ and the expression for $\psi_{sin}$is identical to equation (2.29). If $\psi_{max} \geq -B\ Da$, then the optimal input is singular over the entire range and is equal to (2.29) and hence perfect isothermality is achieved.

However, if $\psi_{max} < -B\ Da$. there will be an initial phase where $\psi = \psi_{max}$. This phase is characterized by temperature decrease initially (when rate of heat absorbed from reaction is larger than ψ_{max}) followed by temperature rise (when rate of heat absorbed from reaction is less than ψ_{max}). The temperature increases until it hits $\theta = 0$ following

which the input switches to the singular arc. These two cases are illustrated in Figure 2.2 for the cases of $\psi_{max} = 25,20$ which correspond to about 11kW/m^3 and 9kW/m^3 respectively.

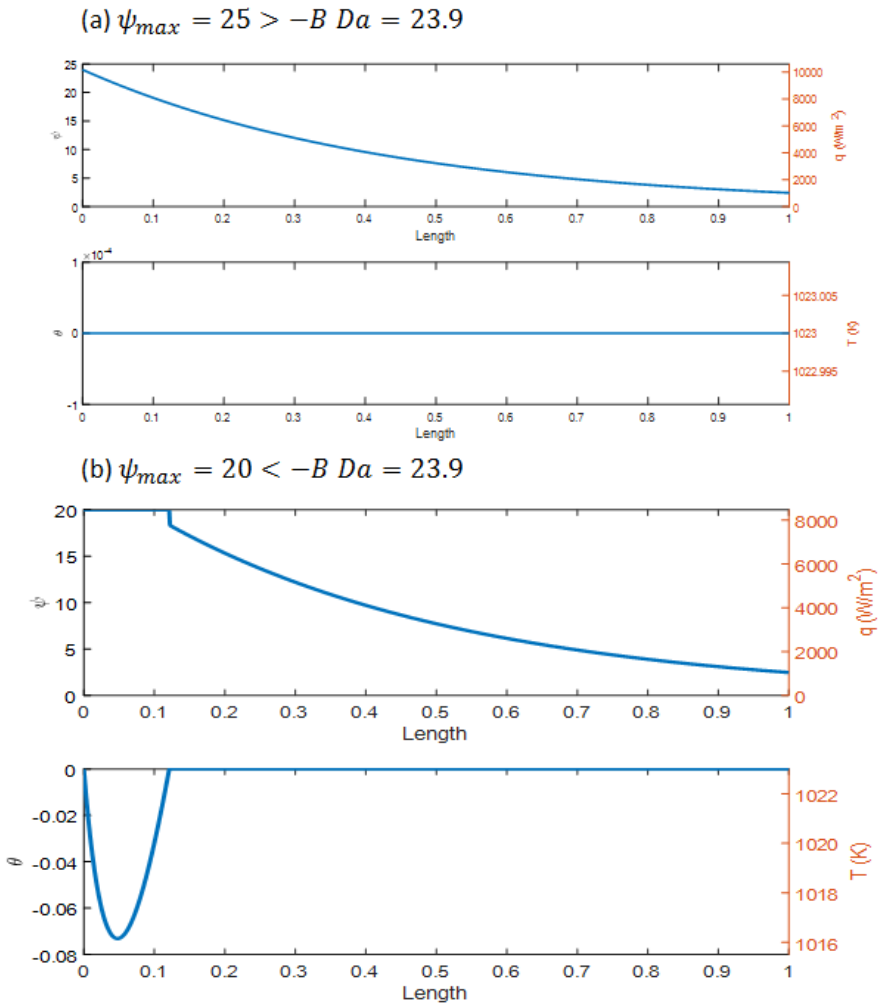

Figure 2.2 Optimal heating rate (ψ) and temperature (θ) profiles (Reprinted with permission from [113]).

2.4.2. Infeasibility of exact isothermality under moderate CP

Having established in the previous subsection that when CP→0, perfect isothermality is possible if $\psi_{max} \geq -B\,Da$, in this subsection it is shown that when CP is non-infinitesimal, perfect isothermality is not possible even if $\psi_{max} \geq -B\,Da$. If reactor phase is isothermal at $\theta = 0\ \forall z\ [0,1]$, then equation (2.7) yields:

$$\theta_w = -B\,\frac{Da}{St}\,e^{-Da\,s} \tag{2.31}$$

and substituting into equation (2.9), yields the heating profile required:

$$\psi = -B\,Da\left[1 - \frac{CP\,Da^2}{St}\right]e^{-Da.s} \tag{2.32}$$

However, the wall temperature necessary for isothermal operation does not satisfy the boundary conditions of the wall. Substituting the obtained wall temperature profile (2.31) in boundary conditions (2.11) yields:

$$\frac{d\theta_w}{ds}(0) = Bi\,\theta_w(0) \rightarrow B\,\frac{Da^2}{St} = -Bi\,B\,\frac{Da}{St}\ \text{i.e.}\ Da = -Bi$$

$$-\frac{d\theta_w}{ds}(1) = Bi\,\theta_w(1) \rightarrow\ -\frac{Da^2}{St}\exp(-Da) = -Bi\,B\frac{Da}{St}\exp(-Da)\ \text{i.e.}\ Da = Bi$$

which leads to contradiction. Thus, applying the isothermal input cannot satisfy the boundary conditions and hence perfect isothermality is shown to be mathematically infeasible under a finite input ψ when CP is non-zero.

2.5. Optimal heating rate under moderate CP- unbounded inputs

In this subsection, the regularized performance index (2.21) with input penalty is considered as it provides a facile way to qualitatively observe the nature of the input as it becomes large in magnitude and de-regularized as the size of the input penalty is reduced.

That is, optimal inputs to minimize the objective function as $\alpha \to 0$ will be calculated, which will turn out to be impulsive.

The boundary value problem (equations 2.6-2.11, equations 2.15-2.20 and equation 2.22) are solved using bvp4c, a finite difference solver that implements the three stage Lobatto formula in MATLAB. α is decreased until near-singularity is observed which would stop numerical calculations. It was observed that as α decreases the appearance of impulses is observed at both ends. In Figures 2.3-2.6, the heating rate, temperature profile, wall temperature profile, and wall temperature derivative for $\alpha = 10^{-23}$ are plotted. The temperature profile along the reactor length is isothermal, and consequently the wall temperature profile is identical to equation (2.31). Furthermore, the heating rate is equal to the isothermal heating rate (2.32), throughout the reactor length except at s=0 and 1. At s=0 and 1, an impulse in the heating rate is observed. As shown in Figure 2.6 these impulses shift $\frac{d\theta_w}{ds}$ at s=0 and s=1 to satisfy the wall boundary conditions.

Motivated by the foregoing numerical findings, one can postulate an impulsive optimal input expression of the form:

$$\psi = -B.Da\left[1 - CP\ \frac{Da^2}{St}\right] e^{-Da.s} + M_1\delta(s) + M_2\delta(s-1)$$

where the first term is identical to equation (2.32) and M_1 and M_2 are calculated to satisfy the boundary conditions (2.11). The resulting heating rate for perfectly isothermal operation is:

$$\psi = -\mathrm{B}.\,\mathrm{Da}\left[1 - \mathrm{CP}\,\frac{\mathrm{Da}^2}{\mathrm{St}}\right] e^{-\mathrm{Da}.s} - \mathrm{CP}\left[\mathrm{Bi}\frac{\mathrm{B\,Da}}{\mathrm{St}} + \mathrm{B}\,\frac{\mathrm{Da}^2}{\mathrm{St}}\right]\delta(s)$$
$$-\mathrm{CP}\left[-\mathrm{B}\,\frac{\mathrm{Da}^2}{\mathrm{St}} + \mathrm{Bi\,B}\frac{\mathrm{Da}}{\mathrm{St}}\right] e^{-\mathrm{Da}}\,\delta(s-1) \qquad (2.32)$$

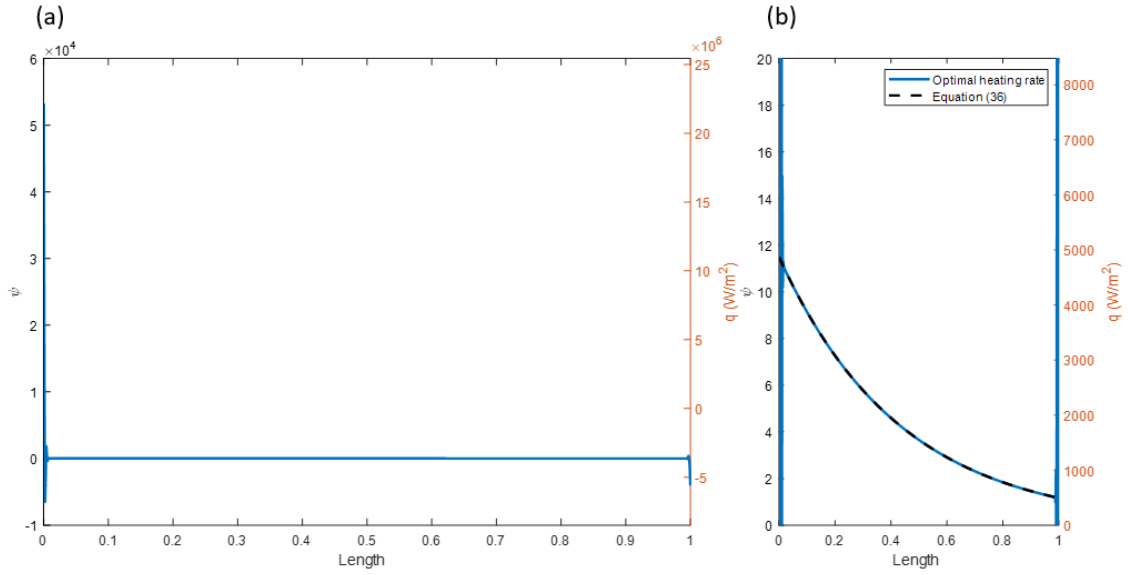

Figure 2.3 (a) Optimal heating rate for $\alpha=10^{-23}$. Impulsive heating rates at the boundaries s=0 and s=1 observed. (b) Optimal heating rate zoomed in to show that the optimal input matches the heating rate given by equation (2.32) in the open interval (0,1) (Reprinted with permission from [113]).

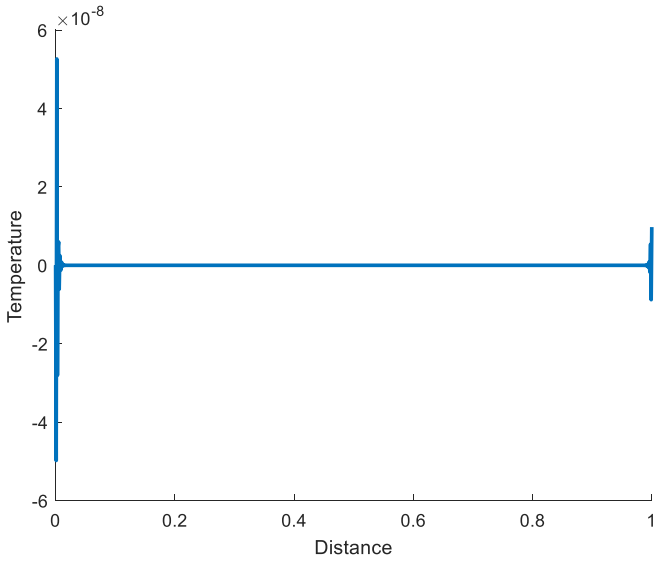

Figure 2.4 Temperature vs distance, $\alpha=10^{-23}$. The reactor is isothermal at $\theta=0$ (Reprinted with permission from [113]).

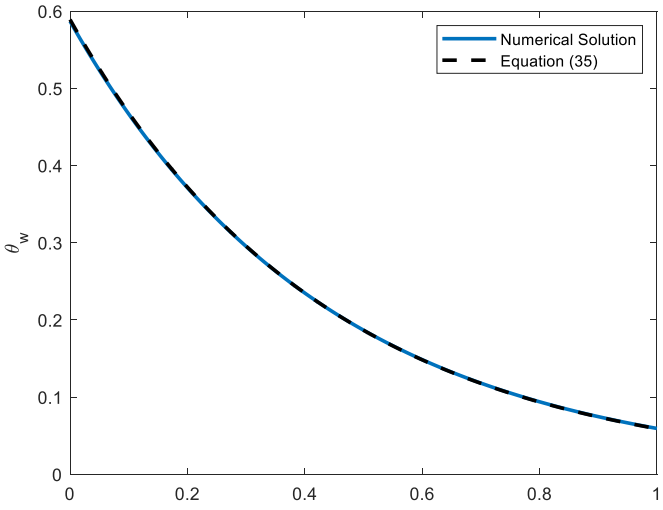

Figure 2.5 Wall temperature, $\alpha=10^{-23}$ (Reprinted with permission from [113]).

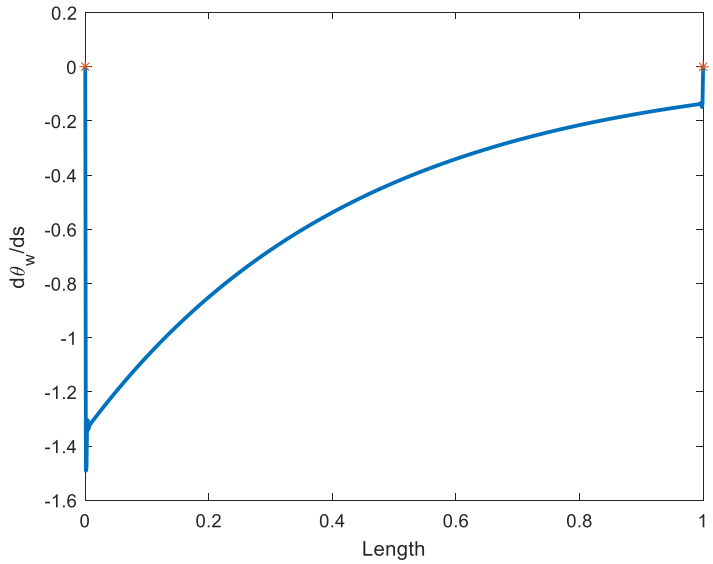

Figure 2.6 Wall temperature derivative vs length. $\alpha=10^{-23}$ * represents the value the derivative should have to satisfy the wall boundary conditions (2.11) (Reprinted with permission from [113]).

It has been established that (i) under a finite input perfectly isothermal operation is infeasible and (ii) to achieve perfect isothermality infinite impulses at the ends would be necessary which of course are infeasible. In this subsection, singular optimal control will be applied to find the optimal heat input to minimize the deviation from perfect isothermality for the case where the input is bounded and, within the finite interval $[0, \psi_{\max}]$. It will turn out that using singular optimal control with bounded input, the optimal input will try to approximate the infinite impulses within the feasible limits. The optimal input will end up having a singular phase in the interior and bang-bang phases at the ends, which will be finite pulses instead of infinite impulses. Again, like in the previous case of CP$\rightarrow$ 0 the input appears linearly in the Hamiltonian. From the Hamiltonian Minimization condition, it is concluded that:

$$\psi = \begin{cases} \psi_{max} & \lambda_4 > 0 \\ \psi_{sin} & \lambda_4 = 0 \\ 0 & \lambda_4 < 0 \end{cases} \tag{2.33}$$

A singular input is possible, when

$$H_\psi = -\frac{\lambda_4}{CP} = 0$$

in an interval. Repeated differentiation of H_ψ with respect to s gives:

$$\frac{dH_\psi}{ds} = 0 \rightarrow \lambda_3 = 0$$

$$\frac{d^2H_\psi}{ds^2} = 0 \rightarrow \lambda_2 = 0$$

$$\frac{d^3H_\psi}{ds^3} = 0 \rightarrow \frac{d\theta}{ds} = 0$$

The latter condition states that along the singular interval θ is constant and differentiating this condition three times gives the necessary singular input:

$$\psi_{sin} = B\ Dae^{\left[\frac{\theta}{1+\frac{\theta}{\gamma}}\right]} u \left[\frac{CP}{St} Da^2\ e^{\left[\frac{2\theta}{1+\frac{\theta}{\gamma}}\right]} - 1\right] \tag{2.34}$$

Even though all the set of possible inputs $[0, \psi_{sin}, \psi_{max}]$ for minimizing deviation from isothermally is known, the challenge is to determine the switching points and define intervals over which singular and bang-bang inputs appear. The following numerical approach was used to determine the sequence in which the bang-bang and singular arcs appear.

The model equations are discretized into 1000 finite nodes using the finite difference scheme and solved using the IPOPT solver [115] in GAMS. This gives an approximate profile where the optimal input sequence is identified.

Once the sequence is identified, a multi-point boundary value problem is formulated with the number of regions equal to the number of optimal input sequences identified in step (i). At the interface of the regions, the boundary conditions are specified to ensure continuity of the state variables.

The exact switching points are identified after solving an optimization problem with switching positions as decision variables. This is done using the fmincon routine, which implements the Interior Point algorithm, wrapped around a function that implements the above multi-point boundary problem using bvp4c and returns the cost calculated using the trapezoidal rule of integration.

2.6. Results

For the simulations, a maximum heating rate of 100 $\frac{\mathrm{kW}}{\mathrm{m}^3}$ and conductivity of 400 W/m/K, 200 W/m/K and 100 W/m/K are considered. In dimensionless terms this corresponds to $\psi = 235.94$ and CP=8.06, 4.03, and 2.01. The optimal heat inputs and the respective temperature, concentration and wall temperature profiles are plotted in Figures 2.7-2.12. For CP =4.03 and CP=2.01 the optimal inputs consist of the singular input sandwiched by bang-bang regions, in effect providing a finite input approximation of the infinite impulse inputs observed in the previous subsection. Along the singular arc, the temperature is observed to be ~ 0, which makes intuitive sense as 0 is the global minimum for the objective function and any other value will increase the objective function. In the

regions corresponding to bang-bang inputs there is, as expected, deviation from isothermality but this is necessary to satisfy the boundary conditions of the wall. In addition, as shown in Figure 2.13, it is observed that the length of the singular interval increases as conductivity decreases. This too, is expected as in the limit CP→0, the optimal input consists of the singular input only for the case when $\psi_{max} \geq -B\ Da$, which holds in our case. For CP=8.06, the optimal input is found to be bang-bang and because in the absence of singular interval, there is significant deviation from isothermality. The critical CP where the transition from partially singular inputs to completely bang-bang inputs is obviously dependent on the reaction parameters and the maximum input available. Hence, numerical simulations over a wide range of CP are required to identify this critical conduction parameter. However, as shown below, it is possible to derive an analytical inequality solely in terms of reactor parameters that, if satisfied, the optimal control is bang-bang control and significant deivation from isothermality is unavoidable.

Indeed, using the fact that the temperature along the singular interval is constant and equal to 0 therefore, the singular input expression can be written as:

$$\psi = B\ Da\ u[\frac{CP}{St} Da^2\ - 1\ ]$$

Since $\psi \geq 0$, singular arc will only be possible if $Da^2 \leq \frac{St}{CP}$. If $Da^2 > \frac{St}{CP}$ the singular input will be necessarily bang-bang. The value of CP when the equality holds is $CP = \frac{St}{Da^2} = 7.73$. Thus, for CP>7.73 the control will be bang-bang. It is to be noted that in the numerical simulations shown in Figure 2.13 the critical CP at which the transition from partially singular inputs to bang-bang inputs occurred was ~ 6. Thus, CP<$\frac{St}{Da^2}$=7.73

is a necessary condition for partially singular inputs and CP>$\frac{\mathrm{St}}{\mathrm{Da}^2} = 7.73$ is a sufficient condition for bang bang inputs and hence significant deviation from isothermality.

For the three cases taken:

$\mathrm{Da}^2 - \frac{\mathrm{St}}{\mathrm{CP}} = 2.29^2 - \frac{40.74}{4.0364} = -4.8103 < 0$- Singular arc feasible

$\mathrm{Da}^2 - \frac{\mathrm{St}}{\mathrm{CP}} = 2.29^2 - \frac{40.74}{2.0192} = -14.9322 < 0$- Singular arc feasible

$\mathrm{Da}^2 - \frac{\mathrm{St}}{\mathrm{CP}} = 2.29^2 - \frac{40.74}{8.0729} = 0.2375 > 0$. Singular arc infeasible. Bang Bang input.

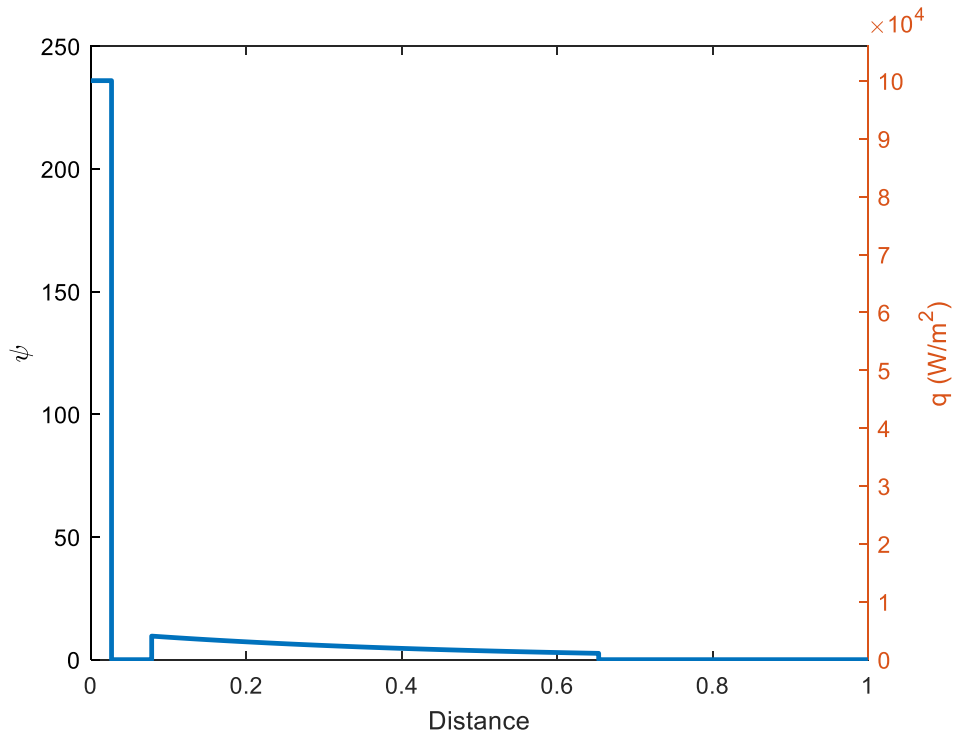

Figure 2.7 Optimal heating rate- case 1 (Reprinted with permission from [113]).

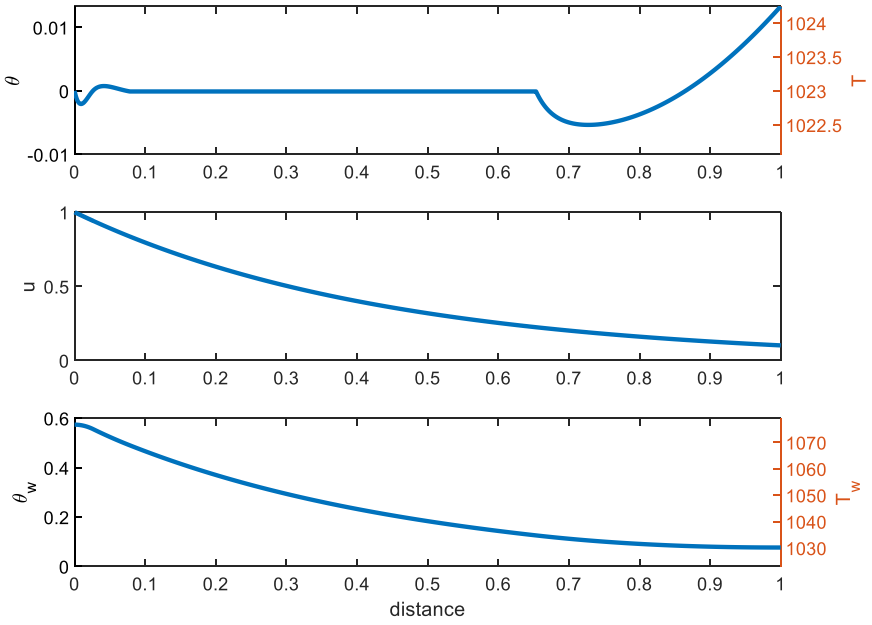

Figure 2.8 Optimum temperature, concentration and wall temperature profiles- case 1 (Reprinted with permission from [113]).

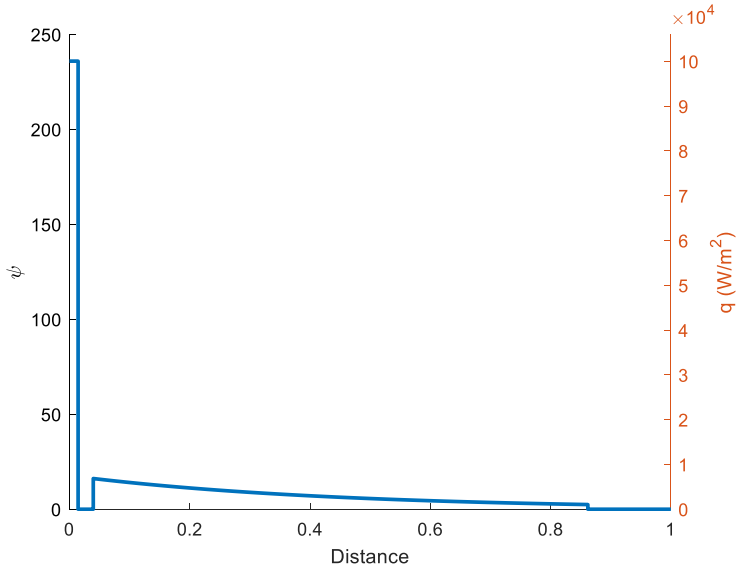

Figure 2.9 Optimal heating rate- case 2 (Reprinted with permission from [113]).

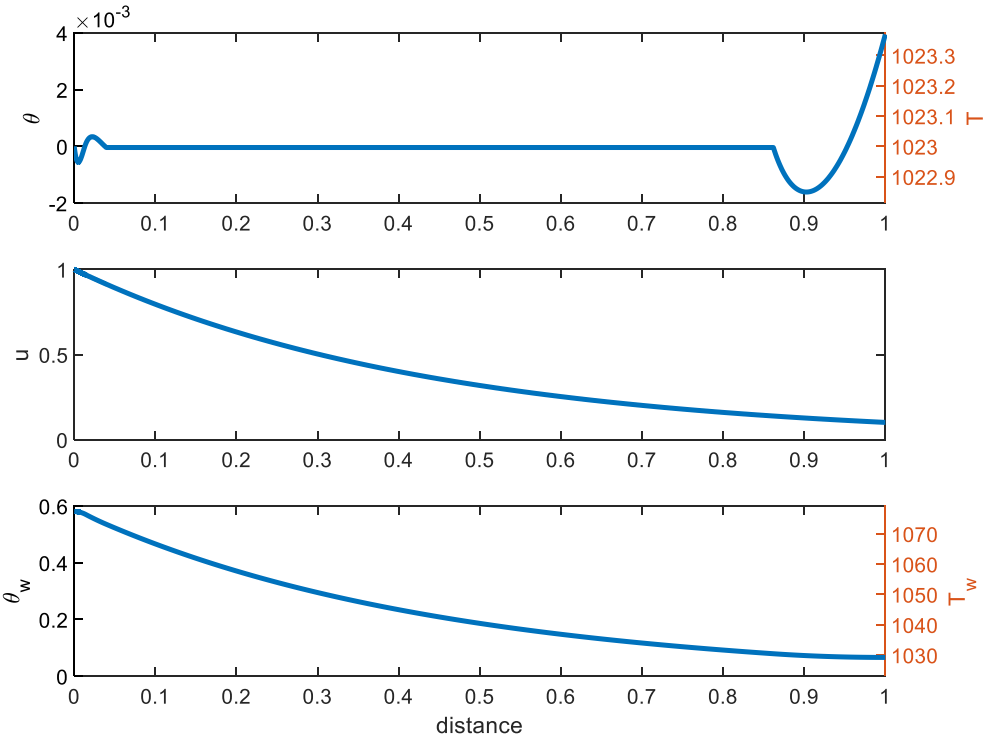

Figure 2.10 Optimal temperature, concentration, wall temperature profiles- case 2 (Reprinted with permission from [113]).

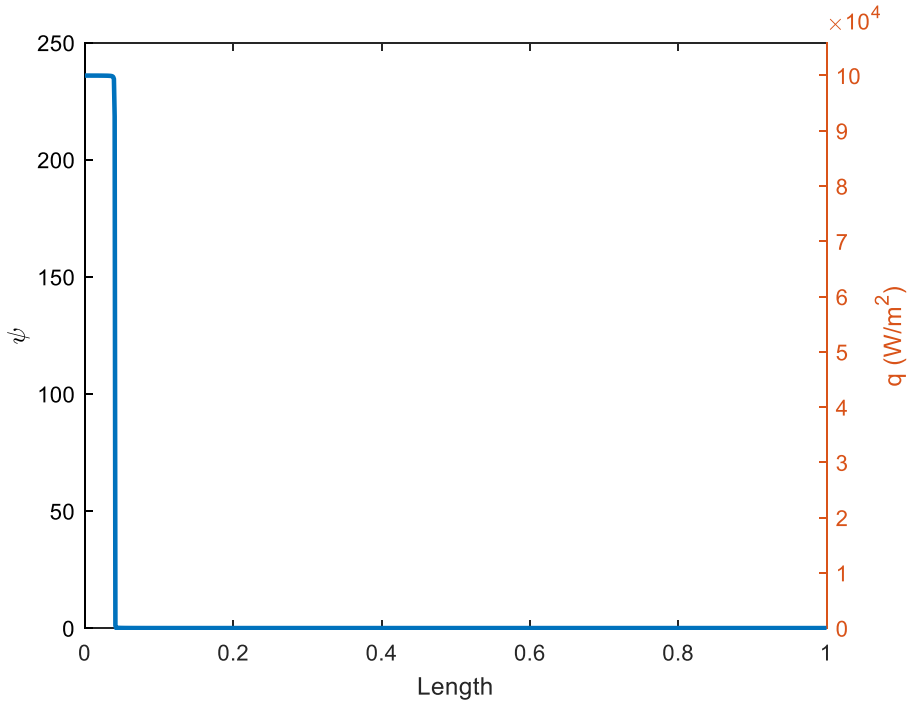

Figure 2.11 Optimal heating rate- case 3 (Reprinted with permission from [113]).

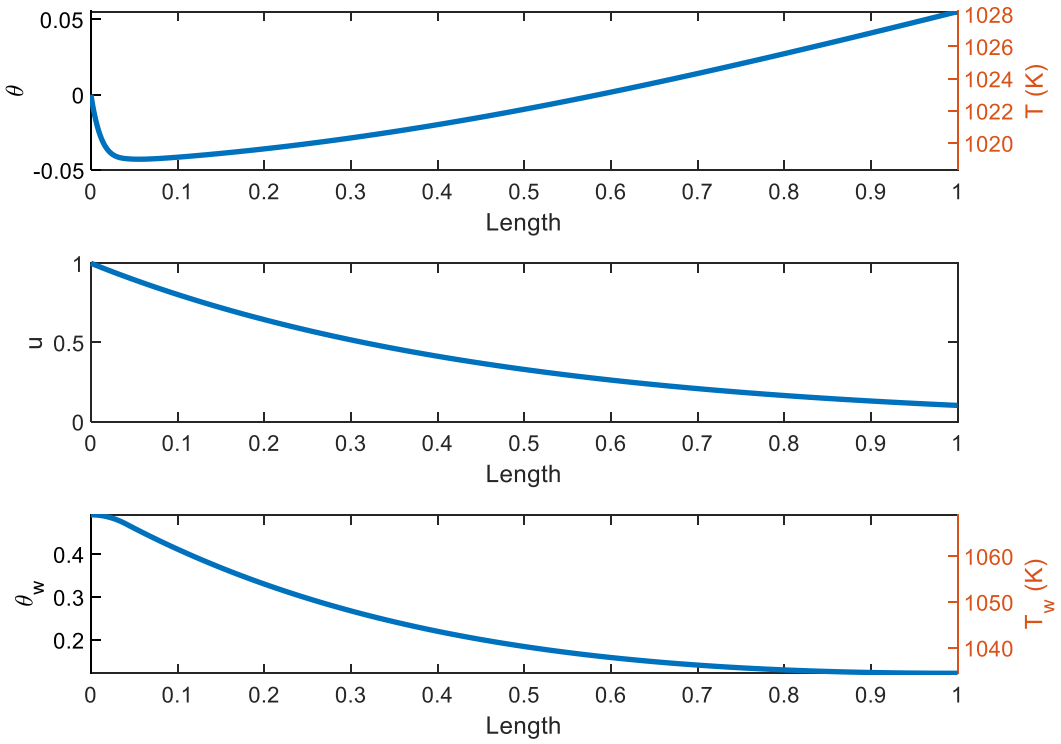

Figure 2.12 Optimal temperature, concentration, wall temperature profiles- case 3 (Reprinted with permission from [113]).

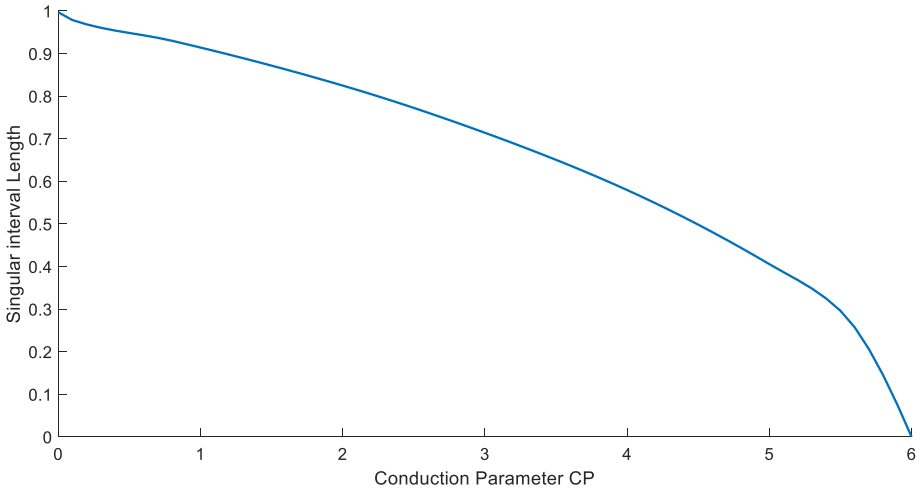

Figure 2.13 Singular interval length vs CP (Reprinted with permission from [113]).

It has been observed in the literature that heat transfer efficiency of microreactor decreases with increase in solid phase axial conduction, since some of the heat from the external source is conducted along the reactor wall and lost to the surroundings rather than reaching the fluid phase[37]. This observation agrees with our analysis. The term $\mathrm{Da}^2 - \frac{\mathrm{St}}{\mathrm{CP}}$. suggests that near- isothermal operation of microreactors hinges on two key factors; (i) the reaction rate (Da^2); this dependence is intuitive, as the magnitude of external heat required increases with reaction rate. (ii) The efficiency of heat transfer from the external heat source to the fluid phase (St/CP); In the limit $\frac{\mathrm{St}}{\mathrm{CP}} \to \infty$, the efficiency of heat transfer to the reactor is maximum, as the heat from the source directly reaches the reactor in the absence of conduction, facilitating perfectly isothermal operation. When St/CP is finite, wall conduction losses to the packaging brings down the efficiency of heat transfer onto the reactor phase, inhibiting isothermal operation. In the limit $\frac{\mathrm{St}}{\mathrm{CP}} \to 0$, the heating element

is unable to transfer heat to the reactor, as all the heat is lost via conduction to the surroundings.

Therefore, to achieve near-isothermal reactors, $\mathrm{Da}^2 - \frac{\mathrm{St}}{\mathrm{CP}}$ should be as low as possible. To illustrate this the objective function vs CP is plotted for three different maximum heat inputs in, (i) $\psi_{\max} = -0.8\ \mathrm{B\ Da}$, (ii) $\psi_{\max} = -\mathrm{B\ Da}$, (iii) $\psi_{\max} = -10\mathrm{B\ Da}$ in Figure 2.14. In the limit CP$\rightarrow 0$, perfect isothermality is observed for the cases (ii) and (iii) since $\psi_{\max} \geq -\mathrm{B\ Da}$, in case (i) where $\psi_{\max} \leq -\mathrm{B\ Da}$ there is an offset from perfect isothermality. As CP is increased but still in the region where $\mathrm{Da}^2 - \frac{\mathrm{St}}{\mathrm{CP}} < 0$,the reactor is not perfectly isothermal, but the objective function is low enough to ensure deviation from isothermal operation is minimum. Furthermore, in this region the effect of the maximum heat input is most significant. As CP is increased even further the objective function keeps increasing and, for large CP where $\mathrm{Da}^2 - \frac{\mathrm{St}}{\mathrm{CP}} > 0$, the effect of $\psi_{\max}$on the objective function value is diminished. In fact, when CP$\rightarrow \infty$, $\frac{\mathrm{St}}{\mathrm{CP}}$ and $\frac{\psi_{\max}}{\mathrm{CP}} \rightarrow 0$, the following reduced model is obtained:

$$\frac{\mathrm{du}}{\mathrm{ds}} = -\mathrm{Da}\ \mathrm{e}^{\left[\frac{\theta}{1+\frac{\theta}{\gamma}}\right]}\ \mathrm{u}$$

$$\frac{\mathrm{d}\theta}{\mathrm{ds}} = \mathrm{B\ Da}\ \mathrm{e}^{\left[\frac{\theta}{1+\frac{\theta}{\gamma}}\right]}\ \mathrm{u} + \mathrm{St}(\theta - \theta_a)$$

Thus, in this limit the model equations are no longer affected by the heat input.

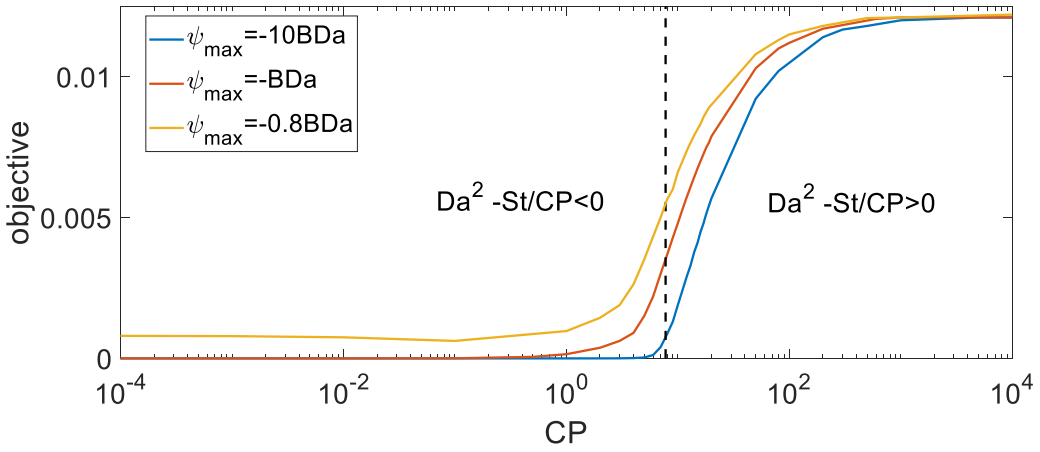

Figure 2.14 Objective function vs conduction parameter (CP) (Reprinted with permission from [113]).

2.7. Conclusions

Using a one-dimensional steady state plug flow model with significant solid phase conduction optimal heat inputs to achieve near-isothermal operation are obtained using singular optimal control theory. Near-isothermal operation is feasible when the magnitude of heat conduction is low. The effect of external heating elements on temperature control is strongly dependent on CP. CP$\rightarrow 0$ reactors are more amenable to isothermal operation due higher heat transfer efficiencies in the absence of conduction. On the other hand, in CP $\rightarrow \infty$ microreactors, fluid phase temperature is unaffected by the heat input. In between these two extremes, the behavior is dictated by the sign of $\mathrm{Da}^2 - \frac{\mathrm{St}}{\mathrm{CP}}$. Positive values signify high rate of heat absorption due to the reaction (Da^2) or low heat transfer efficiency to the fluid phase (St/CP), both contributing to deviation

from isothermal temperature. Negative values mean the opposite i.e low rate of heat absorption and high heat transfer efficiency and enable near-isothermal operation.

3. EXOTHERMIC MICROREACTORS- EFFECT OF SOLID PHASE CONDUCTION ON HOTSPOT FORMATION[*]

3.1. Introduction

The previous section focused on heat transfer limited endothermic processes where achieving temperature uniformity was critical to maintaining high reaction rates throughout the reactor. Now the focus shifts to exothermic reactions. Many industrially relevant exothermic reactions are fast and release large amounts of energy. This makes them susceptible to runaway and explosion hazards. Thanks to high rates of transverse heat exchange between the reacting fluid and the coolant, one of the first opportunities identified for microreactors was ability to safely perform hazardous chemistries, with emphasis on highly exothermic, fast reactions. However, solid-phase axial heat conduction brings out complexities in the heat distribution process. For example, it has been shown experimentally, that high thermal conductivity of the solid-phase from which the device is fashioned (e.g., silicon, steel) axially disperses reaction heat for further prevention of localized hot-spots and/or runaway. Conversely, microreactors fashioned from low thermal conductivity materials (e.g., ceramics) have been explored for exploiting runaway in exothermic reactions to achieve breakthroughs in thermal efficiencies for regenerative combustors or heat-exchanger reactors [6, 12-13, 41-42]. The objective of this

[*] Parts of this section have been reprinted with permission from "Analysis of solid-phase axial heat conduction upon hot-spot formation in a one-dimensional microreactor". Venkateswaran, S., Wilhite, B., & Kravaris, C. (2019). Chemical Engineering Journal, 377, 1250501 Copyright 2019 Elsevier

subsection is to obtain fundamental insights on the effect of solid-phase axial heat conduction on hotspot formation.

For the case of conventional, non-isothermal tubular reactors there exists several published criteria for predicting hot-spot formation (or, runaway behavior). Explicit (or, a priori) criteria are based upon analyzing the geometry of the reactor model equation to derive general criteria for runaway without requiring a rigorous solution of the reactor model[116-118]. While computationally facile, such criteria tend to yield overly conservative reactor designs [117]. For this reason, implicit criteria based upon the parametric sensitivity of the steady-state reacting fluid temperature profile with respect to a particular design parameter have been developed [119-120], culminating in the generalized criteria of Morbidelli and Varma which defines the critical point (corresponding to onset of hot-spot formation or runaway) as occurring at a simultaneous extrema in the parametric sensitivity of the reacting fluid maximum temperature with respect to each design parameter [121]. However, both implicit and explicit criteria reported to-date have been obtained using a classical non-isothermal plug flow reacting fluid model which does not account for any contributions of the solid phase.

What follows is a rigorous mathematical analysis of the impact of solid-phase axial heat conduction (both with and without conductive losses to packaging) via parametric sensitivity analysis of a generalized one-dimensional microreactor model. The generalized model is developed to enable a direct side-by-side comparison with literature findings and explicit criteria obtained for the traditional case of a non-isothermal plug-flow reactor.

3.2. Model

We consider a one-dimensional steady state model describing a single reacting fluid exchanging heat with the microchannel's wall (see also Figure 3.1). The microchannel's wall exchanges heat with a constant-temperature coolant, instead of an external heating source. Finite conductive heat transfer from the solid phase to adjacent fluidic connections is assumed at the inlet and outlet faces of the microchannel network, while heat losses to ambient along the axial length of the microchannel network are assumed negligible relative to heat transfer to coolant flow. The dimensionless model equations are as follows

$$\frac{\mathrm{du}}{\mathrm{ds}} = -\mathrm{Da}\, \mathrm{e}^{\left[\frac{\theta}{1+\frac{\theta}{\gamma}}\right]}\, \mathrm{u} \tag{3.1}$$

$$\frac{\mathrm{d}\theta}{\mathrm{ds}} = \mathrm{B}\, \mathrm{Da}\, \mathrm{e}^{\left[\frac{\theta}{1+\frac{\theta}{\gamma}}\right]}\, \mathrm{u} - \mathrm{St}\,(\theta - \theta_{\mathrm{w}}) \tag{3.2}$$

$$\frac{\mathrm{d}^2\theta_{\mathrm{w}}}{\mathrm{ds}^2} = -\left[\frac{\mathrm{St}}{\mathrm{CP}}(\theta - \theta_{\mathrm{w}}) + \frac{\mathrm{St}}{\mathrm{CP}}\xi(\theta_{\mathrm{c}} - \theta_{\mathrm{w}})\right] \tag{3.3}$$

$$\mathrm{u}(0) = \mathrm{u}_0 = 1, \qquad \theta(0) = \theta_0 = 0 \tag{3.4}$$

$$-\frac{\mathrm{d}\theta_{\mathrm{w}}}{\mathrm{ds}}(0) = \mathrm{Bi}_0\,(\theta_{\mathrm{a}} - \theta_{\mathrm{w}}) \qquad -\frac{\mathrm{d}\theta_{\mathrm{w}}}{\mathrm{ds}}(1) = \mathrm{Bi}_1\,(\theta_{\mathrm{w}} - \theta_{\mathrm{a}}) \tag{3.5}$$

The resulting equations indicate that the state variables $\mathrm{u}(\mathrm{s}), \theta(\mathrm{s}),$ and $\theta_{\mathrm{w}}(\mathrm{s})$ are functions of $[\mathrm{Da}, \mathrm{B}, \gamma, \mathrm{St}, \mathrm{Bi}, \mathrm{CP}, \xi, \theta_{\mathrm{a}}, \theta_{\mathrm{c}}]$. This provides the basis for formulating model expressions for obtaining the corresponding sensitivities of $\mathrm{u}(\mathrm{s}), \theta(\mathrm{s}),$ and $\theta_{\mathrm{w}}(\mathrm{s})$ with respect to each parameter.

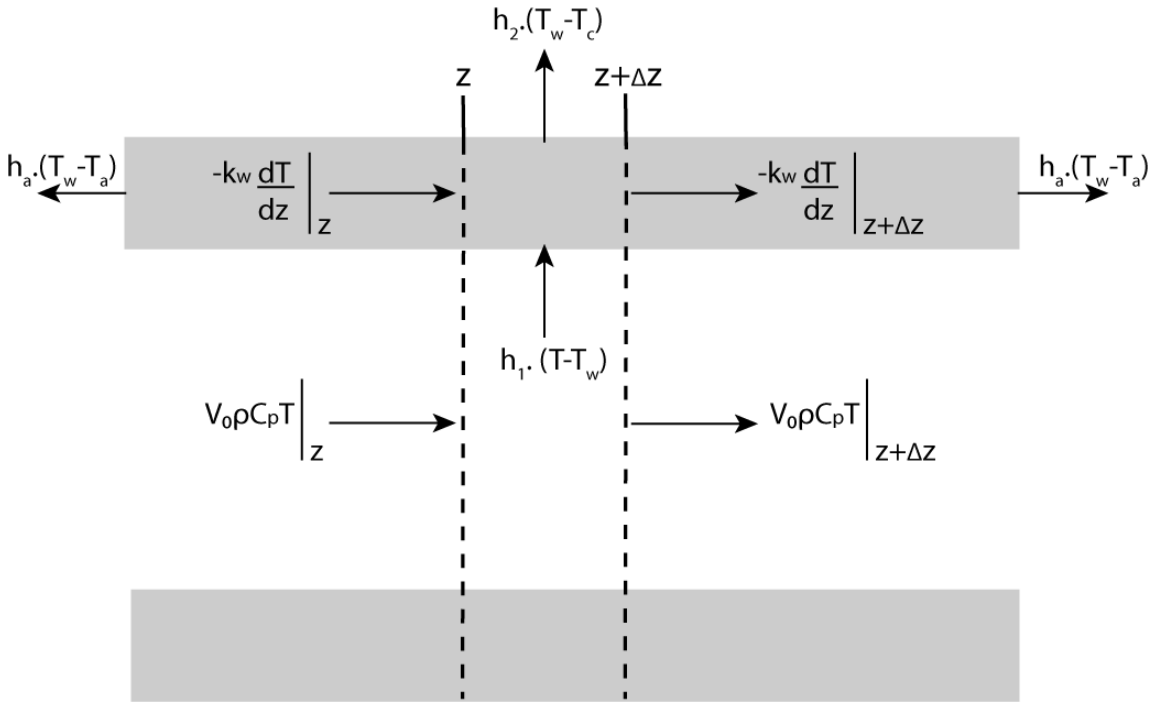

Figure 3.1 Schematic of 1-D model of a heat-exchanger microreactor, in which a pseudo-homogeneous exothermic, first-order reaction exchanges heat via dividing wall with parallel, isothermal coolant fluid (Reprinted with permission from[39]).

3.3. Parameter estimation

In the present work, the objective is to theoretically investigate the impact of solid-phase axial heat conduction and heat-losses to surroundings upon criticality/ runaway in a microchannel reactor under conditions conducive to runaway. Thus, appropriate values of Da, γ, B, previously used for similar analysis of criticality in non-isothermal tubular reactors [117], are selected to ensure the possibility of runaway. For simplicity and clarity of the present analysis, identical heat transfer resistance to end-losses via conduction to packaging/plumbing at either end of the microreactor are assumed (i.e., $Bi_o = Bi_1$). Additionally, both coolant and manifold temperatures are assumed equal to the inlet

temperature, i.e. $\theta_c = \theta_a = 0$, following the approach used for tubular reactors[117]. These assumptions enable analysis to focus solely upon the parameter space relevant to solid-phase conduction contributions to criticality/runaway, $[St, Bi, CP, \xi]$. A span of CP [0-1000] is selected based on previous analysis of typical microchannel dimensions and materials properties reported by Moreno et al., [37] while Bi is selected to range from the case of a perfectly insulated wall at both inlet/outlet (Bi=0) to the case of externally fixed isothermal wall conditions at both inlet/ outlet temperature (Bi=∞). Lastly, the ratio of coolant-to-reacting fluid heat transfer capacity (ξ) is assumed to be unity except in Subsection 3.8.5. The resulting reduced parameter space employed in this work is presented in Table 3.1.

Table 3.1 Reactor parameters (Reprinted with permission from [39]).

Parameters	Value
Da	0.1
B	40 (ϵ [10,100] in Subsection 3.8.4)
γ	20
Bi (= Bi_o = Bi_1)	0-∞
CP (= CP_1 = CP_2)	0-1000
ξ	1(ϵ [1,5] in Subsection 3.8.5)
θ_a	0
θ_a	0

3.4. Reduced model formulations for explicit criteria

Prior to analysis of the complete model, the two asymptotic limits of (i) negligible and ii) near-infinite solid-phase axial heat conduction are considered. The former case corresponds to the classical analysis of a non-isothermal tubular reactor wherein solid-phase axial heat conduction is neglected[117] The latter case corresponds to a spatially isothermal solid phase, in effect also reducing the model form to that of a non-isothermal tubular reactor[117].

3.4.1. Case I: low CP approximation – negligible solid-phase axial conduction

When contribution of solid-phase axial heat conduction relative to fluid phase heat transport is negligible (i.e CP<<1), equations 3.1-3.5 may be reduced to the form of a non-isothermal tubular reactor as $\frac{St}{CP}$ >>1, assuming $\frac{d^2\theta_w}{ds^2}$ in equation 3.3 is always unity order. This reduces the model to a pair of first order differential equations describing only the reacting fluid.

$$\frac{du}{ds} = -Da\, e^{\left[\frac{\theta}{1+\frac{\theta}{\gamma}}\right]} u \tag{3.5}$$

$$\frac{d\theta}{ds} = B\, Da\, e^{\left[\frac{\theta}{1+\frac{\theta}{\gamma}}\right]} u - \frac{\xi}{1+\xi} St(\theta - \theta_c) \tag{3.6}$$

The resulting effective Stanton number ($\frac{\xi}{1+\xi}$St) accounts for both reactant channel-to-solid wall and coolant channel–to-solid wall heat transfer resistances. For the case of ξ =1 (i.e., $h_1 \hat{a}_{f_1 s} \epsilon_{f_1 w} = h_2 \hat{a}_{f_2 s} \epsilon_{f_2 w}$) which is appropriate for equivalent reacting fluid and cooling fluid channel dimensions and heat transfer coefficients, the effective Stanton number in equation 3.7 reduces to $\frac{St}{2}$.

3.4.2. Case II: high CP approximation – isothermal solid-phase

For sufficiently high values of CP, $\frac{St}{CP}$ can be neglected, in turn reducing equation 3.3 to equating the second derivative of the wall temperature to null. Substitution of a constant first order wall temperature derivative into boundary conditions (equation 3.5)

equates wall temperature to the ambient temperature, such that equations 3.1 and 3.2 yield a pair of fluid-phase expressions of identical shape as those obtained for the low-CP case above,

$$\frac{du}{ds} = -k_0 . e^{\left[\frac{\theta}{1+\frac{\theta}{\gamma}}\right]} u \tag{3.7}$$

$$\frac{d\theta}{ds} = B . Da . e^{\left[\frac{\theta}{1+\frac{\theta}{\gamma}}\right]} . u - St . (\theta - \theta_a) \tag{3.8}$$

with one exception being that the effective Stanton Number in equation 3.7 is replaced with the unscaled Stanton Number in equation 3.9. Thus, comparison of equation 3.7 and equation 3.9 indicates that, for the case of $\xi = 1$, the critical Stanton number for the High CP approximation is twice that of the Low CP approximation; this in turn implies that solid phase axial heat conduction can reduce criticality by up to 50% (assuming $\xi \geq 1$). Additionally, the coolant temperature, θ_c, is replaced with the manifold temperature θ_a, indicating that conductive heat losses to adjacent manifolding is the dominant mode of heat transfer from the reactor. This in turn suggests that there are regions in the parameter space where the reactor is stable irrespective of the magnitude of heat transferred to the coolant. This will be discussed in Subsection 3.8.5.

3.5. Application of Van Welsenare and Froment (VWF) explicit criterion for runaway

These reduced models allow the formulation of fast explicit criteria for runaway which, while neglecting any contribution of the solid phase to runaway, provide both an

initial guess of St_c for subsequent sensitivity calculations and the necessary reference point for comparison with parametric sensitivity analysis of the complete model. In the present study, in which reaction order is restricted to unity, the criterion originally developed by Van Welsenare and Froment[116] is applied to the reduced models as follows. Dividing either equation 3.7 or 3.8 by equation 3.6 yields a single ordinary differential equation describing the reactor trajectory along the temperature-conversion plane,

$$\frac{1}{B}\frac{d\theta}{du} = 1 - \frac{St_{eff}\,(\theta - \theta_c)}{B\ Da\ u} e^{\left[\frac{-\theta}{1+\frac{\theta}{\gamma}}\right]} \tag{3.9}$$

where St_{eff} is the effective Stanton Number for either High-CP or Low-CP approximation. This equation yields the temperature maximum (θ^*) along a trajectory specific to a given set of parameter values.

$$u^* = \frac{St_{eff.}\,(\theta^* - \theta_c)}{B.\,Da} e^{\left[\frac{-\theta}{1+\frac{\theta}{\gamma}}\right]} \tag{3.10}$$

The critical trajectory is defined as the one which passes through the maximum of this temperature maxima curve equation 3.10. Hence, differentiating equation 3.10 with respect to θ^* and equating the result to null yields an expression for the critical temperature,

$$\theta^*_{max} = \frac{\gamma}{2}.\left[(\gamma - 2) - \sqrt{\gamma(y-4) - 4\theta_c}\right] \tag{3.11}$$

From this critical temperature, an extrapolation procedure is used to obtain an explicit expression relating the parameters (St_{eff}, B, Da,γ, θ_c) at onset of criticality:

$$\frac{\mathrm{B.\,Da}}{\mathrm{St_{eff}}} = \left(1 + \frac{1}{\mathrm{Q}} + \frac{1}{\mathrm{Q}^2}\right)(\theta^*_{\max} - \theta_c).\, e^{\left[\frac{-\theta^*_{\max}}{1+\frac{\theta^*_{\max}}{\gamma}}\right]} \tag{3.12}$$

where

$$\mathrm{Q} = \frac{\sqrt{1 + 4\left[\frac{\mathrm{B}}{\theta^*_{\max} - \theta_c} - 1\right]} - 1}{2} \tag{3.13}$$

3.6. Parametric sensitivity analysis and application of Morbidelli & Varma (MV) criterion

Parametric sensitivity analysis of the complete reactor model [3.1-3.5] is employed to numerically obtain the steady-state sensitivity profiles of the three state variables $[\mathrm{u(s)}, \theta(\mathrm{s}), \theta_w(\mathrm{s})]$ with respect to the parameter set $[\mathrm{Da}, \mathrm{B}, \gamma, \mathrm{St}, \mathrm{Bi}, \mathrm{CP}, \xi]$, alongside the steady-state solution. Resulting profiles enable application of the Morbidelli and Varma (MV) criterion to obtain the critical parameter values corresponding to runaway

3.6.1. Derivation of the sensitivity equations

Sensitivity equations are derived from equations 3.1-3.5 recognizing that all three are of the general form,

$$\frac{\mathrm{dY}}{\mathrm{ds}} = \mathrm{f(Y, \varphi, s)} \tag{3.14}$$

with boundary conditions,

$$\mathrm{C_1.\, y(0) = d_1, C_2 y(L) = d_2} \tag{3.15}$$

where $\mathrm{Y} = [\mathrm{u(s)}, \theta(\mathrm{s}), \theta_w(\mathrm{s}), \theta'_w]$ are the four state variables, and $\varphi = [\mathrm{Da}, \mathrm{B}, \gamma, \mathrm{St}, \mathrm{Bi}, \mathrm{CP}, \xi]$ are the parameters. $\mathrm{C_1}$ and $\mathrm{C_2}$ are 3×4 and 1×4 matrices,

respectively, while d_1 and d_2 are a 3×1 vector and scalar, respectively. The local sensitivity of the state variables, Y, with respect to parameter φ_j is thus defined as,

$$S(Y;\varphi_j) = \frac{\partial Y}{\partial \varphi_j} \tag{3.16}$$

The local sensitivity profiles are obtained using the direct differential method[117], in which both sides of the model equations are differentiated by the parameter of interest, φ_j. Thus, differentiating equation 3.14 with respect to φ_j yields the general form of the sensitivity equation,

$$\frac{dS(y;\varphi_j)}{ds} = \frac{\partial f(Y(\varphi_i))}{\partial \varphi_j} = \frac{\partial f}{\partial \varphi_j} + \frac{\partial f}{\partial Y}\, S(Y;\varphi_j) \tag{3.17}$$

with boundary conditions:

$$\frac{dC_1}{d\varphi_j}\, y(0) + S(y(0);\varphi_j) = 0, \frac{dC_2}{d\varphi_j}\, y(L) + S(y(0);\varphi_j) = 0 \tag{3.18}$$

Applying equations 3.17 and 3.18 to equations 3.1 to 3.5 yields the sensitivity equations specific to the complete microreactor model:

$$\frac{dS(u;\varphi_j)}{ds} = \begin{Bmatrix} -\frac{dDa}{d\varphi_j} \exp\left[\frac{\theta}{1+\frac{\theta}{\gamma}}\right] u - Da\, \frac{d\gamma}{d\varphi_j} \exp\left[\frac{\theta}{1+\frac{\theta}{\gamma}}\right] \frac{\theta}{\left[1+\frac{\theta}{\gamma}\right]^2}\, u\, \frac{\theta}{\gamma^2} \ldots \\ -Da \exp\left[\frac{\theta}{1+\frac{\theta}{\gamma}}\right] \frac{u}{\left[1+\frac{\theta}{\gamma}\right]^2}\, S(\theta;\varphi_j) - Da \exp\left[\frac{\theta}{1+\frac{\theta}{\gamma}}\right] S(u;\varphi_j) \end{Bmatrix} \tag{3.19}$$

$$\frac{dS(\theta;\varphi_j)}{ds} = \left\{ \begin{array}{l} \exp\left[\frac{\theta}{1+\frac{\theta}{\gamma}}\right]\left(\frac{d(B.Da)}{d\varphi_j}\ u + B\ Da\ \frac{dSt}{d\varphi_j}\ \frac{\theta}{\left[1+\frac{\theta}{\gamma}\right]^2}\ \frac{\theta}{\gamma^2}\right) \\ +B\ Da\exp\left[\frac{\theta}{1+\frac{\theta}{\gamma}}\right]\left(\frac{u}{\left[1+\frac{\theta}{\gamma}\right]^2}\ S(\theta;\varphi_j) + \ S(u;\varphi_j)\right) \\ -\frac{dSt}{d\varphi_j}\ [\theta-\theta_w] - St\left[S(\theta;\varphi_j) - S(\theta_w;\varphi_j)\right] \end{array} \right\} \quad (3.20)$$

$$\frac{\partial^2 S(\theta_w;\varphi_j)}{ds^2} = \left\{ \begin{array}{l} -\frac{d(\frac{St}{CP})}{d\varphi_j}\ [\theta-\theta_w] - \frac{d(\xi\frac{St}{CP})}{d\varphi_j}\ [\theta_c-\theta_w] \ldots \\ -\frac{St}{CP}\ \left[S(\theta;\varphi_j) - S(\theta_w;\varphi_j)\right]\ - \xi\frac{St}{CP}\ [0 - S(\theta_w;\varphi_j)] \end{array} \right\} \quad (3.21)$$

with inlet conditions for concentration and temperature,

$$S(u;\varphi_j) = 0 \text{ at } s = 0, S(\theta;\varphi_j) = 0 \text{ at } s = 0 \quad (3.22)$$

and boundary conditions for the solid-phase (wall),

$$\begin{aligned} -\frac{dS(\theta_w(0);\varphi_j)}{ds} &= -Bi\ S(\theta_w(0);\varphi_j) + \frac{d(Bi)}{d\varphi_j}(\theta_a - \theta_w(0)) \\ -\frac{dS(\theta_w(1);\varphi_j)}{ds} &= Bi\ S(\theta_w(1);\varphi_j) + \frac{d(Bi)}{d\varphi_j}(\theta_w(1) - \theta_a) \end{aligned} \quad (3.23)$$

Finally, the normalized sensitivity can be defined as,

$$S^N(Y;\varphi_j) = \frac{\varphi_j}{y}.\frac{\partial y}{\partial \varphi_j} = \frac{\partial \ln(y)}{\partial \ln(x)} = \frac{\varphi_j}{y}.s(y;\varphi_j) \quad (3.24)$$

3.7. Numerical simulation

Steady-state solutions to the reduced models developed in Subsection 3.4 (equations 3.6 and 3.7 and equations 3.6 and 3.8 were obtained in MATLAB using the ode15s pre-packaged Runge-Kutta numerical solver for stiff equations [122]. However,

obtaining the steady state solution in MATLAB to the complete model developed in Subsection 3.3. (equations 3.1-3.5)) and corresponding steady-state sensitivity expressions developed in Subsection 3.6. (equations 3.19-3.23) via boundary-value problem solver (bvp4c) proved to be problematic and very sensitive to the initial guess, owing to onset of singularities under runaway conditions. For this reason, a time relaxation approach is followed[56] where equations 3.1-3.5 and equations 3.19-3.23 were re-cast in unsteady-state form and spatially discretized across 200 evenly spaced nodes. The discretized expressions are given in the appendix.

The resulting 6×200 system of ordinary differential equations were solved numerically in MATLAB using the prepackaged ode15s algorithm over sufficient time span as to achieve steady-state. In all simulations, results were considered steady-state upon satisfying the criteria ($\left|\frac{\partial Y}{\partial \tau}\right| \leq 10^{-6}$) for all state variables. All simulations were carried out on a Lenovo Yoga710-141SK Signature edition at 2.4 GHz and equipped with 8GB of RAM. Typical solution times ranged 10s to 500s.

3.8. Results and discussions

3.8.1. Analysis of reduced models and comparison with complete model

Results obtained using the complete (Subsection 3.2) and reduced models (Subsection 3.4) were compared to investigate the accuracy of the latter for predicting (i) criticality conditions via explicit criteria of Van Welsenaure and Froment (VWF), and (ii) magnitude and location of resulting hot-spot after criticality is reached. For the case of the low-CP model (Subsection 3.4.1), application of the VWF criterion yields a critical value of $\mathrm{St_c}$ = 16.93 for the nominal parameter values listed in Table 3.1. A comparison of the

steady-state solutions to equations 3.6-3.7 and equations 3.1-3.5 under sub-critical conditions (St = 20), presented in Figure 3.2a, likewise confirms the accuracy of the low-CP reduced model in predicting sub-critical reaction and temperature profiles. However, under runaway conditions (St = 10) the low-CP reduced model fails to accurately predict the location or magnitude of the resulting hot-spot (Figure 3.2b) unless CP is unrealistically low ($< 10^{-6}$), as $\frac{d^2\theta_w}{ds^2}$ ceases to be O(1) and hence cannot be neglected relative to $\frac{St}{CP}$.

For the case of the high-CP reduced model, application of the VWF explicit criterion for runaway, assuming $\xi = 1$, yields a value of $St_c = 8.47$ (half the value obtained from low-CP model) as expected from a comparison of equations 3.7 and 3.8. Under these conditions, the solid-phase (wall) temperature is assumed to be uniform and equal to the ambient/inlet temperature; for the case of $\theta_a = \theta_o = 0$, this means the reacting fluid is effectively exchanging heat with an infinite heat-sink fixed to the manifold temperature such that coolant fluid has no impact upon criticality. A comparison of steady-state profiles obtained via complete model for CP = 1000, Bi = 1, $\xi = 1$ alongside the reduced high-CP model at sub-critical (St = 10) and runaway (St = 5) conditions is presented in Figure 3.2c,d. As was the case for the low-CP reduced model, excellent agreement under sub-critical conditions is obtained; additionally, good agreement under runaway conditions is observed as well, as derivation of the high-CP model did not require assumption of an O(1) derivative term.

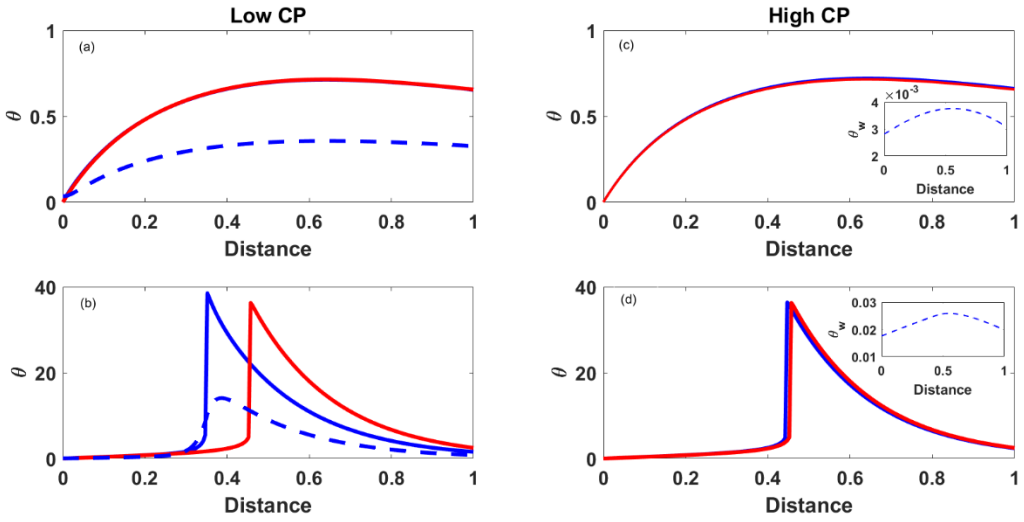

Figure 3.2 Comparison between full (blue) and approximate models (red). Parameters- B=40,γ=20,Da=0.1Bi=1. (a) No runaway, St=20, CP=0.01 (b) Runaway, St=10, CP=0.01, (c) No runaway, St=10, CP=1000 (inset- θ_w-Full model),(d) Runaway, St=20, CP=1000 (inset- θ_w) (Reprinted with permission from [39]).

3.8.2. Parametric sensitivity analysis and Morbidelli & Varma (MV) criteria

Normalized sensitivities of the reacting fluid maximum temperature ($S^N(\theta^*, \varphi)$) with respect to each parameter were analyzed at each set of parameter values over a range of St. Figure 3a presents the normalized sensitivity curves obtained for the specific case of B = 40, CP = 30, Bi = 1, Da = 0.1, γ = 20, $\xi = 1$. It is seen that there exists a single value for St = 9.23 where an extremum in all sensitivity functions occur. This point is identified as the critical Stanton number (St_c), following the Morbidelli and Varma (MV) criteria [117, 120-121]. The criticality of this point is confirmed by Figure 3.3b-c, which presents steady-state reacting-fluid temperature profiles obtained at values for St greater than and equal to (Figure 3.3b), and lesser than, this critical value of 9.23 (Figure 3.3c). This methodology for determining St_c for a given set of parameter values (B, Da, γ, CP, Bi, ξ)

was employed throughout the remainder of the present work; in all cases studied, there existed a single value of St_c which corresponded to an extrema in all sensitivity functions, $S^N(\theta^*, \varphi)$

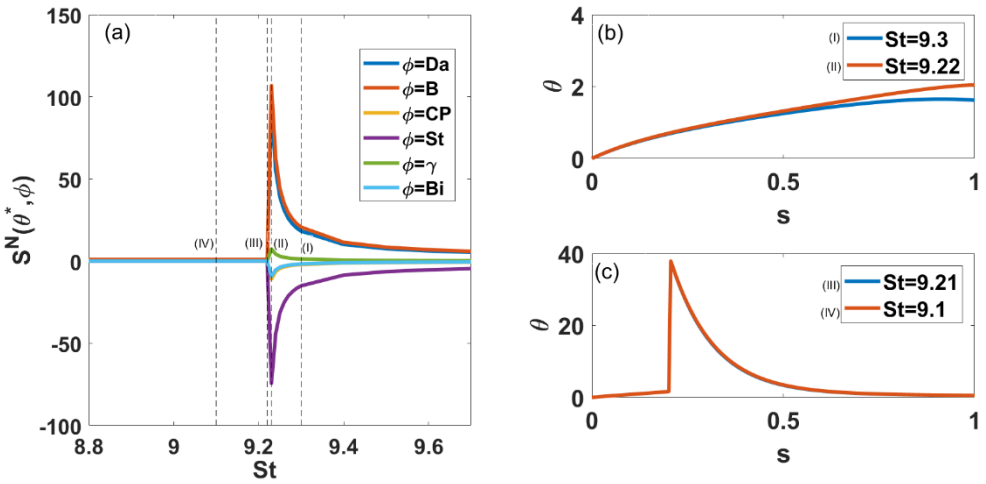

Figure 3.3 (a) Parametric sensitivity of reacting fluid temperature; Normalized sensitivity at maximum temperature vs Stanton number for B=40, CP=30, Bi=1, Da=0.1,γ=20, ξ=1. Critical Stanton number=9.23. (b) fluid phase temperature profiles St≥ St_c (c) fluid phase (Reprinted with permission from [39]).

3.8.3. Comparison of VWF explicit criteria with VM criteria

Values of St_c obtained via the MV criteria were compared with those obtained via the explicit VWF criteria for the two cases of high (CP = 1000) and low (0.01) values of the conduction parameter, over a range of values for the adiabatic dimensionless temperature rise (B) while assuming $\xi = 1$ (Figure 3.4). For each case, MV criteria was evaluated for both perfectly insulated (Bi = 0) and isothermal (Bi =∞) inlet/outlet wall

conditions. For clarity of presentation, results are presented in terms of the normalized critical Stanton number [117].

For the low-CP case, the VWF criterion is conservative compared to the MV criterion for low B, but there is good agreement as B increases for Bi=0 (Figure 3.4a), Bi=1 (Figure 3.4b) and Bi=∞ (Figure 3.4c). This is also observed for the high-CP case when Bi=1 and Bi =∞; however, when Bi=0, the high CP-VWF criterion under predicts the criticality of the complete model. This is because when applying VWF criterion to the High CP reduced model, it is assumed that heat losses to the ambient is dominant and the wall is uniformly equal to θ_a but when Bi=0, the solid-phase is insulated from the ambient and hence there is no heat removal via conduction losses at inlet and outlet wall boundaries. Thus, the low-CP case of the VWF criteria provides a reliable, albeit conservative, criteria for ensuring hot-spot prevention regardless of microreactor design or materials selection.

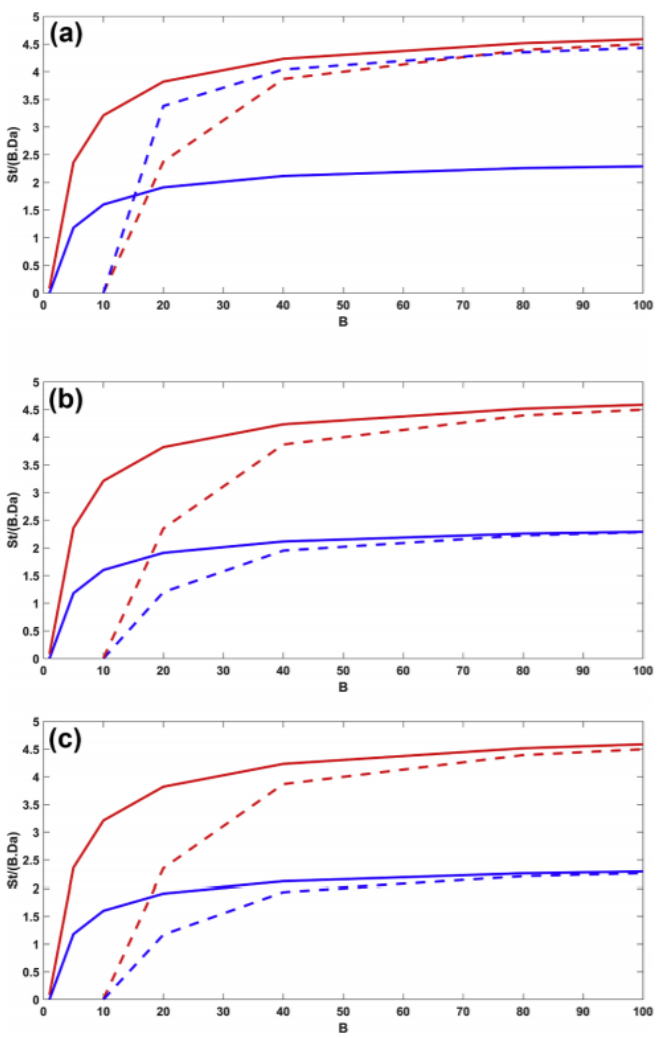

Figure 3.4 Comparison of St_c vs B obtained for Van Welsenare and Froment explicit criterion applied to reduced models (solid) and Morbidelli and Varma (dashed) at Da=0.1, γ=20, CP=0.01 (red). CP=1000 (blue) (a) adiabatic wall conditions Bi=0 (b) Finite heat transfer limited boundary conditions (Bi=1) (c) isothermal wall boundary conditions (Bi=∞) (Reprinted with permission from [39]).

3.8.4. Influence of solid-phase heat conduction and end-losses upon runaway via MV criteria for symmetric channels (ξ=1)

The influence of solid-phase heat conduction and end-losses upon St_c is shown in Figure 3.5 for the case of B = 40, Da = 0.1, γ = 20 and $\xi = 1$. In the absence of any conductive heat losses to packaging (Bi=0), increasing CP raises St_c from a value of 15.46 (at CP = 10^{-8}) to the asymptotic limit of 16.16 (at CP > 10^2). This arises owing to greater recirculation of heat within the reactor in the absence of any heat losses, which facilitates runaway. It should be noted that this upper limit in St_c is still less than the value for St_c obtained from the conservative VWF criteria applied to the case of low-CP (St_c = 16.93). Conversely, for the case of isothermal wall boundaries (Bi=∞), any increase in CP reduces St_c towards an asymptotic limit of 7.73 at CP > 10^2. This asymptotic limit of St_c = 7.73 is exactly half of the critical Stanton number at CP = 10^{-8}, consistent with the reduced model analysis in Subsection 3.4. As was the case for the reduced model at high-CP, the asymptotic limit obtained via MV criteria at high CP and Bi values corresponds to a near-isothermal wall fixed to the manifold temperature, which is in turn equal to the coolant temperature, thus maximizing heat removal. Thus, for any value of CP, Bi at B=40, Da=0.1, γ=20 runaway is assured if St < 7.73 regardless of ξ.

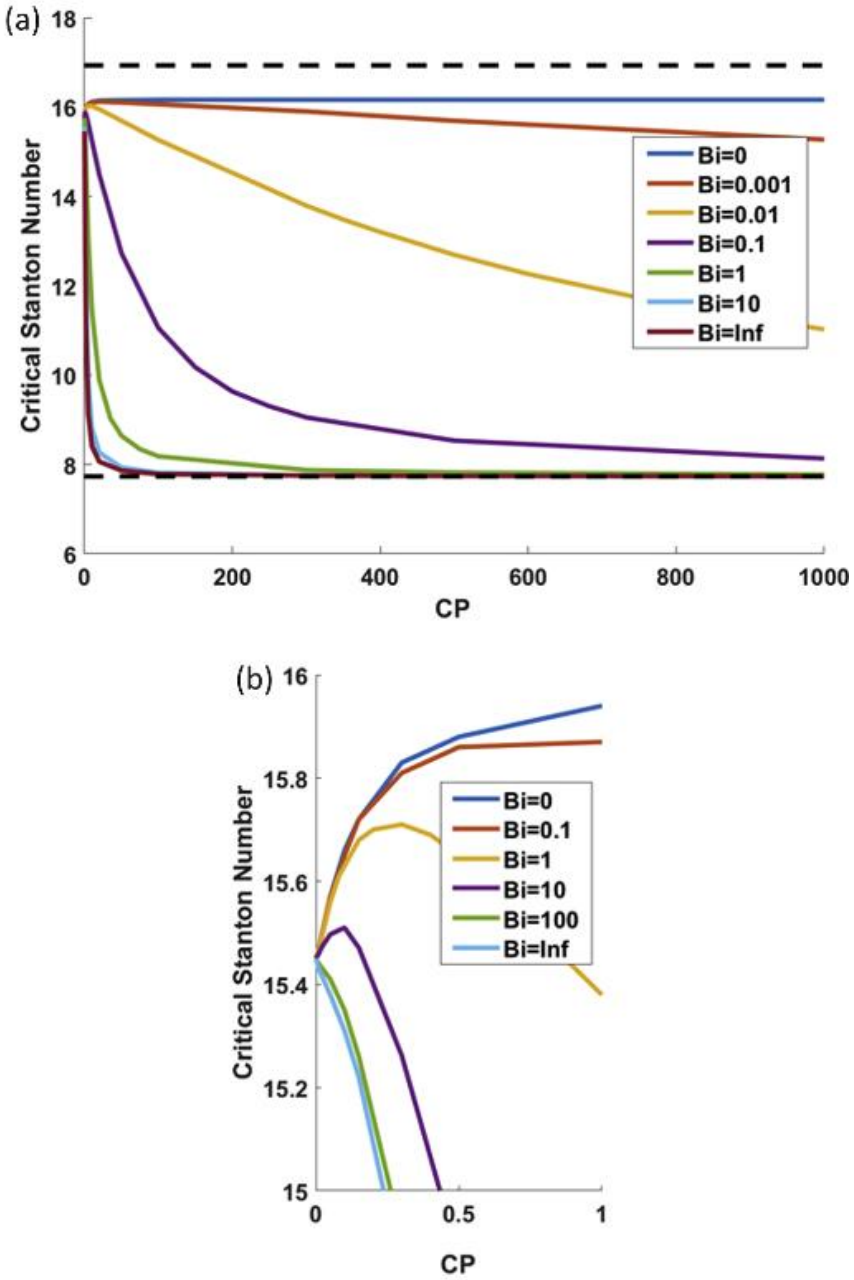

Figure 3.5 (a) Effect of conduction parameter and Biot number on critical Stanton number. Dashed line-(bottom)- critical St high CP approximation, 7.73. Dashed line-(top) critical Stanton number from Van Welsenare and Froment's criterion,16.93. (b) Variation of critical Stanton number for low values of CP (Reprinted with permission from [39]).

In between these two extreme cases of adiabatic and isothermal boundary conditions, a complex behavior is observed wherein at low CP (Figure 3.5b), axial heat conduction raises criticality via enhanced internal heat distribution until stabilizing heat losses become significant; beyond this point a steady decrease in St_c towards the asymptotic limit of 7.73 is observed. This dual role of CP is also manifest in its effect upon the hotspot magnitude and location when runaway occurs. Hotspot temperatures vs CP and Hotspot Location vs CP for insulated (Bi=0), finite heat transfer limited (Bi=1,10), and isothermal wall (Bi=∞) boundary conditions are plotted in Figure 3.6 and Figure 3.7 respectively for a constant value of St=7.72 to ensure runaway in all cases. An initial increase in CP from ∼0 results in a rapid increase and rapid decrease in the hotspot magnitude and location respectively as internal heat circulation enables pre-heating of reacting fluid immediately upstream of the hot-spot [37]. Further increases in CP serve to dissipate the hot-spot across the entire reactor length by bringing heat losses to play, reducing the magnitude of hot-spot and increasing the hot spot position; for the case of an adiabatically packaged reactor (Bi = 0), magnitude (location) of reactor hot-spot remains greater (lesser) than the value obtained when solid-phase is neglected (i.e., CP = 0) due to efficient heat distribution in the absence of heat losses. For the case of finite heat losses to packaging (Bi > 0), axial conduction of heat within the solid-phase serves not only as a means of pre-heating the reacting fluid upstream of the hot-spot but also enables heat dissipation due to heat losses to packaging. Thus, an initial rise (fall) in hot-spot temperature(location) with increasing CP is observed when CP is low, followed by a

steady decrease in hot-spot magnitude as CP increases beyond O(10^{-2}) as heat losses become significant.

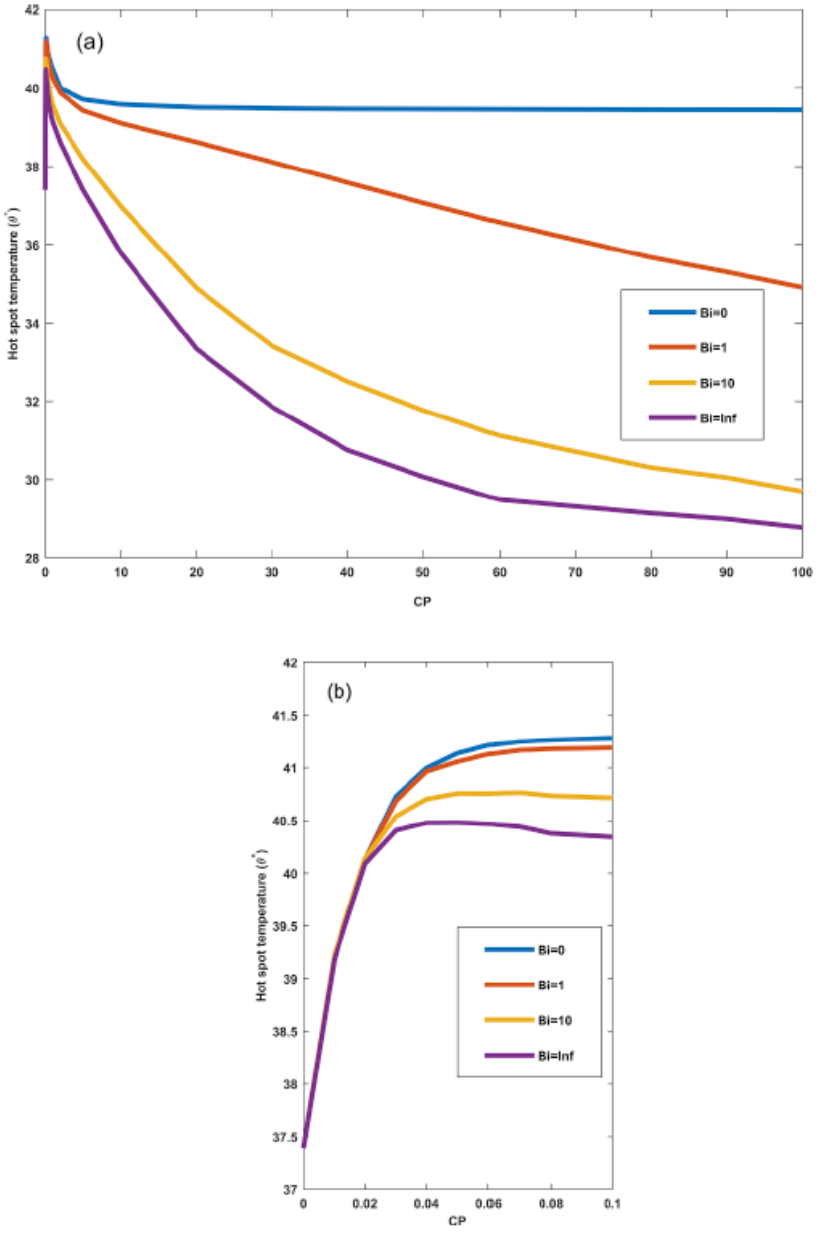

Figure 3.6 (a) Hotspot temperature vs conduction parameter, (b) Hotspot temperature vs conduction parameter for low CP. For B=40,γ=20,Da=0.1, St=7.72 (Reprinted with permission from [39]).

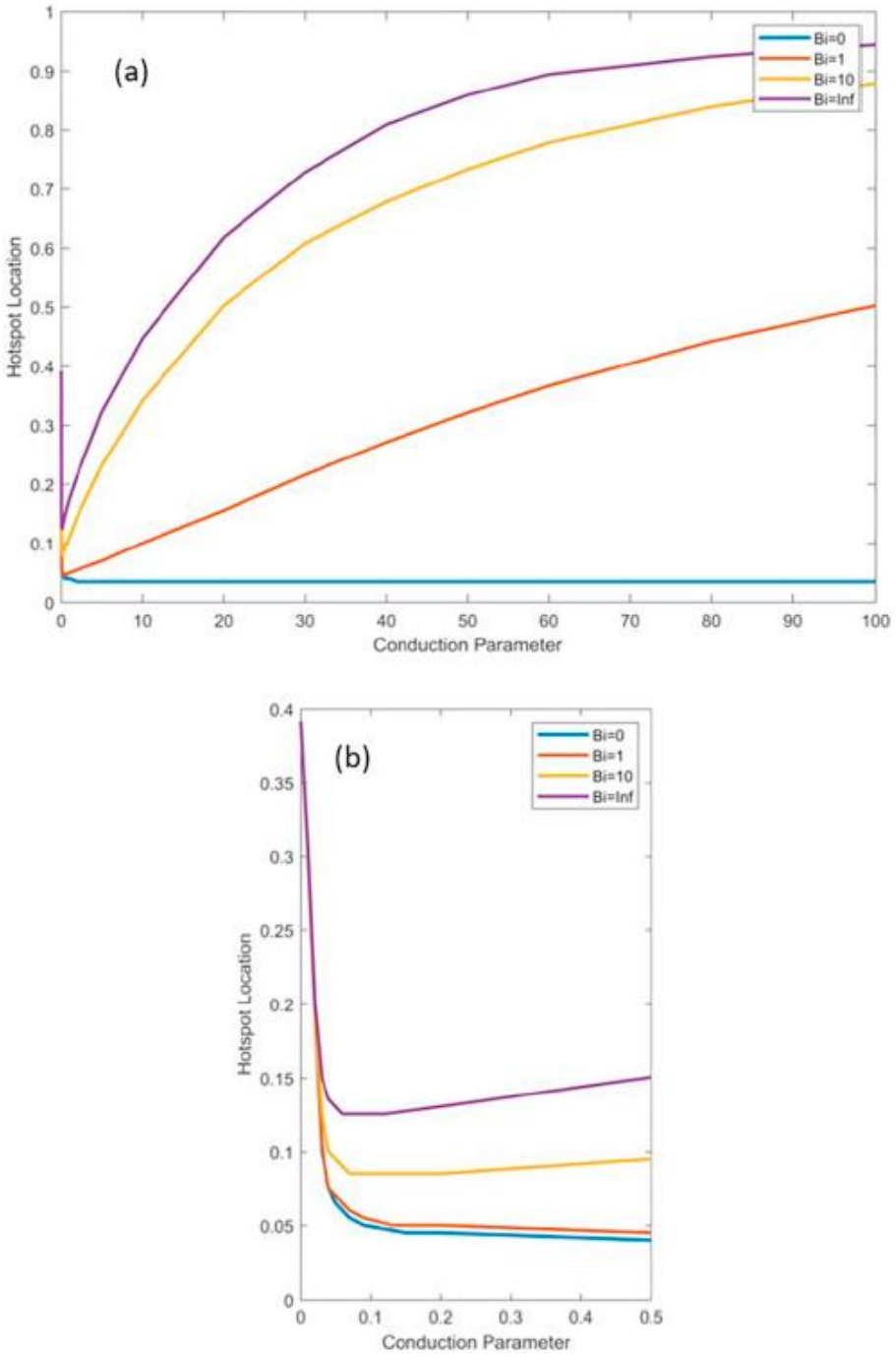

Figure 3.7 (a) Hotspot location vs conduction parameter, (b) Hotspot location vs conduction parameter for low CP. For B=40,γ=20,Da=0.1, St=7.72 (Reprinted with permission from [39]).

3.8.5. Influence of solid-phase heat conduction and end-losses upon runaway via VM criteria for asymmetric channels (ξ>1)

Lastly, the reactant channel-to-wall heat transfer capacity (St) was fixed and the coolant channel-to-wall heat capacity (ξ) varied to identify the critical value, ξ_c, over the range of CP and Bi values employed in Subsection 3.3. A value of St=10 was selected such that for a given pair of CP and Bi there exists a critical value ξ_c, above which cooling channel capacity is sufficiently high to prevent runaway. The results are plotted in Figure 3.8. As observed in Subsection 3.8.4, a slight increase in CP from 0 results in an increase in ξ_c as mild heat dispersion facilitates hot-spot formation. Further increases in CP result in a decrease in ξ_c for Bi $\neq$ 0 as stabilizing heat losses at the reactor inlet/outlet become significant. For any value of Bi $\neq$ 0, it is seen that there exists a value of CP beyond which coolant channels are not required to prevent hot-spot formation (i.e., $\xi_c = 0$). For Bi=0, an increase in CP results in an increase in ξ_c, owing to heat recirculation via solid phase axial heat conduction facilitating runaway in the absence of heat losses

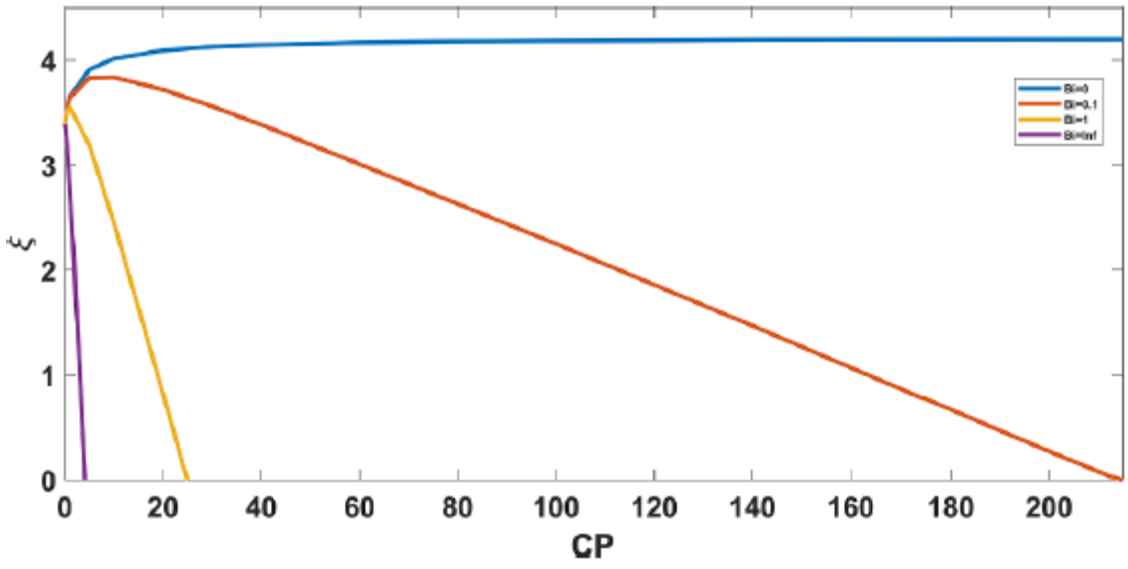

Figure 3.8 Ratio of critical coolant-to-reacting fluid heat transfer capacity to wall ($\boldsymbol{\xi_c}$) vs conduction parameter (CP). B=40,γ=20,Da=0.1, St=10 (Reprinted with permission from [39]).

3.9. Unsteady state sensitivity equations

The discretized unsteady state equations are given below;

$$\frac{du_i}{d\tau} = -\frac{[u_{i+1} - u_i]}{\Delta s} - Da \exp\left[\frac{\theta_i}{1+\frac{\theta_i}{\gamma}}\right].u_i \qquad (3.25)$$

$$\frac{d\theta_i}{d\tau} = -\frac{[\theta_{i+1} - \theta_i]}{\Delta s} + B\ Da.\ e^{\left[\frac{\theta_i}{1+\frac{\theta_i}{\gamma}}\right]} u_i - St\left(\theta_i - \theta_{w,i}\right) \qquad (3.26)$$

$$\frac{d\theta_{w,i}}{d\tau} = F_o\ \frac{\left[\theta_{w,i+1} - 2\theta_{w,i} + \theta_{w,i-1}\right]}{\Delta s^2} + F_o\ \left[\frac{St}{CP}(\theta_i - \theta_{wi}) + \xi\frac{St}{CP}\left(\theta_c - \theta_{w,i}\right)\right] \qquad (3.27)$$

$$\frac{dS(u_i;\varphi_j)}{d\tau}+\frac{S(u_{i+i};\varphi_j)-S(u_i;\varphi_j)}{\Delta s}=\begin{Bmatrix} -\frac{dDa}{d\varphi_j}\, e^{\left[\frac{\theta_i}{1+\frac{\theta_i}{\gamma}}\right]} u_i \\ -Da\ \frac{d\gamma}{d\varphi_j}\, e^{\left[\frac{\theta_i}{1+\frac{\theta_i}{\gamma}}\right]} \frac{\theta_i}{\left[1+\frac{\theta_i}{\gamma}\right]^2}\ u_i\ \frac{\theta_i}{\gamma^2} \\ -Da.\, e^{\left[\frac{\theta_i}{1+\frac{\theta_i}{\gamma}}\right]} \frac{u_i}{\left[1+\frac{\theta_i}{\gamma}\right]^2}\ S(\theta_i;\varphi_j) \\ -Da\, e^{\left[\frac{\theta_i}{1+\frac{\theta_i}{\gamma}}\right]} S(u_i;\varphi_j) \end{Bmatrix} \quad (3.28)$$

$$\frac{\partial S(\theta_i;\varphi_j)}{\partial \tau}+\frac{S(\theta_{i+i};\varphi_j)-S(\theta_i;\varphi_j)}{\Delta s}=$$

$$\begin{Bmatrix} \frac{d(B.Da)}{d\varphi_j} e^{\left[\frac{\theta_i}{1+\frac{\theta_i}{\gamma}}\right]}.u_i \\ +B\ Da\ \frac{d\gamma}{d\varphi_j} e^{\left[\frac{\theta_i}{1+\frac{\theta_i}{\gamma}}\right]} \frac{\theta_i}{\left[1+\frac{\theta_i}{\gamma}\right]^2}\ \frac{\theta_i}{\gamma^2} \\ +B\ Da\ e^{\left[\frac{\theta_i}{1+\frac{\theta_i}{\gamma}}\right]} \frac{u_i}{\left[1+\frac{\theta_i}{\gamma}\right]^2}\ S(\theta_i;\varphi_j) \\ +B\ Da\ e^{\left[\frac{\theta_i}{1+\frac{\theta_i}{\gamma}}\right]} S(u_i;\varphi_j) \\ -\frac{dSt}{d\varphi_j}\ [\theta_i-\theta_w]-St\left[S(\theta_i;\varphi_j)-S(\theta_{w,i};\varphi_j)\right] \end{Bmatrix} \quad (3.29)$$

$$\frac{dS(\theta_i;\varphi_j)}{d\tau}+\frac{S(\theta_{w,i+i};\varphi_j)-2S(\theta_{w,i};\varphi_j)+S(\theta_{w,i-1};\varphi_j)}{\Delta s}$$
$$=\begin{Bmatrix} -\frac{\partial(\frac{St}{CP})}{\partial\varphi_j}\,[\theta-\theta_w] \\ -\frac{\partial(\xi\frac{St}{CP})}{\partial\varphi_j}\,[\theta_c-\theta_w] \\ -\frac{St}{CP}\,[S(\theta;\varphi_j)-S(\theta_w;\varphi_j)] \\ -\xi\frac{St}{CP}\,[0-S(\theta_w;\varphi_j)] \end{Bmatrix} \tag{3.30}$$

with discretized initial and boundary conditions for state variables and sensitivities as follows:

$$\begin{gathered} u_1=1 \\ \theta_1=0 \\ -\frac{[\theta_{w,2}-\theta_{w,1}]}{\Delta s}=Bi\,(\theta_a-\theta_{w,1}) \\ -\frac{[\theta_{w,200}-\theta_{w,199}]}{\Delta s}=Bi\,(\theta_{w,200}-\theta_a) \end{gathered} \tag{3.31}$$

$$\begin{gathered} S(u_1;\varphi_j)=0 \\ S(\theta_1;\varphi_j)=0 \\ -\frac{[S(\theta_{w,2};\varphi_j)-S(\theta_{w,1};\varphi_j)]}{\Delta s}=-Bi.\,S(\theta_{w,1};\varphi_j)+\frac{\partial(Bi)}{\partial\varphi_j}(\theta_a-\theta_{w,1}) \\ -\frac{[S(\theta_{w,200};\varphi_{j,})-S(\theta_{w,199};\varphi_{j,})]}{\Delta s}=Bi.\,S(\theta_{w,200};\varphi_j)+\frac{\partial(Bi)}{\partial\varphi_j}(\theta_{w,200}-\theta_a) \end{gathered} \tag{3.32}$$

Where, Fo=CP* δ , and $\delta=\frac{\rho_g Cp_g}{\rho_w Cp_w}$. δ is taken to be 10^{-4}. Which is the order of magnitude ratio of $\frac{\rho_g Cp_g}{\rho_w Cp_w}$. A cold start-up initial condition is assumed, i.e.

$$\begin{pmatrix} u_i = 1;\ \theta_i = 0; \theta_{w,i} = 0 \\ S(u_i; \varphi_j) = 0; S(\theta_i\ ; \varphi_j) = 0;\ S(\theta_w\ ; \varphi_j) = 0 \end{pmatrix} \quad \text{at } t = 0 \ \text{ for } i = 1,2,3, \dots, 200 \ (3.33)$$

3.10. Conclusions

The analysis in this section has yielded multiple insights into the role of solid-phase axial heat conduction upon hot-spot formation and prevention in microreactors. Application of the VWF criteria to a reduced model corresponding to the limiting case of negligible axial heat conduction and analogous to the traditional non-isothermal plug-flow reactor model provides a reliable, albeit conservative criteria for hot-spot prevention in microreactors which accounts for both reacting-fluid Stanton. Number and microreactor dimensions (specifically, reacting fluid diameter, cooling fluid diameter and dividing wall thickness) via . Conversely, application of MV criteria applied to the microreactor model, assuming sufficient heat conduction in the presence of finite axial heat losses, yields criteria for ensuring hot-spot formation regardless of microreactor dimensions. Analysis using MV criteria indicates that the introduction of mild solid-phase axial heat conduction promotes hot-spot formation so long as heat losses to manifolds is minimal. For the case of a perfectly insulated system (Bi = 0), further increasing solid-phase axial heat conduction parameter results in an asymptotic upper limit in Stc; for all other cases (Bi ≠ 0), Stc eventually reduces to a lower asymptotic limit with sufficient further increase in conduction parameter. For values of St between these two asymptotic limits, there exists a critical ratio of coolant- to reacting-fluid heat transfer capacity to prevent hot-spot formation at low- to intermediate values of CP. It is also shown that within this range of St there exists a critical value of CP for a given non-zero value of Bi, beyond which the

absence of hot-spot formation is ensured. These findings provide new design rules into microreactor design for achieving isothermal reactors for inherently safe operation of fast exothermic chemistries. Likewise, findings provide design rules for ensuring ignition in regenerative microcombustors and heat-exchanger microreactors.

4. INTEGRATING ENDOTHERMIC AND EXOTHERMIC REACTIONS- HEAT EXCHANGER REACTORS*

4.1. Introduction

Effective thermal coupling in heat exchanger reactors remains a significant design challenge. Two commonly encountered extremes in thermal behavior are (i) hotspot formation, occurring when heat generated by the exothermic channel is not consumed at the same rate by the endothermic channel, or (ii) reactor extinction, occurring when endothermic reaction heat duty exceeds that of the exothermic reaction rate. The most common method reported in literature for alleviating hotspot magnitude is to tailor the activity of the catalyst along the reactor length[43, 51, 54-58]. The most studied approach to-date involves introducing inert zones in exothermic and endothermic reaction zones to maximize conversion and while minimizing hotpots [44, 54, 56, 58]. Zanfir and Gavriilidis [57] considered continuously varying linear and parabolic catalyst distributions for the exothermic channel with constant endothermic activity observed considerable decrease in hotspot magnitude at a significant loss of conversion under counter current mode. Ramaswamy et al.,[54] investigated an exponentially decreasing catalyst activity profile($\alpha = 1 - e^{-k_1 \xi}$) for the exothermic channel and observed significant reduction in hotspot magnitude without reducing endothermic conversion under co-current operation.

* Parts of this section have been reprinted with permission from "Identification of Optimal Catalyst Distributions in Heat-Exchanger Reactors". Venkateswaran, S., Wilhite, B., & Kravaris, C. (2020). *Industrial & Engineering Chemistry Research, 59*(13), 5699-5711 Copyright 2020 American Chemical Society

However, for the counter current case, no significant effect of the exponential catalyst profiling was observed; instead an on/off (0-1) configuration for both exothermic and endothermic channels resulted in appreciable reduction in hotspot temperature with a slight decrease in endothermic conversion[54]. Thus, while both discretized and continuous catalyst activity profiles have been proposed and optimized for counter- current and co-current modes of heat exchanger reactor operation, a systematic framework to identify the best catalyst profile for a given set of reactor parameters, conditions and flow arrangement is still lacking. In this work, the challenge of optimizing both endothermic and exothermic catalyst activity profiles in a heat exchanger reactor is addressed using optimal control theory[114] by considering both catalyst distributions as inputs and defining an objective function that maximizes the sum of the conversion of both endothermic and exothermic reactions. The catalyst distributions appear linearly in the model equations and hence in the Hamiltonian formulated for the optimal control problem, implying that the problem is singular[114]. This in turn indicates that optimal profiles consist of both practically implementable discrete inert/active zones, and unimplementable continuously varying regions due to the singular arcs and/or constraint arcs in the optimal solution[114]. While such optimal profiles might not be realized exactly in practice, they provide a best-case profile for the reaction parameters and flow configuration considered. Piecewise constant approximations of the continuously varying portions consisting of a series of constant activity zones are investigated and compared with the aforementioned best-case scenario obtained from optimal control.

The organization of the section is as follows. The model is described in the next subsection and then the optimal control problem is defined and analyzed. Following this, the results are discussed for two sets of parameters for both co and counter current reactors. Then finally, piecewise approximations of the optimal profiles are obtained and compared with the true optimal profiles following which the work is concluded.

4.2. Theoretical

4.2.1. Model

A one-dimensional plug flow model with irreversible first order exothermic and endothermic reactions is considered following the previous analysis by R.C Ramaswamy et al[54]. A schematic illustrating the main transport phenomena in the model is shown in Figure 4.1. The following assumptions are made in the development of the model:

1) Heat and mass transfer resistances across the gas-catalyst film are assumed to be negligible.
2) Axial mass and heat dispersions in both fluid and solid phases is neglected.
3) Physical properties of fluids and the heat of reactions are assumed to be independent of the temperature, and
4) The pressure drop across the reactor is assumed to be negligible.

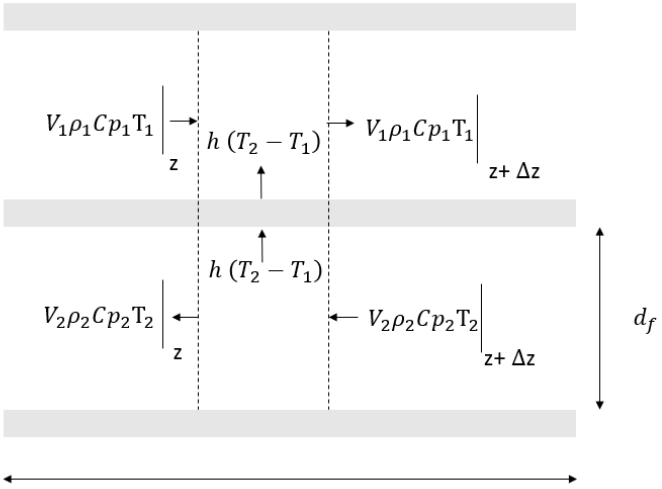

Figure 4.1 Model formulation for counter-current flow heat exchanger reactor- counter current flow (Reprinted with permission from [123]).

The resulting model equations for endothermic and exothermic volumes (equations 4.1-4.4) for either co-current or counter-current flow are:

Endothermic side

$$v_1 \frac{dC_1}{dz} = -\sigma_1(z) k_{01}\, e^{\left[\frac{-E_{a1}}{R.T_1}\right]}.\, C_1 \tag{4.1}$$

$$v_1 \frac{dT_1}{dz} = \frac{-\Delta H_{r1}}{\rho_1 C_{p_1}}\, \sigma_1(z) k_{01}\, e^{\left[-\frac{E_a}{R.T_1}\right]} C_1 - \frac{h_1 \hat{a}_1}{\rho_1 C_{p1}}\, (T_1 - T_2) \tag{4.2}$$

Exothermic side

$$\pm v_2 \frac{dC_2}{dz} = -\sigma_2(z) k_{02}\, e^{\left[\frac{-E_{a_2}}{R.T_2}\right]}.\, C_2 \tag{4.3}$$

$$\pm v_2 \frac{dT_2}{dz} = \frac{-\Delta H_{r2}}{\rho_2\, C_{p2}}\, \sigma(z) k_{02}\, e^{\left[-\frac{E_{a_2}}{R.T_2}\right]} C_2 - \frac{h_2 \hat{a}_2}{\rho_2 C_{p_2}}\, (T_2 - T_1) \tag{4.4}$$

where $\sigma_1(z)$, $\sigma_2(z)$ represent the position dependent catalyst activity and sign of v_2 indicating flow configuration (+ for co-current flow and – for counter current flow).

Boundary conditions for co-current and counter-current (equations 4.5 and 4.6 respectively) are given as:

$$C_1(0) = C_{10}, \qquad T_1(0) = T_{10}, C_2(0) = C_{20}, T_2(0) = T_{20} \tag{4.5}$$

$$C_1(0) = C_{10}, \qquad T_1(0) = T_{10}, C_2(L) = C_{20}, T_2(L) = T_{20} \tag{4.6}$$

In the above system of equations it is assumed the inlet temperatures of both the endothermic and exothermic streams are equal i.e., $T_{10} = T_{20} = T_0$.The above system of equations can be cast in dimensionless form in terms of Damkohler number ($Da_i = \frac{k_{0i} e^{\left[\frac{-E_{ai}}{R.T_0}\right]} L}{v_i}$), Stanton number ($St_i = \frac{h_i \hat{a}_i L}{\rho_i C_{pi} v_i}$), dimensionless activation energies ($\gamma_i = \frac{E_{ai}}{RT_0}$) and dimensionless heat of reaction ($B_i = \frac{-\Delta H_{ri}\, C_{i0}}{\rho_i C_{pi}\, T_0}$), where i=1 and 2 for endothermic and exothermic streams respectively.

$$\frac{du_1}{ds} = -\sigma_1(s) Da_1\, e^{\left[\frac{\gamma_1\theta_1}{1+\theta_1}\right]} u_1 = f_1 \tag{4.7}$$

$$\frac{d\theta_1}{ds} = \sigma_1(s) B_1\, Da_1\, e^{\left[\frac{\gamma_1\theta_1}{1+\theta_1}\right]} u_1 - St_1\,(\theta_1 - \theta_2) = f_2 \tag{4.8}$$

$$\frac{du_2}{ds} = -\sigma_2(s) Da_2\, e^{\left[\frac{\gamma_2\theta_2}{1+\theta_2}\right]} u_2 = f_3 \tag{4.9}$$

$$\frac{d\theta_2}{ds} = \sigma_2(s) B_2\, Da_2\, e^{\left[\frac{\gamma_2\theta_2}{1+\theta_2}\right]} u_2 - St_2\,(\theta_2 - \theta_1) = f_4 \tag{4.10}$$

where $u_1 = \frac{C_1}{C_{10}}, u_2 = \frac{C_2}{C_{20}}, \theta_1 = \frac{T_1 - T_0}{T_0}$, and $\theta_2 = \frac{T_2 - T_0}{T_0}$. In the above equations, $Da_2, St_2 > 0$ for co-current flow and $Da_2, St_2 < 0$ for counter-current flow. The corresponding dimensionless boundary conditions are:

$$u_1(0) = 1, \qquad \theta_1(0) = 0, u_2(0) = 1, \theta_2(0) = 0 \tag{4.11}$$

$$u_1(0) = 1, \qquad \theta_1(0) = 0, u_2(1) = 1, \theta_2(1) = 0 \tag{4.12}$$

4.3. Defining the optimal control problem

The goal of the study is to find the right catalyst distribution in both the endothermic and exothermic channels to maximize conversion while keeping the exothermic channel temperature below a certain critical value. While this is a standard optimization problem, that can be solved by many off-the-shelf solvers currently available, an optimal control approach is chosen as it enables us to predict the different inputs that would be part of the optimal solution. Furthermore, it provides a theoretical basis to the existence of inert and fully active catalyst regions in reactor channels that have been proposed in reaction engineering literature. The objective of the optimization is to: (i) Maximize conversion (or minimize reactant concentration) of the endothermic and exothermic streams (ii) Ensure hotspot temperature is below a pre-defined value. For co-current flow, the optimization problem is to find $\sigma_1 \epsilon [0,1]$ and $\sigma_2 \epsilon [0,1]$ that minimizes the following objective function:

$$J_1 = u_1(L) + u_2(L) \tag{4.13}$$

Subject to:

$$\theta_2(s) \leq \theta_c \tag{4.14}$$

and the model (equations 4.7-4.12) while for counter-current flow, the objective is:

$$\min J_2 = u_1(L) + u_2(0) \tag{4.15}$$

where θ_c is the maximum allowable temperature of the exothermic channel. Furthermore, the domain the inputs imply that the catalyst distribution ranges from fully active ($\sigma = 1$) to inert ($\sigma = 0$). Following Pontriyagin's Maximum Principle, the optimization problem above can be reformulated as that of minimizing the Hamiltonian as given below [114],

Co-current

Min

$$\text{Min } H\big(X(s), \sigma(s), \lambda(s), \mu(s)\big) = \lambda^T F + \mu^T S \tag{4.16}$$

s.t

$$\dot{X} = F(X, \sigma),\ X(0) = X_0 \tag{4.17}$$

$$\dot{\lambda} = -\frac{\partial H}{\partial X}, \qquad \lambda(1) = \frac{dJ_1}{dX}\Big|_{s=1} \tag{4.18}$$

where F represents the model equations (equations 4.7-4.10) and S represents the state and input constraints in vector forms. For counter current, the equations are similar except that for one stream there is a terminal condition instead of an initial condition. Thus, the equations are of the form:

Counter current

$$\text{Min } H\big(X(s), \sigma(s), \lambda(s), \mu(s)\big) = \lambda^T F + \mu^T S \tag{4.19}$$

s.t

$$\dot{X} = F(X, \sigma), \qquad X_i(0) = X_{i0}, \qquad X_j(1) = X_{j1} \tag{4.20}$$

$$\dot{\lambda} = -\frac{\partial H}{\partial X}, \qquad \lambda_j(1) = \frac{dJ_2}{dX}|_{s=1}, \qquad \lambda_i(0) = \frac{dJ_2}{dX}|_{s=0} \tag{4.21}$$

where $X = [X_i, X_j]$ and X_i and X_j represent the state variabl es of the two streams in the model. A necessary condition for the optimum is:

$$H_{\sigma_1} = \lambda^T F_{\sigma_i} + \mu^T S_{\sigma_i} = 0 \tag{4.22}$$

In general, it is not possible to obtain a complete analytical solution to the above optimization problem. However, it is possible to obtain analytical expressions of different arcs/pieces that constitute the optimal solution. This will help us understand the possible solutions to the optimization problem and, as we will see, allude to the existence of inert/fully active regions in the optimal solution.

The necessary condition (equation 4.22) gives rise to two possibilities, one is when $\lambda^T F_{\sigma_i} \neq 0$ which implies $\mu \neq 0$ and hence one of the constraints is active and the second case another being when $\lambda^T F_{\sigma_i} = 0$. When one of the constraints are active the input σ_i can be inferred from the active constraint. Thus, the possible arcs when the constraints are active are(i) $\sigma_i = 0$, (ii)$\sigma_i = 1$ or (iii) σ_i is such that $\theta_2 = \theta_c$ in an interval $s \in [s_1, s_2]$. For the third case, the catalyst distributions can be readily obtained by the fact that if $\theta_2 = \theta_c$ in an interval then $\frac{d\theta_2}{ds}$ should vanish. Thus, from equation (4.10),

$$\sigma_2 = St_2 \frac{(\theta_c - \theta_1)}{B_2\, Da_2\, e^{\left[\frac{\gamma_2\theta_c}{1+\theta_c}\right]} u_2} \tag{4.23}$$

The expression for σ_1 can be obtained using the fact that $\frac{d^2\theta_2}{ds^2}$ should also vanish if $\theta_2 = \theta_c$in an interval, which gives the following expression,

$$\sigma_1 = \frac{-\frac{d\sigma_2}{ds} B_2 Da_2 e^{\left[\frac{\theta_c\gamma_2}{1+\theta_c}\right]} u_2 + \sigma_2 B_2 Da_2^2 e^{\left[\frac{2\theta_c\gamma_2}{1+\theta_c}\right]} u_2 + St_2 St_1(\theta_1 - \theta_c)}{St_2 B_1 Da_1 e^{\left[\frac{\gamma_1\theta_1}{1+\theta_1}\right]} u_1} \tag{4.24}$$

In the case when $\lambda^T F_{\sigma_i} = 0$, the input can be obtained from this condition. However, in cases where the input appears linearly in the Hamiltonian (such as the problem considered in this study) the above condition would not give the expression for the optimal input. In such cases, the input is obtained by repeatedly differentiating $\lambda^T F_{\sigma_i}$ with respect to time along the trajectories of the model equations. The singular arc analysis is done below for σ_1 and the same process can be followed for σ_2. Since for a first order reaction concentration cannot be zero in finite length:

$$\lambda^T F_{\sigma_i} = 0 \rightarrow (-\lambda_1 + \lambda_2 B_1) Da_1 e^{\frac{\gamma_1\theta_1}{1+\theta_1}} u_1 = 0 \rightarrow (-\lambda_1 + \lambda_2 B_1) = 0 \tag{4.25}$$

$$\frac{d\left(\lambda^T F_{\sigma_i}\right)}{ds} = 0 \rightarrow B_1(\lambda_2 St_1 - \lambda_4 St_2) Da_1 e^{\frac{\gamma_1\theta_1}{1+\theta_1}} u_1 = 0 \rightarrow B_1(\lambda_2 St_1 - \lambda_4 St_2) = 0 \tag{4.26}$$

$$\frac{d^2\left(\lambda^T F_{\sigma_i}\right)}{ds^2} = 0 \rightarrow \frac{\gamma_2(-\lambda_3 + B_2\lambda_4)\sigma_2 Da_2 e^{\frac{\gamma_2\theta_2}{1+\theta_2}}}{(1+\theta_2)^2} u_2 B_1 St_2 Da_1 e^{\frac{\gamma_1\theta_1}{1+\theta_1}} u_1 = 0 \tag{4.27}$$

The above equation implies that either $\sigma_2 = 0$ or $(-\lambda_3 + B_2\lambda_4) = 0$. However, if $(-\lambda_3 + B_2\lambda_4) = 0$, the co-state equations for λ_3 and λ_4,

$$\frac{d\lambda_3}{ds} = (\lambda_3 - \lambda_4 B_2)\sigma_2 Da_2 e^{\frac{\gamma_2\theta_2}{1+\theta_2}} = 0 \tag{4.28}$$

$$\frac{d\lambda_4}{ds} = (\lambda_3 - \lambda_4 B_2)\frac{\sigma_2 Da_2 e^{\frac{\gamma_2\theta_2}{1+\theta_2}} u_2}{(1+\theta_2)^2} + \lambda_4 St_2 - \lambda_2 St_1 = 0 \tag{4.29}$$

along with (equation 4.26) imply that an expression for σ_2 inside the feasible region can never be obtained[124]. Thus, the input will always be along the active constraints. This means that the input either consists of practically implemenTable inert/ active regions or practically unimplementable constraint arcs given by equations 4.23 and 3.24.

Having found the possible arcs that could appear in the optimal catalyst distributions, in the subsequent subsections these arcs will be pieced together for different reactor parameters which will provide significant insights into the heat transfer characteristics of heat-exchanger reactors.

4.4. Parameters

In this study, two sets of nominal reactor parameters are selected as follows. The first set of reactor parameters (shown in Table 4.1), corresponds to the case where the heat released by the exothermic reaction is not enough to prevent quenching unless it is distributed optimally throughout the reactor. To obtain this set of parameters, the ratio of endothermic Damkohler number to exothermic Damkohler number was increased until quenching was observed in the simulation for uniform catalyst distribution in the reactor

($\sigma_1 = 1, \sigma_2 = 1$). While doing this we ensured the parameter values stayed in range reported in literature[54]. The second set of parameters in Table 4.2 are similar to those used by [54] and lead to hotspot formation when a uniform catalyst distribution is used.

Table 4.1 Parameter sets. Case I: quenching for $\sigma_1 = \sigma_2 = 1$ (Reprinted with permission from [123]).

Parameters	Endothermic	Exothermic
Da	2	0.5
B	-1	1
γ	12	12
St	10	10
θ_c		0.4

Table 4.2: Parameter sets. Case II: hotspot formation for $\sigma_1 = \sigma_2 = 1$ (Reprinted with permission from [123]).

Parameters	Endothermic	Exothermic
Da	5	2
B	-1	1
γ	12	12
St	10	10
θ_c		0.4

4.5. Numerical calculations

A two-step process is employed to obtain optimal endothermic and exothermic catalytic activity profiles. During the first step, approximate profiles are obtained by converting the model equations to non-linear algebraic equations using finite difference methods with 1000 equally spaced nodes. The resulting non-linear program (NLP) is solved using the IPOPT[115] solver in GAMS. The approximate profiles give the sequence of the possible inputs derived in the previous subsection. In the 2nd step, a second optimization problem is solved to find the final profiles with switching points as the variables by wrapping a fmincon solver over a function (using the ode 15s routine) to solve the model equations using the sequence determined in step 1. If $\theta_2 \neq \theta_c$ along the constraint arcs, a very high cost(10^{10}) is returned to the fmincon solver. The function that solves the model equations for counter-current flow uses the shooting method and in this case the cost returned to the fmincon solver is:

$$\text{cost} = \alpha[(u_2(L) - 1)^2 + \theta_2(L)^2] + u_1(L) + u_2(0)$$

where $\alpha = 10^{10}$ is a large number that ensures the term in the brackets is infinitesimally small. The approximate profiles derived in the first step provide excellent initial guesses for the shooting method. The tolerances for the ode solvers was chosen to be10^{-13} to ensure the effect of numerical artifacts was minimal.

For the co-current configuration, the model equations represent an initial value problem, and thus the cost returned is $u_1(L) + u_2(0)$. All the simulations were performed in an Intel Core 2 Duo Processor with 8.00 GB RAM and 3.16 GHz with simulation times varying from 10s to 300s.

4.6. Results

4.6.1. Parameter set 1- counter current reactor (quench prevention)

The optimal catalyst distribution is obtained by piecing together the arcs obtained in Subsection 4.3 for parameter set 1, which results in quenching of the reactor when a uniform catalyst distribution is employed for both endo- and exothermic reaction volumes. The concentration and temperature profiles for three different catalyst distributions, i) Uniform catalyst distribution (ii) Optimal Catalyst distribution without temperature constraints (iii) Optimal catalyst distributions with temperature constraints, are shown in Figure (4.2) respectively. As shown in the figure, a uniform catalyst distribution results in quenching of the reactor. In the next two subsections the catalyst distributions are optimized with and without temperature constraints to prevent quenching

4.6.1.1. Optimal catalyst distribution without temperature constraints

Without temperature constraints, the results in Subsection 4.3 imply that the optimum will consist of solely active/ inert regions. As shown in Figure 4.2a numerical simulations show that the optimal catalyst distribution is to place inert material at the inlet of the exothermic channel. The inert brings the exothermic reaction interval inside the reactor and in turn preventing extinction[43-44, 59]. However, the concentration profiles in Figure 4.2b show that the exothermic reaction is extremely fast and goes to completion in a narrow length interval resulting in inefficient thermal coupling between the two reactions and giving rise to hotspot formation.

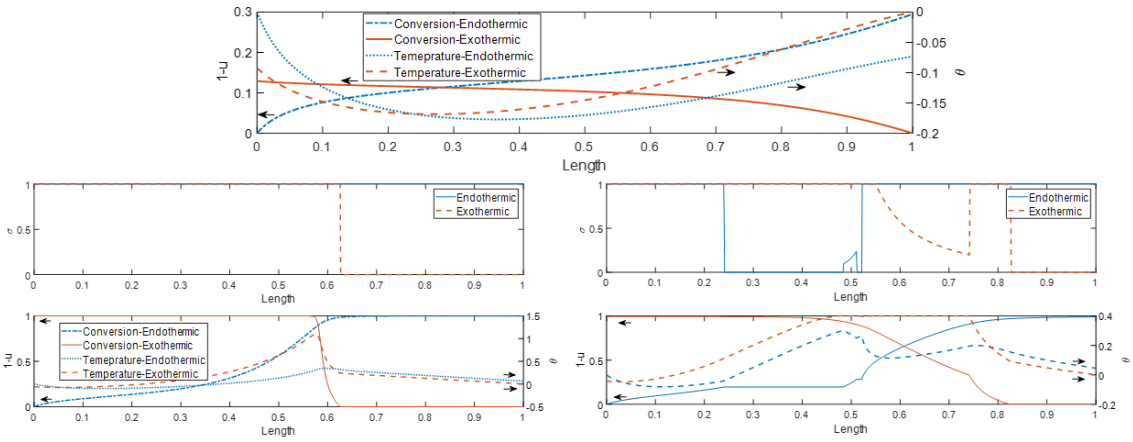

Figure 4.2 Counter-current, parameter set 1. (i) Temperature and conversion vs length-uniform catalyst distribution (1). (ii) Optimal catalyst distribution without temperature constraints (2a), temperature and conversion (2b). (iii) optimal catalyst distribution (Reprinted with permission from [123]).

4.6.1.2. Optimal catalyst distributions with temperature constraints

Incorporating temperature constraints to the optimization leads to non-intuitive combinations of maximum/minimum and constraint arc patterns which results in an overlap of the exothermic and endothermic reaction intervals as shown in Figures (4.3a, 4.3b). In this way, the heat released by the exothermic reactor is effectively consumed by endothermic reaction such that hotspots are eliminated.

4.6.2. Parameter set 1- co- current reactor

In this subsection, the optimal sequence of the input arcs is obtained for co-current flow. The concentration and temperature profiles for three different catalyst distributions, i) Uniform catalyst distribution (ii) Optimal Catalyst distribution without temperature constraints (iii) Optimal catalyst distributions with temperature constraints, are shown in

Figure 4.3. As observed in counter current case, a uniform catalyst distribution causes reactor extinction/quenching albeit at a lower extent as there is no axial separation of the reactor zones like in counter-current flow.

4.6.2.1. Optimal catalyst distribution without temperature constraints

The optimal catalyst distribution to minimize the concentration without temperature constraints consists of inert at the endothermic reactor inlet. The exothermic reaction occurring in the adjacent channel heats up the endothermic reactants in the inert zone so that when the reactants reach the active catalyst portion, the reaction occurs at an elevated temperature, thereby preventing reactor extinction. There are hotspots in the endothermic channel, though it is of lesser magnitude compared to counter current flow.

4.6.2.2. Optimal catalyst distribution with temperature constraints

As shown in Figures (4.3a, 4.3b), addition of temperature constraints to the optimization, gives rise to a region in the reactor space where the temperature constraint is active. In this region the catalyst distribution is governed by the constraint arcs derived in Subsection 4.3. Due to the constraint arc, a more gradual exothermic reaction is observed which consequently decreases hotspot magnitude further.

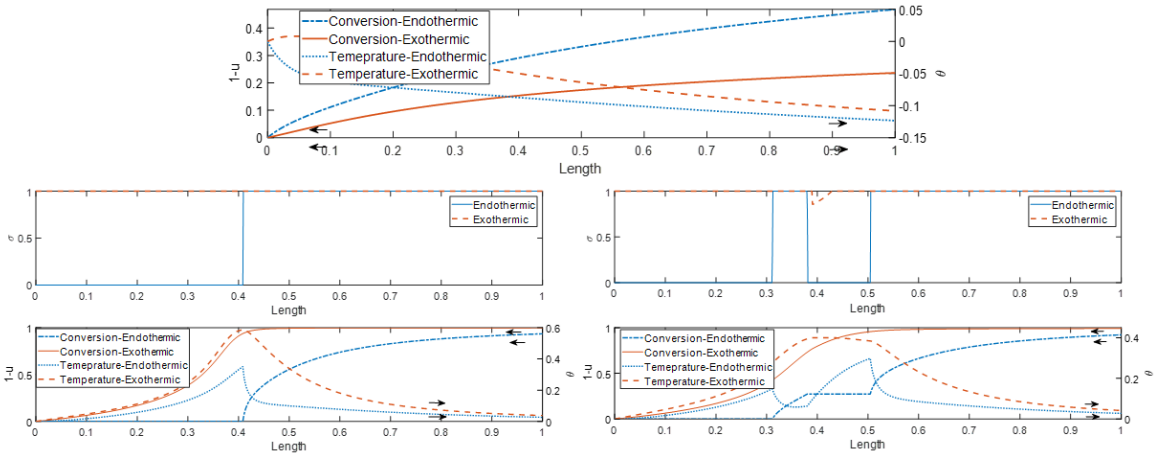

Figure 4.3 Co-current, parameter set 1. (i) Temperature and conversion vs length- uniform catalyst distribution (1). (ii) Optimal catalyst distribution without temperature constraints (2a), temperature and conversion (2b). (iii) Optimal catalyst distribution with temperature constraints for parameter set 1 (3a), conversion and temperature (3b) (Reprinted with permission from [123]).

4.6.3. Parameter set 2- counter- current reactor

In this subsection, the optimal input sequence is obtained for parameter set 2 which corresponds to hotspot formation in a reactor employing uniform catalyst distributions for both endothermic and exothermic volumes. Since the reaction proceeds to near-complete conversion with a uniform catalyst distribution, optimizing the catalyst distribution without temperature constraints doesn't add any value. Thus, given the stated goal of attaining high conversion while preventing hotspots, two catalyst distributions are considered (Figure 4.4): (i) Uniform catalyst distribution and (ii) Optimal catalyst distribution with temperature constraints corresponding to parameter set 2. For uniform catalyst distribution and counter current flow, the exothermic reaction goes to completion in a small interval which gives rise to hotspot formation.

4.6.3.1. Optimal catalyst distribution without temperature constraints

As shown in Figure 4.4 (2a and 2b), the optimal catalyst distribution in this case comprises an inert zone at the exothermic inlet followed by constraint arcs that bring the exothermic reaction inside the reactor and closer to the endothermic reaction, such that the two reaction zones overlap, and the heat released by the exothermic reaction is efficiently consumed by the endothermic reaction.

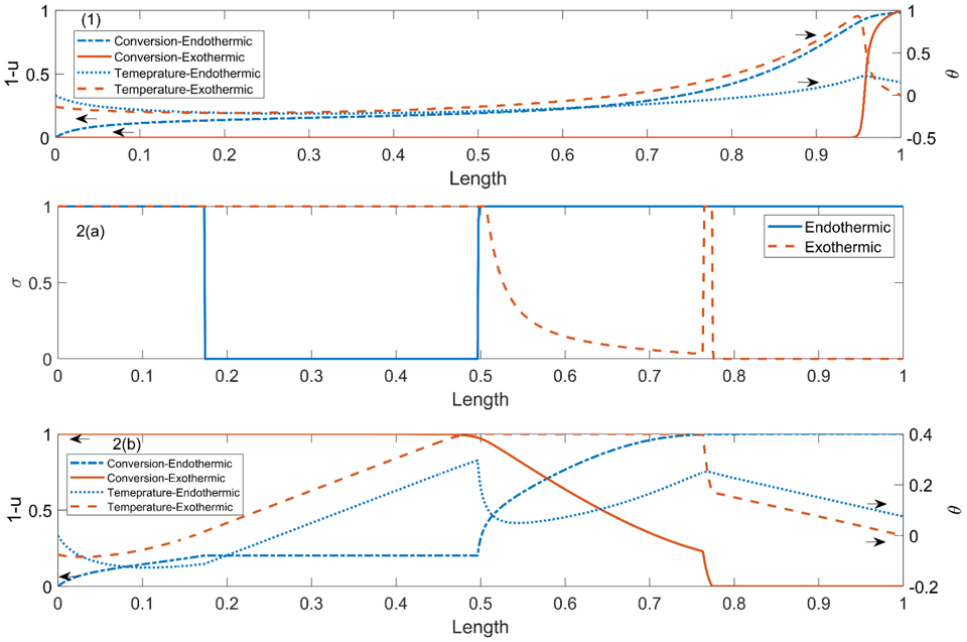

Figure 4.4 Counter-current, parameter set 2. (i) Temperature and conversion vs length-uniform catalyst distribution (1). (ii) Optimal catalyst distribution with temperature constraints (2a), temperature and conversion (2b) (Reprinted with permission from [123]).

4.6.4. Parameter set 2- co-current reactor

Again, like the counter-current case, since the reaction proceeds to full conversion for a uniform catalyst distribution, optimizing without temperature constraints doesn't add much value. Thus, two catalyst distributions are considered (i) Uniform catalyst distribution (ii) Optimal catalyst distribution with temperature constraints (Figure 4.5). In this case, the uniform catalyst distribution gives rise to hotspots albeit of lesser magnitude than the counter current case because there is no axial separation between the two reaction zones.

4.6.4.1. Optimal catalyst distributions with temperature constraints

When temperature constraints are added, the optimal distribution comprises of a combination of inert zones in the endothermic channel and constraint arcs in the exothermic channel, which prevent hotspot formation in the reactor (Figure 4.5 (2a and 2b)). The inert regions in the endothermic channel help pre-heating the endothermic reactants, thereby increasing the heat absorbed in the interior of the reaction channel.

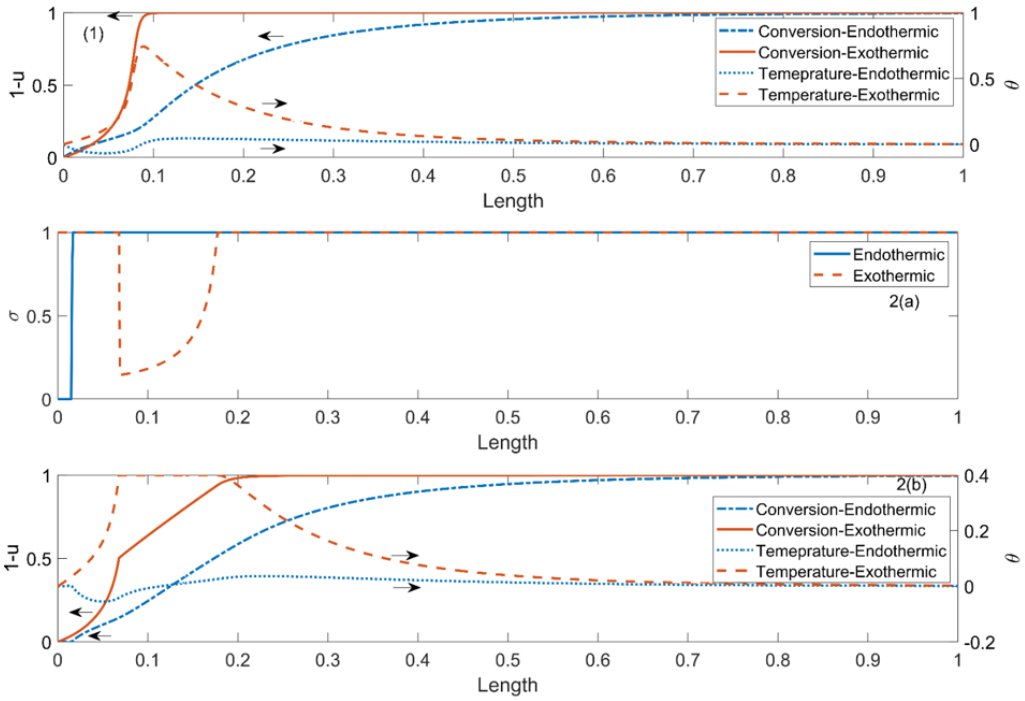

Figure 4.5 Co-current, parameter set 2. (i) Temperature and conversion vs length- uniform catalyst distribution (1). (ii) Optimal catalyst distribution with temperature constraints (2a), temperature and conversion (2b) (Reprinted with permission from [123]).

4.6.5. Effect of St-counter current reactor

Optimal catalyst activity distribution profiles with temperature constraints for three Stanton numbers (St=2,5,10) (Figure 4.6), illustrate how placements of inerts vary with the Stanton number. For low Stanton number (St=2), there are no inert zones in either the endothermic or exothermic channel because heat transfer between the two volumes is low enough that placing inerts to match the reaction intervals does not significantly affect thermal coupling. Instead, a constraint arc in the exothermic channel is required to limit the exothermic temperature rise. At higher Stanton numbers (St=5 and 10), the magnitude of heat transfer between channels increases so that inerts are required for efficient thermal

coupling via matching reaction intervals. It is observed that the length of inert region increases, and the length of the constraint arc decreases with increasing Stanton number as matching reaction intervals becomes more important than limiting exothermic reaction heat generation.

Optimizing catalyst distribution has another interesting effect on the counter-current reactor. In counter current mode, cold pinch crossover, defined as the point where the endothermic and exothermic temperatures are equal, may occur near the endothermic inlet[54]. The presence of cold pinch crossover is undesirable, as in the region from the endothermic inlet to the cold pinch crossover point, the endothermic stream loses energy to the exothermic stream[54]. Thus, the farther away from the endothermic inlet that this cold-pinch point occurs, the higher the additional energy loss, which consequently decreases reactor conversion. To illustrate the evolution of cold pinch points, the temperature profiles for three different Stanton numbers (St=2,5 and 10) are plotted in Figure 4.7. For St=2, due to low heat transfer between the two channels, there is no cold pinch point. When St is increased to 5, a cold pinch point appears for the uniform catalyst distribution case but is absent in the optimal catalyst distribution. Further increase to St=10, results in a cold pinch appearing for both the uniform catalyst and optimal catalyst distribution cases, due to high heat transfer between the two channels. However, it is to be noted that the magnitude of the cold pinch temperature is lower, and the position is closer to the endothermic reactor inlet, in the optimal catalyst distribution. A plot of cold pinch point and corresponding temperature vs Stanton number in Figure 4.8a shows that for $4 < St < 5.4$ pinch point only occurs for the uniform catalyst case, while at $St > 5.4$ pinch

point occurs in the optimal catalyst case too. The magnitude and axial position of the cold pinch point are much higher for uniform catalyst distribution as compared to the optimal catalyst distribution.

To illustrate the effect of cold pinch points on conversion, the endothermic conversion vs Stanton number is plotted in Figure 4.8b. For low Stanton numbers, even in the absence of cold pinch temperatures, endothermic conversion for both the uniform catalyst and optimal catalyst is low as the magnitude of heat transfer between endothermic and exothermic volumes is insufficient regardless of catalyst distribution. As St increases, the endothermic conversion increases for both uniform catalyst and optimal catalyst distributions, due to the increased heat transfer between the two channels which initially outweighs the adverse effects of pinch point. However, for $St \geq 5.4$ heat loss due to cold pinch point become significant and endothermic conversion for uniform catalyst distribution drops drastically. It is in this region that the gains of optimization become significant, as inerts and constraint arcs successfully mitigate cold pinch temperature and position (as shown in Figure 4.8a) so that conversion continues to increase with Stanton number.

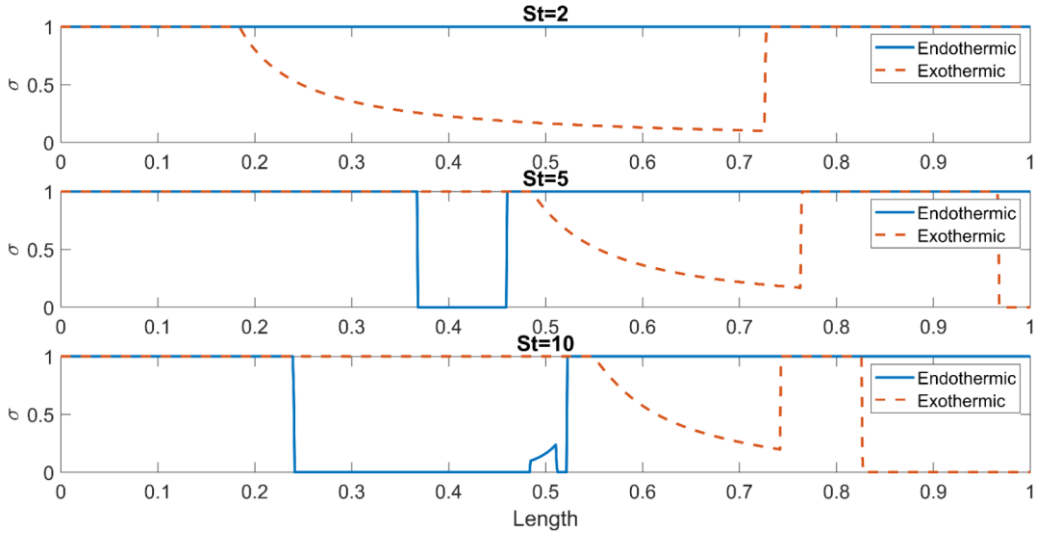

Figure 4.6 Optimal catalyst distribution for different Stanton numbers. Parameter set 1 (counter current flow) (Reprinted with permission from [123]).

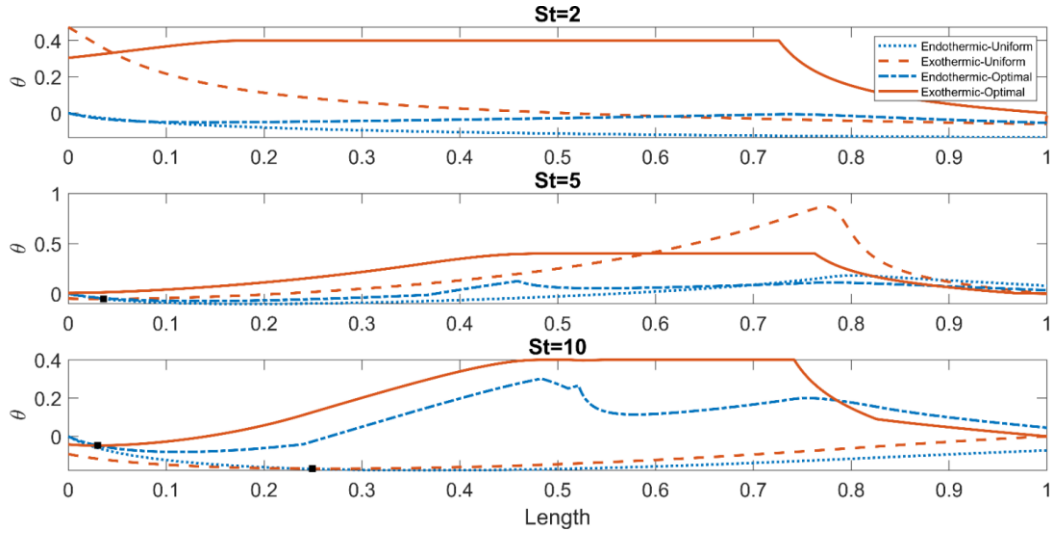

Figure 4.7 Temperature vs length for different Stanton numbers. Parameter set 1(counter-current) •-cold pinch point (Reprinted with permission from [123]).

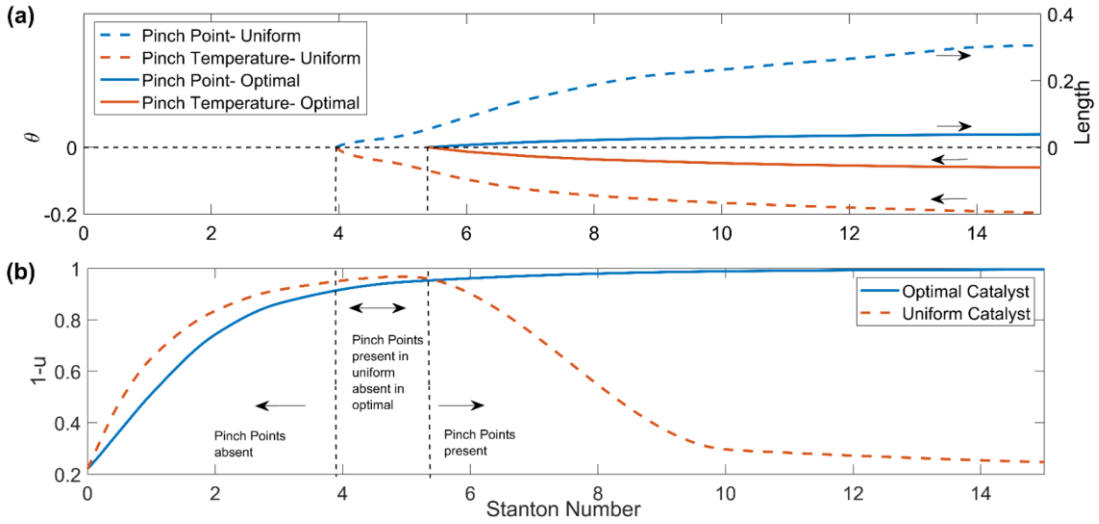

Figure 4.8 (a) Cold pinch crossover point and temperature vs Stanton number for optimal and uniform catalyst distribution. Parameters from set 1 (counter-current flow). (b) Endothermic conversion vs stanton number for optimal and uniform catalyst distribution. parameter set 1 (counter-current flow) (Reprinted with permission from [123]).

4.6.6. Effect of St-co-current reactor

Like the counter-current case, the optimal catalyst distribution is plotted for 3 different Stanton numbers (St=2,5, and 10) in Figure 4.9. For low Stanton numbers (St=2) due to reduced heat transfer the length of the constraint arc is large and inert regions are diminished. As Stanton number increases, chances of extinction increase due to increased heat transfer between the two channels. Thus, an increase in the length of inert material is observed for high Stanton numbers

The endothermic conversion for uniform catalyst and optimal catalyst distribution are plotted in Figure 4.10 for different Stanton numbers. For low St, an increase in the endothermic conversion is observed because of increased thermal coupling where the

exothermic reaction is driven by the endothermic reaction. However, for higher Stanton numbers there is very strong interaction between the two reactions and since the rate of endothermic reaction is greater than exothermic reaction ($Da_1 > Da_2$), the exothermic reaction is quenched. Thus, in the absence of a heat source to drive the endothermic reaction the conversion decreases.

On the other hand, for optimal catalyst distributions, endothermic conversion increases monotonically with Stanton number. This is because for higher St, a large part of the optimal catalyst distribution in the endothermic channel consists of inerts (Figure 4.9) that help the exothermic reaction proceed and heat up the reactor, which in turn drives the endothermic reaction to high conversion.

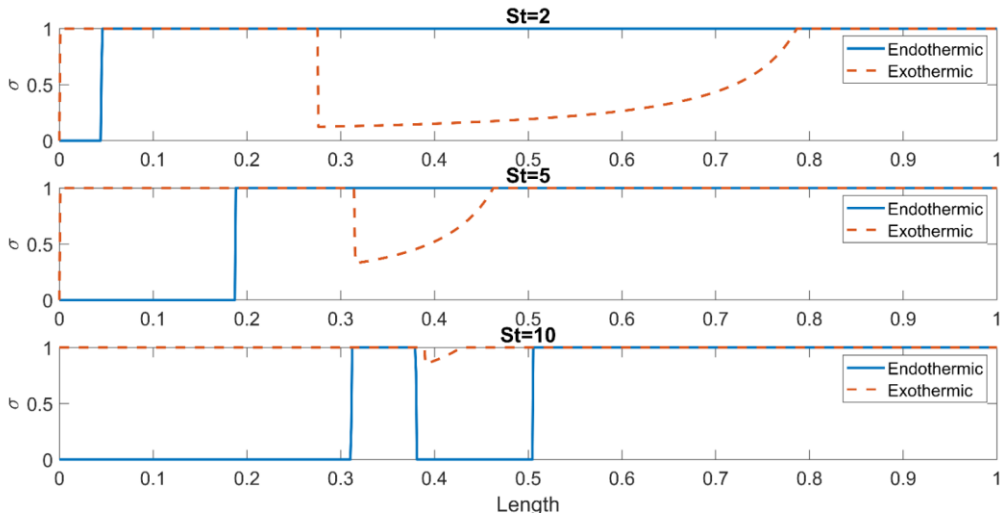

Figure 4.9 Optimal catalyst distribution vs length for different Stanton numbers. Parameter set 1 (co-current flow) (Reprinted with permission from [123]).

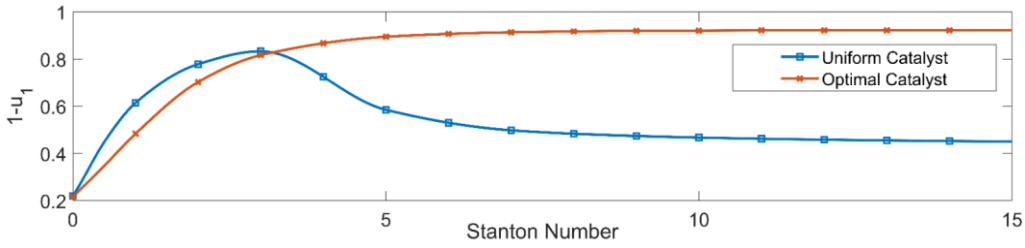

Figure 4.10 Endothermic conversion vs Stanton number for optimal and uniform catalyst distribution. Parameters set 1. (co-current flow) (Reprinted with permission from [123]).

4.6.7. Effect of Da_2- counter-current

In this subsection the goal is to study the effect of fuel consumption rate (characterized by the exothermic Damkolher number) on endothermic (process gas) reactor performance for both uniform and optimal catalyst distributions with all other parameters taken from set 1. The effect of exothermic Damkohler number on the optimal catalyst distribution for counter current is plotted in Figure 4.11 for Da_2=0.5,1 and 2. For low exothermic Damkohler numbers, the inert regions in the endothermic channel are large to prevent reactor extinction. However, as Da_2 increases, the need for inerts in the endothermic channel to prevent reactor extinction is diminished due to higher exothermic reaction rates. Hence, the inert regions get smaller for higher exothermic Damkohler numbers. The effect of exothermic Damkohler number (Da_2) on endothermic conversion is shown in Figure 4.12. Comparing the uniform catalyst and optimal catalyst distributions, the optimal catalyst distribution yields higher conversions for the same Da_2. In fact, even for $Da_2 \in [0.1, 0.6]$ the difference in conversion is greater than 50 %. This is because, in the case of uniform catalyst distribution, the endothermic reaction suppresses

the exothermic reaction for low Da_2. However, optimizing the catalyst distribution results in the intelligent utilization of the low exothermic reaction rate by optimally placing inert and constraint arcs in the channels, and hence higher endothermic conversion/ ignition can be obtained using lesser fuel (Da_2).

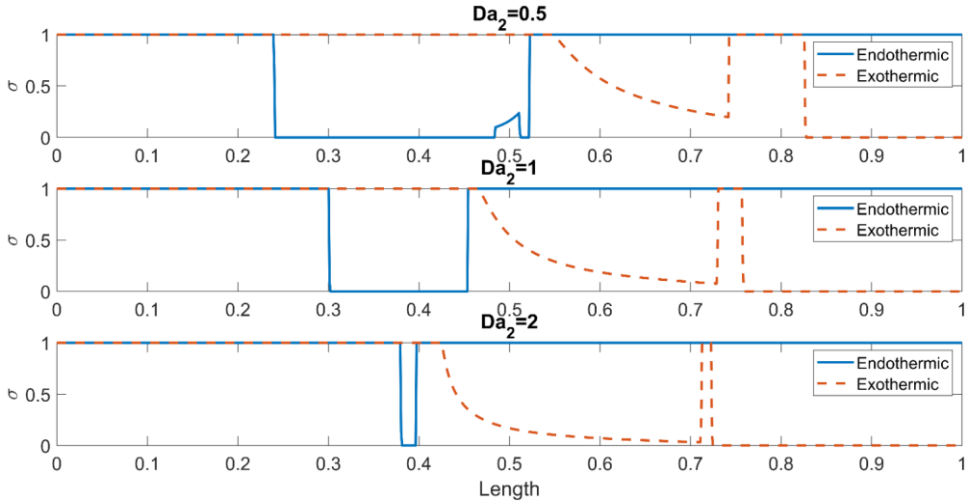

Figure 4.11 Optimal catalyst distribution vs length for different Damkohler numbers- parameter set 1 (counter-current flow) (Reprinted with permission from [123]).

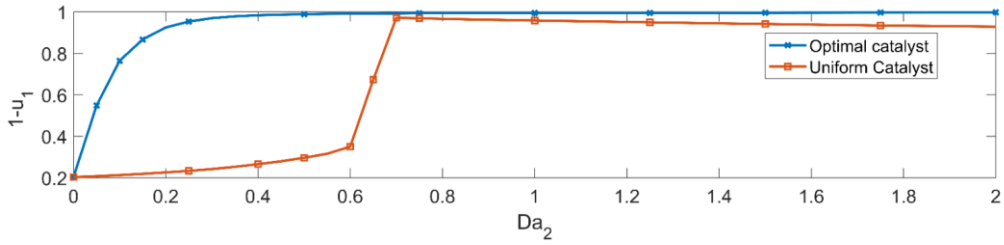

Figure 4.12 Endothermic conversion vs exothermic Damkohler number- parameter set 1 (counter current flow) (Reprinted with permission from [123]).

4.6.8. Effect of Da_2- co-current case

The optimal catalyst distribution is plotted in Figure 4.13 for Da_2=0.5,1 and 2. Like the counter current case, there are significant inert regions for lower exothermic Damkohler numbers to prevent reactor extinction which get smaller as Da_2 increases. The endothermic conversion vs exothermic Damkohler number is plotted in Figure 4.14. Endothermic conversion for the optimal catalyst distribution is little lower than the uniform catalyst distribution for low Da_2. This is because in the optimal catalyst distribution inerts are placed in the endothermic region to prevent the quenching of the exothermic channel. Thus, while the endothermic conversion is a little lower for lower Da_2, the exothermic conversion is much higher in the optimal case. On the other hand, for higher Da_2 that optimal placement of catalysts results in higher conversion in both the streams.

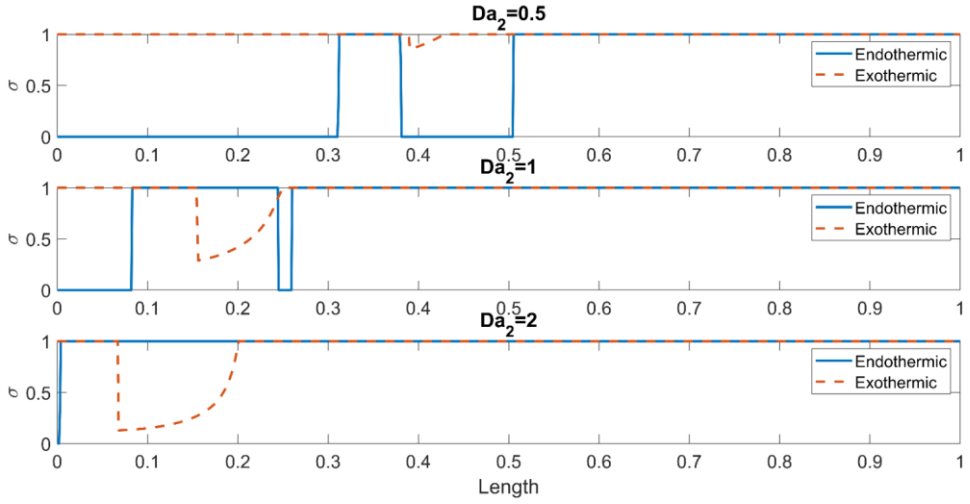

Figure 4.13 Optimal catalyst distribution vs length for different Damkohler numbers. Parameter set 1 (co-current) (Reprinted with permission from [123]).

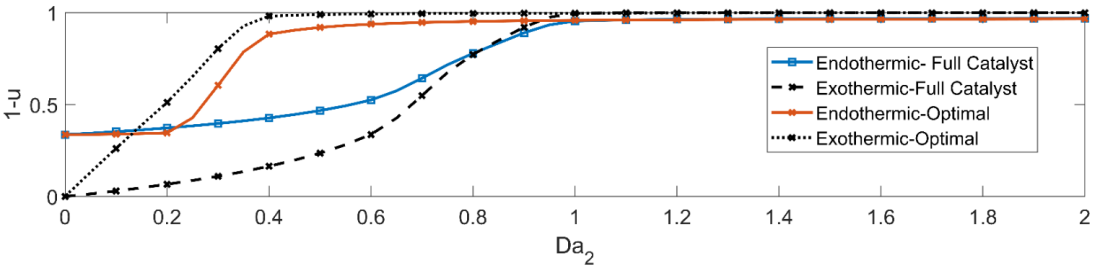

Figure 4.14 Conversion vs exothermic Damkohler number (Da_2)- rest of the parameters from set 1 (co-current) (Reprinted with permission from [123]).

4.6.9. Piecewise constant approximations

The catalyst distributions obtained in the previous subsections consist of continuously varying portions which are practically difficult to implement. Thus, in this subsection, piecewise constant approximations of the optimal catalyst profiles found in the previous subsections are considered. One way to do this would be to ensure a binary

activity of the profiles ($\sigma = 0$ or 1) and measure the deviation of the approximate profiles from the true optimal profiles. However, one of the goals of this subsection is to show that the true optimal profiles provide important information regarding the placement of inert zones and full catalyst activity zones. That is, the location of inerts and full activity zones remains unchanged for piecewise constant approximations. If a binary condition is enforced, it cannot be said for sure whether the inert/full activity zones are due to the binary condition or the optimal control analysis. Thus, partial activity zones are allowed (σ= [0,1]) and the optimization problem is like the one considered before, except that now the catalyst profiles are piece-wise constant. The optimal piecewise constant inputs are calculated using the parameters listed in Table 4.1 (Case 1) for the counter current case, a similar approach could be done for the co-current flow too. The procedure followed is given below:

i. The optimal profile is divided into discrete zones. A transition from one zone to another occurs if any one of the inputs in the optimal profile changes its nature i.e. from 1 to 0 or 1 to constraint arc etc. For the parameter set considered in this subsection there are 8 such zones.

ii. The zones with constraint arcs are further divided depending on the number (n) of piecewise constant approximations needed. Thus, the number of piece-wise constant inputs to be optimized in each channel equals to the sum of the zones obtained in step (i) and step (ii).

iii. The model equations are discretized into 1000 nodes using a finite difference scheme and optimized using the IPOPT solver in GAMS.

Optimal catalyst activity, concentration, and temperature profiles for different are shown in Figures (4.15 and 4.16) for n=1,2,3 and 4. It is observed that the piece-wise constant approximation matches the true optimal in almost all the regions where the true optimal profiles are bang-bang. Furthermore, the deviation in the conversion and temperature profiles from the true optimal is minimal even for n=1. Thus, though the results of the optimal control problem might give practically unimplementable results in some regions of the reactor space, it provides important information as to where the maximum catalyst activity, intermediate catalyst activity and inerts should be placed.

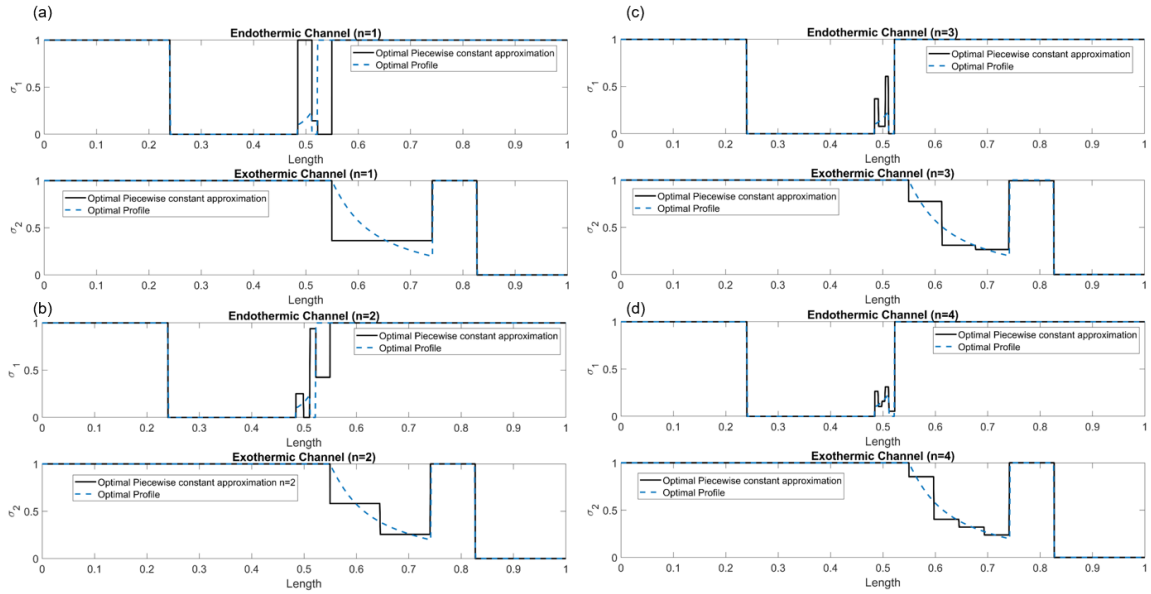

Figure 4.15 Optimal piece-wise catalyst activity profile vs length. Parameter set 1 (counter-current flow) (Reprinted with permission from [123]).

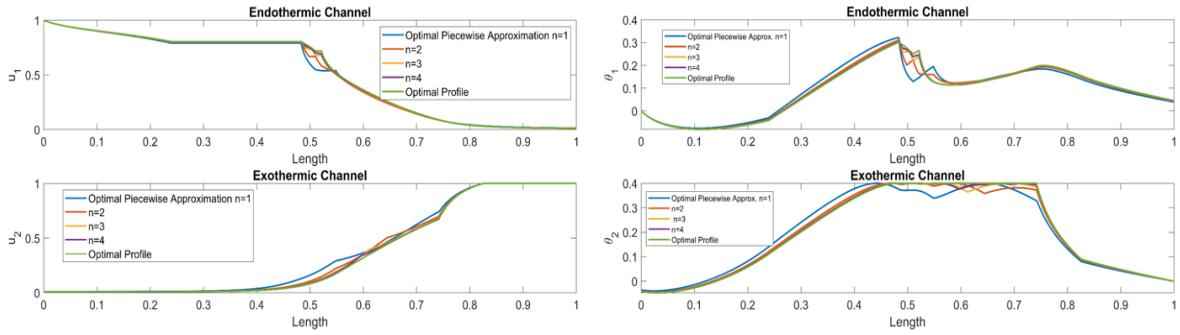

Figure 4.16 Optimal piece-wise catalyst activity approximation. Temperature vs length. Parameter set 1(counter current flow) (Reprinted with permission from [123]).

4.7. Conclusions

In this section optimal control theory is used to develop a systematic way of obtaining the right catalyst distribution in counter current and co-current heat exchanger reactors using a pseudo-homogenous plug flow reactor model. Due to the singular nature of the problem, the optimal catalyst distribution consists of practically implementable bang-bang regions and unimplementable constraint arcs.

There are several scenarios where optimizing catalyst distribution is shown to be beneficial to heat exchanger reactors. Separation of reaction zones, small exothermic reaction intervals, high endothermic reaction rates are some of the cases considered in this section where the gains of optimization are clear. For example, in the case where separation of reaction zones leads to reactor quenching, optimizing catalyst distribution lead to 70% increase in endothermic conversion. Thus, whatever the reason be for inefficiency of heat transfer, optimizing catalyst distribution results in the intelligent placements of inerts and constraint arcs for a given set of reaction parameters which in

turn ensures safe and efficient operation of the reactor. Moreover, the practically unimplementable constraint arc profiles could be divided into discrete zones and further optimized to obtain approximate piecewise constant profiles with minimal deviation from true optimal profiles. For more complex flows and geometries, an optimization like this would give the approximate location and length of the inerts/ active regions a priori. This can be a useful starting point for parameter optimization problems (where catalyst bed activity (0/1) and bed length are parameters) that have been studied a lot in literature. For high order systems as the nature of the optimization will remain the same i.e. maximizing conversion subject to model equations and an exothermic temperature constraint. Moreover, if gas-solid resistances are assumed to be negligible it can be again said that the optimal input will consist of inter/active regions and continuously varying constraint/singular arcs. Thus, extending the present work to higher order reactive systems should be straight forward. However, for multiple reactions in addition to thermal balancing and maximizing conversion high selectivity is also desirable and hence there is a requirement to reformulate the optimization problem to include selectivity.

Another important complexity in heat exchanger reactors is the presence of solid-phase axial conduction in the walls. In this present work solid-phase conduction is neglected as the goal of the section was to provide a fundamental study of how altering catalyst distribution can help in ensuring efficient heat transfer between endothermic and exothermic streams. However, given the nature of the optimization addition of a solid wall in the model equations won't change the analysis drastically as problem remains singular.

5. FAULT DIAGNOSIS USING OBSERVERS IN CONTINUOUS TIME SYSTEMS-APPLIED TO CONVENTIONAL CHEMICAL REACTORS*

5.1. Introduction

This section marks the transition from tackling design problems in unconventional chemical reactors to diagnosis problems in conventional reactors with the goal to make them safer and reliable. This will be accomplished by designing a robust observer-based fault detection and isolation (FDI) scheme for nonlinear processes that will then be applied to chemical reactors. We will approach functional observer-based FDI for nonlinear systems from the point of view of exact observer error linearization[101]. The functional observer in the absence of faults has linear disturbance-decoupled error dynamics, with the observer output (residual) function identically vanishing on the observer invariant manifold. Such functional observers are also known as residual generators. It will be shown that, with the proposed formulation, easy-to-check necessary and sufficient conditions for the existence of such a residual generator can be derived, leading to simple formulas for functional observer design with eigenvalue assignment. Moreover, fault isolation can be accomplished via multiple residual generators, one for each fault, decoupled from the other faults and the system disturbances. The proposed formulation and results provide a direct nonlinear generalization of standard linear FDI methods[61].

* Parts of this section have been reprinted with permission from "Design of linear residual generators for fault detection and isolation in nonlinear systems". Venkateswaran, S., Liu, Q., Wilhite, B.A. and Kravaris, C., 2020. *International Journal of Control*, pp.1-17.Copyright 2020 Taylor and Francis.

In the following subsections, the notion of functional observer for nonlinear systems in a completely analogous manner to Luenberger's definition for linear systems will be defined. Then, the notions of observer error linearization will be defined. Following this the problem of fault detection, isolation and estimation using residual generators (a special case of a functional observer) will be presented. Finally, the fault diagnosis scheme will be applied to a variety of chemical engineering case studies involving conventional chemical reactors namely, bio-reactors, CSTRs, and process network.

5.1.1. Functional observers for non-linear systems

Consider an unforced non-linear system of the form

$$\dot{x} = F(x)$$

$$y = H(x)$$

$$r_o = q(x)$$

where $x \epsilon R^n$ denotes the vector of states, $y \epsilon R^p$ denotes the vector of measured outputs

The objective is to construct a functional observer of order $s < n$, which generates an estimate of the output r_o, driven by the output measurement y. For the following system $z \in R^s, r \in R$,

$$\frac{dz}{dt} = \phi(z, y)$$

$$r = \omega(z, y)$$

to act as an observer, the overall dynamics, in the series connection,

$$\dot{x} = F(x)$$

$$\frac{dz}{dt} = \phi(z, H(x))$$

Must possess an invariant manifold $z = T(x)$ (where $T(x): R^n \rightarrow R^s$) with the property that $r(x) = \omega(T(x), H(x))$

In the above definition, the requirement that $z = T(x)$ is an invariant manifold of the series connection, i.e. that $z(0) = T(x(0)) \Rightarrow z(t) = T(x(t)) \forall t > 0$, translates to

$$\frac{\partial T}{\partial x}(x)F(x) = \varphi\big(T(x), H(x)\big)$$

If the functional observer is initialized consistently with the system i.e. if $z(0) = T(x(0))$, then $z(t) = T(x(t))$, and therefore $r(t) = \omega\big(\hat{\xi}(t), y(t)\big) = \omega\big(T(x(t)), H(x(t))\big) = q(x(t)) \forall t > 0$. which means that the functional observer will be able to exactly reproduce z(t). In the presence of initialization errors, additional stability requirements will need to be imposed on the z-dynamics, for the estimate r(t) to asymptotically converge to $r_o(t)$.

Of particular interest is the linear form for the observer dynamics $\phi(z, y) = Az +$ By as the eigenvalues of A will determine the stability of the functional observer and the rate of decay of the error. If we can find a continuously differentiable map T(x) to be a solution of the linear partial differential equation

$$\frac{\partial T}{\partial x}(x)F(x) = AT(x) + BH(x)$$

for some Hurwitz matrix A, and if in addition T(x) satisfies condition (IV), i.e. that q(x) can be expressed as a function of $T(x) \text{and} H(x)$, then we have a stable functional observer

with linear dynamics. Throughout this subsection, we will consider linear output maps of the form $\omega(z, y) = Cz + Dy$. Thus, our goal is to find an observer of the form

$$\frac{dz}{dt} = Az + By$$

$$r = Cz + Dy$$

where A, B, C, and, D are $s \times s, s \times p, 1 \times s, \text{and } 1 \times p$ matrices respectively and A having stable eigenvalues and equivalently, find a continuously differentiable mapping $T(x)\colon R^n \to R^s$ such that

$$\frac{\partial T}{\partial x}(x)F(x) = AT(x) + BH(x)$$

$$q(x) = CT(x) + DH(x)$$

Assuming that the above problem can be solved, the resulting error dynamics will be linear:

$$\frac{d}{dt}\big(z - T(x)\big) = A\big(z - T(x)\big)$$

$$r - r_o = C(z - T(x))$$

from which $r(t) - r_o(t) = Ce^{At}(z(0) - T(x(0)))$. With the matrix A having stable eigenvalues, the effect of the initialization error $z(0) - T(x(0))$ will die out, and $r(t)$ will approach $r_o(t)$ asymptotically. While the above problem has been solved and explicit design conditions for the design of linear observers have been derived[125] in the following subsections a special case of a functional observer that tracks the identically $q(x) = 0$ output will be considered. This will be the basis of the fault diagnosis approach presented in the rest of the subsection.

5.1.2. Disturbance decoupled fault detection

Consider a nonlinear process described by:

$$\dot{x} = F(x) + G(x)f + \sum_{i=1}^{m} E_i(x)\, w_i \qquad (5.1)$$

$$y = H(x) + J(x)f + \sum_{i=1}^{m} K_i(x)\, w_i$$

where $x \epsilon R^n$ denotes the vector of states, $y \epsilon R^p$ denotes the vector of measured outputs. $f \epsilon R$ and $w_i \epsilon R, i = 1,2, \ldots, m$ are the fault and the disturbances/uncertainties respectively (system inputs) and $F(x), G(x), E_i(x), H(x), J(x), K_i(x)$ are smooth functions. Under normal operation of the process, the input f (fault) is identically equal to zero, however in an abnormal situation (equipment failure), f becomes nonzero, and this is what needs to be detected on the basis of the measurements. The inputs w_i describe normal variability of process conditions (disturbances) and/or model uncertainty. It is in the presence of this variability that the fault must be detected, and the conclusion (normal or faulty operation) must be unaffected by the presence of w_i (disturbance-decoupled detection).

In this work, we will study the problem of disturbance-decoupled fault detection on the basis of calculating a quantity r called the residual, which is identically zero under normal operation (i.e. when f(t)=0) and nonzero under an abnormal situation (i.e. when f(t)≠0), and is unaffected by the disturbances w_i. More specifically, this work will study the design of a **linear** functional observer, called the residual generator, of the form

$$\dot{z} = Az + By \qquad (5.2)$$

$$r = Cz + Dy$$

with state $z \epsilon R^s$, output $r \epsilon R$ (the residual), and parameters A, B,C, D being $s \times s$, $s \times p$, $1 \times s$ and $1 \times p$ matrices respectively with (C, A) observable pair, so that the response of the residual r in the series connection of (5.1) followed by (5.2)

$$\frac{d}{dt}\begin{bmatrix} x \\ z \end{bmatrix} = \begin{bmatrix} F(x) \\ Az + BH(x) \end{bmatrix} + \begin{bmatrix} G(x) \\ BJ(x) \end{bmatrix} f + \sum_{i=1}^{m} \begin{bmatrix} E_i(x) \\ BK_i(x) \end{bmatrix} w_i \tag{5.3}$$

$$r = [Cz + DH(x)] + [DJ(x)]f + \sum_{i=1}^{m} [DK_i(x)]w_i$$

has the following properties:

r(t) asymptotically approaches zero when f is identically zero

r(t) is unaffected by the disturbances w_i

r(t) is affected by the fault f

In other words, for any initial conditions $\begin{bmatrix} x(0) \\ z(0) \end{bmatrix}$ and any disturbances $w_i(t)$,

$$\lim_{t \to \infty} r(t) = 0 \text{ if } f(t) = 0$$
$$\lim_{t \to \infty} r(t) \neq 0 \text{ if } f(t) \neq 0$$

The responsiveness of r to faults and insensitivity to disturbances ensures fault detection while precluding the possibility of false alarms.

The present study focuses on designing **linear** residual generators for nonlinear systems given by (5.1) because of the practicality of linear observers in design and implementation. We will derive necessary and sufficient conditions for the existence of a linear residual generator based on a disturbance-decoupled linear functional observer. As long as these conditions are satisfied, we will derive simple design formulas for the residual generator, with eigenvalue assignment capability.

5.2. Design conditions for the residual generator for disturbance decoupled fault detection

In this subsection we derive specific design conditions that the residual generator must satisfy to meet the requirements (i)-(iii). The first and foremost requirement of the residual generator is that the residual must vanish in the absence of faults or disturbances (asymptotically converge to zero in the presence of initialization errors). In other words, the residual generator should act as a functional observer that tracks an output identically equal to zero. Consequently[61, 68, 70, 125-126], there must exist a differentiable map $\mathrm{T}(\mathrm{x})$ from P^{n} to P^{s} such that :

$$\frac{\partial \mathrm{T}(\mathrm{x})}{\partial \mathrm{x}} \mathrm{F}(\mathrm{x}) - \mathrm{AT}(\mathrm{x}) - \mathrm{BH}(\mathrm{x}) = 0 \tag{5.4}$$

$$\mathrm{CT}(\mathrm{x}) + \mathrm{DH}(\mathrm{x}) = 0 \tag{5.5}$$

Conditions (5.4) and (5.5) state that z=T(x) is an invariant manifold of the zero-input dynamics of system (5.3), on which the residual r is identically equal to zero. It will be seen in Proposition 1 in the next subsection that the necessary and sufficient conditions for existence of such an invariant manifold depend on F(x) and H(x) only, and not on the (A, B, C, D) matrices of the residual generator. If conditions (5.4) and (5.5) are satisfied, the observer error dynamics (expressed in terms of the off-the-manifold coordinate $\mathrm{e} = \mathrm{z} - \mathrm{T}(\mathrm{x})$) and the residual are given by:

$$\frac{\mathrm{d}\big(\mathrm{z} - \mathrm{T}(\mathrm{x})\big)}{\mathrm{dt}} = \mathrm{A}\big(\mathrm{z} - \mathrm{T}(\mathrm{x})\big) + \left(\mathrm{BJ}(\mathrm{x}) - \frac{\partial \mathrm{T}(\mathrm{x})}{\partial \mathrm{x}} \mathrm{G}(\mathrm{x})\right) \mathrm{f} + \sum_{\mathrm{i}=1}^{\mathrm{m}} \left(\mathrm{BK}_{\mathrm{i}}(\mathrm{x}) - \frac{\partial \mathrm{T}(\mathrm{x})}{\partial \mathrm{x}} \mathrm{E}_{\mathrm{i}}(\mathrm{x})\right) \mathrm{w}_{\mathrm{i}} \tag{5.6}$$

$$r = C\big(z - T(x)\big) + DJ(x)f + \sum_{i=1}^{m} DK_i(x)w_i \tag{5.7}$$

It should be noted here that the zero-input dynamics of (5.6) - (5.7) is exactly linear and moreover, if the matrix A is Hurwitz, the zero-input response is

$$z(t) - T\big(x(t)\big) = e^{At}\Big(z(0) - T\big(x(0)\big)\Big) \to 0$$

$$r(t) = Ce^{At}\Big(z(0) - T\big(x(0)\big)\Big) \to 0$$

which means that the manifold z=T(x) is attractive and the residual r(t) asymptotically approaches zero.

The second requirement for the residual generator is that the residual must remain completely unaffected by any disturbances $w_i(t)$ present in the system. Disturbance decoupling can be achieved if the coefficients of w_i in (5.6) and (5.7) vanish, i.e, for all i=1,..,m,

$$\frac{\partial T(x)}{\partial x} E_i(x) - BK_i(x) = 0 \tag{5.8}$$

$$DK_i(x) = 0 \tag{5.9}$$

The third requirement for the residual generator is that the residual r must be affected by the input f, so that the fault can be detected by monitoring the residual. Therefore, the coefficients of the input f in (5.6) and (5.7) must not be all zero:

$$\begin{bmatrix} \frac{\partial T}{\partial x}(x)G(x) - BJ(x) \\ DJ(x) \end{bmatrix} \neq \begin{bmatrix} 0 \\ 0 \end{bmatrix} \tag{5.10}$$

In summary, the residual generator should satisfy the following design conditions:

i) The functional observer conditions (5.4) and (5.5)

ii) The disturbance decoupling conditions (5.8) and (5.9) for all disturbances

iii) The fault detectability condition (5.10)

Remark 2.1: Some parallels can be drawn between the observer approach formulated here and the differential geometric perspective in [95]. Specifically, the disturbance decoupling and fault detectability conditions can be expressed in geometric terms as $\begin{bmatrix} E_i(x) \\ K_i(x) \end{bmatrix} \in \Omega^{\perp} \ \forall\, i = 1, .., m$ and $\begin{bmatrix} G(x) \\ J(x) \end{bmatrix} \notin \Omega^{\perp}$, where $\Omega^{\perp}$ is the annihilator of the codistribution Ω spanned by the rows of the matrix $\begin{bmatrix} \frac{\partial T(x)}{\partial x} & -B \\ 0 & D \end{bmatrix}$.

5.3. Solution of the design conditions

For the design of the residual generator (5.2), one must be able to find the matrices A, B, C and D and a differentiable map T(x) so that the design conditions (5.4), (5.5), (5.8) and (5.9) are satisfied. In addition, it is desired that the matrix A is Hurwitz with prescribed eigenvalues for stability and fast response of the error dynamics. The following proposition provides necessary and sufficient conditions for the residual generator (5.2) to satisfy (5.4) and (5.5).

Proposition 1**:** *There exists a residual generator of the form (5.2) satisfying the functional observer design conditions (5.4) and (5.5) if and only if there exist constant row vectors* $v_0, v_1, \ldots, v_{s-1}, v_s \in R^p$ *that satisfy:*

$$V_0 H(x) + L_F\big(v_1 H(x)\big) + \cdots + L_F^{s-1}\big(v_{s-1} H(x)\big) + L_F^{s}\big(v_s H(x)\big) = 0 \qquad (5.11)$$

where L_F *denotes the Lie derivative operator* $L_F = \sum_{j=1}^{n} F_j(x) \frac{\partial}{\partial x_j}$.

Proof: i) Necessity: Suppose that there exists $T(x) = \begin{bmatrix} T_1(x) \\ T_2(x) \\ \vdots \\ T_s(x) \end{bmatrix}$ such that (5.4) is satisfied,

i.e.

$$\begin{bmatrix} L_F T_1(x) \\ L_F T_2(x) \\ \vdots \\ L_F T_s(x) \end{bmatrix} = A \begin{bmatrix} T_1(x) \\ T_2(x) \\ \vdots \\ T_s(x) \end{bmatrix} + \begin{bmatrix} B_1 H(x) \\ B_2 H(x) \\ \vdots \\ B_s H(x) \end{bmatrix}$$

where $B_1, \dots, B_s$ denote the rows of the matrix B. Applying the Lie derivative operator L_F to each component of the above equation (k–1) times, we find that for k=1,2,3…

$$\begin{bmatrix} L_F^k T_1(x) \\ L_F^k T_2(x) \\ \vdots \\ L_F^k T_s(x) \end{bmatrix} = A^k \begin{bmatrix} T_1(x) \\ T_2(x) \\ \vdots \\ T_s(x) \end{bmatrix} + \begin{bmatrix} (A^{k-1}B)_1 H(x) + L_F((A^{k-2}B)_1 H(x)) + \cdots + L_F^{k-1}(B_1 H(x)) \\ (A^{k-1}B)_2 H(x) + L_F((A^{k-2}B)_2 H(x)) + \cdots + L_F^{k-1}(B_2 H(x)) \\ \vdots \\ (A^{k-1}B)_s H(x) + L_F((A^{k-2}B)_s H(x)) + \cdots + L_F^{k-1}(B_s H(x)) \end{bmatrix}$$

and we can calculate

$$(L_F^s + \alpha_1 L_F^{s-1} + \cdots + \alpha_s I)T_i(x) = ((A^{s-1}B)_i + \alpha_1 (A^{s-2}B)_i + \cdots + \alpha_{s-1} B_i)H(x)$$

$$+ L_F(((A^{s-2}B)_i + \cdots + \alpha_{s-2} B_i)H(x))) + \cdots + L_F^{s-1}(B_i H(x)) \qquad (5.12)$$

where $\alpha_1, \dots, \alpha_s$ are the coefficients of the characteristic polynomial of the matrix A.

At the same time, the mapping $T(x)$ must satisfy (5.5), hence applying $(L_F^s + \alpha_1 L_F^{s-1} + \cdots + \alpha_s I)$ on each component of equation (5.5) and using (5.12) gives:

$$0 = (CA^{s-1}B + \alpha_1 CA^{s-2}B + \cdots + \alpha_{s-1} CB + \alpha_s D)H(x)$$

$$+ L_F((CA^{s-2}B + \cdots + \alpha_{s-2} CB + \alpha_{s-1} D)H(x))) + \cdots + L_F^{s-1}((CB + \alpha_1 D)H(x))$$

$$+ L_F^s(DH(x))$$

which proves that (5.11) is satisfied. ,

ii) Sufficiency: Suppose that there exist constant row vectors $v_0, v_1, \ldots, v_{s-1}, v_s$ that satisfy (3.1). Consider the following choices of (A, B, C, D) matrices:

$$A = \begin{bmatrix} 0 & 0 & \cdots & 0 & -\alpha_s \\ 1 & 0 & \cdots & 0 & -\alpha_{s-1} \\ 0 & 1 & \cdots & 0 & \alpha_{s-2} \\ \vdots & \vdots & \ddots & \vdots & \vdots \\ 0 & 0 & \cdots & 1 & -\alpha_1 \end{bmatrix}, \qquad B = \begin{bmatrix} \alpha_s \\ \alpha_{s-1} \\ \vdots \\ \alpha_2 \\ \alpha_1 \end{bmatrix} v_s - \begin{bmatrix} v_0 \\ v_1 \\ \vdots \\ v_{s-2} \\ v_{s-1} \end{bmatrix}, \qquad C = [0\ 0 \cdots 0\ 1],$$

$$D = -v_s \tag{5.13}$$

For the above A and C matrices (in observer canonical form), the design conditions (2.4) and (5.5) can be written component-wise as follows:

$$\frac{\partial T_1(x)}{\partial x} F(x) + \alpha_s T_s(x) - B_1 H(x) = 0 \tag{5.14}$$

$$\frac{\partial T_2(x)}{\partial x} F(x) - T_1(x) + \alpha_{s-1} T_s(x) - B_2 H(x) = 0 \tag{5.15}$$

$$\vdots$$

$$\frac{\partial T_s(x)}{\partial x} F(x) - T_{s-1}(x) + \alpha_1 T_s(x) - B_s H(x) = 0 \tag{5.16}$$

$$T_s(x) + DH(x) = 0 \tag{5.17}$$

We observe that the above equations are easily solvable sequentially for $T_s(x), T_{s-1}(x), \ldots, T_1(x)$, starting from the last equation and going up. In particular, for the chosen B and D matrices, we find from (5.17), (5.16), … ,(5.15):

$$T_s(x) = v_s H(x)$$

$$T_{s-1}(x) = L_F\big(v_s H(x)\big) + v_{s-1} H(x)$$

$$\vdots$$

$$T_2(x) = L_F^{s-2}\big(v_s H(x)\big) + \cdots + v_2 H(x)$$

$$T_1(x) = L_F^{s-1}\big(v_s H(x)\big) + \cdots + L_F\big(v_2 H(x)\big) + v_1 H(x)$$

whereas (5.14) gives:

$$L_F^s(v_s H(x)) + L_F^{s-1}(v_{s-1} H(x)) + \cdots + L_F(v_1 H(x)) + v_0 H(x) = 0$$

which is exactly (5.11). Thus, we have proved that

$$T(x) = \begin{bmatrix} v_1 H(x) + L_F(v_2 H(x)) + \cdots + L_F^{s-1}(v_s H(x)) \\ v_2 H(x) + \cdots + L_F^{s-2}(v_s H(x)) \\ \vdots \\ v_{s-1} H(x) + L_F(v_s H(x)) \\ v_s H(x) \end{bmatrix} \tag{5.18}$$

satisfies the design conditions (5.4) and (5.5) when v_0 , v_1, …, v_{s-1}, v_s satisfy (5.1) and the A, B, C, D matrices are chosen according to (5.13).

It is important to observe that the sufficiency part of the proof is constructive: it gives an explicit solution of the design equations (5.4) and (5.5) in terms of the vectors v_0 , v_1, …, v_{s-1}, v_s that satisfy (5.11). Moreover the eigenvalues of matrix A don't appear in the (5.11) and can hence be freely assigned. The following Proposition provides necessary and sufficient conditions for the derived residual generator to meet the disturbance decoupling specifications (5.8) and (5.9).

Proposition 2**:** *Suppose that there exist constant row vectors* v_0 , v_1, …, v_{s-1}, $v_s \in R^p$ *that satisfy (5.11) and that the residual generator matrices (A, B, C, D) have been chosen according to (5.13), so that the functional observer conditions hold with* T(x) *given by (5.18). The residual generator will satisfy the disturbance decoupling conditions if and only if for all i=1,2…,m:*

$$v_0 K_i(x) + L_{E_i}(v_1 H(x)) + L_{E_i} L_F(v_2 H(x)) + \cdots + L_{E_i} L_F^{s-1}(v_s H(x)) = 0$$

$$v_1 K_i(x) + L_{E_i}(v_2 H(x)) + \cdots + L_{E_i} L_F^{s-2}(v_s H(x)) = 0$$

$$\vdots \tag{5.19}$$

$$v_{s-2}K_i(x) + L_{E_i}\left(v_{s-1}H(x)\right) + \cdots + L_{E_i}L_F\left(v_sH(x)\right) = 0$$

$$v_{s-1}K_i(x) + L_{E_i}\left(v_sH(x)\right) = 0$$

$$v_sK_i(x) = 0$$

Proof: The disturbance decoupling conditions (5.8) and (5.9) can be written in component form, for i=1,2,…m, as follows:

$$\frac{\partial T_1(x)}{\partial x}E_i(x) - B_1K_i(x) = 0$$

$$\frac{\partial T_2(x)}{\partial x}E_i(x) - B_2K_i(x) = 0$$

$$\vdots$$

$$\frac{\partial T_{s-1}(x)}{\partial x}E_i(x) - B_{s-1}K_i(x) = 0$$

$$\frac{\partial T_s(x)}{\partial x}E_i(x) - B_sK_i(x) = 0$$

$$DK_i(x) = 0$$

Substituting the expressions for B, D and $T(x)$ from (5.3) and (5.8) to the above equations lead to the following conditions:

$$L_{E_i}L_F^{s-1}\left(v_sH(x)\right) + \cdots + L_{E_i}L_F\left(v_2H(x)\right) + L_{E_i}\left(v_1H(x)\right) - \alpha_sv_sK_i(x) + v_0K_i(x) = 0$$

$$L_{E_i}L_F^{s-2}\left(v_sH(x)\right) + \cdots + L_{E_i}\left(v_2H(x)\right) - \alpha_{s-1}v_sK_i(x) + v_1K_i(x) = 0$$

$$\vdots$$

$$L_{E_I}L_F^2\left(v_sH(x)\right) + L_{E_i}L_F\left(v_{s-1}H(x)\right) + L_{E_i}\left(v_{s-2}H(x)\right) - \alpha_3v_sK_i(x) + v_{s-3}K_i(x) = 0$$

$$L_{E_i}L_F\left(v_sH(x)\right) + L_{E_i}\left(v_{s-1}H(x)\right) - \alpha_2v_sK_i(x) + v_{s-2}K_i(x) = 0$$

$$L_{E_i}\left(v_s H(x)\right) - \alpha_1 v_s K_i(x) + v_{s-1} K_i(x) = 0$$

$$-v_s K_i(x) = 0$$

which can be written equivalently as

$$L_{E_i} L_F^{s-1}\left(v_s H(x)\right) + \cdots + L_{E_i} L_F\left(v_2 H(x)\right) + L_{E_i}\left(v_1 H(x)\right) + v_0 K_i(x) = 0$$

$$L_{E_i} L_F^{s-2}\left(v_s H(x)\right) + \cdots + L_{E_i} L_F\left(v_3 H(x)\right) + L_{E_i}\left(v_2 H(x)\right) + v_1 K_i(x) = 0$$

$$\vdots$$

$$L_{E_I} L_F^{2}\left(v_s H(x)\right) + L_{E_i} L_F\left(v_{s-1} H(x)\right) + L_{E_i}\left(v_{s-2} H(x)\right) + v_{s-3} K_i(x) = 0$$

$$L_{E_i} L_F\left(v_s H(x)\right) + L_{E_i}\left(v_{s-1} H(x)\right) + v_{s-2} K_i(x) = 0$$

$$L_{E_i}\left(v_s H(x)\right) + v_{s-1} K_i(x) = 0$$

$$v_s K_i(x) = 0$$

This completes the proof. ,

The following Proposition provides necessary and sufficient conditions for the derived residual generator to meet the fault detectability condition (5.10).

Proposition 3**:** *Suppose that there exist constant row vectors* $v_0, v_1, \ldots, v_{s-1}, v_s \in R^p$ *that satisfy (5.11) and that the residual generator matrices (A, B, C, D) have been chosen according to (5.13), so that (5.4) and (5.5) hold with* $T(x)$ *given by (5.18). The residual generator will satisfy the fault detectability condition (5.10) if and only if*

$$\begin{bmatrix} V_0 J(x) + L_G(v_1 H(x)) + L_G L_F(v_2 H(x)) \ldots + L_G L_F^{s-1}\left(v_s H(x)\right) \\ v_1 J(x) + L_G(v_2 H(x)) + \cdots + L_G L_F^{s-2}\left(v_s H(x)\right) \\ \vdots \\ v_{s-2} J(x) + L_G\left(v_{s-1} H(x)\right) + L_G L_F\left(v_s H(x)\right) \\ v_{s-1} J(x) + L_G\left(v_s H(x)\right) \\ v_s J(x) \end{bmatrix} \neq \begin{bmatrix} 0 \\ 0 \\ \vdots \\ 0 \\ 0 \\ 0 \end{bmatrix} \qquad (5.20)$$

Proof: For B and D defined via (5.13) and T(x) given by (5.18), condition (5.10) is equivalent to: is "either $v_s J(x) \neq 0$

or

$$\begin{bmatrix} \alpha_s \\ \alpha_{s-1} \\ \vdots \\ \alpha_2 \\ \alpha_1 \end{bmatrix} v_s J(x) - \begin{bmatrix} v_0 J(x) + L_G(v_1 H(x)) + L_G L_F\left(v_2 H(x)\right) + \cdots + L_G L_F^{s-1}\left(v_s H(x)\right) \\ v_1 J(x) + L_G(v_2 H(x)) + \cdots + L_G L_F^{s-2}\left(v_s H(x)\right) \\ \vdots \\ v_{s-2} J(x) + L_G(v_{s-1} H(x)) + L_G L_F\left(v_s H(x)\right) \\ v_{s-1} J(x) + L_G(v_s H(x)) \end{bmatrix} \neq \begin{bmatrix} 0 \\ 0 \\ \vdots \\ 0 \\ 0 \end{bmatrix}$$

and further to

$$\begin{bmatrix} v_0 J(x) + L_G(v_1 H(x)) + L_G L_F\left(v_2 H(x)\right) + \cdots + L_G L_F^{s-1}\left(v_s H(x)\right) \\ v_1 J(x) + L_G(v_2 H(x)) + \cdots + L_G L_F^{s-2}\left(v_s H(x)\right) \\ \vdots \\ v_{s-2} J(x) + L_G(v_{s-1} H(x)) + L_G L_F\left(v_s H(x)\right) \\ v_{s-1} J(x) + L_G\left(v_s H(x)\right) \\ v_s J(x) \end{bmatrix} \neq \begin{bmatrix} 0 \\ 0 \\ \vdots \\ 0 \\ 0 \\ 0 \end{bmatrix}$$

Summarizing the results of Propositions 1-3, we conclude that the design of a an s-th order linear residual generator is feasible if and only if there exist constant row vectors $v_0, v_1, \ldots, v_{s-1}, v_s \in R^p$ that satisfy

1) $L_F^s\left(v_s H(x)\right) + L_F^{s-1}\left(v_{s-1} H(x)\right) + \cdots + L_F\left(v_1 H(x)\right) + v_0 H(x) = 0$

2) $\Omega \begin{bmatrix} E_i(x) \\ K_i(x) \end{bmatrix} = 0 \quad \forall\, i = 1, .., m$ and

3) $\Omega \begin{bmatrix} G(x) \\ J(x) \end{bmatrix} \neq 0$

where $\Omega = \begin{bmatrix} \frac{\partial}{\partial x}\left[L_F^{s-1}(v_s H(x))\right] + \cdots + \frac{\partial}{\partial x}\left[L_F(v_2 H(x))\right] + \frac{\partial}{\partial x}(v_1 H(x)) & v_0 \\ \frac{\partial}{\partial x}\left[L_F^{s-2}(v_s H(x))\right] + \cdots + \frac{\partial}{\partial x}(v_2 H(x)) & v_1 \\ \vdots & \vdots \\ \frac{\partial}{\partial x}\left[L_F(v_s H(x))\right] + \frac{\partial}{\partial x}(v_{s-1} H(x)) & v_{s-2} \\ \frac{\partial}{\partial x}(v_s H(x)) & v_{s-1} \\ 0 & v_s \end{bmatrix}$.

The last two conditions state that the vectors $\begin{bmatrix} E_i(x) \\ K_i(x) \end{bmatrix}$, $i = 1, .., m$ belong to the annihilator of the codistribution spanned by the rows of the matrix Ω, whereas $\begin{bmatrix} G(x) \\ J(x) \end{bmatrix}$ does not (cf. Remark 5.1). Also, it is important to note that all three conditions are independent of the choice of eigenvalues for the residual generator; if constant row vectors v_0 , v_1, …, v_{s-1}, v_s can be found to satisfy them, any arbitrary eigenvalues can be assigned.

Remark 5.1: In case $\begin{bmatrix} G(x) \\ J(x) \end{bmatrix} \in \text{span}\left(\begin{bmatrix} E_1(x) \\ K_1(x) \end{bmatrix}, \begin{bmatrix} E_2(x) \\ K_2(x) \end{bmatrix}, \dots, \begin{bmatrix} E_m(x) \\ K_m(x) \end{bmatrix}\right)$ for all x, the disturbance decoupling conditions become incompatible with the fault detectability condition, hence fault detection is infeasible in the presence of disturbances.

Remark 5.2: Using the Lie derivative notation on a vector function as the vector of the Lie derivatives of its components, e.g. $L_F \begin{bmatrix} H_1(x) \\ \vdots \\ H_p(x) \end{bmatrix} = \begin{bmatrix} L_F H_1(x) \\ \vdots \\ L_F H_p(x) \end{bmatrix}$, and accordingly notation for higher-order Lie derivatives of vector functions, the conditions of Propositions 1-3 may be written in a compact form as

$$[v_0\ v_1 \dots v_{s-1}\ v_s]\left[\Gamma_o(x)\ \ \Gamma_{w_1}(x)\ \dots\ \Gamma_{w_m}(x)\ \ \Gamma_f(x)\right] = [0\ 0\ *] \qquad (5.21)$$

where:

$$\Gamma_o(x) = \begin{bmatrix} H(x) \\ L_F H(x) \\ \vdots \\ L_F^{s-1} H(x) \\ L_F^{s} H(x) \end{bmatrix}$$

$$\Gamma_{w_i}(x) = \begin{bmatrix} K_i(x) & 0 & \cdots & 0 & 0 \\ L_{E_i} H(x) & K_i(x) & \cdots & 0 & 0 \\ \vdots & \vdots & \ddots & \vdots & \vdots \\ L_{E_i} L_F^{s-2} H(x) & L_{E_i} L_F^{s-3} H(x) & \cdots & K_i(x) & 0 \\ L_{E_i} L_F^{s-1} H(x) & L_{E_i} L_F^{s-2} H(x) & \cdots & L_{E_i} H(x) & K_i(x) \end{bmatrix}$$

$$\Gamma_f(x) = \begin{bmatrix} J(x) & 0 & \cdots & 0 & 0 \\ L_G H(x) & J(x) & \cdots & 0 & 0 \\ \vdots & \vdots & \ddots & \vdots & \vdots \\ L_G L_F^{s-2} H(x) & L_G L_F^{s-3} H(x) & \cdots & J(x) & 0 \\ L_G L_F^{s-1} H(x) & L_G L_F^{s-2} H(x) & \cdots & L_G H(x) & J(x) \end{bmatrix}$$

and the symbol * indicates a nonzero matrix block. In this form, the linear dependence of the conditions on the unknown vectors $v_0, v_1, \ldots, v_{s-1}, v_s$ becomes explicit.

For the special case when the system (5.1) is linear, i.e.

$$\dot{x} = Fx + Gf + \sum_{i=1}^{m} E_i w_i \tag{5.22}$$

$$y = Hx + Jf + \sum_{i=1}^{m} K_i w_i$$

the design conditions (5.4), (5.5), (5.8) and (5.9) become the standard design conditions for linear residual generators for linear system [61]

$$TF - AT - BH = 0 \tag{5.23}$$

$$CT + DH = 0 \tag{5.24}$$

$$TE - BK = 0 \tag{5.25}$$

$$DK = 0 \tag{5.26}$$

where $E = [\,E_1 \ldots E_m]$ and $K = [\,K_1 \ldots K_m]$, whereas the fault detectability condition (2.10) becomes $\begin{bmatrix} TG - BJ \\ DJ \end{bmatrix} \neq 0$.

For the choices of A,B,C,D matrices given by (5.13),

$$T = \begin{bmatrix} v_1 H + v_2 HF + \cdots + v_s HF^{s-1} \\ v_2 H + \cdots + v_s HF^{s-2} \\ \vdots \\ v_{s-1} H + v_s HF \\ v_s H \end{bmatrix}$$

and the conditions on the residual generator can be combined in a compact form as

$$[v_0, v_1, \ldots, v_{s-1}, v_s]\left[\tilde{\Gamma}_o \tilde{\Gamma}_w \; \tilde{\Gamma}_f\right] = [0\ 0\ *] \tag{5.27}$$

where

$$\tilde{\Gamma}_o = \begin{bmatrix} H \\ HF \\ \vdots \\ HF^{s-1} \\ HF^{s} \end{bmatrix}$$

$$\tilde{\Gamma}_w = \begin{bmatrix} K & 0 & \cdots & 0 & 0 \\ HE & K & \cdots & 0 & 0 \\ \vdots & \vdots & \ddots & \vdots & \vdots \\ HF^{s-2}E & HF^{s-3}E & \cdots & K & 0 \\ HF^{s-1}E & HF^{s-2}E & \cdots & HE & K \end{bmatrix}$$

$$\tilde{\Gamma}_f = \begin{bmatrix} J & 0 & \cdots & 0 & 0 \\ HG & J & \cdots & 0 & 0 \\ \vdots & \ddots & \ddots & \vdots & \vdots \\ HF^{s-2}G & HF^{s-3}G & \ddots & J & 0 \\ HF^{s-1}G & HF^{s-2}G & \cdots & HG & J \end{bmatrix}$$

and the symbol * indicates a nonzero matrix block. Equation (5.27) is exactly the condition given by Ding [61] for linear systems of the form (5.22). Thus, the results of Propositions 1, 2 and 3 provide a direct generalization of standard results on linear systems to nonlinear systems.

Remark 5.3: In the linear systems literature [61], the vectors $v_0, v_1, \dots, v_{s-1}, v_s$ that satisfy (5.27) are called parity vectors, and the set of parity vectors, when nonempty, defines a linear space which is called the parity space[127]. The nonlinear generalization developed in this subsection offers a nonlinear analog of parity vectors, defined as the ones satisfying (5.11), (5.19) and (5.20) or equivalently (5.21).

Remark 5.4: The parity vectors $v_0, v_1, \dots, v_{s-1}, v_s$ provide information about the measurements that are being used in the residual generator. If the j-th element of all of these vectors happens to be 0, this means that the measurement y_j is not used for fault detection since both B and D will have their j-th column identically zero. This situation may arise in applications and will be discussed in the applications subsection. In the event of multiple solutions for the set of parity vectors $v_0, v_1, \dots, v_{s-1}, v_s$, this feature might be used minimize the total number of sensors that are used.

Remark 5.5: In the majority of applications, process disturbances do not affect sensors and sensor disturbances do not affect the process. This motivates considering the following special case:

$$\dot{x} = F(x) + G(x)f + \sum_i E_i(x) w_i^p \tag{5.28}$$

$$y = H(x) + J(x)f + \sum_i K_i(x) w_i^s$$

where w_i^p denotes a process disturbance and w_i^s a sensor disturbance. For this special class of systems, the disturbance decoupling conditions (5.19) get simplified since for every disturbance, either $E_i(x)$ or $K_i(x)$ vanishes, depending on whether it is a process or sensor

disturbance. A sensor disturbance generally places more restrictions than a process disturbance. In particular, we see from (5.19) that

a) A process disturbance w_i^p places no restriction on v_0 since the corresponding $K_i(x) = 0$.

b) A sensor disturbance w_i^s imposes the restriction that $[v_0\ v_1\ \dots v_{s-1}\ v_s]K_i(x) = 0$. In case a disturbance affects only a specific sensor measuring y_j , this implies that the j-th element of $v_0, v_1, \dots, v_{s-1}, v_s$ must equal to 0, hence the measurement y_j must not be used in the residual generator.

Remark 5.6: For the special case of a scalar residual generator (s=1), the design conditions become

$$v_0 H(x) + L_F(v_1 H(x)) = 0$$

$$v_0 K_i(x) + L_{E_i}\big(v_1 H(x)\big) = 0\,, \qquad i = 1, \dots, m$$

$$v_1 K_i(x) = 0\,, \qquad i = 1, \dots, m$$

$$\begin{bmatrix} v_0 J(x) + L_G(v_1 H(x)) \\ v_1 J(x) \end{bmatrix} \neq \begin{bmatrix} 0 \\ 0 \end{bmatrix}$$

The above conditions take an even simpler form in case all states are measurable, i.e. $H(x) = x$:

$$v_0 x + v_1 F(x) = 0$$

$$v_0 K_i(x) + v_1 E_i(x) = 0\,, \qquad i = 1, \dots, m$$

$$v_1 K_i(x) = 0\,, \qquad i = 1, \dots, m$$

$$\begin{bmatrix} v_0 J(x) + v_1 G(x) \\ v_1 J(x) \end{bmatrix} \neq \begin{bmatrix} 0 \\ 0 \end{bmatrix}$$

5.4. Fault isolation

Till now we considered the problem of detecting a single scalar fault in the presence of disturbances. However, for systems with multiple faults, in addition to detecting the occurrence of faults it is necessary to correctly identify which fault/faults have occurred. To this end, consider the following system involving n_f possible faults:

$$\dot{x} = F(x) + \sum_{i=1}^{n_f} G_i(x) f_i \tag{5.29}$$

$$y = H(x) + \sum_{i=1}^{n_f} J_i(x) f_i$$

with state $x \epsilon P^n$, output $y \epsilon R^p$ and inputs $f_i \epsilon R$, $i = 1,2, \dots, n_f$, and with $F(x), H(x), G_i(x)$, $J_i(x)$ smooth functions, and assume that

(i) $n_f \leq p$ i.e. that the number of faults does not exceed the number of measurements.

(ii) the vectors $\begin{bmatrix} G_i(x) \\ J_i(x) \end{bmatrix}, i = 1, \dots, n_f$ are linearly independent for every x. In other words, that no fault can enter the model equations the same way as a linear combination of some other faults.

The above are clearly necessary conditions fault distinguishability.

Remark 5.7: In general, fault distinguishability may be defined as injectivity or left invertibility of the input/output map $(f_1, \dots, f_{nf}) \circ y$. Sufficient conditions may be derived by taking derivatives of each output of order up to the relative orders, and checking the left invertibility of the matrix of the coefficients of the input vector. Specifically, denoting

by ρ_j the relative order of output y_j with respect to the input vector and by $C(x)$ the $p \times n_f$ characteristic matrix, with entries

$$C_{ji}(x) = \begin{cases} L_{G_i} L_F^{\rho_j - 1} H_j(x), \text{if} \rho_j > 0 \\ J_{ji}(x), \text{if} \rho_j = 0 \end{cases}$$

a sufficient condition for left invertibility of the input/output map is $\text{Rank} C(x) = n_f$.

The residual generator formulated in Subsection 5.3 can be applied to build a fault isolation scheme in a straightforward manner. To isolate a specific fault f_k, one can try to construct a residual generator of the form:

$$\dot{z_k} = Az_k + B_k y \tag{5.30}$$
$$r_k = Cz_k + D_k y$$

which satisfies the fault detectability condition (5.20) for fault f_k and the disturbance decoupling conditions (5.19) for $w_i = f_i$, $i \neq k$, along with the functional observer condition (5.11).

If this is feasible for every fault, then one can build an overall system of residual generators, working in parallel, and each one detecting a specific fault (see also Figure 5.1):

$$\begin{gathered} \dot{z_1} = Az_1 + B_1 y \\ \vdots \\ \dot{z_{n_f}} = Az_{n_f} + B_{n_f} y \\ r_1 = Cz_1 + D_1 y \\ \vdots \end{gathered} \tag{5.31}$$

$$\mathrm{r}_{\mathrm{n_f}} = \mathrm{C}z_{\mathrm{n_f}} + \mathrm{D}_{\mathrm{n_f}}\mathrm{y}$$

where for any initial condition $\begin{bmatrix} x(0) \\ z_1(0) \\ \vdots \\ z_{n_f}(0) \end{bmatrix}$, $\lim_{t\to\infty} \mathrm{r_i}(t) = 0$ if $\mathrm{f_i}(t) = 0$
$\lim_{t\to\infty} \mathrm{r_i}(t) \neq 0$ if $\mathrm{f_i}(t) \neq 0$

This will solve the fault isolation problem.

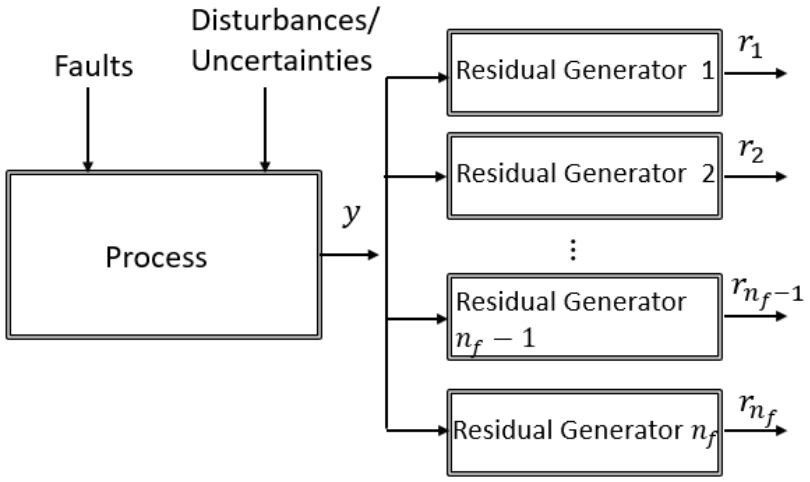

Figure 5.1 Fault isolation scheme (Reprinted with permission from [104]).

Remark 5.8: In the foregoing formulation, the same pair of (C, A) matrices are used in all residual generators, leading to the same assigned eigenvalues for all residual generators. More generally, different pairs of (C, A) matrices could be used.

Remark 5.9: System (5.29) involves faults but no disturbances. More generally, one could consider

$$\dot{x} = F(x) + \sum_{i=1}^{n_f} G_i(x) f_i + \sum_{i=1}^{m} E_i(x)\, w_i \tag{5.32}$$

$$y = H(x) + \sum_{i=1}^{n_f} J_i(x) f_i + \sum_{i=1}^{m} K_i(x)\, w_i$$

Every residual generator in this case, must satisfy disturbance decoupling conditions for all w_i in addition to the disturbance decoupling conditions for the other faults. In general, the disturbance decoupling conditions for w_i may impose an increase in the number of necessary measurements p, beyond the number of faults n_f.

5.5. Representative applications to chemical processes

In this subsection, case studies are presented to demonstrate the use of linear residual generators for fault diagnosis in nonlinear chemical process systems. In chemical processes, dynamic models are generally composed of conservation equations and inventory rate equations of the form: (Accumulation) = (In) – (Out) + (Generation), with the nonlinearities often appearing only in the generation terms, associated with kinetic rate expressions. This makes them amenable to the design conditions, with parity vectors that are independent of the reaction rates, which are often uncertain. Three application examples are studied in this subsection, specifically an anaerobic digester (bio-reactor), a continuous stirred tank reactor (CSTR) and a process network consisting of a CSTR and flash separator with a recycle stream.

5.5.1. Bioreactor

Anearobic digestion is a complex biochemical system, in which organic compounds are converted to biogas, consisting primarily of methane and carbon dioxide.

Anerobic digestion of a soluble susbtrate can be modeled as a two-step process: The acidogenic bacteria first convert the organic soluble substrate to a volatile fatty acid mixture and then the acids are utilized by methanogenic bacteria to produce the biogas. It is assumed that the digestion occurs in a CSTR (see Figure 5.2) and the feed only consists of soluble substrates and no biomass and no volatile fatty acids. The mathematical model is as follows:

$$\frac{dX_1}{dt} = -(D_r+f(t))X_1 + \frac{(\mu_{max1} + w(t))S_1}{K_{s1} + S_1}X_1$$

$$\frac{dS_1}{dt} = (D_r + f(t))(S_0 - S_1) - \frac{1}{Y_1}\frac{(\mu_{max1} + w(t))S_1}{K_{s1} + S_1}X_1$$

$$\frac{dX_2}{dt} = -\big(D_r + f(t)\big)X_2 + \frac{\mu_{max2}S_2}{K_{s2} + S_2}X_2 \qquad (5.33)$$

$$\frac{dS_2}{dt} = -(D_r + f(t))S_2 + \frac{c_{12}}{Y_1}\frac{(\mu_{max1} + w(t))S_1}{K_{s1} + S_1}X_1 - \frac{\mu_{max2}S_2}{K_{s2} + S_2}\frac{X_2}{Y_2}$$

$$y_1 = X_1$$

$$y_2 = S_1$$

$$y_3 = X_2$$

$$y_4 = S_2$$

where S_1 and S_2 are the concentration of the soluble organic substrate and volatile fatty acids respectively, X_1 and X_2 are the concentration of acidogenic and methanogenic biomass respectively, $\mu_1(S_1) = \frac{\mu_{max1}S_1}{K_{s1}+S_1}$ and $\mu_2(S_2) = \frac{\mu_{max2}S_2}{K_{s2}+S_2}$ are the specific growth rates of acidogenic and methanogenic bacteria respectively, with μ_{max1}, μ_{max2}, the corresponding maximum specific growth rates and K_{S1}, K_{S2} the saturation constants,

Y_1, Y_2 are the biomass yield coefficients, c_{12} is the stoichiometric coefficient of conversion of S_1 to S_2, S_0 is the concentration of organic substrate in the feed and D_r is the dilution rate. f(t) represents a fault in the dilution rate and w(t) represents the uncertainty in the maximum growth rate of acidogenic bacteria.

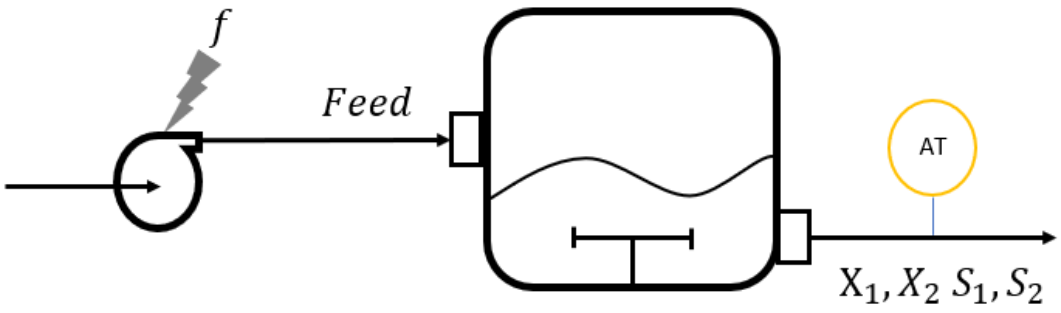

Figure 5.2 Bioreactor parameters (Reprinted with permission from [104]).

Table 5.1 Bioreactor parameters (Reprinted with permission from [104]).

Parameter	Value	Parameter	Value
D_r	0.2 d^{-1}	μ_{max2}	0.36 d^{-1}
μ_{max1}	4d^{-1}	Y_1	0.11 g/g
K_{s1}	0.023g/L	Y_2	0.003 g/mmol
S_0	10 g/L	c_{12}	16.95 mmol/g
K_{s2}	2.3 mmol/L		

The bio-reactor parameters are listed in Table 5.1 and the initial conditions are $X_1(0) = 0.1\text{g/L}\,, X_2(0) = 40\ \text{g/L}\,, S_1(0) = 10\text{g/L}, S_2(0) = 0.1\ \text{mmol/L}\,.$

The model (5.33) can be converted to deviation form, relative to reference steady state conditions corresponding to absence of faults or uncertainties: $X_1' = X_1 - X_{1,\text{ref}}, S_1' = S_1 - S_{1,\text{ref}}, X_2' = X_2 - X_{2,\text{ref}}\,, S_2' = S_2 - S_{2,\text{ref}}$ and $y_1' = X_1',\ y_2' = S_1',\ y_3' = X_2',\ y_4' = S_2'$, where the subscript ref denotes reference steady state value. The goal is to build a residual generator to detect the dilution rate fault f(t) in the presence of the disturbance w(t) in the acidogenic reaction rate expression.

To this end, a scalar residual generator is built (s=1), with the design conditions satisfied for following choice of parity vectors

$$v_0 = \left[D_r, D_r, D_r\left(-1 + \frac{1}{Y_1}\right)\frac{Y_1}{Y_2 c_{12}}, D_r\left(-1 + \frac{1}{Y_1}\right)\frac{Y_1}{c_{12}}\right] \tag{5.34}$$

$$v_1 = \left[1, 1, \left(-1 + \frac{1}{Y_1}\right)\frac{Y_1}{Y_2 c_{12}}, \left(-1 + \frac{1}{Y_1}\right)\frac{Y_1}{c_{12}}\right]$$

Using the parity vectors (5.34) and the design parameters $A = -\alpha_1 = -1,\ B = \alpha_1 v_1 - v_0,\ C = 1,\ D = -v_1$, leads to the following first order residual generator:

$$\frac{dz}{dt} = -z + (1 - D_r)\left(y_1' + y_2' + \left(-1 + \frac{1}{Y_1}\right)\frac{Y_1}{Y_2 c_{12}} y_3' + \left(-1 + \frac{1}{Y_1}\right)\frac{Y_1}{c_{12}} y_4'\right)$$

$$r = z - \left(y_1' + y_2' + \left(-1 + \frac{1}{Y_1}\right)\frac{Y_1}{Y_2 c_{12}} y_3' + \left(-1 + \frac{1}{Y_1}\right)\frac{Y_1}{c_{12}} y_4'\right) \tag{5.35}$$

From (5.3), we see that at steady state, the residual is given by

$$r_s = -D_r\left(X_{1,s}' + S_{1,s}' + \left(-1 + \frac{1}{Y_1}\right)\frac{Y_1}{Y_2 c_{12}} X_{2,s}' + \left(-1 + \frac{1}{Y_1}\right)\frac{Y_1}{c_{12}} S_{2,s}'\right) \tag{5.36}$$

and it is zero in the absence of fault and disturbances (when system is at reference steady state). One can also observe, from the steady state equations of the system (5.33) in deviation form, that the new steady state obtained in the presence of only disturbances and no fault, satisfies (5.36) with $r_s = 0$, as a result of the disturbance-decoupling property of the residual generator. On the other hand, again from (5.33) in deviation form, in the presence of a constant fault of size f_s,

$$D_r\left(X'_{1,s} + S'_{1,s} + \left(-1 + \frac{1}{Y_1}\right)\frac{Y_1}{Y_2 c_{12}}X'_{2,s} + \left(-1 + \frac{1}{Y_1}\right)\frac{Y_1}{c_{12}}S'_{2,s}\right)$$
$$+f_s\left(X_{1,s} + S_{1,s} + \left(-1 + \frac{1}{Y_1}\right)\frac{Y_1}{Y_2 c_{12}}X_{2,s} + \left(-1 + \frac{1}{Y_1}\right)\frac{Y_1}{c_{12}}S_{2,s}\right) = 0 \qquad (5.37)$$

where the subscript s denotes the new steady state of the bioreactor.

Combining (5.36) and (5.37), the conclusion is that

$$R_s = f_s\left(X_{1,s} + S_{1,s} + \left(-1 + \frac{1}{Y_1}\right)\frac{Y_1}{Y_2 c_{12}}X_{2,s} + \left(-1 + \frac{1}{Y_1}\right)\frac{Y_1}{c_{12}}S_{2,s}\right) \qquad (5.38)$$

From (5.38) it is clear that a constant fault of size $f_s \neq 0$, leads to a residual $r_s \neq 0$.

The residual generator is simulated for two cases: (i) No fault in the dilution rate but under uncertainty in the maximum growth rate of acidogenic bacteria of size $w(t) = 0.5\,\mu_{max1}$. (ii) A fault in the dilution rate which is a step of size 0.5 applied at t = 2 and $w(t) = 0.5\,\mu_{max1}$.

The residuals for cases (i) and (ii) are plotted in Figure 5.3. For the fault-free case the residual shows no deviation for all times whereas in case (ii), there is a deviation that starts at time t = 2 d (when the fault occurs) and settles at $r_s = 1.431$.

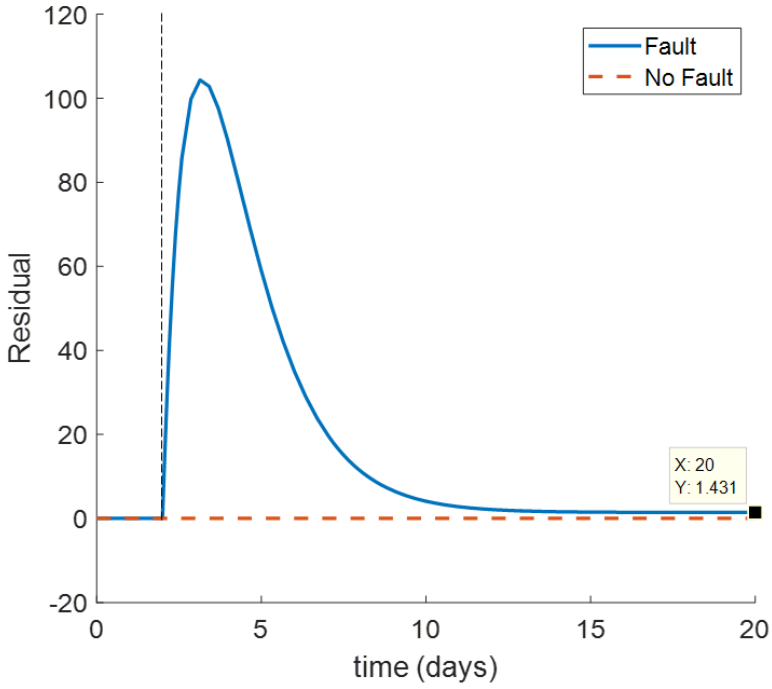

Figure 5.3 Residual as a function of time. Fault f(t)=0.5 occurs at time t= 2 d. The final value of the residual is 1.431 (Reprinted with permission from [104]).

Remark 5.10: As noted in Remark 5.4, parity vectors are not uniquely defined; multiple solutions could exist for v_0, v_1. For example, in the present problem,

$$v_0 = \left[\frac{1}{Y_1}\ 1\ 0\ 0\right] \tag{5.39}$$

$$v_1 = [\frac{D}{Y_1}\ D\ 0\ 0]$$

is an alternative pair of parity vectors. With this choice, only two measurements are required namely, the acidogenic biomass $y_1 = X_1$ and the soluble organic substrate $y_2 = S_1$.

5.5.2. Non-isothermal continuous stirred tank reactor (CSTR)

Consider a non-isothermal continuous stirred rank reactor (see Figure 5.4) where a chemical reaction A→ B takes place. It is assumed the reactor is well-mixed and has constant volume and the feed does not contain species B. The dynamics of the reactor are as follows:

$$\frac{dC_A}{dt} = \frac{F}{V}\left(C_{A,in} - C_A\right) - \left(k_0 + w(t)\right) \cdot R(C_A, \theta)$$

$$\frac{d\theta}{dt} = \frac{F}{V}(\theta_{in} - \theta) - \frac{UA}{\rho c_p V}\left(\theta - \theta_j\right) + \frac{-\Delta H_R}{\rho c_p}\left(k_0 + w(t)\right) \cdot R(C_A, \theta) \qquad (5.40)$$

$$\frac{d\theta_j}{dt} = \frac{F_j}{V_j}\left(\theta_{j,in} + f_2(t) - \theta_j\right) + \frac{UA}{\rho_j\, c_{p_j} V_j}\left(\theta - \theta_j\right)$$

$$y_1 = C_A + f_1(t)$$

$$y_2 = \theta$$

$$y_3 = \theta_j$$

where C_A, θ, θ_j and $C_{A,in}, \theta_{in}, \theta_{j,in}$ represent the concentration, reactor temperature and coolant temperature of the outlet and inlet streams respectively. F and F_j are the feed and coolant flowrates respectively. V and V_j are the reactor volume and cooling jacket volume respectively. $k_0 R(C_A, \theta)$ is the reaction rate, with $R(C_A, \theta) = e^{\frac{-E}{R\theta}} C_A^{1.2}$. ΔH_R is the enthalpy of the reaction. ρ, c_p and ρ_j, c_{p_j} are the densities and heat capacities of the reactor contents and cooling fluid respectively. All three states are assumed to be measurable. There is an uncertainty in the pre-exponential factor $w(t)$ of the reaction rate. Two faults are

considered namely a sensor fault in the concentration measurement ($f_1(t)$) and a process fault in the inlet jacket temperature ($f_2(t)$).

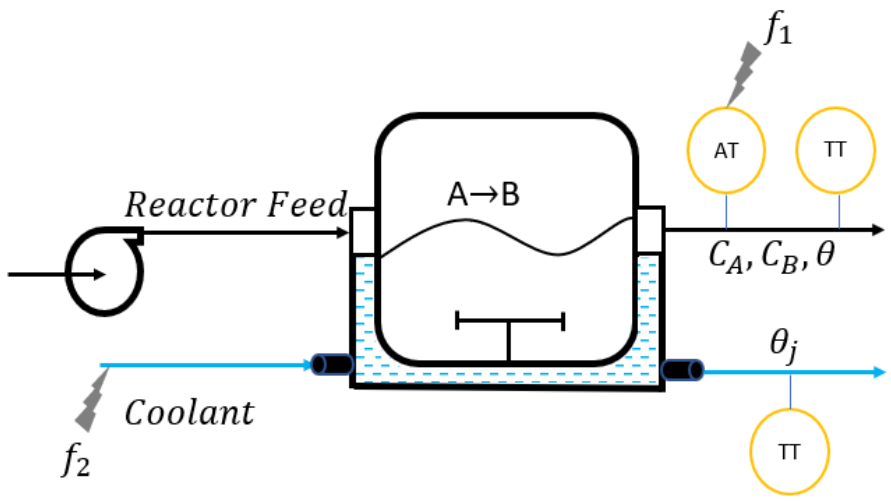

Figure 5.4 Continuous stirred tank reactor schematic (Reprinted with permission from [104]).

The model (5.8) can be converted to deviation form relative to reference conditions corresponding to absence of faults and uncertainties: $C'_A = C_A - C_{A,ref}, \theta' = \theta - \theta_{j,ref}$, $\theta'_j = \theta_j - \theta_{j,ref}$, where the subscript ref denotes reference steady state value.

Our goal is to design a fault diagnosis scheme that can detect and isolate faults f_1 and f_2 in the presence of uncertainties in the reaction rate. To this end, two scalar residual generators are built (i) to estimate the analytical sensor fault (f_1) while considering f_2 as an additional disturbance. (ii) to estimate inlet jacket temperature fault f_2 considering f_1 as an additional disturbance.

Residual generator 1: Detection of the analytical sensor fault f_1 while considering f_2 as an additional disturbance.

A scalar (s=1) residual generator can be designed with the following parity vectors:

$$v_0 = -\left[1, \frac{F\rho c_p + UA}{F(-\Delta H_R)}, \frac{-UA}{F(-\Delta H_R)}\right] \tag{5.41}$$

$$v_1 = -\left[\frac{V}{F}, \frac{V\rho c_p}{F(-\Delta H_R)}, 0\right]$$

and design parameters $A = -\alpha_1 = -1,\ B = \alpha_1 v_1 - v_0,\ C = 1,\ D = -v_1$:

$$\frac{dz_1}{dt} = -z_1 + \left(-\frac{V}{F} + 1\right)y_1' + \left(-\frac{V\rho c_p}{F(-\Delta H_R)} + \frac{F\rho c_p + UA}{F(-\Delta H_R)}\right)y_2' - \frac{UA}{F(-\Delta H_R)}y_3'$$

$$r_1 = z_1 + \frac{V}{F}y_1' + \frac{V\rho c_p}{F(-\Delta H_R)}y_2' \tag{5.42}$$

From (5.42), we see that at steady state, the residual is given by

$$r_{1,s} = (C_{A,s}' + f_{1,s}) + \frac{\rho c_p}{(-\Delta H_R)}\theta_s' + \frac{UA}{F(-\Delta H_R)}(\theta_s' - \theta_{j,s}') \tag{5.43}$$

On the other hand, from the first two steady state equations of the system in deviation form,

$$C_{A,s}' + \frac{\rho c_p}{(-\Delta H_R)}\theta_s' + \frac{UA}{F(-\Delta H_R)}(\theta_s' - \theta_{j,s}') = 0 \tag{5.44}$$

irrespective of the presence or absence of disturbance w or fault f_2. Therefore,

$$r_{1,s} = f_{1,s} \tag{5.45}$$

The steady state of the residual is nonzero when fault f_1 is nonzero.

Residual generator 2: Detection of the inlet cooling jacket temperature fault f_2 considering f_1 as an additional disturbance.

A scalar (s=1) residual generator can be designed with the following parity vectors:

$$v_0 = \left[0, +\frac{UA}{\rho_j C_{pj} F_j}, -1 - \frac{UA}{\rho_j C_{pj} F_j}\right] \tag{5.46}$$

$$v_1 = -\left[0, 0, \frac{V_j}{F_j}\right]$$

and design parameters $A = -\alpha_1 = -1,\ B = \alpha_1 v_1 - v_0,\ C = 1,\ D = -v_1$:

$$\frac{dz_2}{dt} = -z_2 - \left(\frac{UA}{\rho_j c_{p_j} F_j}\right) y_2' - \left(\frac{V_j}{F_j} - 1 - \frac{UA}{\rho_j c_{pj} F_j}\right) y_3'$$

$$r_2 = z_2 + \frac{V_j}{F_j} y_3' \tag{5.47}$$

From (5.47), we see that at steady state, the residual is given by

$$r_{2,s} = -\left(\frac{UA}{\rho_j c_{p_j} F_j}\right) \theta_s' + \left(1 + \frac{UA}{\rho_j c_{pj} F_j}\right) \theta_{j,s}' \tag{5.48}$$

On the other hand, from the third steady state equation of the system in deviation form,

$$\left(f_{2,s} - \theta_{j,s}'\right) + \frac{UA}{\rho_j\, c_{p_j} V_j} \left(\theta_s' - \theta_{j,s}'\right) = 0 \tag{5.49}$$

From (5.48) and (5.49), it is evident that the residual tracks the closure of the jacket energy balance with or without the fault and we have

$$r_{2,s} = f_{2,s} \tag{5.50}$$

The two residual generators are tested on the following scenario: $f_1(t) = \begin{cases} 0, & t < 1 \\ 0.1, & t \geq 1 \end{cases}, f_2(t) = \begin{cases} 0, & t < 2 \\ 10, & t \geq 2 \end{cases}$, $w(t)$ is uniformly distributed in the interval $[-0.05k_0, 0.05k_0]$. The data used for simulations are in Table 5.2 and the initial

conditions of the state variables are $C_A(0) = 0, \theta(0) = 300, \theta_j(0) = 278.15$. The residuals are plotted in Figure 5.6. Both residuals from time t =0 to 1 hr are identically 0. When the sensor fault occurs at time t=1hr a deviation is seen in r_1 whereas r_2 is identically zero. At time t=2hr a deviation is observed in r_2 indicating the presence of a fault in the inlet coolant temperature.

Table 5.2 CSTR parameters (Reprinted with permission from [104]).

Parameter	Value	Parameter	Value
F	4 m^3/hr	ρ	1000 kg/m^3
V	1 m^3	c_p	0.23 kJ/ (kg K)
V_j	0.03 m^3	ρ_j	1000 kg/m^3
$C_{A,in}$	$kmol/m^3$	c_{pj}	4 kJ/ (kg K)
θ_{in}	300K	U	500 W/(m^2 K)
$\theta_{j\,in}$	278.15 K	A	10 m^2
k_0	$3 \times 10^8 hr^{-1} m^{0.6} kmol^{-0.2}$	A_j	1 m^2
E	5×10^4 kJ/kmol	ΔH_R	-5×10^4 kJ /kmol

Remark 5.2: We see from (5.13) and (5.18) that in this particular application, the residuals at steady state are equal to the values of the respective faults. This can also be seen in Figure 5.5 where the residuals r_1 and r_2 tend to $f_1$and f_2 asymptotically. Thus, in addition to disturbance decoupled fault detection and isolation, the residuals provide estimates of the sizes of the faults.

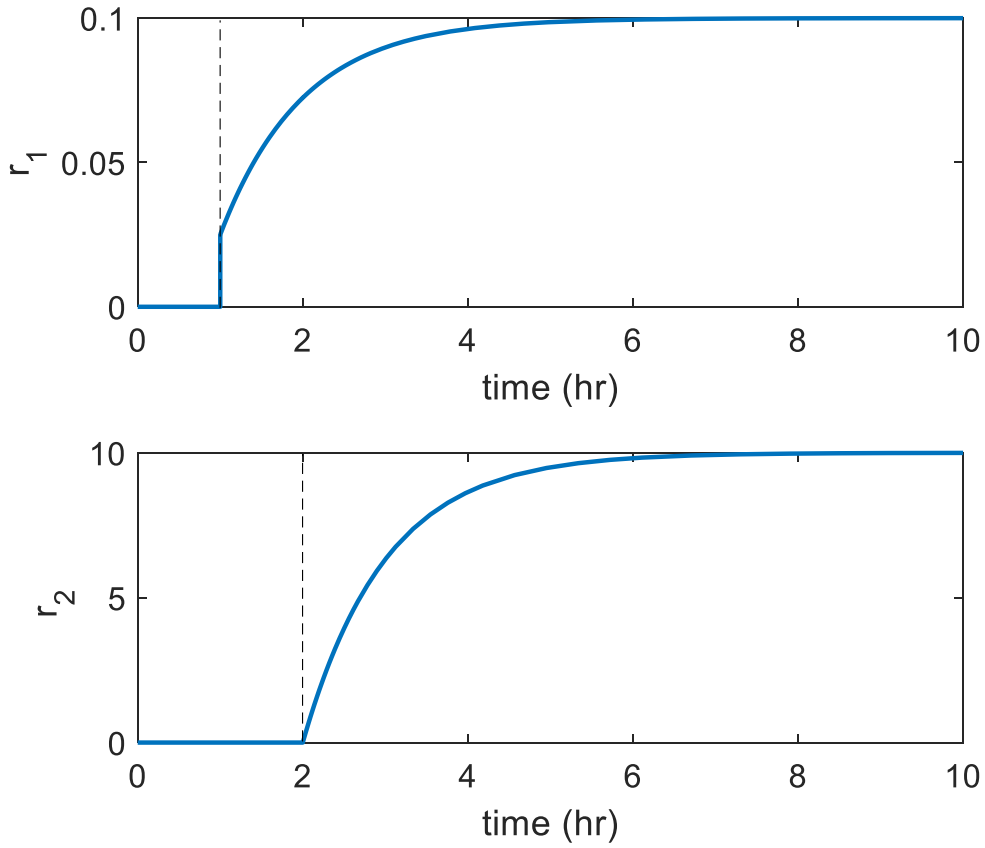

Figure 5.5 Residuals vs time for non-isothermal CSTR. Fault f_1 occurs at t=1 hr and f_2 at t=2 hr (Reprinted with permission from [104]).

5.5.3. Process network

As our final example, we consider a process network consisting of a CSTR and a flash separator (see Figure 5.6). This process is considerably more complex than the previous two case studies due to the presence of parallel reactions and a recycle stream. In this plant, two parallel exothermic chemical reactions $A \rightarrow B, A + A \rightarrow C$ with B being the desired product. The outlet stream of the reactor goes to the separator and a part of it is recycled back to the reactor. The mathematical model of the process takes the following form:

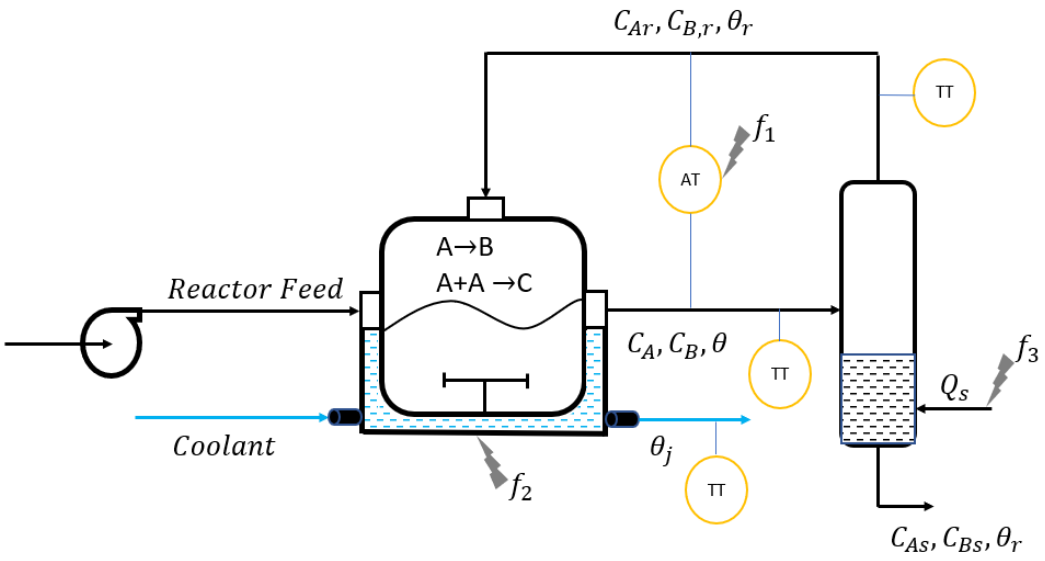

Figure 5.6 Reactor separator network (Reprinted with permission from [104]).

Reactor Mass Balance

$$\frac{dC_A}{dt} = \frac{F}{V}\left(C_{A,in} - C_A\right) + \frac{F_r}{V}(C_{Ar} - C_A) - \left(k_1 + w_1(t)\right) \cdot e^{\frac{-E_1}{R\theta}} C_A - \left(k_2 + w_2(t)\right) \cdot e^{\frac{-E_2}{R\theta}} C_A^2$$

$$\frac{dC_B}{dt} = \frac{F_r}{V}(C_{Br} - C_B) - \frac{F}{V}C_B + \left(k_1 + w_1(t)\right) \cdot e^{\frac{-E_1}{R\theta}} C_A$$

Reactor Energy Balance

$$\frac{d\theta}{dt} = \frac{F}{V}(\theta_{in} - \theta) + \frac{F_r}{V}(\theta_r - \theta) - \frac{\left(U + f_2(t)\right)A}{\rho c_p V}\left(\theta - \theta_J\right) + \frac{-\Delta H_{R1}}{\rho c_p}\left(k_1 + w_1(t)\right) \cdot e^{\frac{-E_1}{R\theta}} C_A + \frac{-\Delta H_{R2}}{\rho c_p}\left(k_2 + w_2(t)\right) \cdot e^{\frac{-E_2}{R\theta}} C_A^2$$

Cooling Jacket Energy Balance

$$\frac{d\theta_j}{dt} = \frac{F_j}{V_j}\left(\theta_{j,in} - \theta_j\right) + \frac{\left(U + f_2(t)\right)A}{\rho_j\, c_{p_j} V_j}\left(\theta - \theta_j\right) \tag{5.51}$$

Flash Separator Mass Balance

$$\frac{dC_{Af}}{dt} = \frac{F_b}{V_f}(C_A - C_{Af}) + \frac{F_r}{V_f}(C_A - C_{Ar}) + w_3$$

$$\frac{dC_{Bf}}{dt} = \frac{F_b}{V_f}(C_B - C_{Bf}) + \frac{F_r}{V_f}(C_B - C_{Br}) + w_4$$

$$C_{Ar} = \frac{\alpha_A C_{Bf} \rho}{\rho + (\alpha_A - 1) C_{Bf} MW_A}$$

$$C_{Br} = \frac{\alpha_B C_{Bf} \rho}{\rho + (\alpha_B - 1) C_{Bf} MW_B}$$

Flash Separator Energy Balance

$$\frac{d\theta_r}{dt} = \frac{F_b + F_r}{V_f}(\theta - \theta_r) + \frac{Q_f + f_3(t)}{\rho C p V_f}$$

Outputs

$$y_1 = C_A + f_1(t)$$

$$y_2 = C_B - f_1(t)$$

$$y_3 = \theta$$

$$y_4 = \theta_j$$

$$y_5 = C_{Ar} + f_1(t)$$

$$y_6 = C_{Br} - f_1(t)$$

$$y_7 = \theta_r$$

The reactor contains an inlet feed F consisting of only species A with concentration $C_{A,in}$ and a recycle feed F_r consisting of both A and B (C_{Ar} and C_{Br}). C_A and C_B are the concentrations of A and B in the reactor and the reactor temperature is θ, the inlet feed temperature is θ_{in} and heat is removed from the reactor via a coolant jacket with inlet temperature $\theta_{j,in}$ and outlet temperature θ_j. V and V_j are the reactor and cooling jacket volumes respectively. The desired reaction A→ B has a rate given by $k_1 e^{-\frac{E_1}{R\theta}} C_A$ and the undesired parallel reaction has a rate given by $k_2 e^{-\frac{E_2}{R\theta}} C_A^2$ where E_1, E_2 and k_1, k_2 are the activation energies and pre-exponential factors of the two reactions respectively and R in the exponential term of the reaction rate is the universal gas constant. ΔH_{R1} and ΔH_{R2} are the enthalpies of the two reactions respectively. ρ, c_p and ρ_j, c_{p_j} are the densities and heat capacities of the reactant and cooling fluid respectively. The outlet of the reactor feeds into a separator with volume V_f, operated at a temperature θ_r and has a heat input Q_f. The

concentrations of A and B at the bottom of the flash separator are given by C_{Af} and C_{Bf} respectively with a flow rate F_b. The relative volatilities and molecular weights of the two compounds are given by α_A, α_b and MW_A, MW_B respectively. The parameters used for the simulations are obtained from[104] and the initial conditions are $C_A(0) = 0, C_B(0) = 0, \theta(0) = 300, \theta_j(0) = 300, C_{As}(0) = 0, C_{Bs}(0) = 0, \theta_r(0) = 300$.

It is assumed that there are uncertainties, given by w_1 and w_2, in the pre-exponential factors of both the reaction rates. In addition, there are modeling uncertainties in the concentration equations for the flash separator characterized by w_3 and w_4. Three different faults are considered namely, (i) a sensor fault f_1 affecting the measurements of C_A, C_B, C_{Ar} and C_{Br}. (ii) a fault in the cooling jacket given by f_2, (iii) a fault in the heat input to the separator given by f_3. Our goal is to detect and isolate the presence of the three faults decoupled from the four uncertainties in the system. To this end, three residual generators are built, one for each fault of interest.

Like in the previous applications, the model is converted to deviation form relative to reference conditions corresponding to absence of faults and uncertainties: $C'_A = C_A - C_{A,ref}$, $C'_B = C_B - C_{B,ref}$, $\theta' = \theta - \theta_{j,ref}$, $\theta'_j = \theta_j - \theta_{j,ref}$, $C'_{Af} = C_{Af} - C_{Af,ref}$, $C'_{Bf} = C_{Bf} - C_{Bf,ref}, \theta'_r = \theta_r - \theta_{r.ref}$, where the subscript ref denotes reference steady state value.

Residual generator 1: Detection of sensor fault f_1 with all the other faults as disturbances. A scalar (s=1) residual generator can be designed with the following parity vectors:

$$v_0 = \left[\frac{-\Delta H_{R2}\left(\frac{F}{V}+\frac{F_r}{V}\right)}{\rho c_p}, \left(\frac{-\Delta H_{R2}}{\rho c_p} - \frac{-\Delta H_{R1}}{\rho c_p}\right)\left(\frac{F_r}{V}+\frac{F}{V}\right), \left(\frac{F_r}{V}+\frac{F}{V}\right), \frac{F_j \rho_j c_{pj}}{\rho c_p V}, -\frac{-\Delta H_{R2} F_r}{\rho c_p V}, \right.$$

$$\left. \frac{\left(\frac{-\Delta H_{R1}}{\rho c_p} - \frac{-\Delta H_{R2}}{\rho c_p}\right) F_r}{V}, -\frac{F_r}{V}\right]$$

$$v_1 = \left[\frac{-\Delta H_{R2}}{\rho c_p}, \left(\frac{-\Delta H_{R2}}{\rho c_p} - \frac{-\Delta H_{R1}}{\rho c_p}\right), 1, \frac{\rho_j c_{pj} V_j}{\rho c_p V}, 0, 0, 0\right] \tag{5.52}$$

and design parameters $A = -\alpha_1 = -1,\ B = \alpha_1 v_1 - v_0,\ C = 1,\ D = -v_1$:

$$\frac{dZ'}{dt} = -z' + \left(\frac{-\Delta H_{R2}}{\rho c_p} - \frac{-\Delta H_{R2}\left(\frac{F}{V}+\frac{F_r}{V}\right)}{\rho c_p}\right) y_1' + \left(\frac{-\Delta H_{R2}}{\rho c_p} - \frac{-\Delta H_{R1}}{\rho c_p}\right)\left(1 - \left(\frac{F_r}{V}+\frac{F}{V}\right)\right) y_2' + \left(1 - \right.$$

$$\left.\left(\frac{F_r}{V}+\frac{F}{V}\right)\right) y_3' + \left(\frac{\rho_j c_{pj} V_j}{\rho c_p V} - \frac{F_j \rho_j c_{pj}}{\rho c_p V}\right) y_4' + \frac{-\Delta H_{R2} F_r}{\rho c_p V} y_5' - \frac{\left(\frac{-\Delta H_{R1}}{\rho c_p} - \frac{-\Delta H_{R2}}{\rho c_p}\right) F_r}{V} y_6' + \frac{F_r}{V} y_7'$$

$$r_1 = z' - \frac{-\Delta H_{R2}}{\rho c_p} y_1' - \left(\frac{-\Delta H_{R2}}{\rho c_p} - \frac{-\Delta H_{R1}}{\rho c_p}\right) y_2' - y_3' - \frac{\rho_j c_{pj} V_j}{\rho c_p V} y_4' \tag{5.53}$$

Following the same steps as before, we have the following expression of the residual in terms of the fault of interest at steady state:

$$r_{1,s} = \left(-\left(\frac{-\Delta H_{R2}\left(\frac{F}{V}+\frac{F_r}{V}\right)}{\rho c_p}\right) + \left(\frac{-\Delta H_{R2}}{\rho c_p} - \frac{-\Delta H_{R1}}{\rho c_p}\right)\left(\left(\frac{F_r}{V}+\frac{F}{V}\right)\right)\right) f_{1,s} +$$

$$\left(\frac{-\Delta H_{R2} F_r}{\rho c_p V} + \frac{\left(\frac{-\Delta H_{R1}}{\rho c_p} - \frac{-\Delta H_{R2}}{\rho c_p}\right) F_r}{V}\right) f_{1,s} \tag{5.54}$$

Residual generator 2: Detection of cooling jacket fault f_2 with all the other faults as disturbances. A scalar (s=1) residual generator can be designed with the following parity vectors:

$$v_0 = \left[0,0,-\frac{UA}{\rho_j c_{pj} V_j}, \frac{UA}{\rho_j c_{pj} V_j} + \frac{F_j}{V_j}, 0,0,0\right]$$

$$v_1 = [\,0,0,0,1,0,0,0]$$

and design parameters $A = -\alpha_1 = -1,\ B = \alpha_1 v_1 - v_0,\ C = 1,\ D = -v_1$:

$$\frac{dZ'}{dt} = -z' + \left(\frac{UA}{\rho_j c_{p_j} F_j}\right) y_3' + \left(1 - \frac{UA}{\rho_j c_{pj} V_j} - \frac{F_j}{V_j}\right) y_4'$$

$$r_2 = z' - y_4' \tag{5.55}$$

Following the same steps as before, we have the following expression of the residual in terms of the fault of interest at steady state.

$$r_{2,s} = -\frac{f_{2,s} A}{\rho_j c_{p_j} F_j}\left(\theta_s - \theta_{j,s}\right) \tag{5.56}$$

Residual generator 3: Detecting fault in flash separator heat input f_3 with all the other faults as disturbances. A scalar (s=1) residual generator can be designed with the following parity vectors:

$$v_0 = \left[0,0,-\frac{F_b + F_r}{V_f}, 0,0,0, \frac{F_b + F_r}{V_f}\right]$$

$$v_1 = [\,0,0,0,0,0,0,1]$$

and design parameters $A = -\alpha_1 = -1,\ B = \alpha_1 v_1 - v_0,\ C = 1,\ D = -v_1$:

$$\frac{dZ'}{dt} = -z' + \left(\frac{F_b + F_r}{V_f}\right) y_3' + \left(1 - \frac{F_b + F_r}{V_f}\right) y_8'$$

$$r_3 = z' - y_8' \tag{5.57}$$

Following the same steps as before, we have the following expression of the residual in terms of the fault of interest at steady state.

$$r_{3,s} = \frac{-f_{3,s}}{\rho C p V_f} \tag{5.58}$$

The three residual generators are tested in a scenario with faults occurring in the following way: $f_1(t) = \begin{cases} 0, & t < 1 \\ 0.1, & t \geq 1 \end{cases}, f_2(t) = \begin{cases} 0, & t < 2 \\ -100e^{0.01t}, & t \geq 2 \end{cases}, f_3(t) = \begin{cases} 0, & t < 3 \\ 1000, & t \geq 3 \end{cases}$

Uncertainties w_1 and w_2 are uniformly distributed in the intervals $[-0.05k_{10}, 0.05k_{10}]$ and $[-0.05k_{20}, 0.05k_{20}]$ respectively. w_3 and w_4 are Gaussian distributions $N(0,1)$ and $N(0,2)$ respectively. The plots of the three residuals are shown in Figure 5.7. In the interval t=[0,1] all residuals are identically zero. When the sensor fault occurs at time t= 1hr there is a deviation in r_1 from sensor fault f_1 whereas residuals r_2 and r_3 are unaffected. After the onset of cooling jacket fault f_2 at time t=2hr, r_2 shows a deviation but r_3 remains identically equal to zero, until the fault f_3 in the heat input to the flash separator occurs at time t=3hr.

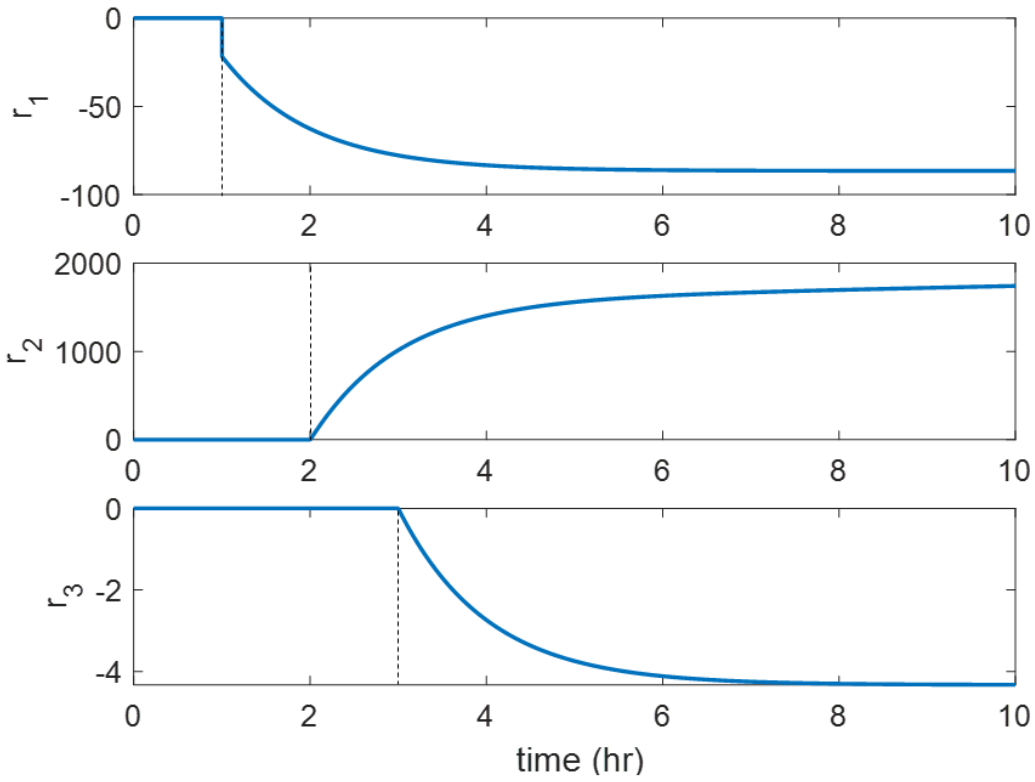

Figure 5.7 Residuals vs time for process network. Faults f_1, f_2, f_3 occur at t=1,2,3 hr respectively (Reprinted with permission from [104]).

Remark 5.11: It is to be noted that the requirement of full state measurements can be done away with if f_1 is absent or is assumed to be an additional disturbance. Isolation of faults f_2 and f_3 requires only the 3 temperature measurements, namely reactor, cooling jacket, and separator temperature.

5.5.4. Fault diagnosis in a CSTR with a general reaction model

The fault diagnosis scheme can be easily extended to a reactor undergoing with n species undergoing m reactions. The reactions occurring are as follows

$$\phi_{1,1}A_1 + \phi_{2,1}A_2 + \cdots + \phi_{n,1}A_n \leftrightarrow 0$$

$$\phi_{1,2}A_1 + \phi_{2,2}A_2 + \cdots + \phi_{n,2}A_n \leftrightarrow 0$$

$$\vdots$$

$$\phi_{1,m-1}A_1 + \phi_{2,m-1}A_2 + \cdots + \phi_{n,m-1}A_n \leftrightarrow 0$$

$$\phi_{1,m}A_1 + \phi_{2,m}A_2 + \cdots + \phi_{n,m}A_n \leftrightarrow 0$$

where $\phi_{i,j}$ is the stoichiometric coefficient for species A_i in reaction j.

The CSTR equations are as shown:

Species balance

$$\frac{dC_A}{dt} = \frac{F}{V}\left(C_{A,in} - C_A\right) + \Phi^T R$$

Reactor energy balance

$$\frac{dT}{dt} = \frac{F}{V}(T_{in} - T) + \frac{1}{\rho c_p}(-\Delta H)R - \frac{UA}{\rho c_p V}(T - T_j)$$

Jacket energy balance

$$\frac{dT_j}{dt} = \frac{F_j}{V_j}\left(T_{j,in} - T_j\right) + \frac{UA}{\rho c_p V}(T - T_j)$$

It is assumed that all the states are measurable. In the above equations C_A is the concentration vector for the species in the reactor, T and T_j are the reactor and coolant temperatures respectively $R = \begin{bmatrix} r_1 \\ r_2 \\ \vdots \\ r_m \end{bmatrix}$ and $-\Delta H = [-\Delta H_1, \ldots., -\Delta H_m]$ are the reaction rate and enthalpy vectors. $\Phi = \begin{bmatrix} \phi_{1,1} & \cdots & \phi_{n,1} \\ \vdots & \ddots & \vdots \\ \phi_{1,m} & \cdots & \phi_{n,m} \end{bmatrix}$ is the stoichiometric coefficient matrix.

5.5.4.1. Relationship between the scalar functional observer design condition and reaction invariants

The scalar functional observer design condition (for fault detection) in deviation form is as follows

$$v_0\begin{bmatrix} C_A' \\ T' \\ T_j' \end{bmatrix} + v_1\begin{bmatrix} \frac{F}{V}(-C_A') + \Phi^T(R' - R_s) \\ \frac{F}{V}(-T') + \frac{1}{\rho c_p}(-\Delta H)(R' - R_s) - \frac{UA}{\rho c_p V}(T' - T_j') \\ \frac{F_j}{V_j}(-T_j') + \frac{UA}{\rho_j c_{pj} V_j}(T' - T_j') \end{bmatrix} = 0$$

Where $v_0, v_1 \in R^{n+2}$For the nonlinearity in the reaction rate to cancel we must have

$$[v_{1,1} \dots, v_{1,n+1}, v_{1,n+2}]\begin{bmatrix} \Phi^T \\ -\frac{\Delta H}{\rho c_p} \\ 0 \end{bmatrix} = 0$$

$\begin{bmatrix} \Phi^T \\ -\Delta H \end{bmatrix}$ is of dimension $n + 2 \times m$.

Remark 5.12: Taking the transformation $\psi = [v_{1,1}, \dots, v_{1,n+1}]\begin{bmatrix} C_A' \\ T' \end{bmatrix}$ one can observe that

$$\frac{d\psi}{dt} = -\frac{F}{V}\psi - v_{1,n+1}\frac{UA}{\rho c_p V}(T' - T_j')$$

transformation vector $[v_{1,1}, \dots, v_{1,n+1}]$ is such that the dynamics of

$\psi = [v_{1,1}, \dots, v_{1,n+1}]\begin{bmatrix} C_A' \\ T' \end{bmatrix}$ is not explicitly dependent on the reaction rate.

5.5.4.2. Detecting a fault in a species measurement, in the presence of reaction rate uncertainties and disturbances in the heat transfer coefficient

Consider the following CSTR system

Species balance

$$\frac{dC_A}{dt} = \frac{F}{V}\left(C_{A,in} - C_A\right) + \Phi^T(R + W_R)$$

Reactor energy balance

$$\frac{dT}{dt} = \frac{F}{V}(T_{in} - T) + \frac{1}{\rho c_p}(-\Delta H)(R + W_R) - \frac{(UA)}{\rho c_p V}(T - T_j)$$

Jacket energy balance

$$\frac{dT_j}{dt} = \frac{F_j}{V_j}\left(T_{j,in} + f_c - T_j\right) + \frac{(UA)}{\rho c_p V}(T - T_j)$$

where $W_R \in R^m$ is the set of uncertainties in the reaction rates and w_c is the fault in the inlet coolant temperature. All states are measurable but out of n concentration measurements, 1 is susceptible to large faults and other n_w measurements are corrupted by disturbances (these could be large faults but are not of interest currently). WLOG it is assumed that the C_{A1} is the measurement that is susceptible to large faults and C_{Ai} with $i = 2, \ldots, n_w + 1$ are corrupted by disturbances.

5.5.4.2.1. Detecting fault in C_{A1}measurement while considering f_c as an additional disturbance

The functional observer condition is

$$v_0 \begin{bmatrix} C_A' \\ T' \\ T_j' \end{bmatrix} + v_1 \begin{bmatrix} \frac{F}{V}(-C_A') + \Phi^T(R' - R_s) \\ \frac{F}{V}(-T') + \frac{1}{\rho c_p}(-\Delta H)(R' - R_s) - \frac{UA}{\rho c_p V}\left(T' - T_j'\right) \\ \frac{F_j}{V_j}\left(-T_j'\right) + \frac{UA}{\rho_j c_{pj} V_j}(T' - T_j') \end{bmatrix} = 0$$

For the reaction rate nonlinearities to cancel,

$$[v_{1,1} \cdots, v_{1,n+1}, v_{1,n+2}] \begin{bmatrix} \Phi^T \\ -\frac{\Delta H}{\rho cp} \\ 0 \end{bmatrix} = 0$$

This leads to the following m equations

$$v_{1,1}\phi_{1,1} + \cdots + v_{1,n}\phi_{n,1} + v_{1,n+1}(-\Delta H_1) = 0$$

$$v_{1,1}\phi_{1,1} + \cdots + v_{1,n}\phi_{n,2} + v_{1,n+1}(-\Delta H_2) = 0$$

$$\vdots$$

$$v_{1,1}\phi_{i,m-,1} + \cdots + v_{1,n}\phi_{n,m-1} + v_{1,n+1}(-\Delta H_{m1}) = 0$$

The above set of equations will always have a non-trivial solution if rank $\begin{bmatrix} \Phi^T \\ -\frac{\Delta H}{\rho cp} \end{bmatrix} < n + 1$

Now other terms in the functional observer equation also must be cancelled this leads to the following $n + 2$ equations,

Species concentration elimination:

$$v_{0,1}C_{A,1} - v_{1,1}\frac{F}{V}C_{A,1} = 0$$

$$\vdots$$

$$v_{0,n}C_{A,n} - v_{1,n}\frac{F}{V}C_{A,n} = 0$$

Reactor temperature elimination

$$v_{0,n+1}T - v_{1,n+1}\frac{F}{V}T - v_{1,n+1}\frac{UA}{\rho c_p V}T + v_{1,n+2}\frac{UA}{\rho_j c_{pj} V_j}T = 0$$

Coolant jacket elimination

$$v_{0,n+2}T_j - v_{1,n+2}\frac{F_j}{V_j}T_j + v_{1,n+1}\frac{UA}{\rho c_p V}T_j - v_{1,n+2}\frac{UA}{\rho_j c_{pj} V_j}T_j = 0$$

For sensor disturbance decoupling, we have the following $2n_w$ equations $\forall j = 2,3 \ldots n_w + 1$

$$v_{1,j} = 0$$

$$v_{0,j} = 0$$

Finally, the coolant temperature disturbance decoupling condition results in an addition equation

$$v_{1,n+1} = 0$$

In summary, there are $n + m + 2n_w + 3$ homogenous equations with $2(n + 2)$ variables. A non-trivial solution always exists if $n - m > 2n_w - 1$

For fault detectability, from all the possible solutions we must choose one where $v_{1,1} \neq 0$.

Note: If we n_f concentration sensors are faulty in the system, then to isolate a particular fault say, in sensor i, we consider all other faults as disturbances i.e $n_w = n_f - 1$ and repeat the analysis before.

5.5.4.2.2. Detecting f_c while considering fault in C_{A1}as an additional disturbance

As we saw in the previous CSTR example (Subsection 5.5.2), no concentration measurements are required to detect f_c. Thus, following choice of $v_0$and v_1 can be chosen for the same,

$$v_0 = \left[\underbrace{0,0,\ldots,0}_{\text{n terms}}, +\frac{UA}{\rho_j C_{pj} F_j}, -1 - \frac{UA}{\rho_j C_{pj} F_j}\right]$$

$$v_1 = -\left[\underbrace{0,0,\ldots,0}_{\text{n terms}}, 0, \frac{V_j}{F_j}\right]$$

5.5.4.3. Detecting a fault in the inlet concentration, in the presence of reaction rate uncertainties and disturbances in the heat transfer coefficient

Consider the following CSTR system

Species balance $i = 1$

$$\frac{dC_{A1}}{dt} = \frac{F}{V}\left(C_{A1,in} + f - C_{A_1}\right) + \phi_1^T R$$

Species balance $i = 2, \dots, n_w + 1$

$$\frac{dC_{Ai}}{dt} = \frac{F}{V}\left(C_{Ai,in} + w_i - C_{A_i}\right) + \phi_i^T R$$

Species balance $i = n_w + 2, \dots, n$

$$\frac{dC_{Ai}}{dt} = \frac{F}{V}\left(C_{Ai,in} - C_{A_i}\right) + \phi_i^T R$$

Reactor energy balance

$$\frac{dT}{dt} = \frac{F}{V}(T_{in} - T) + \frac{1}{\rho c_p}(-\Delta H)(R + W_R) - \frac{(UA + w_h)}{\rho c_p V}(T - T_j)$$

Jacket energy balance

$$\frac{dT_j}{dt} = \frac{F_j}{V_j}\left(T_{j,in} - T_j\right) + \frac{(UA + w_h)}{\rho c_p V}\left(T - T_j\right)$$

where $W_R \in R^m$ is the set of uncertainties in the reaction rates and $f_i \in R$ is the fault affecting the inlet concentration of species $i = 1,2,3, \dots n_f$ and $\phi_i^T \in R^m$ represents the stoichiometric coefficients of species i in all the m reactions. The goal is to detect fault in the inlet concentration of species i.

For the reaction rate nonlinearities to cancel,

$$[v_{1,1}, v_{1,2}, \dots, v_{1,n}, v_{1,n+1}]\begin{bmatrix} \phi_1^T \\ \phi_2^T \\ \vdots \\ \phi_n^T \\ -\Delta H \end{bmatrix} = 0$$

This leads to the following m equations

$$v_{1,i}\phi_{i,1} + v_{1,n_f+1}\phi_{n_f+1,1} + \cdots + v_{1,n}\phi_{n,1} + v_{1,n+1}(-\Delta H_1) = 0$$

$$v_{1,i}\phi_{i,1} + v_{1,n_f+1}\phi_{n_f+1,2} + \cdots + v_{1,n}\phi_{n,2} + v_{1,n+1}(-\Delta H_2) = 0$$

$$\vdots$$

$$v_{1,i}\phi_{i,m-,1} + v_{1,n_f+1}\phi_{n_f+1,m-1} + \cdots + v_{1,n}\phi_{n,m-1} + v_{1,n+1}(-\Delta H_{m-1}) = 0$$

In addition, the following equations in the functional observer condition must hold Species concentration elimination:

$$v_{0,1}C_{A,1} - v_{1,1}\frac{F}{V}C_{A,1} = 0$$

$$\vdots$$

$$v_{0,n}C_{A,n} - v_{1,n}\frac{F}{V}C_{A,n} = 0$$

Reactor temperature elimination

$$v_{0,n+1}T - v_{1,n+1}\frac{F}{V}T - v_{1,n+1}\frac{UA}{\rho c_p V}T + \frac{UA}{\rho_j c_{pj} V_j}T = 0$$

Coolant jacket elimination

$$v_{0,n+2}T_j - v_{1,n+2}\frac{F_j}{V_j}T_j + v_{1,n+1}\frac{UA}{\rho c_p V}T_j - v_{1,n+2}\frac{UA}{\rho_j c_{pj} V_j}T_j = 0$$

The heat transfer coefficient disturbance decoupling condition results in an addition equation

$$v_{1,n+1}\frac{UA}{\rho c_p V}\left(T' - T_j'\right) - v_{1,n+2}\frac{UA}{\rho_j c_{pj} V_j}\left(T' - T_j'\right) = 0$$

Finally, there are n_w equations to decouple faults that are not of interest i.e $\forall j = 2, \ldots n_w + 1$

$$v_{1,j} = 0$$

In summary, there are $m + n + 2 + 1 + n_w$ equations and $2(n + 2)$ variables. There will always be a solution if $n - m > n_w - 1$. For fault detectability, from all the possible solutions we must choose one where $v_{1,1} \neq 0$.

Note: If we n_f faulty species inlets in the system, then to isolate a particular fault say, in species i, we consider all other faults as disturbances i.e $n_w = n_f - 1$ and repeat the analysis before.

5.6. Conclusion

This section derived necessary and sufficient conditions of existence of a linear residual generator for disturbance-decoupled fault detection in a nonlinear system. As long as, these conditions are satisfied, we have shown that the design of residual generators with eigenvalue assignment is straightforward. Using a linear residual generator for every fault, decoupled from the other faults and the system disturbances, immediately gives rise to a linear fault diagnoser for the nonlinear system. Not every nonlinear system satisfies the feasibility conditions for a linear residual generator. However, a large class of chemical processes involve “localized” nonlinearities in a way that they permit the design of linear residual generators. Therefore, the results of this work are expected to enable future industrial fault diagnosis applications.

6. FUNCTIONAL OSBERVERS FOR DISCRETE TIME NONLINEAR SYSTEMS- A PRELUDE TO FAULT DETECTION IN THE PRESENCE OF NOISES

6.1. Introduction

The goal of this section is to develop a direct generalization of Luenberger's functional observers to discrete time nonlinear systems. The concept of functional observers for discrete-time nonlinear systems is defined and the observer design problem is considered from the point of view of observer error linearization and is analogous to the methods in [70, 104]. It will be shown that, with the proposed formulation, easy-to-check necessary and sufficient conditions for the existence of such a functional observer can be derived, leading to simple formulas for observer design with eigenvalue assignment. Furthermore, the formulation also lends itself to fault detection and estimation in discrete-time nonlinear systems and this will also be investigated.

The outline of the section is as follows. In the next couple of subsections, the notion of functional observer for discrete time nonlinear systems will be defined in a manner completely analogous to Luenberger's definition [68-69] for linear systems and different approaches to solve the functional observer design problem will be outlined. Following this, notions of observer error linearization will be defined, and then necessary and sufficient conditions will be derived for the solution of the linearization problem, as well as a simple formula for the resulting functional observer. Subsequent subsections will study the use of the functional observers to detect and estimate faults in the presence of uncertainties/disturbances. Throughout the section, the functional observer design scheme

and the fault detection and estimation capabilities will be tested on a non-isothermal CSTR case study.

6.2. Functional observers for discrete-time nonlinear systems

Consider a discrete- time nonlinear system described by:

$$x(k+1) = F\big(x(k)\big) \tag{6.1}$$

$$y(k) = H\big(x(k)\big)$$

$$z(k) = q(x(k))$$

where:

$x \in \mathbb{R}^n$ is the system state

$y \in \mathbb{R}^p$ is the vector of measured outputs

$z \in \mathbb{R}$ is the (scalar) output to be estimated

and $F: \mathbb{R}^n \to \mathbb{R}^n, H: \mathbb{R}^n \to \mathbb{R}^p, q: \mathbb{R}^n \to \mathbb{R}$ are smooth nonlinear functions. The objective is to construct a functional observer of order $\nu < n$, which generates an estimate of the output z, driven by the output measurement y. In complete analogy to Luenberger's construction for the linear case, we seek a mapping

$$\xi = T(x) = \begin{bmatrix} T_1(x) \\ \vdots \\ T_\nu(x) \end{bmatrix}$$

from $\mathbb{R}^n$ to $\mathbb{R}^\nu$, to immerse system (6.1) to a ν -th order system ($\nu < n$), with input y and output z:

$$\xi(k+1) = \varphi(\xi(k), y(k)) \tag{6.2}$$

$$z(k+1) = \omega(\xi(k), y(k))$$

But in order for system (6.1) to be mapped to system (6.2) under the mapping $T(x)$, the following relations have to hold

$$\varphi(T(x), H(x)) = T\big(F(x)\big) \tag{6.3}$$

$$\omega\big(T(x), H(x)\big) = q(x) \tag{6.4}$$

The foregoing considerations lead to the following definition of a functional observer:

Definition 1: Given a dynamic system

$$x(k+1) = F\big(x(k)\big) \tag{6.1}$$

$$y(k) = H(x(k))$$

$$z(k) = q(x(k))$$

where $F: \mathbb{R}^n \to \mathbb{R}^n, H: \mathbb{R}^n \to \mathbb{R}^p, q: \mathbb{R}^n \to \mathbb{R}$ are smooth nonlinear functions, y is the vector of measured outputs and z is the scalar output to be estimated, the system

$$\hat{\xi}(k+1) = \varphi(\hat{\xi}(k), y(k)) \tag{6.5}$$

$$\hat{z}(k+1) = \omega(\hat{\xi}(k), y(k))$$

is a functional observer for (6.1) if the overall dynamics of (6.1) and (6.5) in series

$$x(k+1) = F(x(k))$$

$$\hat{\xi}(k+1) = \varphi(\hat{\xi}(k), H(x(k)))$$

possesses an invariant manifold $\hat{\xi} = T(x)$ with the property that $q(x) = \omega(T(x), H(x))$. If the functional observer (6.5) is initialized consistently with the system (6.1) i.e. if $\hat{\xi}(0) = T(x(0))$, then $\hat{\xi}(k) = T(x(k)),\ \forall\, k \in \mathbb{N}$ and therefore $\hat{z}(k) = \omega\left(\hat{\xi}(k), y(k)\right) = \omega\left(T\big(x(k)\big), H\big(x(k)\big)\right) = q\big(x(k)\big) \quad \forall\, k \in \mathbb{N}$, which means that the functional observer will be able to exactly reproduce z(k). In the presence of

initialization errors, additional stability requirements will need to be imposed on the $\hat{\xi}$-dynamics, for the estimate $\hat{z}(k)$ to asymptotically converge to $z(k)$. At this point, it is important to examine the special case of a linear system, where $F(x) = Fx, H(x) = Hx, q(x) = qx$ with F, H, q being $n \times n, p \times n, 1 \times n$ matrices respectively, and a linear mapping $T(x) = Tx$ is considered. Definition 1 tells us that for a linear time-invariant system

$$x(k+1) = Fx(k) \tag{6.6}$$

$$y(k) = Hx(k)$$

$$z(k) = qx(k)$$

the system

$$\hat{\xi}(k+1) = A\hat{\xi}(k) + By(k) \tag{6.7}$$

$$\hat{z}(k) = C\hat{\xi}(k) + Dy(k)$$

will be a functional observer if the following conditions are met:

$$TF = AT + BH$$

$$q = CT + DH$$

for some $\nu \times n$ matrix T. These are exactly the discrete-time version of Luenberger's conditions for a functional observer for linear continuous time-invariant systems [68-69]

6.3. Designing lower-order functional observers

For the design of a functional observer, one must be able to find a continuous map $T(x) = \begin{bmatrix} T_1(x) \\ \vdots \\ T_\nu(x) \end{bmatrix}$ to satisfy conditions (6.3) and (6.4) i.e. such that $T_j\big(F(x)\big), j = 1, \cdots, \nu$ is a function of $T_1(x), \cdots, T_\nu(x), H(x)$ and $q(x)$ is a function of $T_1(x), \cdots, T_\nu(x), H(x)$

However, such scalar functions $T_1(x), \cdots, T_\nu(x)$ may not exist, if ν is too small. Moreover, even when they do exist, there is an additional very important requirement: Since $T(F(x)) = \varphi(T(x), H(x))$ will define the right-hand side of the functional observer's dynamics, it must be such that the functional observer's dynamics is stable and the decay of the error is sufficiently rapid. All the above requirements can be satisfied if $\begin{cases} x(k+1) = F(x(k)) \\ y(k) = H(x(k)) \end{cases}$ is linearly observable and $\nu = n - p$:

Available design methods for reduced-order state observers [128] generate a functional observer of order $\nu = n - p$, by only modifying the output map of the observer (so that the estimate of z is the observer output instead of the entire state vector). The question is whether a lower order $\nu < n - p$ would be feasible and how to go about designing the functional observer. This is not an easy question because we will be trying to impose too many requirements at the same time.

For constructing the functional observer, one possible way involves identifying functions $T_1(x), \cdots, T_\nu(x)$ such that $T_j\big(F(x)\big), j = 1, \cdots, \nu$ and $q(x)$ can be expressed as functions of $T_1(x), \cdots, T_\nu(x)$ and the measured output. The second step is then to check stability of the error dynamics. This approach might be successful if the selection of $T_1(x), \cdots, T_\nu(x)$ could be directed by physical intuition.

Alternatively, one could try to follow the opposite path. As a first step, try to enforce stability: given some desirable dynamics for the observer $\hat{\xi}(k+1) = \varphi(\hat{\xi}, y)$, with φ so as to guarantee stability and rapid decay of the error, find $T(x) = \begin{bmatrix} T_1(x) \\ \vdots \\ T_\nu(x) \end{bmatrix}$ so that

$T(F(x)) = \varphi(T(x), H(x))$. The second step will then be to check if q(x) can be expressed as a function of $T(x)$ and $H(x)$.

6.4. Exact linearization of the functional observer

Along the second line of attack of the functional observer design problem, the most natural φ - function to work with is the linear one:

$$\varphi(\xi, y) = A\xi + By$$

It will then be the eigenvalues of the matrix A that will determine stability of the functional observer and the rate of decay of the error.

If we can find a continuously differentiable map $T(x)$ to satisfy the corresponding condition (6.3), i.e. to be a solution of the functional equation

$$T(F(x)) = AT(x) + BH(x)$$

for some Hurwitz matrix A, and if in addition $T(x)$ satisfies condition (6.4), i.e. that q(x) can be expressed as a function of $T(x)$ and $H(x)$, then we have a stable functional observer with linear dynamics. This leads to the Functional Observer Linearization Problem.

Given a system of the form (6.1), find a functional observer of the form

$$\hat{\xi}(k+1) = A\hat{\xi}(k) + By(k) \tag{6.8}$$

$$\hat{z}(k) = C\hat{\xi}(k) + Dy(k)$$

where A, B, C, D are $\nu \times \nu, \nu \times p, 1 \times \nu, 1 \times p$ matrices respectively, with A having stable eigenvalues. Equivalently, find a continuously differentiable mapping $T: \mathbb{R}^n \to \mathbb{R}^\nu$ such that

$$T(F(x)) = AT(x) + BH(x) \tag{6.9}$$

and

$$q(x) = CT(x) + DH(x) \tag{6.10}$$

Assuming that the above problem can be solved, the resulting error dynamics will be linear:

$$\hat{\xi}(k+1) - T(x(k+1)) = A\left(\hat{\xi}(k) - T\big(x(k)\big)\right)$$

$$\hat{z}(k) - z(k) = C\left(\hat{\xi}(k) - T\big(x(k)\big)\right) \tag{6.11}$$

from which $\hat{z}(k) - z(k) = CA^k\big(\hat{\xi}(0) - T(x(0))\big)$, with the matrix A having eigenvalues in the interior of the unit disc, the effect of the initialization error $\hat{\xi}(0) - T(x(0))$ will die out, and $\hat{z}(k)$ will approach $z(k)$ asymptotically.

Remark: It is possible to formulate a linearization problem in a slightly more general manner by including additive nonlinear output injection terms in the functional observer and a possibly nonlinear output map

$$\hat{\xi}(k+1) = A\hat{\xi}(k) + \mathcal{B}\big(y(k)\big) \tag{6.12}$$

$$\hat{z}(k) = \omega(\hat{\xi}(k), y(k))$$

where $\mathcal{B}$ (.) $\mathbb{R}^p \to \mathbb{R}^v$is the nonlinear output injection term. This generalization will also be considered in the next subsection.

In order to solve the Functional Observer Linearization Problem, it is natural to first try to solve the system of functional equations (6.9) given some small-size matrix A with fast enough eigenvalues, and then check to see if q(x) can be expressed as a function of $T(x)$ and $H(x)$ according to (6.10). If it can, we have a functional observer with linear

error dynamics; if not, we can try a different matrix A with different eigenvalues and/or larger size, up until we can satisfy both conditions.

The above approach will be feasible as long as the system of functional equations (6.9) is solvable. The following Proposition is an immediate consequence of Smajdor's Theorem [129]. (See also [130])

Proposition 1: *Let* $\mathrm{F}: \mathbb{R}^{\mathrm{n}} \to \mathbb{R}^{\mathrm{n}}, \eta: \mathbb{R}^{\mathrm{n}} \to \mathbb{R}^{\nu}$ *be real analytic functions with* $\mathrm{F}(0) = 0, \eta(0) = 0$ *and denote by* $\sigma(\mathrm{F})$ *the set of eigenvalues of* $\frac{\partial \mathrm{F}}{\partial \mathrm{x}}(0)$ *that are all either entirely inside or outside the unit disc. Also, let* A *be a* $\nu \times \nu$ matrix. *Suppose the eigenvalues* $\sigma(\mathrm{F})$*are not related to the eigenvalues* $\lambda_{\mathrm{j}}(\mathrm{j} = 1,2, \dots, \nu)$ *of* A *through any equation of the form* $\prod_{i=1}^{n} k_i^{m_i} = \lambda_j$with $\mathrm{k_i} \in \sigma(\mathrm{F})$, and m_i *are nonnegative integers, not all zero. Then the system of functional equations*

$$\mathrm{T}\big(\mathrm{F}(\mathrm{x})\big) = \mathrm{AT}(\mathrm{x}) + \eta(\mathrm{x}) \tag{6.13}$$

with initial condition $\mathrm{T}(0) = 0$, *admits a unique real analytic solution* $\mathrm{T}(\mathrm{x})$ *in a neighborhood of* $\mathrm{x} = 0$.

6.5. Necessary and sufficient conditions for solvability of the functional observer linearization problem

The trial-and-error approach outlined in the previous subsection is in principle feasible, but it is far from being practical due to the computational effort involved in solving (6.9), which will be multiplied by the number of trials until (6.10) is satisfied.

To be able to develop a practical approach for designing functional observers, it would be helpful to develop criteria to check if for a given set of ν eigenvalues, there exists a

functional observer whose error dynamics is governed by these eigenvalues. This will be done in the present subsection for the Functional Observer Linearization Problem.

The main result is as follows:

Proposition 2: *Under the assumptions of Proposition 1, for a real analytic nonlinear system of the form (2.1), there exists a functional observer of the form*

$$\hat{\xi}(k+1) = A\hat{\xi}(k) + By(k) \tag{6.8}$$

$$\hat{z}(k) = C\hat{\xi}(k) + Dy(k)$$

with the eigenvalues of A *being the roots of a given polynomial* $\lambda^{\nu} + \alpha_1\lambda^{\nu-1} + \cdots + \alpha_{\nu-1}\lambda + \alpha_{\nu}$,

if and only if $qF^{\nu}(x) + \alpha_1 qF^{\nu-1}(x) + \cdots + \alpha_{\nu-1}qF(x) + \alpha_{\nu}q(x)$ *is* $\mathbb{R}$*-linear combination of* $H_j(x), H_jF(x), \ldots, H_jF^{\nu}(x), j = 1, \cdots, p,$ *where in the above we have used the notation* $F^j(x) = \underbrace{F \circ F \ldots F \circ F(x)}_{j \text{ times}}$ *and* $H_jF(x) = (H_j \circ F)(x)$

Proof: Necessity: Suppose that there exists $T(x) = \begin{bmatrix} T_1(x) \\ T_2(x) \\ \vdots \\ T_{\nu}(x) \end{bmatrix}$ such that (6.9) is satisfied,

i.e

$$\begin{bmatrix} T_1F(x) \\ T_2F(x) \\ \vdots \\ T_{\nu}F(x) \end{bmatrix} = A\begin{bmatrix} T_1(x) \\ T_2(x) \\ \vdots \\ T_{\nu}(x) \end{bmatrix} + \begin{bmatrix} B_1H(x) \\ B_2H(x) \\ \vdots \\ B_{\nu}H(x) \end{bmatrix}$$

where $B_1, \ldots, B_{\nu}$ denote the rows of the matrix B. Now, we find that for k=1,2,3…

$$\begin{bmatrix} T_1F^k(x) \\ T_2F^k(x) \\ \vdots \\ T_{\nu}F^k(x) \end{bmatrix} = A^k\begin{bmatrix} T_1(x) \\ T_2(x) \\ \vdots \\ T_{\nu}(x) \end{bmatrix} + \begin{bmatrix} (A^{k-1}B)_1H(x) + (A^{k-2}B)_1HF(x) + \cdots + (B_1HF^{k-1}(x)) \\ (A^{k-1}B)_2H(x) + (A^{k-2}B)_2HF(x) + \cdots + (B_2HF^{k-1}(x)) \\ \vdots \\ (A^{k-1}B)_{\nu}H(x) + (A^{k-2}B)_{\nu}HF(x) + \cdots + (B_{\nu}HF^{k-1}(x)) \end{bmatrix}$$

and we can calculate

$$T_iF^{\nu}(x) + \alpha_1 T_iF^{\nu-1}(x) + \cdots + \alpha_\nu T_i(x) = ((A^{\nu-1}B)_i + \alpha_1(A^{\nu-2}B)_i + \cdots + \alpha_{\nu-1}B_i)H(x)$$
$$+((A^{\nu-2}B)_i + \cdots + \alpha_{\nu-2}B_i)HF(x)) + \cdots + (B_iHF^{\nu-1}(x))$$

where $\alpha_1, \alpha_2, \ldots, \alpha_\nu$ are the coefficients of the characteristic polynomial of the matrix A. At the same time the mapping $T(x)$ must satisfy (6.10) and we can calculate

$$qF^{\nu}(x) + \alpha_1 qF^{\nu-1}(x) + \cdots + \alpha_\nu q(x)$$
$$= (CA^{\nu-1}B + \alpha_1 CA^{\nu-2}B + \cdots + \alpha_{\nu-1}CB + \alpha_\nu D)H(x) +$$
$$(CA^{\nu-2}B + \cdots + \alpha_{\nu-2}CB + \alpha_{\nu-1}D)HF(x) + \cdots + (CB + \alpha_1 D)HF^{\nu-1}(x) + DHF^{\nu}(x)$$

That is,

$$qF^{\nu}(x) + \alpha_1 qF^{\nu-1}(x) + \cdots + \alpha_\nu q(x)$$
$$= \beta_0 HF^{\nu}(x) + \beta_1 HF^{\nu-1}(x) + \cdots + \beta_{\nu-1}HF(x) + \beta_\nu H(x) \qquad (6.14)$$

where

$$\beta_0 = D$$
$$\beta_1 = CB + \alpha_1 D$$
$$\beta_2 = CAB + \alpha_1 CB + \alpha_2 D$$
$$\vdots$$
$$\beta_{\nu-1} = CA^{\nu-2}B + \cdots + \alpha_{\nu-2}CB + \alpha_{\nu-1}D \qquad (6.15)$$
$$\beta_\nu = CA^{\nu-1}B + \alpha_1 CA^{\nu-2}B + \cdots + \alpha_{\nu-1}CB + \alpha_\nu D$$

Which proves that $qF^{\nu-1}(x) + \alpha_1 qF^{\nu-1}(x) + \cdots + \alpha_{\nu-1}qF(x) + \alpha_\nu q(x)$ is $\mathbb{R}$-linear combination of $H_j(x), H_jF(x), \ldots, H_jF^{\nu}(x), j = 1, \cdots, p,$

Sufficiency: Suppose that there exist constant row vectors β_0 , β_1, …, $\beta_{\nu-1}$, β_ν that satisfy (6.14). Consider the following choices of (A, B, C, D) matrices:

$$A = \begin{bmatrix} 0 & 0 & \cdots & 0 & -\alpha_\nu \\ 1 & 0 & \cdots & 0 & -\alpha_{\nu-1} \\ \vdots & \vdots & \ddots & \vdots & \vdots \\ 0 & \cdots & 1 & 0 & -\alpha_2 \\ 0 & \cdots & 0 & 1 & -\alpha_1 \end{bmatrix}, \qquad B = \begin{bmatrix} \beta_\nu - \alpha_\nu \beta_0 \\ \beta_{\nu-1} - \alpha_{\nu-1}\beta_0 \\ \beta_{\nu-2} - \alpha_{\nu-2}\beta_0 \\ \vdots \\ \beta_1 - \alpha_1 \beta_0 \end{bmatrix},$$

$$C = [0\ 0 \cdots 0\ 1], \qquad D = \beta_0 \tag{6.16}$$

For the above A and C matrices (in observer canonical form), the design conditions (6.9) and (6.10) can be written component-wise as follows:

$$T_1 F(x) + \alpha_\nu T_\nu(x) - B_1 H(x) = 0 \tag{6.17}$$

$$T_2 F(x) - T_1(x) + \alpha_{\nu-1} T_\nu(x) - B_2 H(x) = 0 \tag{6.18}$$

$$\vdots$$

$$T_\nu F(x) - T_{\nu-1}(x) + \alpha_1 T_\nu(x) - B_\nu H(x) = 0 \tag{6.19}$$

$$T_\nu(x) + DH(x) = q(x) \tag{6.20}$$

We observe that the above equations are easily solvable sequentially for $T_\nu(x), T_{\nu-1}(x), \ldots, T_1(x)$, starting from the last equation and going up. In particular, for the chosen B and D matrices, we find from (6.20), (6.19), … , (6.18):

$$T_\nu(x) = -\beta_0 H(x) + q(x)$$

$$T_{\nu-1}(x) = -\beta_0 HF(x) - \beta_1 H(x) + qF(x) + \alpha_1 q(x)$$

$$\vdots$$

$$T_1(x) = -\beta_0 HF^{\nu-1}(x) - \cdots - \beta_{\nu-2} HF(x) - \beta_{\nu-1} H(x) + qF^{\nu-1}(x) + \alpha_1 qF^{\nu-2}(x) + \cdots + \alpha_{\nu-1} q(x)$$

whereas (6.17) gives:

$$\beta_0 HF^{\nu}(x) + \beta_1 HF^{\nu-1}(x) + \cdots + \beta_{\nu-1} HF(x) + \beta_{\nu} H(x)$$

$$= qF^{\nu}(x) + \alpha_1 qF^{\nu-1}(x) + \cdots + \alpha_{\nu} q(x)$$

which is exactly (6.14). Thus, we have proved that

$$T(x) = \begin{bmatrix} \begin{pmatrix} -\beta_0 HF^{\nu-1}(x) - \cdots - \beta_{\nu-2} HF(x) - \beta_{\nu-1} H(x) + \\ qF^{\nu-1}(x) + \alpha_1 qF^{\nu-2}(x) + \cdots + \alpha_{\nu-1} q(x) \end{pmatrix} \\ \vdots \\ -\beta_0 HF(x) - \beta_1 H(x) + qF(x) + \alpha_1 q(x) \\ -\beta_0 H(x) + q(x) \end{bmatrix} \tag{6.21}$$

satisfies the design conditions (6.9) and (6.10) when β_0 , β_1, …, $\beta_{\nu-1}$, β_{ν} satisfy (6.14) and the A, B, C, D matrices are chosen according to (6.16).

It is important to observe that the sufficiency part of the proof is constructive: it gives an explicit solution of the design equations (6.9) and (6.10) in terms of the vectors β_0 , β_1, …, $\beta_{\nu-1}$, β_{ν} that satisfy (6.14).

6.6. Lower order functional observers for linear systems

The results of the previous subsection can now be specialized to linear time-invariant systems. The following is a Corollary to Proposition 2.

Proposition 3: For a linear time-invariant system of the form

$$x(k+1) = Fx(k) \tag{6.6}$$

$$y(k) = Hx(k)$$

$$z(k) = qx(k)$$

there exists a functional observer of the form

$$\hat{\xi}(k+1) = A\hat{\xi}(k) + By(k) \tag{6.7}$$

$$\hat{z}(k) = C\hat{\xi}(k) + Dy(k)$$

with the eigenvalues of A being the roots of a given polynomial $\lambda^{\nu} + \alpha_1\lambda^{\nu-1} + \cdots + \alpha_{\nu-1}\lambda + \alpha_{\nu}$, if and only if

$$(qF^{\nu} + \alpha_1 qF^{\nu-1} + \cdots + \alpha_{\nu-1}qF + \alpha_{\nu}q) \in \text{span}\{H_j, H_jF, \ldots, H_jF^{\nu}, j = 1, \cdots, p\} \quad (6.22)$$

The above Proposition provides a simple and easy-to-check feasibility criterion for a lower-order functional observer with a pre-specified set of eigenvalues governing the error dynamics. Moreover, an immediate consequence of the Proposition 3 is the following:

Corollary: Consider a linear time-invariant system of the form (6.6) with observability index ν_o. Then, there exists a functional observer of the form (6.7) of order $\nu = \nu_o - 1$ and arbitrarily assigned eigenvalues.

The result of the Corollary, derived through a different approach, is exactly the discrete-time version of Luenberger's result for functional observers for continuous linear time-invariant systems [68-69].

6.7. Non-isothermal CSTR case study

Consider a non-isothermal Continuous Stirred Tank Reactor (CSTR) undergoing N-alkyl pyridine oxidation with hydrogen peroxide. The product of the reaction, Alkyl Pyridine N-Oxides is an important intermediate in several important reactions in pharmaceutical industry including the production of anti-ulcer and anti-inflammatory drugs [131]. It is assumed the reactor is well-mixed and has constant volume with an inlet stream containing N-methyl pyridine (A) + catalyst Z (assumed to be fully dissolved) and hydrogen peroxide (B). The catalyst is assumed to be completely dissolved in the pyridine

stream and its concentration is assumed to be constant in the reactor [131] The dynamics of the reactor [131] is described by:

$$\frac{dC_A}{dt} = \frac{F}{V}\left(C_{A,in} - C_A\right) - R(C_A, C_B, \theta)$$

$$\frac{dC_B}{dt} = \frac{F}{V}\left(C_{B,in} - C_B\right) - R(C_A, C_B, \theta)$$

$$\frac{d\theta}{dt} = \frac{F}{V}(\theta_{in} - \theta) - \frac{US_A}{\rho c_p V}\left(\theta - \theta_j\right) + \frac{-\Delta H_R}{\rho c_p} R(C_A, C_B, \theta) \tag{6.23}$$

$$\frac{d\theta_j}{dt} = \frac{F_j}{V_j}\left(\theta_{j,in} - \theta_j\right) + \frac{US_A}{\rho_j\, c_{p_j} V_j}\left(\theta - \theta_j\right)$$

$$y_1 = \theta$$

$$y_2 = \theta_j$$

where $R(C_A, C_B, \theta) = \frac{A_1 e^{-\frac{E_1}{\theta}} A_2 e^{-\frac{E_2}{\theta}} C_A C_B Z}{1 + A_2 e^{-\frac{E_2}{\theta}} C_B} + A_3 e^{-\frac{E_3}{\theta}} C_A C_B$ is the reaction rate and

the state vector $x = \left[C_A, C_B\, \theta, \theta_j\right]$ consists of N-methyl pyridine concentration, hydrogen peroxide concentration, reactor temperature and coolant temperature of the outlet and $C_{A,in}, C_{B,in}, \theta_{in}, \theta_{j,in}$ represent the inlet values of the state values. F and F_j are the inlet feeds and coolant flowrates respectively. V and V_j are the reactor volume and cooling jacket volume respectively. Parameters A_1, A_2, A_3 are the pre-exponential factors in the reaction rate. ΔH_R is the enthalpy of the reaction. ρ, c_p and ρ_j, c_{p_j} are the densities and heat capacities of the reactor contents and cooling fluid respectively.

The parameter values are as follows, $C_{A,in} = 2\,\frac{mol}{L}, C_{B,in} = 1.5\,\frac{mol}{L}, \theta_{in} = 373\ K, \theta_{j,in} = 300\ K, F = 0.1\,\frac{L}{min}, F_j = 1\,\frac{L}{min}, V = 0.5\ L, V_j = 3 \times 10^{-2} L, A_1 = e^{8.08} L\ mol^{-1} s^{-1}, A_2 = e^{28.12} L\ mol^{-1} s^{-1}, A_3 = e^{25.12} L\ mol^{-1}. \Delta H_R = -160\,\frac{kJ}{mol}, \rho = 1200\,\frac{g}{L}, \rho_j = 1000\,\frac{g}{L}$ $c_{p_j} = 3\,\frac{J}{gK}$. c_p=3.4$\frac{J}{gK}$ U=0.942 $\frac{W}{m^2 K}, S_A = 1\ m^2$, Z=0.0021 $\frac{mol}{L}$, E_1 =3952 K, E_2 =7927 K, E_3 =12989 K.

The model equations (6.23) are discretized using Euler's method. This is easy to implement and preserves the nonlinearities of the original continuous-time system. The discretized equations are

$$C_A(k+1) = C_A(k) + \delta_t \left(\frac{F}{V}\left(C_{A,in} - C_A(k)\right) - R(C_A(k), C_B(k), \theta(k)) \right)$$

$$C_B(k+1) = C_B(k) + \delta_t \left(\frac{F}{V}\left(C_{B,in} - C_B(k)\right) - R(C_A(k), C_B(k), \theta(k)) \right)$$

$$\begin{aligned} \theta(k+1) = \theta(k) &+ \delta_t \left(\frac{-\Delta H_R}{\rho c_p} R\left(C_A(k), C_B(k), \theta(k)\right) \right) \\ &+ \delta_t \left(\frac{F}{V}\left(\theta_{in} - \theta(k)\right) - \frac{U S_A}{\rho c_p V}\left(\theta(k) - \theta_j(k)\right) \right) \end{aligned} \tag{6.24}$$

$$\theta_j(k+1) = \theta_j(k) + \delta_t \left(\frac{F_j}{V_j}\left(\theta_{j,in} - \theta_j(k)\right) + \frac{U S_A}{\rho_j\, c_{p_j} V_j}\left(\theta(k) - \theta_j(k)\right) \right)$$

$$y_1(k) = \theta(k)$$

$$y_2(k) = \theta_j(k)$$

where $\delta_t = 0.05s$ is the sampling period. The reactor temperature θ and the coolant temperature θ_j are measured. Both N-methyl pyridine and hydrogen peroxide are hazardous chemicals and it is important to monitor the sum of the concentration of these chemicals in the reactor. Thus, our goal is to design a functional observer that tracks the total concentration of the reactants $z(k) = C_A(k) + C_B(k)$ in the reactor.

The initial condition of the reactor is $C_A(0) = 0, C_B(0) = 0, \theta(0) = 300, \theta_j(0) = 300$ and the model is can be converted to deviation form $C_A' = C_A - C_{A,ref}, C_B' = C_B - C_{B,ref}\, \theta' = \theta - \theta_{ref},\ \theta_j' = \theta_j - \theta_{j,ref}$ and $y_1' = \theta',\ y_2' = \theta_j'$ where the subscript ref denotes reference steady state value, with $C_{A,ref} = 0.6718 \frac{mol}{L}, C_{B,ref} = 0.1718 \frac{mol}{L}, \theta_{ref} = 409.8698, \theta_{j,ref} = 300.0254$

A scalar functional observer is built (ν =1) and the necessary and sufficient condition (6.14) is satisfied for the following choice of $\beta_0, \beta_1 \in \mathbb{R}^2$ and $\alpha_1 \in \mathbb{R}$

$$\beta_0 = \left[-\frac{2\rho c_p}{-\Delta H_R}, 1\right]$$

$$\beta_1 = \left[\frac{2\rho c_p}{-\Delta H_R}\left(1 - \frac{F\delta_t}{V} - \frac{US_A\delta_t}{\rho c_p V}\right) - \frac{US_A\delta_t}{\rho_j c_{pj} V_j}, \frac{F_j\delta_t}{V_j} + \frac{US_A\delta_t}{\rho_j c_{pj} V_j} + \frac{2US_A\delta_t}{-\Delta H_R V} - 1\right] \quad (6.25)$$

$$\alpha_1 = \frac{\delta_t F}{V} - 1$$

Remark 6.2: A sampling rate δ_t that satisfies $\delta_t < 2\left(\frac{V}{F}\right)$ ensures $-1 < \alpha_1 < 1$.

The resulting functional observer is

$$\hat{\xi}(k+1) = -\left(\frac{\delta_t F}{V} - 1\right)\hat{\xi}(k) - \delta_t\left[\frac{2US_A}{(-\Delta H_R)V} + \frac{US_A}{\rho_j c_{pj} V_j}\right] y_1'(k)$$
$$+\delta_t\left[\frac{F_j}{V_j} - \frac{F}{V} + \frac{US_A}{\rho_j c_{pj} V_j} + \frac{2US_A}{-\Delta H_R V}\right] y_2'(k) \qquad (6.26)$$

$$\hat{z}(k) = \hat{\xi}(k) - \frac{2\rho c_p}{(-\Delta H_R)} y_1'(k) + y_2'(k)$$

The estimate generated by the functional observer (in non-deviation form) and the estimation error plotted in Figure 6.1.

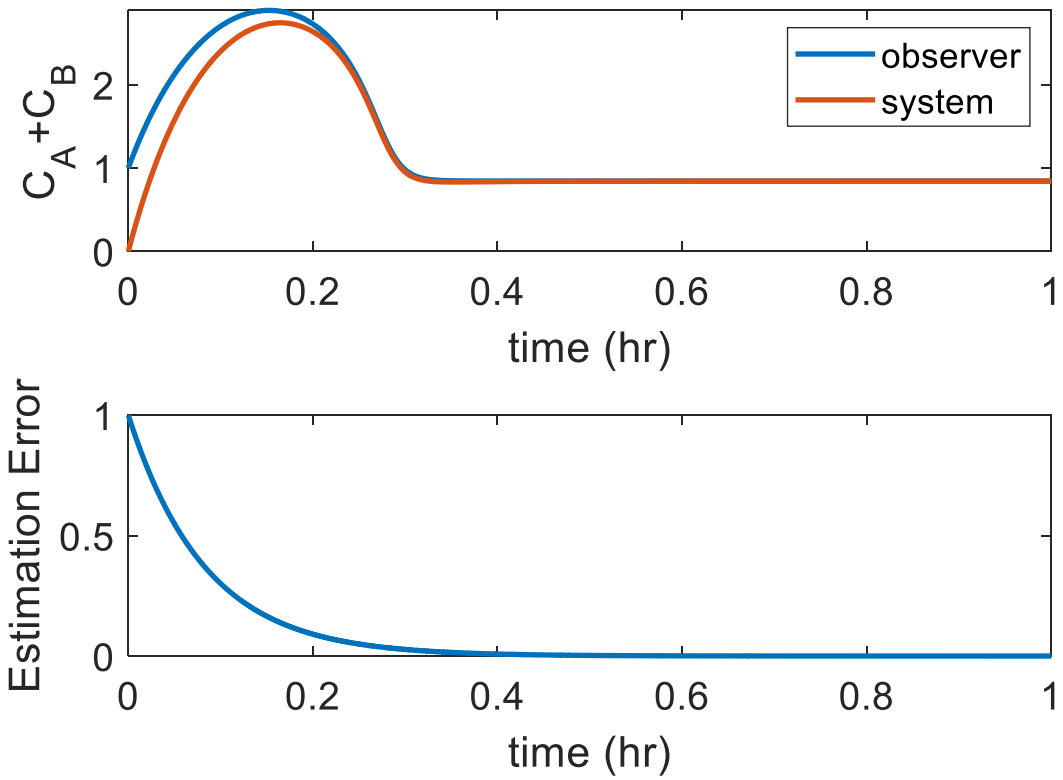

Figure 6.1 Top-Estimates and true profiles in non-deviation form in the presence of initialization error =1 where T(x) is given by equation 6.21. Bottom- estimation error.

6.8. Application 1- fault detection

In this subsection the problem of fault detection will be studied on the basis of estimating an output z (also known as the residual in fault diagnosis literature), that is identically zero under normal operation, nonzero under an abnormal situation, and is unaffected by a set of prespecified potential disturbances. Thus, the fault detection problem is in a sense a special case of the functional observer problem, where the tracked output has $q(x) = 0$, however the functional observer (also called a residual generator) must satisfy additional conditions of disturbance decoupling. Consider a nonlinear process described by:

$$x(k+1) = F\big(x(k), W(k), f(k)\big)$$

$$y(k) = H\big(x(k)\big) + G(x)W(x) + E(x)f(k) \qquad (6.27)$$

$$z = q(x) = 0$$

where $x \epsilon R^n$ denotes the vector of states, $y \epsilon R^p$ denotes the vector of measured outputs. $f \epsilon R$ and $W \epsilon R^m, i = 1,2, \dots, m$ are the fault and the disturbances/uncertainties respectively (system inputs) and $E(x), F(x), G(x), H(x)$ are smooth functions. Under normal operation of the process, the input f (fault) is identically equal to zero, however in an abnormal situation (equipment failure, human errors, power failures etc.), f becomes nonzero, and this what needs to be detected based on the measurements. The input W describes the normal variability of process conditions (disturbances) and/or model uncertainty. It is in the presence of this variability that the fault must be detected, and the conclusion (normal

or faulty operation) must be unaffected by the presence of W (disturbance-decoupled detection).

A linear functional observer

$$\hat{\xi}(k+1) = A\hat{\xi}(k) + By(k) \tag{6.28}$$

$$\hat{z}(k) = C\hat{\xi}(k) + Dy(k)$$

is built to track the output z in (6.27). To this end, it is desired that the response of the residual $\hat{z}$ in the series connection of (6.27) followed by (6.28)

$$\begin{bmatrix} x(k+1) \\ \hat{\xi}(k+1) \end{bmatrix} = \begin{bmatrix} F\big(x(k), W(k), f(k)\big) \\ A\hat{\xi}(k) + B\big[H\big(x(k)\big) + G\big(x(k)\big)W(k) + E\big(x(k)\big)f(k)\big] \end{bmatrix} \tag{6.29}$$

$$\hat{z}(k) = \Big[C\hat{\xi} + D\big[H\big(x(k)\big) + G(x)W(x) + E(x)f(k)\big]\Big]$$

has the following properties:

(i) $\hat{z}(k)$ asymptotically approaches zero when f is identically zero

(ii) $\hat{z}(k)$ is unaffected by the disturbances W

(iii) $\hat{z}(k)$ is affected by the fault f.

In other words, for any initial conditions $\begin{bmatrix} x(0) \\ \hat{\xi}(0) \end{bmatrix}$ and any disturbances W(k),

$$\lim_{k\to\infty} \hat{z}(k) = 0 \text{ if } f(k) = 0$$
$$\lim_{k\to\infty} \hat{z}(k) \neq 0 \text{ if } f(k) \neq 0$$

The responsiveness of $\hat{z}$ to faults and insensitivity to disturbances ensures fault detection while precluding the possibility of false alarms.

For (i) to hold in the absence of disturbances, there must exist a differentiable map $T(x)$ from R^n to R^v such that:

$$T\big(F_*(x)\big) = AT(x) + BH(x) \tag{6.30}$$

$$0 = CT(x) + DH(x) \tag{6.31}$$

where $F_*(x) = F(x, 0,0)$. The functional observer's error dynamics then follows:

$$\hat{\xi}(k+1) - T\big(x(k+1)\big) = A\left(\hat{\xi}(k) - T\big(x(k)\big)\right) + \underbrace{B[G(x(k))W(k) + E(x(k))f(k)] - [T(F(x(k), W(k), f(k))\,) - T(F_*(x(k)))]}_{\Omega(x(k),W(k),f(k))} \tag{6.32}$$

$$\hat{z}(k) = C(\hat{\xi}(k) - T\big(x(k)\big) + D[G(x(k))W(k) + E(x(k))f(k)]$$

It should be noted here that the zero-input dynamics of (6.32) is exactly linear and moreover, if the matrix A has eigenvalues in the unit disc, the zero-input response is

$$\hat{\xi}(k) - T\big(x(k)\big) = A^k\left(\hat{\xi}(0) - T\big(x(0)\big)\right) \to 0$$

$$\hat{z}(k) = CA^k\left(z(0) - T\big(x(0)\big)\right) \to 0$$

which means that the residual $\hat{z}(k)$ asymptotically approaches zero. But as an immediate consequence of proposition 2, (6.30) and (6.31) will be satisfied if and only if there exist $\beta_0, \beta_1, \dots, \beta_v \in R^p$ such that:

$$\beta_0 H\, {F_*}^v(x) + \beta_1 H\, {F_*}^{v-1}(x) + \cdots + \beta_{v-1} H F_*(x) + \beta_v H(x) = 0 \tag{6.33}$$

with A, B, C, D given by (6.16) and

$$T(x) = \begin{bmatrix} -\beta_0 HF_*{}^{\nu-1}(x) - \cdots - \beta_{\nu-2} HF_*(x) - \beta_{\nu-1} H(x) \\ \vdots \\ -\beta_0 HF_*(x) - \beta_1 H(x) \\ -\beta_0 H(x) \end{bmatrix} \tag{6.34}$$

The second requirement for the functional observer is that the residual $\hat{z}$ must remain completely unaffected by any disturbances $W(t)$ present in the system. From (6.32), disturbance decoupling can be achieved if

$$\Omega(x, W, 0) = 0 \text{ and } \frac{\partial \Omega(x, W, f)}{\partial W} = 0 \; \forall \; W$$

$$DG(x) = 0 \tag{6.35}$$

where $\Omega(x, W, f) = B[G(x)W + E(x)f] - [T(F(x, W, f)) - T(F_*(x))]$. The third and final requirement for the functional observer is that the residual must be affected by the input f, so that the fault can be detected by monitoring the residual. For this to be possible the following equations must hold,

$$\Omega(x, W, f) \neq 0 \; \forall \; f \neq 0$$

Or

$$DE(x) \neq 0 \tag{6.36}$$

Thus, to construct a functional observer (6.28) for fault detection in the process (6.27):

(i) Find a set of constant row vectors $\beta_0, \beta_1, \ldots, \beta_\nu$ that satisfy (6.33)

(ii) Construct T(x) and (A, B, C, D) using (6.34) and (6.16) respectively

(iii) Substitute in (6.35) and (6.36) to see if the disturbance decoupling and fault detectability condition hold. If they hold, the residual generator matrices (A,B,C,D) given by (6.16), else, look a different set of vectors in step (i).

The above fault detection methodology will be applied to the non-isothermal CSTR example considered in the previous subsection

Consider the CSTR reactor presented before with an added concentration measurement and possible faults in the concentration sensor (f_1) and inlet coolant temperature (f_2) and uncertainty (w_1) in the pre-exponential factor(A_1) of the reaction rate. The reaction rate expression with the uncertainty is $R(C_A, C_B, \theta, w) = \frac{(A_1+w)e^{-\frac{E_1}{\theta}}A_2 e^{-\frac{E_2}{\theta}}C_A C_B Z}{1+A_2 e^{-\frac{E_2}{\theta}}C_B} + A_3\, e^{-\frac{E_3}{\theta}}C_A C_B$. The discretized model equations are as follows.

$$C_A(k+1) = C_A(k) + \delta_t\left(\frac{F}{V}\left(C_{A,in} - C_A(k)\right) - R(C_A(k), C_B(k), \theta(k), w(k))\right)$$

$$C_B(k+1) = C_B(k) + \delta_t\left(\frac{F}{V}\left(C_{B,in} - C_B\right) - R(C_A(k), C_B(k), \theta(k), w(k))\right)$$

$$\theta(k+1) = \theta(k) + \delta_t\left(\frac{F}{V}\left(\theta_{in} - \theta(k)\right) - \frac{US_A}{\rho c_p V}\left(\theta(k) - \theta_j(k)\right)\right) + \frac{\delta_t(-\Delta H_R)}{\rho c_p}\left(R(C_A(k), C_B(k), \theta(k), w(k))\right) \tag{6.37}$$

$$\theta_j(k+1) = \theta_j(k) + \delta_t\left(\frac{F_j}{V_j}\left(\theta_{j,in}(k) + f_2(k) - \theta_j(k)\right) + \frac{US_A}{\rho_j\, c_{p_j} V_j}\left(\theta(k) - \theta_j(k)\right)\right)$$

$$y_1 = C_A(k) + f_1(k)$$

$$y_2 = \theta(k)$$

$$y_3 = \theta_j(k)$$

The initial condition of the reactor is $C_A(0) = 0, C_B(0) = 0, \theta(0) = 300, \theta_j(0) = 300$ and the model is converted to deviation form $C'_A = C_A - C_{A,ref}, C'_B = C_B - C_{B,ref}\ \theta' = \theta - \theta_{ref},\ \theta'_j = \theta_j - \theta_{j,ref}$ and $y'_1 = C'_A,\ y'_2 = \theta', y'_3 = \theta'_j$ where the subscript ref denotes reference steady state value. The goal is to detect and isolate these faults $f_1(k)$ and $f_2(k)$ in the presence of uncertainties $w(k)$ in the reaction rate. To this end, two scalar functional observers ($(\nu = 1)$) are built (i) to detect the analytical sensor fault (f_1) while considering f_2 as an additional disturbance. (ii) to detect the inlet coolant temperature fault f_2 considering f_1 as an additional disturbance.

Functional observer 1: Detection of the analytical sensor fault f_1 while considering f_2 as an additional disturbance. For a scalar functional observer ($\nu = 1$) the matrices A, B, C, D of the functional observer (6.16) are $A = -\alpha_1,\ B = \beta_1 - \alpha_1\beta_0,\ C = 1,\ D = \beta_0$, the transformation matrix (6.34) is $T(x) = -\beta_0 Hx$ where $H = \begin{bmatrix} 1 & 0 & 0 & 0 \\ 0 & 0 & 1 & 0 \\ 0 & 0 & 0 & 1 \end{bmatrix}$. For the design conditions to be satisfied, there must exist $\beta_0, \beta_1 \in R^3$ satisfying $\beta_0 HF_*(x) + \beta_1 Hx = 0$. For model equations (6.37), disturbance decoupling (6.35) and fault detectability conditions (6.36) take the following forms $\begin{bmatrix} \beta_1 G_1(x) - \beta_0 HJ_1(x) \\ \beta_0 G_1(x) \end{bmatrix} = \begin{bmatrix} 0 \\ 0 \end{bmatrix}$ and $\begin{bmatrix} \beta_1 E_1(x) - \beta_0 HK_1(x) \\ \beta_0 E_1(x) \end{bmatrix} \neq \begin{bmatrix} 0 \\ 0 \end{bmatrix}$ respectively. Where,

$$J_1(x) = \begin{bmatrix} -\delta_t \frac{\partial R}{\partial w} & 0 \\ \frac{\delta_t(-\Delta H_R)}{\rho c_p}\left(\frac{\partial R}{\partial w}\right) & 0 \\ 0 & \frac{\delta_t F_j}{V_j} \end{bmatrix}, \quad G_1(x) = \begin{bmatrix} 0 & 0 \\ 0 & 0 \\ 0 & 0 \end{bmatrix}, E_1(x) = \begin{bmatrix} 1 \\ 0 \\ 0 \end{bmatrix}, K_1(x) = 0.$$ The conditions are satisfied for the following choice of $\beta_0, \beta_1 \in R^3$,

$$\beta_0 = \left[1, \frac{\rho c_p}{(-\Delta H)}, 0\right]$$

$$\beta_1 = \left[\left(\frac{\delta_t F}{V} - 1\right), -\frac{\rho c_p}{(-\Delta H)}\left(1 - \frac{\delta_t F}{V} - \frac{US_A\delta_t}{\rho c_p V}\right), -\frac{US_A}{(-\Delta H)V}\delta_t\right]$$

The resulting functional observer (with $\alpha_1 = -0.999$) is

$$\hat{\xi}(k+1) = -\alpha_1\hat{\xi}(k) + \left[\frac{\delta_t F}{V} - 1 - \alpha_1\right]y_1'(k) - \frac{\rho c_p}{(-\Delta H)}\left(1 + \alpha_1 - \frac{\delta_t F}{V} - \frac{US_A\delta_t}{\rho c_p V}\right)y_2'(k)$$

$$- \frac{US_A\delta_t}{(-\Delta H)V}y_3'(k)$$

$$\hat{z}_1(k) = \hat{\xi}(k) + y_1'(k) + \frac{\rho c_p}{(-\Delta H)}y_2'(k)$$

Functional observer 2: Detection of inlet coolant temperature fault f_2 while considering f_1 as an additional disturbance. For a scalar functional observer ($\nu = 1$) to be possible there must exist $\beta_0, \beta_1 \in R^3$ that satisfy $\beta_0 H F_*(x) + \beta_1 H x = 0$, and the disturbance decoupling and fault detectability conditions $\begin{bmatrix}\beta_1 G_2(x) - \beta_0 H J_2(x) \\ \beta_0 G_2(x)\end{bmatrix} = \begin{bmatrix}0 \\ 0\end{bmatrix}$ and $\begin{bmatrix}\beta_1 E_2(x) - \beta_0 H K_2(x) \\ \beta_0 E_2(x)\end{bmatrix} \neq \begin{bmatrix}0 \\ 0\end{bmatrix}$ respectively where

$J_2(x) = \begin{bmatrix} -\delta_t\frac{\partial R}{\partial w} & 0 \\ \frac{\delta_t(-\Delta H_R)}{\rho c_p}\left(\frac{\partial R}{\partial w}\right) & 0 \\ 0 & 0\end{bmatrix}$, $G_2(x) = \begin{bmatrix}0 & 1 \\ 0 & 0 \\ 0 & 0\end{bmatrix}$, $E_2(x) = \begin{bmatrix}0 \\ 0 \\ 0\end{bmatrix}$ and $K_2(x) = \begin{bmatrix}0 \\ 0 \\ \frac{\delta_t F_j}{V_j}\end{bmatrix}$. The conditions are satisfied for the following choice of $\beta_0, \beta_1 \in R^3$,

$$\beta_0 = [0,0,1]$$

$$\beta_1 = \left[0, -\frac{US_A\delta_t}{\rho_j c_{p_j} V_j}, -\left(1 - \frac{\delta_t F_j}{V_j} - \frac{US_A\delta_t}{\rho_j cp_j V_j}\right)\right]$$

The resulting functional observer constructed using (5.3) and with $\alpha_1 = -0.9$. is:

$$\hat{\xi}(k+1) = -\alpha_1\hat{\xi}(k) - \frac{US_A\delta_t}{\rho_j cp_j V_j}y_2'(k) - \left[1 + \alpha_1 - \frac{\delta_t F_j}{V_j} - \frac{US_A\delta_t}{\rho_j cp_j V_j}\right]y_3'(k)$$

$$\hat{z}_2(k) = \hat{\xi}(k) + y_3'(k)$$

The two residual generators are tested on the following scenario: $f_1(t) = \begin{cases} 0, & t < 0.1 \\ 0.5, & t \geq 0.1 \end{cases}$, $f_2(t) = \begin{cases} 0, & t < 0.2 \\ 20, & t \geq 0.2 \end{cases}$, $w(t) = 10^5$. The residuals are plotted in Figure 6.2. Both residuals from time t =0 to 0.1hr are identically 0. When the sensor fault occurs at time t=0.1hr a deviation is seen in $\hat{z}_1$ whereas $\hat{z}_2$ is identically zero. At time t=0.2hr a deviation is observed in $\hat{z}_2$ indicating the presence of a fault in the inlet coolant temperature.

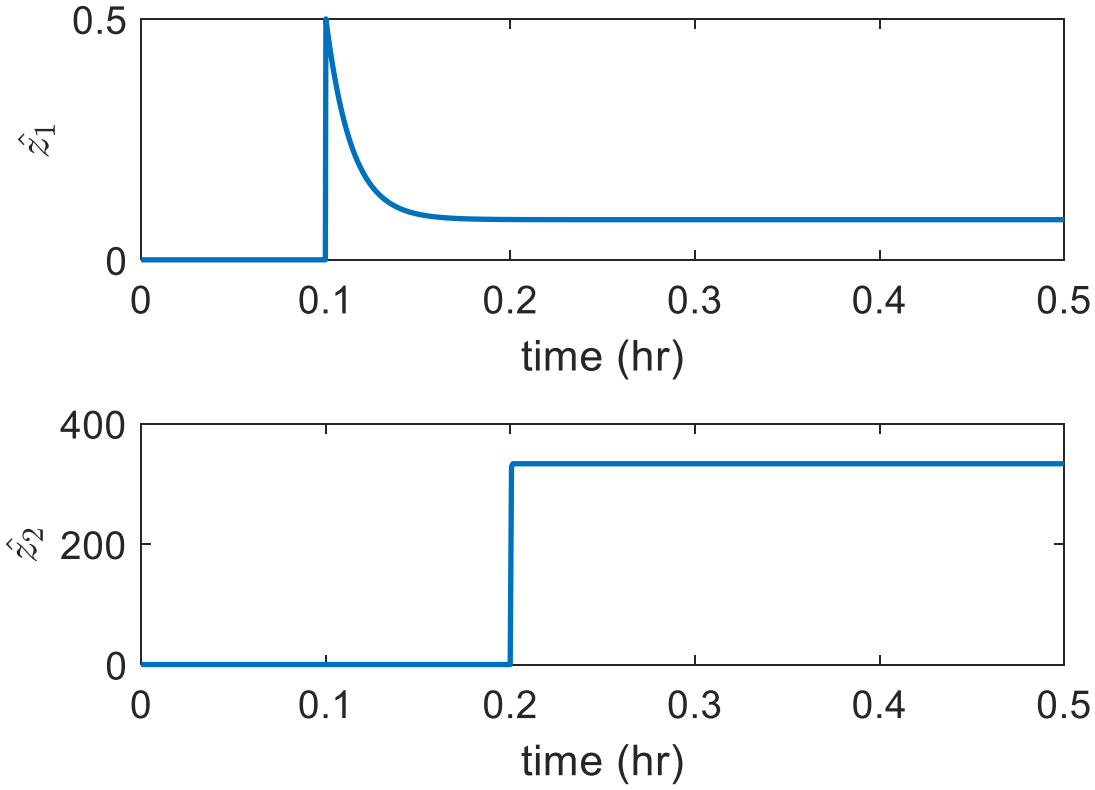

Figure 6.2 Residuals vs time in the absence of initialization errors.

6.9. Application 2- step fault estimation

Consider a nonlinear system of the form

$$x(k+1) = F\big(x(k), x_0, W(k)\big) \tag{6.38}$$

$$y(k) = H(x(k)) + x_0 E(x(k)) + G\big(x(k)\big)W(k)$$

and the where $x_0 \in \mathbb{R}$ represents a potential fault arising from equipment malfunction, such that x_0 is zero under normal operation, but x_0 assumes a constant nonzero value in the event of a sudden malfunction. To be able to detect the occurrence of a fault and at the

same time estimate its size, one can design a functional observer of the form (6.8) for the extended system:

$$x_0(k+1) = x_0(k)$$

$$x(k+1) = F\big(x(k), x_0(k), W(k)\big) \tag{6.39}$$

$$y(k) = H(x(k)) + x_0(k)E(x(k)) + G(x(k))W(k)$$

$$z = x_0$$

Defining$F_*(x, x_0) = F(x, x_0, 0)$. Such an observer will exist if there exists a mapping $T(x, x_0)$: $\mathbb{R}^{n+1} \to \mathbb{R}^{\nu}$ such that

$$T(F_*(x, x_0), x_0) = AT(x, x_0) + B[H(x) + x_0E(x)] \tag{6.40}$$

$$x_0 = CT(F_*(x, x_0), x_0) + D[H(x) + x_0E(x)]$$

and consequently, the functional observer error dynamics is the functional observer's error dynamics then follows:

$$\hat{\xi}(k+1) - T(x(k+1), x_0) = A\left(\hat{\xi}(k) - T(x(k), x_0)\right) +$$
$$B[G(x)W(k)] - [T\left(F\left(\left(x(k), x_0, W(k)\right)\right), x_0\right) - T(F_*(x(k), x_0), x_0)]$$

$$\hat{z}(k) - x_0 = C(\hat{\xi}(k) - T(x(k), x_0) + D\big[G\big(x(k)\big)W(k)\big] \tag{6.41}$$

As an immediate consequence of proposition 2 we have the following conditions in terms of the constant row vectors $\beta_0, \ldots, \beta_{\nu} \in R^p$.

$$\begin{gathered}\beta_0(HF_*^{\nu}(x,x_0)+x_0EF_*^{\nu}(x,x_0)+\beta_1\big(HF_*^{\nu-1}(x,x_0)+x_0EF_*^{\nu-1}(x,x_0)\big)+\cdots\\ +\beta_{\nu-1}\big(HF_*(x,x_0)+x_0EF_*(x,x_0)\big)+\beta_{\nu}\big(H(x)+x_0E(x)\big)\\ =(1+\alpha_1+\cdots+\alpha_{\nu-1}+\alpha_{\nu})x_0\end{gathered} \tag{6.42}$$

where $HF_*(x,x_0)=H\big(F_*(x,x_0)\big)$, $HF_*^2(x,x_0)=HF_*((F_*(x,x_0),x_0))$ and so on. With $T(x,x_0)=$

$$\begin{bmatrix}\begin{pmatrix}-\beta_0\big(HF_*^{\nu-1}(x,x_0)+x_0EF_*^{\nu-1}(x,x_0)\big)-\cdots-\beta_{\nu-1}\Big(\big(H(x)+x_0E(x)\big)\Big)+\\ (1+\alpha_1+\cdots+\alpha_{\nu-1})x_0\end{pmatrix}\\ \vdots\\ -\beta_0\big(HF_*(x,x_0)+x_0EF_*(x,x_0)\big)-\beta_1\Big(\big(H(x)+x_0E(x)\big)\Big)+(1+\alpha_1)x_0\\ -\beta_0\big(H(x)+x_0E(x)\big)+x_0\end{bmatrix} \tag{6.43}$$

and for fault estimate to be uncorrupted by uncertainties/disturbances the following condition must hold

$$B[G(x)W]-\big[T\big(F\big((x,x_0,W)\big),x_0\big)-T(F_*(x,x_0),x_0)\big]\forall\, W \tag{6.44}$$

$$DG(x)=0$$

Revisiting the example in the previous subsection, the fault estimation methodology will be used to estimate the value of step-faults f_1 and f_2. To this end, two scalar functional observers ($\nu=1$) are built (i) to estimate the analytical sensor fault (f_1) while considering f_2 as an additional disturbance. (ii) to estimate the inlet coolant temperature fault f_2 considering f_1 as an additional disturbance.

Functional observer 1: Estimating the analytical sensor fault f_1 while considering f_2 as an additional disturbance. A scalar functional observer is built ($\nu=1$). The design conditions (6.42) and (6.44) are satisfied for the following choice of $\beta_0,\beta_1\in R^3$,

$$\beta_0 = \left[1, \frac{\rho c_p}{(-\Delta H)}, 0\right]$$

$$\beta_1 = \left[\left(\frac{\delta_t F}{V} - 1\right), \frac{\rho c_p}{(-\Delta H)}\left(\frac{\delta_t F}{V} - 1\right) + \frac{US_A \delta_t}{(-\Delta H)}, -\frac{US_A \delta_t}{\rho c_p V}\right]$$

And $\alpha_1 = \frac{\delta_t F}{V} - 1$. The functional observer is

$$\hat{\xi}(k+1) = -\left[\frac{\delta_t F}{V} - 1\right]\hat{\xi}(k) + \frac{US_A \delta_t}{(-\Delta H)} y_2'(k) - \frac{US_A \delta_t}{\rho c_p V} y_3'(k)$$

$$\hat{z}_1(k) = \hat{\xi}(k) + y_1'(k) + \frac{\rho c_p}{(-\Delta H)} y_2'(k)$$

Functional observer 2: Estimating inlet coolant temperature fault f_2 while considering f_1 as an additional disturbance. A scalar functional observer is built ($\nu = 1$). The design conditions (6.42) and (6.44) are satisfied for the following choice of $\beta_0, \beta_1 \in R^3$,

$$\beta_0 = \left[0,0, \frac{(1+\alpha_1)V_j}{F_j \delta_t}\right]$$

$$\beta_1 = \left[0, -\frac{(1+\alpha_1)}{F_j}\frac{US_A}{\rho_j c_{p_j}}, -\frac{(1+\alpha_1)V_j}{F_j \delta_t}\left(1 - \frac{\delta_t F_j}{V_j} - \frac{US_A \delta_t}{\rho_j c_{p_j} V_j}\right)\right]$$

and $\alpha_1 = -0.99$. The resulting residual generator is

$$\hat{\xi}(k+1) = \alpha_1 \hat{\xi}(k) - \frac{(1+\alpha_1)}{F_j}\frac{US_A}{\rho_j c_{p_j}} y_2'(k) - \frac{(1+\alpha_1)V_j}{F_j \delta_t}\left(1 - \frac{\delta_t F_j}{V_j} - \frac{US_A \delta_t}{\rho_j c_{p_j} V_j}\right) y_3'(k)$$

$$- \frac{\alpha_1 (1+\alpha_1) V_j}{F_j \delta_t} y_3'(k)$$

$$\hat{z}_2(k) = \hat{\xi}(k) - \frac{(1+\alpha_1)V_j}{F_j \delta_t} y_3'(k)$$

The two residual generators are tested on the following scenario: $f_1(t) = \begin{cases} 0, & t < 0.1 \\ 0.5, & t \geq 0.1 \end{cases}$, $f_2(t) = \begin{cases} 0, & t < 0.2 \\ 20, & t \geq 0.2 \end{cases}$, $w(t) = 10^5$. The residuals are plotted in Figure 6.3. Both residuals from time t =0 to 0.1 hr are identically 0.When the sensor fault occurs at time t=0.1hr $\hat{z}_1$converges to the fault value 0.1 whereas $\hat{z}_2$ is identically zero. At time t=0.2hr when the inlet coolant temperature fault occurs $\hat{z}_2$ converges to its respective fault value.

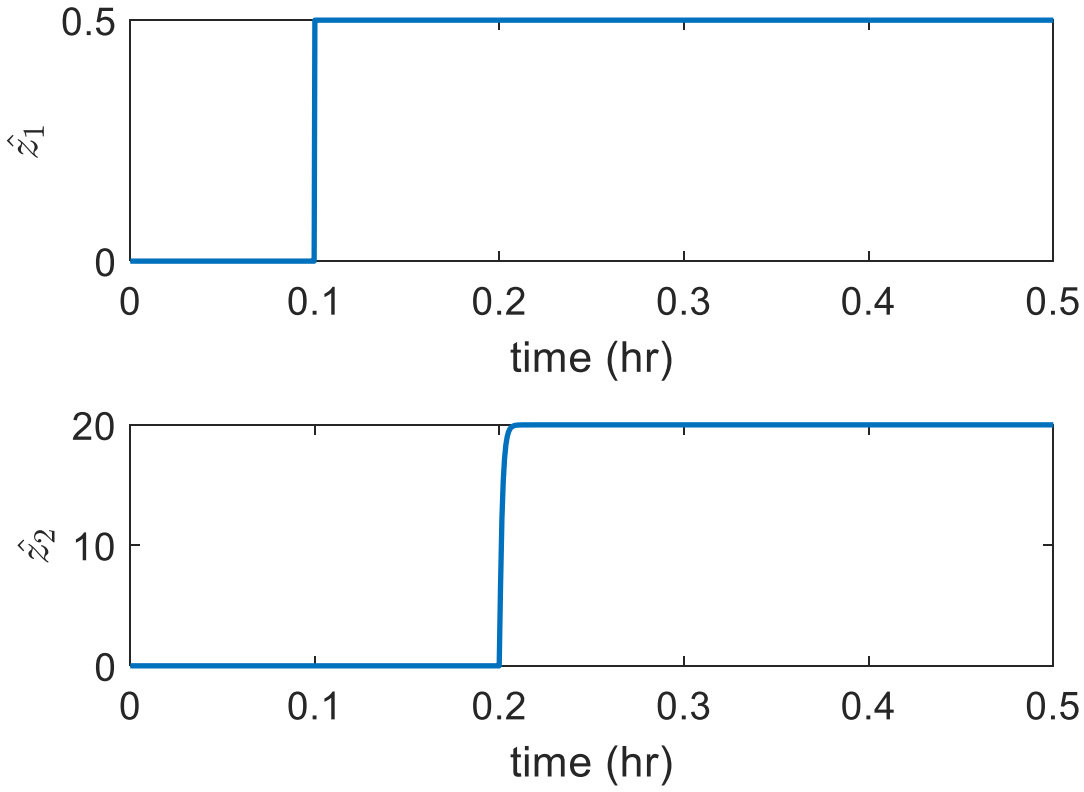

Figure 6.3 Fault estimates vs time in the absence of initialization errors.

6.10. Conclusions

A generalization of Luenberger's functional observer to the discrete-time nonlinear systems is presented in this section. The problem of exact linearization of the functional observer dynamics has been studied and conditions for the linearization to be feasible have been derived including a simple formula for the design of the resulting functional observer. The fault detection and estimation capabilities of the functional observer design scheme have also been studied and conditions for disturbance decoupling and fault detectability were presented. Throughout the study, the functional observer design scheme, and the fault detection and estimation capabilities have been tested on a non-isothermal CSTR example.

7. FAULT DETECTION IN THE PRESENCE OF NOISES

7.1. Introduction

One major limitation of the fault diagnosis approach presented in the previous sections is that it doesn't take measurement noise and state noise into consideration. In the presence of noises the residual will no longer decay to zero. Figure 7.1 below shows the sensitivity of the residuals in the absence of faults to even small measurement and process noises. The presence of noises brings a stochastic element to the fault diagnosis problem and has lent itself to different approaches in literature ranging from purely data driven methods[23-25] to integrated schemes with both model-based and data-driven components[61, 132].

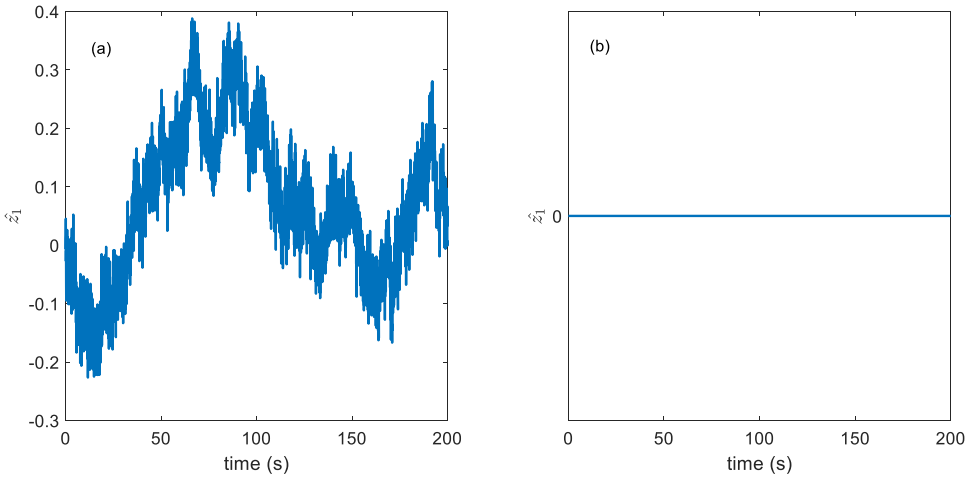

Figure 7.1 Residuals (fault free) vs time. (a) in the presence of noises (b) noises absent.

Purely data-driven methods require no knowledge of a quantitative model and is based on the availability of large amount of historical process data[24-25]. Methods that extract quantitative information can be broadly classified as non-statistical or statistical methods[25]. Neural networks are an important class of non-statistical classifiers. Principal component analysis (PCA)/partial least squares (PLS) and statistical pattern classifiers such as Generalized Likelihood Ratios (GLR) form a major component of statistical feature extraction methods[23-25]. Schemes that integrate model-based and data driven methods, however, make use of quantitative models and model based fault diagnosis techniques augmented with statistical classification techniques to tackle any noises and uncertainties prevalent in the system[25, 61]. In general, such schemes use the model-based fault diagnosis for residual generation and statistical methods for residual evaluation. For linear systems, prior research has focused on integrating Kalman filters with Generalized likelihood ratios[25, 61, 133-134], parity space methods with temporal and spatial whitening of the residuals[133], and Markov models with Monte Carlo estimation[132]. For nonlinear systems however, methods integrating model-based with statistical methods have been limited. The goal of this section is to design a robust fault diagnosis scheme for nonlinear processes with sensor and measurement noises that utilizes the functional observers designed in the previous subsection for residual generation and generalized likelihood ratios for residual evaluation.

In the next subsection, the problem of disturbance decoupled detection of a single fault in the presence of only sensor noises will be considered. Here the fault free distribution of the residual will be derived analytically, and subsequent residual evaluation

will be done using Generalized Likelihood Ratios. Following this, both process noises and sensor noises will be considered where a numerical approach will be used to obtain the fault free distribution before using GLR to evaluate the residual.

7.2. Disturbance decoupled detection of a single fault in the presence of sensor noises

Consider a nonlinear process described by:

$$x(k+1) = F\big(x(k), W(k), f(k)\big) \tag{7.1}$$

$$y(k) = H\big(x(k)\big) + G(x)W(x) + E(x)f(k) + \eta(k)$$

where $x \epsilon R^n$ denotes the vector of states, $y \epsilon R^p$ denotes the vector of measured outputs. $f \epsilon R$ and $W \epsilon R^m$ are the fault and the disturbances/uncertainties respectively (system inputs) and $E(x), F(x), G(x), H(x), J(x), K(x)$ are smooth functions and η is the gaussian noise vector with mean 0 and covariance Σ_η^2 gaussian. We wish to use the following linear functional observer to detect faults

$$\hat{\xi}(k+1) = A\hat{\xi}(k) + By(k) \tag{7.2}$$

$$\hat{z}(k) = C\hat{\xi}(k) + Dy(k)$$

Following the methods in the previous subsection one can show that the error dynamics of the observer in the absence of faults and with disturbance decoupling is

$$(e(k+1)) = A(e(k)) + B\eta(k) \tag{7.3}$$

$$\hat{z}(k) = C(e(k)) + D\eta(k) \tag{7.4}$$

Now, the error at time k can be expressed in terms of the error l time steps before as follows

$$e(k) = A^k e(0) + \sum_{i=0}^{k-1} A^{k-i-1} B\eta(i) \tag{7.5}$$

If the eigenvalues of A lie in the unit disc, for large k, $e(k) = \sum_{i=0}^{k-1} A^{k-i-1} B\eta(i)$. Thus, for large times the observer output (residual) $\hat{z}(k)$ is

$$\hat{z}(k) = C \sum_{i=0}^{k-1} A^{k-i-1} B\eta(i) \; + D\eta(k) \tag{7.6}$$

From the above equation, one can see that the residual for large times follows a gaussian distribution with mean $\mu_0 = 0$ and variance $\sigma_0^2 = D\left(\Sigma_\eta^2\right)D^T + \sum_{i=0}^{k-1}(CA^{k-i-1}B)\,\Sigma_\eta^2\left(CA^{k-i-1}B\right)^T$

The foregoing conclusions lead to the null hypothesis H_0, i.e in the absence of faults the residual $\hat{z}(k)$, at large times k, follows a Gaussian distribution $N\left(\mu_0 = 0, \sigma_0^2 = D\left(\Sigma_\eta^2\right)D^T + \sum_{i=0}^{k-1}(CA^{k-i-1}B)\,\Sigma_\eta^2\left(CA^{k-i-1}B\right)^T\right)$.

7.3. Generalized likelihood ratios

Suppose the residual generated from the functional observer designed in the previous subsection has a $N(\mu_r, \sigma_r^2)$ distribution. We know the fault free distribution is $N(\mu_0, \sigma_0^2)$. In this subsection, we would like to detect any fault that produces a shift in μ_r away from μ_0. To this end, say we have k observations, $r_1, \ldots., r_k$ and consider the hypothesis that a mean shift of some value $\mu_1 \neq \mu_0$ has occurred at some time τ^* between samples τ and $\tau + 1$ where $\tau < k$. The likelihood function at sample k is[24]

$$L(\tau, \mu_1 | r_1, r_2, \dots, r_k) = (2\pi)^{-k/2}\sigma_0^{-k/2} \times \exp\left(-\frac{1}{2\sigma_0^2}\left(\sum_{i=1}^{\tau}(r_i - \mu_0)^2 + \sum_{i=\tau+1}^{k}(r_i - \mu_1)^2\right)\right)$$

Under the hypothesis that there has been no mean shift, the likelihood function at sample k can be represented as

$$L(\infty, \mu_0 | r_1, r_2, \dots, r_k) = (2\pi)^{-k/2}\sigma_0^{-k/2} \times \exp\left(-\frac{1}{2\sigma_0^2}\left(\sum_{i=1}^{k}(r_i - \mu_0)^2\right)\right)$$

If there has been a shift to some unknown μ_1 between samples τ and $\tau + 1$, then the maximum likelihood estimator of μ_1 is

$$\hat{\mu}_{1,\tau,k} = \frac{1}{k - \tau}\sum_{i=\tau+1}^{k} r_i$$

Then a log likelihood-ratio statistic for determining whether there has in fact been a mean shift is

$$GLR_k = \ln \frac{\max\limits_{0 \le \tau < k, -\infty < \mu_1 < \infty} L(\tau, \mu_1 | r_1, r_2, \dots., r_k)}{L(\infty, \mu_0 | r_1, r_2, \dots., r_k)}$$

$$= \max_{0 \le \tau \le k} \frac{\left(\hat{\mu}_{1,\tau,k} - \mu_0\right)}{\sigma_0} \sum_{i=\tau+1}^{k} \left[(r_i - \mu_0) - \frac{1}{2}\left(\hat{\mu}_{1,\tau,k} - \mu_0\right)\right]$$

From the maximum likelihood estimate $\hat{\mu}_{1,\tau,k}$ the above equation reduces to

$$GLR_k = \max_{0 \le \tau < k} \frac{k - \tau}{2\sigma_0}\left(\hat{\mu}_{1,\tau,k} - \mu_0\right)^2$$

We will use the above equation to calculate the GLR statistic at any time k given the data from $[0, k]$.

Below an algorithm is presented to calculate the threshold for the GLR statistic for a residual dataset with a given mean and variance of the fault free distribution and a desired false alarm rate.

Obtaining the threshold for the GLR Statistic

1. Generate random normal distribution of a sufficiently large size (10000 observations) using known mean (μ_0) and variance (σ_0^2).
2. Compute GLR statistic using the random normal distribution that was generated: To monitor mean

$$\mathrm{GLR_k} = \max_{0 \le \tau < k} \frac{(k-\tau)}{2\sigma_0^2}\left(\hat{\mu}_{1,\tau,k} - \mu_0\right)^2 \tag{7.7}$$

where, $\hat{\mu}_{1,\tau,k}$ is the maximum likelihood estimates (MLEs) of the mean computed utilized the available data. k and τ correspond to the current time instant, and the position in the time window that provides the maximum detection rate for a fixed false alarm rate.

3. Use the computed generalized likelihood ratio statistic to compute its empirical distribution.
4. Use the specific confidence interval (α), e.g., 99% to obtain the fault detection threshold by extracting the corresponding percentile from the computed cumulative empirical distribution.

$$\mathrm{GLR_{treshold,\alpha}} = \mathrm{ecdf_\alpha}\left(\mathrm{GLR_k(mean)}\right)$$

Using the threshold to detect faults

1. Compute the GLR statistic online using the available formula:
    a. To monitor mean:

$$\mathrm{GLR_{test,k}} = \max_{0 \le \tau < k} \frac{(k-\tau)}{2\sigma_0^2}\left(\hat{\mu}_{1,\tau,k} - \mu_0\right)^2$$

2. Declare fault if:

$$\mathrm{GLR_{test,k}} > \mathrm{GLR_{lim,\alpha}}$$

7.4. Simulations- sensor noises

Consider the CSTR seen in the previous subsection

$$C_A(k+1) = C_A(k) + \delta_t\left(\frac{F}{V}\left(C_{A,in} - C_A(k)\right) - R(C_A(k), C_B(k), \theta(k), w(k))\right)$$

$$C_B(k+1) = C_B(k) + \delta_t\left(\frac{F}{V}\left(C_{B,in} - C_B\right) - R(C_A(k), C_B(k), \theta(k), w(k))\right)$$

$$\theta(k+1) = \theta(k) + \delta_t\left(\frac{F}{V}\left(\theta_{in} - \theta(k)\right) - \frac{US_A}{\rho c_p V}\left(\theta(k) - \theta_j(k)\right)\right) + \frac{\delta_t(-\Delta H_R)}{\rho c_p}\left(R(C_A(k), C_B(k), \theta(k), w(k))\right) \tag{7.8}$$

$$\theta_j(k+1) = \theta_j(k) + \delta_t\left(\frac{F_j}{V_j}\left(\theta_{j,in}(k) + f_2(k) - \theta_j(k)\right) + \frac{US_A}{\rho_j\, c_{p_j} V_j}\left(\theta(k) - \theta_j(k)\right)\right)$$

$$y_1 = C_A(k) + f_1(k) + \eta_1(k)$$

$$y_2 = \theta(k) + \eta_2(k)$$

$$y_3 = \theta_j(k) + \eta_3(k)$$

The noise vector $H = [\eta_1, \eta_2, \eta_3]$ is of zero mean and variance $\Sigma_\eta^2 = \begin{bmatrix} 0.001 & 0 & 0 \\ 0 & 0.01 & 0 \\ 0 & 0 & 0.01 \end{bmatrix}$. The same two functional observers used in the previous section (Subsection 6.6) are used here.

Functional observer 1: Detection of the analytical sensor fault f_1 while considering f_2 as an additional disturbance.

$$\beta_0 = \left[1, \frac{\rho c_p}{(-\Delta H)}, 0\right]$$

$$\beta_1 = \left[\left(\frac{\delta_t F}{V} - 1\right), -\frac{\rho c_p}{(-\Delta H)}\left(1 - \frac{\delta_t F}{V} - \frac{US_A \delta_t}{\rho c_p V}\right), -\frac{US_A}{(-\Delta H)V}\delta_t\right]$$

The resulting functional observer (with $\alpha_1 = -0.999$) is

$$\hat{\xi}(k+1) = -\alpha_1 \hat{\xi}(k) + \left[\frac{\delta_t F}{V} - 1 - \alpha_1\right] y_1'(k) - \frac{\rho c_p}{(-\Delta H)}\left(1 + \alpha_1 - \frac{\delta_t F}{V} - \frac{US_A \delta_t}{\rho c_p V}\right) y_2'(k)$$

$$- \frac{US_A \delta_t}{(-\Delta H)V} y_3'(k)$$

$$\hat{z}_1(k) = \hat{\xi}(k) + y_1'(k) + \frac{\rho c_p}{(-\Delta H)} y_2'(k)$$

At large times($k \to \infty$) the residual follows a gaussian distribution with mean 0 and variance $\sigma_r^2 = \sigma_0^2 = D\left(\Sigma_\eta^2\right)D^T + \sum_{i=0}^{k-1}\left(CA^{k-i-1}B\right)\Sigma_\eta^2\left(CA^{k-i-1}B\right)^T = 0.001$ in the absence of faults.

Functional Observer 2: Detection of inlet coolant temperature fault f_2 while considering f_1 as an additional disturbance.

$$\beta_0 = [0,0,1]$$

$$\beta_1 = \left[0, -\frac{US_A \delta_t}{\rho_j c_{p_j} V_j}, -\left(1 - \frac{\delta_t F_j}{V_j} - \frac{US_A \delta_t}{\rho_j c p_j V_j}\right)\right]$$

The resulting functional observer with $\alpha_1 = -0.999$. is:

$$\hat{\xi}(k+1) = -\alpha_1 \hat{\xi}(k) - \frac{US_A \delta_t}{\rho_j c p_j V_j} y_2'(k) - \left[1 + \alpha_1 - \frac{\delta_t F_j}{V_j} - \frac{US_A \delta_t}{\rho_j c p_j V_j}\right] y_3'(k)$$

$$\hat{z}_2(k) = \hat{\xi}(k) + y_3'(k)$$

At large times ($k \to \infty$) the residual follows a gaussian distribution with mean 0 and variance $\sigma_r^2 = \sigma_0^2 = D\left(\Sigma_\eta^2\right)D^T + \sum_{i=0}^{k-1}(CA^{k-i-1}B)\,\Sigma_\eta^2\left(CA^{k-i-1}B\right)^T = 1.4506$ in the absence of faults.

The fault scenario is as follows $f_1(t) = \begin{cases} 0, & t < 1000s \\ 1, & t \geq 1000s \end{cases}$, $f_2(t) = \begin{cases} 0, & t < 1200s \\ 20, & t \geq 1200s \end{cases}$, $w(t) = 10^5$. A false alarm rate of less than 1% is desired and the GLR threshold for sensor fault and coolant fault residuals are 3.411 and 3.477 respectively.

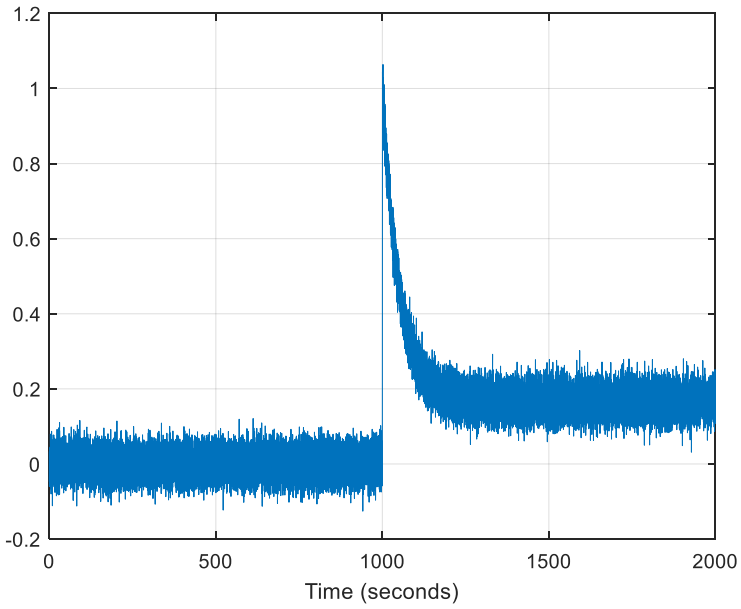

Figure 7.2 Residual vs time (seconds) for sensor faults.

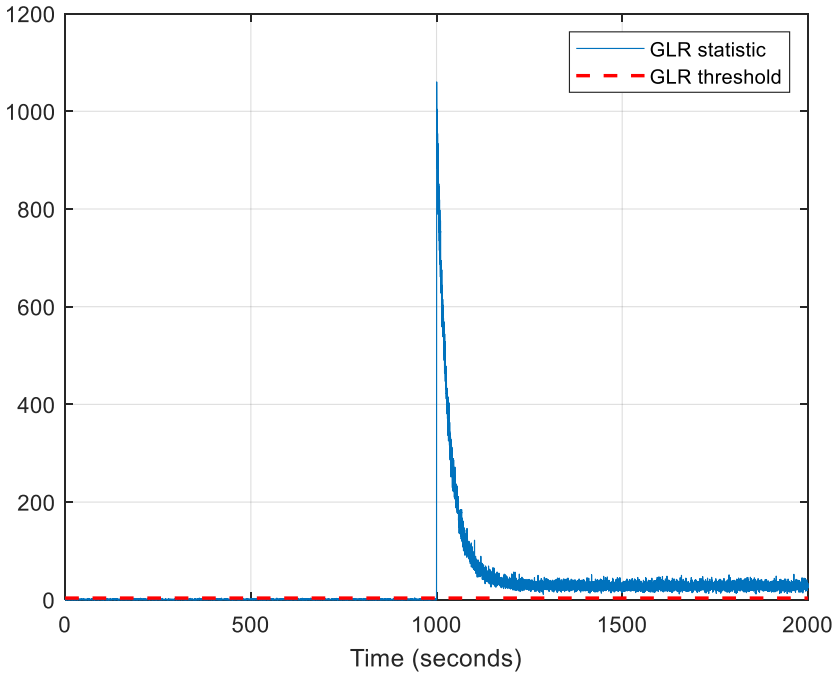

Figure 7.3 GLR statistic vs time for sensor fault residual.

The residuals for the sensor fault and the corresponding GLR statistic are plotted in Figures 7.2 and 7.3. The coolant fault residuals and their corresponding GLR statistic are plotted in Figures 7.4 and 7.5. In both cases the when a fault occurs a sharp increase GLR statistic is observed which then settles to a value higher that the threshold for fault free data facilitating rapid fault detection rate with near 0 missed detection rate. The fault detection metrics are in Table 7.1. The missed detection rate in both the cases is 0 and the average run length is 1; meaning only 1 observation is required since fault occurrence to detect faults. The false alarm rate for both the cases is 0.06%.

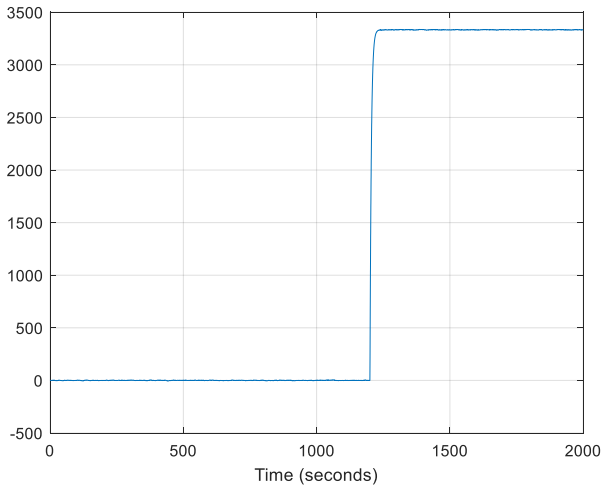

Figure 7.4 Residual vs time for coolant temp fault.

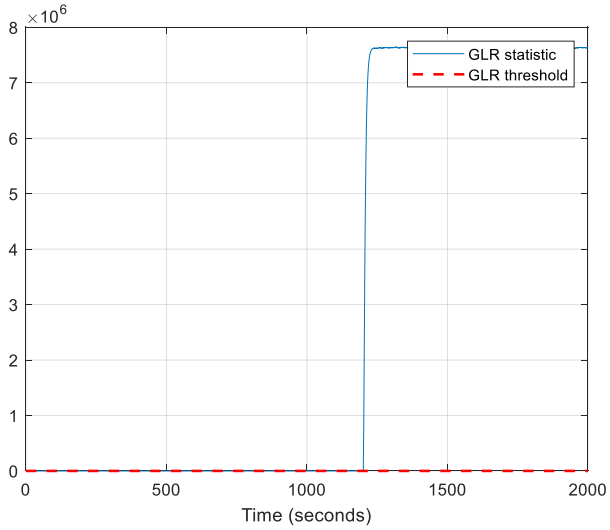

Figure 7.5 GLR statistic vs time for coolant fault.

Table 7.1 Fault detection metrics.

	Sensor fault	Coolant fault
Missed Detection Rate (%)	0.00	0.00
False Alarm Rate (%)	0.06	0.06
ARL_1	1.00	1.00

7.5. Disturbance decoupled detection of a single fault in the presence of sensor and process noises

Consider a nonlinear process described by:

$$x(k+1) = F\big(x(k), W(k), f(k)\big) + \zeta_1(k) \tag{7.9}$$

$$y(k) = H\big(x(k)\big) + G(x)W(x) + E(x)f(k) + \eta(k)$$

where $x \epsilon R^n$ denotes the vector of states, $y \epsilon R^p$ denotes the vector of measured outputs. $f \epsilon R$ and $W \epsilon R^m$ are the fault and the disturbances/uncertainties respectively (system inputs) and $E(x), F(x), G(x), H(x), J(x), K(x)$ are smooth functions and η is the gaussian sensor noise vector with mean 0 and covariance Σ_η^2 gaussian and ζ_1 is the process noise vector with mean 0 and covariance Σ_η^2. We wish to use the linear functional observer (7.2) to detect faults.

It is assumed that the response of the residual in the absence of faults at large times follows a Gaussian distribution of unknown mean and variance. The user needs to specify a fault-free region in the testing data set that can be utilized to compute the "training" GLR statistic that will allow its empirical cumulative distribution function to be computed in

order to obtain a fault detection threshold. Once the fault-free distribution is found the same steps in the algorithm for solely sensor noises in the previous subsection for can be followed.

7.6. Simulations- process and sensor noises

Consider the CSTR seen in the previous subsection

$$C_A(k+1) = C_A(k) + \delta_t\left(\frac{F}{V}\left(C_{A,in} - C_A(k)\right) - R(C_A(k), C_B(k), \theta(k), w(k))\right) + \zeta_1(k)$$

$$C_B(k+1) = C_B(k) + \delta_t\left(\frac{F}{V}\left(C_{B,in} - C_B\right) - R\left(C_A(k), C_B(k), \theta(k), w(k)\right)\right) + \zeta_2(k)$$

$$\theta(k+1) = \theta(k) + \delta_t\left(\frac{F}{V}\left(\theta_{in} - \theta(k)\right) - \frac{US_A}{\rho c_p V}\left(\theta(k) - \theta_j(k)\right)\right) + \frac{\delta_t(-\Delta H_R)}{\rho c_p}\left(R(C_A(k), C_B(k), \theta(k), w(k))\right) + \zeta_2(k) \tag{7.10}$$

$$\theta_j(k+1) = \theta_j(k) + \delta_t\left(\frac{F_j}{V_j}\left(\theta_{j,in}(k) + f_2(k) - \theta_j(k)\right) + \frac{US_A}{\rho_j\, c_{p_j} V_j}\left(\theta(k) - \theta_j(k)\right)\right) + \zeta_3(k)$$

$$y_1 = C_A(k) + f_1(k) + \eta_1(k)$$

$$y_2 = \theta(k) + \eta_2(k)$$

$$y_3 = \theta_j(k) + \eta_3(k)$$

The noise vectors H= $[\eta_1, \eta_2, \eta_3]$ and N = $[\zeta_1, \zeta_2, \zeta_3]$ are gaussian with zero mean and variance $\Sigma_\eta^2 = \begin{bmatrix} 0.001 & 0 & 0 \\ 0 & 0.01 & 0 \\ 0 & 0 & 0.01 \end{bmatrix}$ and $\Sigma_\zeta^2 = \begin{bmatrix} 0.016 & 0 & 0 \\ 0 & 0.16 & 0 \\ 0 & 0 & 0.16 \end{bmatrix}$ The same functional observers as in Subsection 6.6 are used to generate the residuals. The fault scenario is as follows $f_1(t) = \begin{cases} 0, & t < 360s \\ 1, & t \geq 360s \end{cases}$, $f_2(t) = \begin{cases} 0, & t < 720s \\ 20, & t \geq 720s \end{cases}$, $w(t) = 10^5$. A false alarm rate of less than 1% is desired and the GLR threshold for both sensor fault and coolant fault residuals is 3.477 respectively.

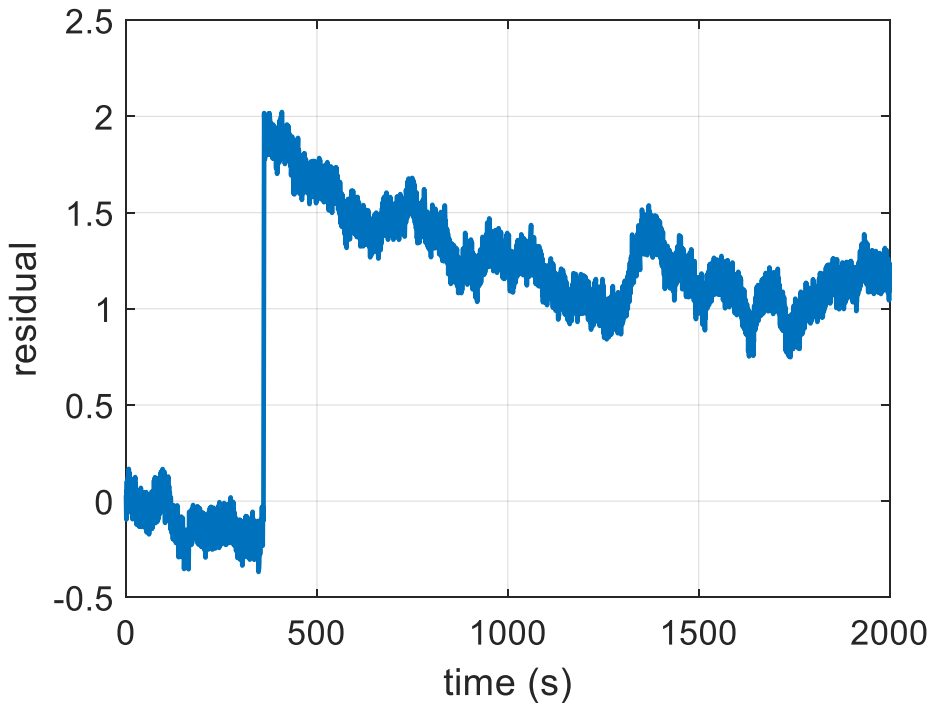

Figure 7.6 Residual vs time for sensor faults.

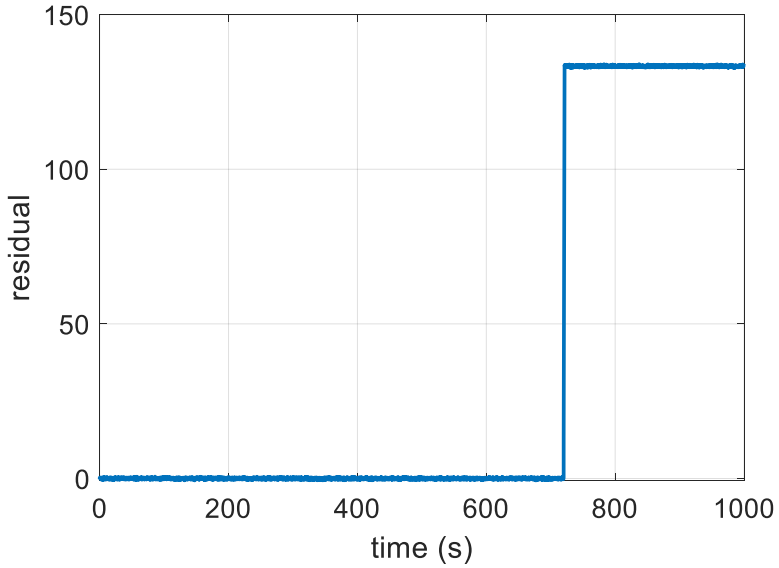

Figure 7.7 Residual vs time for coolant fault.

The residuals for the sensor fault and the corresponding GLR statistic are plotted in Figures 7.6 and 7.7. The coolant fault residuals and their corresponding GLR statistic are plotted in Figures 7.8 and 7.9. In both cases the when a fault occurs a sharp increase GLR statistic is observed which then settles to a value higher that the threshold for fault free data facilitating rapid fault detection rate with near 0 missed detection rate. The fault detection metrics are in Table 7.2. The missed detection rate in for sensor faults is 0.01% and 0% for coolant fault and the average run length is 3 and 1 for sensor and coolant faults respectively; meaning only 3 observations are required since fault occurrence to detect sensor fault (1 observation for coolant fault). The false alarm rate is 0.5% for sensor fault and 0% for coolant fault.

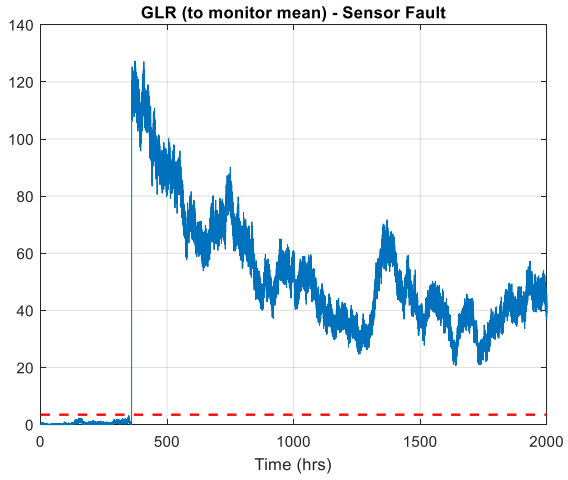

Figure 7.8 GLR statistic for sensor fault.

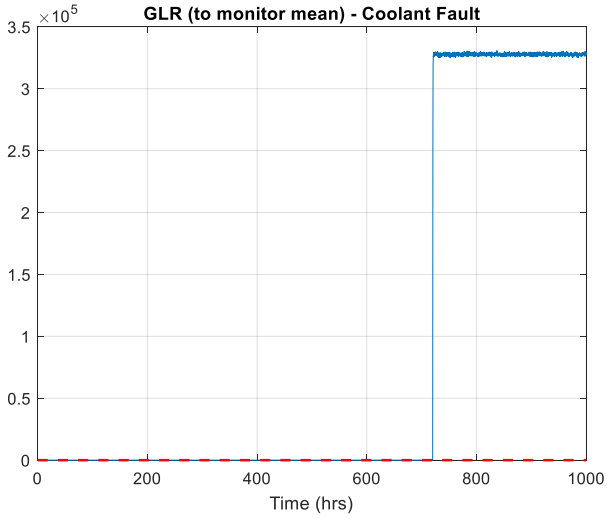

Figure 7.9 GLR statistic for coolant fault.

Table 7.2 Fault detection metrics.

	Dataset 1	Dataset 2
Missed Detection Rate (%)	0.01	0.00
False Alarm Rate (%)	0.50	0.00
ARL_1	3.00	1.00

7.7. Eigenvalue tuning

The eigenvalue of the functional observers plays a crucial role in the ability to detect faults both accurately and rapidly. In most cases there is a trade-off between sensitivity to faults and sensitivity to noises. The effect of eigenvalue on the variance of the residual in the fault free case and the mean of the residual for large times vs eigenvalue are plotted in Figures 7.10, 7.11 and 7.12. In general, when the eigenvalues tend to 1, the fault free residual variance (Figure 7.11) is the highest. This implies that the effect of noises are more pronounced for higher eigenvalues. However, on the flip side, the mean of the residual in the presence of faults is the highest for eigenvalues tending to 1 (Figures 7.11 and 7.12) which might make fault detection easier. In summary, a careful tuning of the eigenvalues is necessary so as to minimize the effect of noises while maximizing the effect of faults so as to facilitate fault detection.

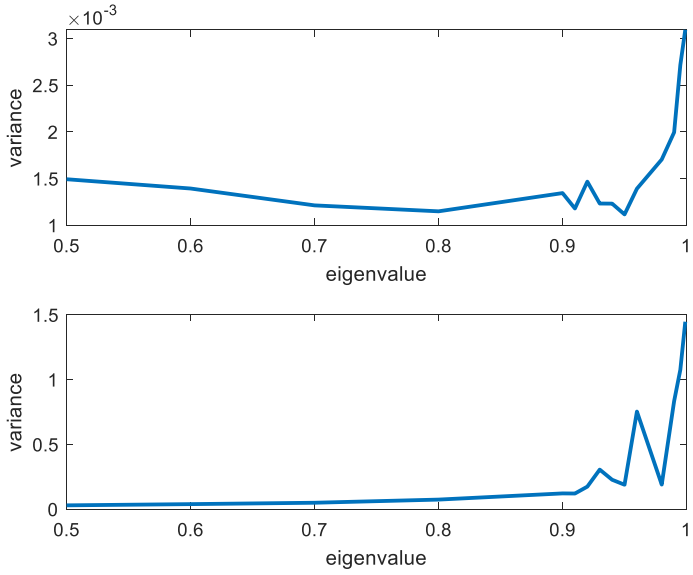

Figure 7.10 Residual variance vs eigenvalue for observers dedicated to sensor fault detection (top) and coolant temp fault detection (bottom).

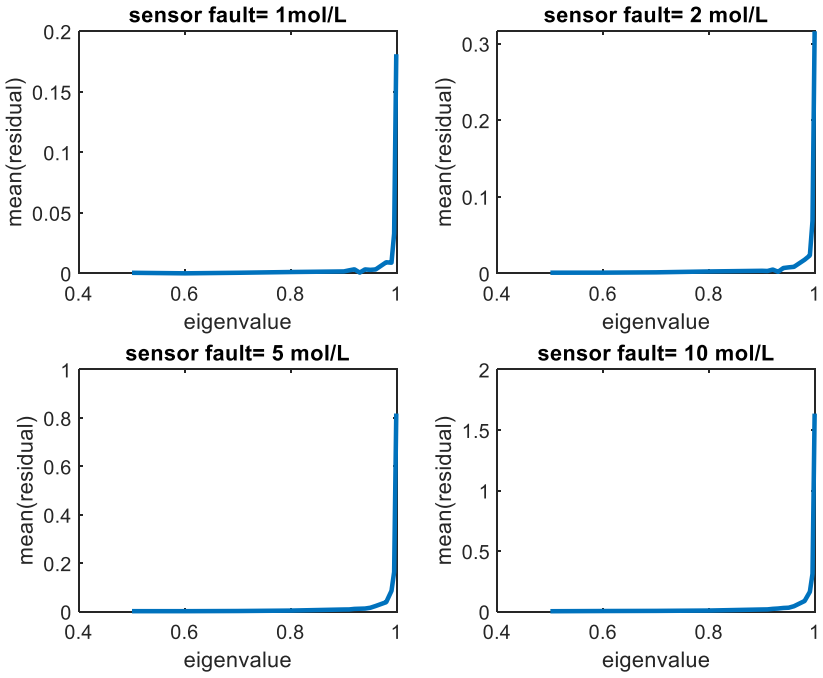

Figure 7.11 Residual mean vs eigenvalue for different sensor fault magnitudes.

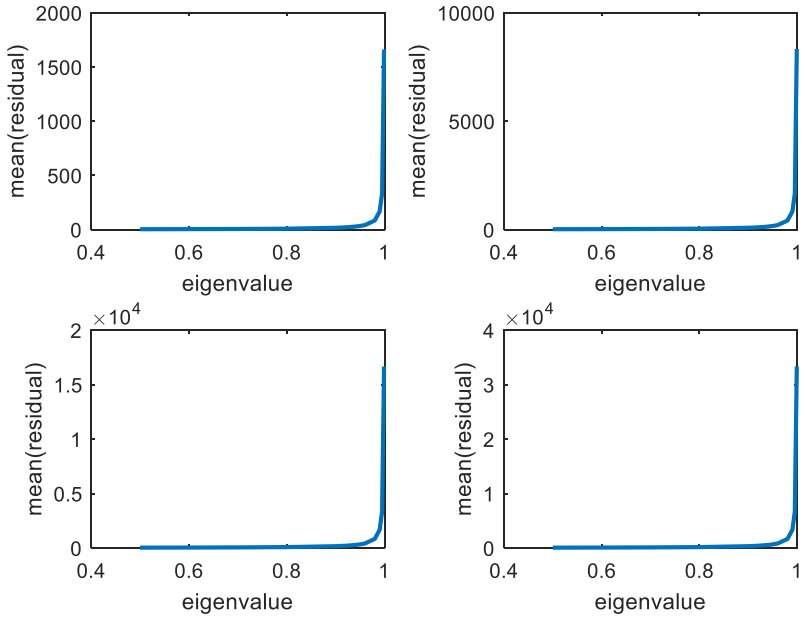

Figure 7.12 Residual Mean vs eigenvalue for different coolant fault magnitudes.

7.8. Fault detection metrics for different fault magnitudes

In this subsection, the capabilities of the fault diagnosis scheme presented is tested for different sensor fault magnitudes in the presence of both sensor and process noises. The following scenario is assumed to occur $f_1 = \begin{cases} 0, & t < 1000s \\ M, & x \geq 1000s \end{cases}$, $M = 0.05, 0.1, 0.5, 1, 2,$ 5 mol/L. As in the previous subsection, a false alarm rate of below 1% was desired for the fault free distribution and the GLR threshold remained the same at 3.477. In Figure, 7.13 the missed detection rate for different fault sizes is plotted. As expected, the number of observations incorrectly classified as fault-free increases as fault size decreases. For

fault sizes less than 1 mol/L, the missed detection rate is greater than 20% whereas large fault sizes (2-5 mol/L), the missed detection rate tends to 0%.

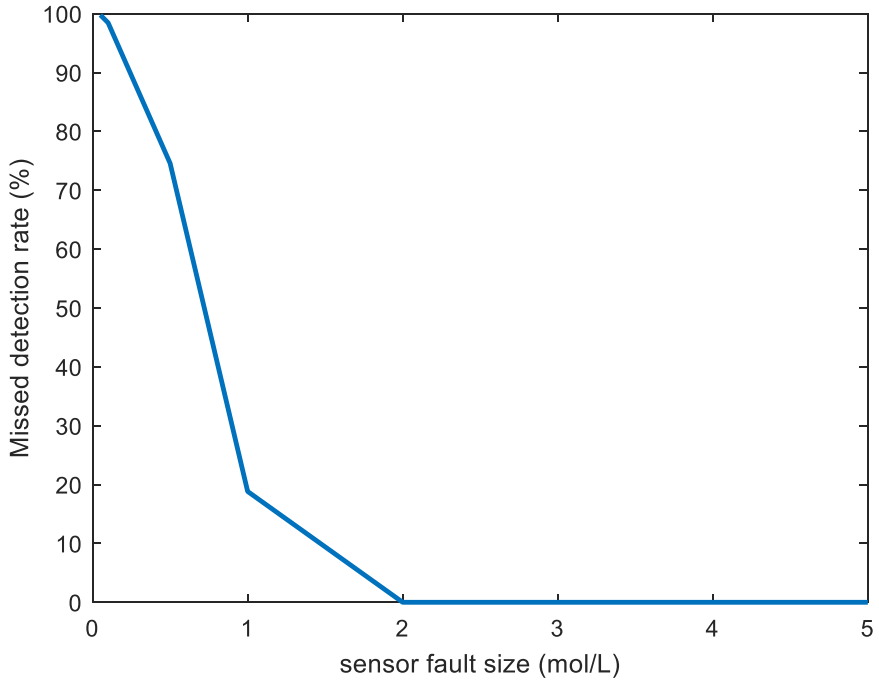

Figure 7.13 Missed detection rate (%) vs sensor fault size.

7.9. Conclusions

This section tackled the problem of detecting faults in the presence of noises in nonlinear systems by integrating discrete-time functional observers (Section 6) with statistical methods like Generalized Likelihood Ratios. A threshold on the residual data is calculated on the basis of GLR by deriving the fault free distribution analytically (when only sensor noises are present) and empirically (process and sensor noises). The GLR of

the residual is then tracked online and faults are flagged when the ratio violates the threshold. The scheme was successfully tested on a non-isothermal CSTR example first in the presence of only sensor noises and then with both sensor and process noises. In either case (absence or presence of process noises) it is important to optimally tune to eigenvalues of the functional observer to maximize and minimize the sensitivity to faults and noises respectively.

8. CONCLUSIONS AND SUGGESTED FUTURE WORK

8.1. Conclusions

The overarching goal of this dissertation was making chemical reactors safer and more efficient. The first part (Sections 2,3 and 4) of the dissertation focused on design problems in inherently safer and compact unconventional reactors. The role of solid-phase axial heat conduction in maintaining temperature uniformity and hotspot formation was studied in endothermic and exothermic microreactors respectively. The main takeaways from this part are endothermic microreactors with relatively low solid phase axial heat conduction are more amenable to isothermal or near isothermal operation and too much of axial heat conduction can lead to loss of controllability. In exothermic microreactors, high axial heat conduction is more amenable for decreasing possibility of hotspot formation/runaway. In heat exchanger reactors the role of catalyst distribution in preventing hotspot formation and quenching was investigated using optimal control. It was shown that using that strategically placing inerts in the reactor channels can prevent quenching. For hotspot control, constraint arcs are necessary to ensure efficient thermal coupling between exothermic and endothermic streams. The exact location of the inert regions and the constraint arcs can be calculated using optimal control.

The second part focused on diagnosing faults/ mishaps in inherently unsafe conventional reactor systems. Here, an observer-based fault detection scheme was designed for a general class of continuous input affine nonlinear systems and necessary and sufficient conditions were derived for the existence of linear functional observers

(residual generators) for non-linear systems. Following this, the problem of noises in the dynamics and measurements was tackled. To do this, a discrete time version of the functional observer design with application to fault diagnosis was studied. Then, noises were incorporated in the system and the residuals from the discrete time functional observer were evaluated using Generalized Likelihood Ratios. Throughout the study, the fault diagnosis methodology was tested on chemical reactor systems including bioreactors and CSTRs.

8.2. Suggested future work- fault tolerant control

To make any process completely resilient to sudden faults, data from fault diagnosis algorithms need to be integrated with a control strategy that would take corrective action when a fault has been detected, isolated and/or estimated. This leads to what is known as fault tolerant control in literature. Fault tolerant control has been an active area of research over the past 20 years. In general fault tolerant control can be divided into two categories, (i) Passive Fault tolerant control (ii) Active fault tolerant control. Passive fault tolerant control schemes are developed to be robust to all conceivable cases of faults[26, 135-156]. They don't include data from fault diagnosis schemes, and a fixed controller is commissioned regardless of whether faults are present[26, 140, 156]. Passive schemes are conservative from a performance aspect since they consider normal operation and faulty scenarios simultaneously[26, 140, 156]. Active fault tolerant schemes, on the other hand, utilize information from fault detection and isolation schemes to reconfigure control algorithms to ensure safe operation under faulty conditions[26, 140, 156]. Thus, in contrast to a one size fits all approach in passive schemes, active fault tolerant

schemes strive for optimal performance for each faulty scenario based on inputs from the FDI schemes[26, 140, 156]. There has been active research in active fault tolerant control schemes for non-linear systems over the past 30 years[26, 140, 156]. A conventional approach has been to design controllers based on linear approximations of the system around the operating points[157-162]. Beyond linearization, several reconfigurable control schemes have also been studied such as, feedback linearization[163-164] , nonlinear dynamic inversion[165], backstepping[166], Lyapunov Methods[167], neural networks[168-170]. However, none of the methods provide effective schemes for active fault tolerant control in the presence of state and/or input constraints. There has been some progress in this regard, in [17, 19] fault tolerant control designs were developed for systems in the presence of input constraints where the reconfiguration of the control system is done based on stability regions, derived using level sets of the Lyapunov function, of the back-up configurations.

To achieve resilience to sudden faults and mishaps, the next logical step is to derive active fault-tolerant controllers using data from fault detection, isolation and estimation schemes presented in this dissertation while considering input and state constraints. In a recent paper[171], the concept of a Dynamic Safe Set (DSS) was formulated and mathematically defined in terms of maximal admissible sets. The DSS characterizes the region in state space where, not only safety constraints on the states are satisfied at every point, but also all the system trajectories originating from every point of the DSS satisfy the safety constraints, without any possibility of "escaping". The presence of a major fault can significantly alter the DSS and drive the system outside, resulting in safety threats, unless appropriate control action is taken. The idea is to use the DSS as a basis of switching

control configuration, so that the system remains within DSS with an adequate margin. The overall fault tolerant control strategy will be as follows. Consider the nonlinear dynamic system

$$\frac{dx}{dt} = f(x) + p(x)(u^{(k)} + f_k^a) + \sum_{i=1}^{n_p} g_i(x) f_i^p$$

$$y = h(x) + \sum_{i=1}^{n_s} k(x) f_j^s$$

where f_i^p, f_j^s, f_k^a represent the process faults, sensor fault and actuator fault respectively and $u^{(k)}$, $k = 1,2,\ldots$ represents the control input vector under alternative configurations, with $k = 1$ corresponding to the nominal configuration that is used under normal operating conditions. The proposed fault tolerant control strategy will involve the following offline calculations:

i) A safety assessment and HAZOP analysis to determine all the possible faults in the system. The faults in general can in general be can be grouped as (a) actuator faults- these are faults that affect the controller (b) process faults- All non-actuator faults that affect the process (c) sensor faults- These affect the measurements.

ii) Calculate the DSS for each control configuration and for different fault sizes. This will provide information about the size of the DSS and sensitivity to different faults.

iii) Build FDI algorithms to detect and isolate a possible fault f_i, as well as state observer algorithms to estimate the unmeasurable states and the size of f_i.

During the operation of the process, the estimates from the state observer will locate the system in state space and define the corresponding DSS. The default fault tolerant control strategy is to monitor the distance of the system state from the boundary of the DSS (including the fault estimates from step (iii)) and change the control configuration when it drops below a certain acceptable limit. In particular, if T_r is the earliest time at which the distance drops below the acceptable limit, can use the following switching rule to change the control configuration:

$$k = \begin{cases} 1, & 0 < t < T_r \\ j \neq 1, & t \geq T_r \text{ , } x(T_r) \epsilon \Omega_j \end{cases}$$

where Ω_j is the DSS of the system under control configuration j and highest DSM amongst all other configurations.

In some cases, the effect of the fault on the process might be miniscule, wherein one might just retune the control parameters. In another extreme, the fault might be highly sensitive and an imminent safety threat. In such cases, instead of waiting for the fault estimates to converge one could change to a fault free configuration immediately (for actuator faults), employ fail safe configurations (process faults) or discard faulty measurements (sensor faults). The fault tolerant control strategy is summarized in the following Table 8.1.

Table 8.1 FTC strategy summary.

Fault type → **Sensitivity ↓**	Actuator Faults	Process Faults	Sensor Faults
Low	Retune Controller (optionally)	Retune controller (optionally)	Retune controller (optionally)
Normal	Use estimates from FDI to possibly reconfigure controller	Use estimates from FDI to possibly reconfigure controller	Use estimates from FDI to possibly reconfigure controller
High	Change to fault free configuration	Employ Fail- safe configuration	Discard measurement

REFERENCES

1. Kockmann, N., A Brief History of Chemical Reactor and Reaction Technology. *Chemie Ingenieur Technik* 2019, *91* (7), 941-952.

2. Fogler, H. S., *Elements of chemical reaction engineering*. 4th ed.; Prentice Hall PTR: Upper Saddle River, NJ, 2006.

3. Ehrfeld, W.; Hessel, V.; Haverkamp, V., *Microreactors*. Wiley Online Library: 2000.

4. Theis, A. E., Case study: T2 Laboratories explosion. *Journal of Loss Prevention in the Process Industries* 2014, *30*, 296-300.

5. Ajmera, S. K.; Delattre, C.; Schmidt, M. A.; Jensen, K. F., Microfabricated differential reactor for heterogeneous gas phase catalyst testing. *Journal of Catalysis* 2002, *209* (2), 401-412.

6. Blakeley, B.; Sullivan, N., Fuel processing in a ceramic microchannel reactor: Expanding operating windows. *International Journal of Hydrogen Energy* 2016, *41* (6), 3794-3802.

7. Cao, C.; Wang, Y.; Rozmiarek, R. T., Heterogeneous reactor model for steam reforming of methane in a microchannel reactor with microstructured catalysts. *Catalysis Today* 2005, *110* (1-2), 92-97.

8. Cao, C.; Xia, G.; Holladay, J.; Jones, E.; Wang, Y., Kinetic studies of methanol steam reforming over Pd/ZnO catalyst using a microchannel reactor. *Applied Catalysis A: General* 2004, *262* (1), 19-29.

9. Hasebe, S., Design and operation of micro-chemical plants—bridging the gap between nano, micro and macro technologies. *Computers & chemical engineering* 2004, *29* (1), 57-64.

10. Jensen, K. F., Microreaction engineering—is small better? *Chemical Engineering Science* 2001, *56* (2), 293-303.

11. Jensen, K. F., Microchemical systems: status, challenges, and opportunities. *AIChE Journal* 1999, *45* (10), 2051-2054.

12. Kee, R. J.; Almand, B. B.; Blasi, J. M.; Rosen, B. L.; Hartmann, M.; Sullivan, N. P.; Zhu, H.; Manerbino, A. R.; Menzer, S.; Coors, W. G., The design, fabrication, and evaluation of a ceramic counter-flow microchannel heat exchanger. *Applied Thermal Engineering* 2011, *31* (11-12), 2004-2012.

13. Wilhite, B. A., Unconventional microreactor designs for process intensification in the distributed reforming of hydrocarbons: a review of recent developments at Texas A&M University. *Current Opinion in Chemical Engineering* 2017, *17*, 100-107.

14. Zhang, J.; Wang, K.; Teixeira, A. R.; Jensen, K. F.; Luo, G., Design and Scaling Up of Microchemical Systems: A Review. *Annual review of chemical and biomolecular engineering* 2017, *8*, 285-305.

15. Anxionnaz, Z.; Cabassud, M.; Gourdon, C.; Tochon, P., Heat exchanger/reactors (HEX reactors): concepts, technologies: state-of-the-art. *Chemical Engineering and Processing: Process Intensification* 2008, *47* (12), 2029-2050.

16. Stief, T.; Langer, O. U.; Schubert, K., Numerical investigations of optimal heat conductivity in micro heat exchangers. *Chemical Engineering & Technology: Industrial Chemistry-Plant Equipment-Process Engineering-Biotechnology* 1999, *22* (4), 297-303.

17. Mhaskar, P.; Gani, A.; El-Farra, N. H.; McFall, C.; Christofides, P. D.; Davis, J. F., Integrated fault-detection and fault-tolerant control of process systems. *AIChE Journal* 2006, *52* (6), 2129-2148.

18. Mhaskar, P.; Liu, J.; Christofides, P. D., *Fault-tolerant process control: methods and applications*. Springer Science & Business Media: 2012.

19. Mhaskar, P.; McFall, C.; Gani, A.; Christofides, P. D.; Davis, J. F., Isolation and handling of actuator faults in nonlinear systems. *Automatica* 2008, *44* (1), 53-62.

20. Du, M.; Mhaskar, P., Isolation and handling of sensor faults in nonlinear systems. *Automatica* 2014, *50* (4), 1066-1074.

21. Du, M.; Scott, J.; Mhaskar, P., Actuator and sensor fault isolation of nonlinear process systems. *Chemical Engineering Science* 2013, *104*, 294-303.

22. Shahnazari, H.; Mhaskar, P., Actuator and sensor fault detection and isolation for nonlinear systems subject to uncertainty. *International Journal of Robust and Nonlinear Control* 2018, *28* (6), 1996-2013.

23. Basha, N.; Sheriff, M. Z.; Kravaris, C.; Nounou, H.; Nounou, M., Multiclass data classification using fault detection-based techniques. *Computers & Chemical Engineering* 2020, *136*, 106786.

24. Sheriff, M. Z.; Mansouri, M.; Karim, M. N.; Nounou, H.; Nounou, M., Fault detection using multiscale PCA-based moving window GLRT. *Journal of Process Control* 2017, *54*, 47-64.

25. Venkatasubramanian, V.; Rengaswamy, R.; Kavuri, S. N.; Yin, K., A review of process fault detection and diagnosis: Part III: Process history based methods. *Computers & chemical engineering* 2003, *27* (3), 327-346.

26. Yu, X.; Jiang, J., A survey of fault-tolerant controllers based on safety-related issues. *Annual Reviews in Control* 2015, *39*, 46-57.

27. Stankiewicz, A. I.; Moulijn, J. A., Process intensification: transforming chemical engineering. *Chemical engineering progress* 2000, *96* (1), 22-34.

28. Van Gerven, T.; Stankiewicz, A., Structure, energy, synergy, time The fundamentals of process intensification. *Industrial & engineering chemistry research* 2009, *48* (5), 2465-2474.

29. Kolb, G., Microstructured reactors for distributed and renewable production of fuels and electrical energy. *Chemical Engineering and Processing: Process Intensification* 2013, *65*, 1-44.

30. Srinivasan, R.; Hsing, I. M.; Berger, P. E.; Jensen, K. F.; Firebaugh, S. L.; Schmidt, M. A.; Harold, M. P.; Lerou, J. J.; Ryley, J. F., Micromachined reactors for catalytic partial oxidation reactions. *AIChE Journal* 1997, *43* (11), 3059-3069.

31. De Mas, N.; Günther, A.; Schmidt, M. A.; Jensen, K. F., Microfabricated multiphase reactors for the selective direct fluorination of aromatics. *Industrial & Engineering Chemistry Research* 2003, *42* (4), 698-710.

32. Inoue, T.; Schmidt, M. A.; Jensen, K. F., Microfabricated multiphase reactors for the direct synthesis of hydrogen peroxide from hydrogen and oxygen. *Industrial & Engineering Chemistry Research* 2007, *46* (4), 1153-1160.

33. Deshmukh, S. R.; Tonkovich, A. L. Y.; Jarosch, K. T.; Schrader, L.; Fitzgerald, S. P.; Kilanowski, D. R.; Lerou, J. J.; Mazanec, T. J., Scale-up of microchannel reactors for Fischer− Tropsch synthesis. *Industrial & Engineering Chemistry Research* 2010, *49* (21), 10883-10888.

34. Lerou, J.; Tonkovich, A.; Silva, L.; Perry, S.; McDaniel, J., Microchannel reactor architecture enables greener processes. *Chemical Engineering Science* 2010, *65* (1), 380-385.

35. Yang, Y.; Brandner, J. J.; Morini, G. L. In *Hydraulic and thermal design of a gas microchannel heat exchanger*, Journal of Physics: Conference Series, IOP Publishing: 2012; p 012023.

36. Kaisare, N. S.; Deshmukh, S. R.; Vlachos, D. G., Stability and performance of catalytic microreactors: Simulations of propane catalytic combustion on Pt. *Chemical Engineering Science* 2008, *63* (4), 1098-1116.

37. Moreno, A.; Murphy, K.; Wilhite, B. A., Parametric study of solid-phase axial heat conduction in thermally integrated microchannel networks. *Industrial & Engineering Chemistry Research* 2008, *47* (23), 9040-9054.

38. Moreno, A. M.; Wilhite, B. A., Autothermal hydrogen generation from methanol in a ceramic microchannel network. *Journal of Power Sources* 2010, *195* (7), 1964-1970.

39. Venkateswaran, S.; Kravaris, C.; Wilhite, B., Analysis of solid-phase axial heat conduction upon hot-spot formation in a one-dimensional microreactor. *Chemical Engineering Journal* 2018.

40. Avci, A.; Trimm, D.; Önsan, Z. İ., Heterogeneous reactor modeling for simulation of catalytic oxidation and steam reforming of methane. *Chemical Engineering Science* 2001, *56* (2), 641-649.

41. Moreno, A. M.; Damodharan, S.; Wilhite, B., Influence of two-dimensional distribution schemes upon reactor performance in a ceramic microchannel network for autothermal methanol reforming. *Industrial & Engineering Chemistry Research* 2010, *49* (21), 10956-10964.

42. Norton, D. G.; Vlachos, D. G., A CFD study of propane/air microflame stability. *Combustion and Flame* 2004, *138* (1-2), 97-107.

43. Kolios, G.; Frauhammer, J.; Eigenberger, G., Autothermal fixed-bed reactor concepts. *Chem. Eng. Sci.* 2000, *55* (24), 5945-5967.

44. Frauhammer, J.; Eigenberger, G.; Hippel, L.; Arntz, D., A new reactor concept for endothermic high-temperature reactions. *Chem. Eng. Sci.* 1999, *54* (15-16), 3661-3670.

45. Zanfir, M.; Gavriilidis, A., Catalytic combustion assisted methane steam reforming in a catalytic plate reactor. *Chem. Eng. Sci.* 2003, *58* (17), 3947-3960.

46. Rahimpour, M.; Dehnavi, M.; Allahgholipour, F.; Iranshahi, D.; Jokar, S., Assessment and comparison of different catalytic coupling exothermic and endothermic reactions: a review. *Appl. Energy* 2012, *99*, 496-512.

47. De Groote, A.; Froment, G.; Kobylinski, T., Synthesis gas production from natural gas in a fixed bed reactor with reversed flow. *Can. J. Chem. Eng.* 1996, *74* (5), 735-742.

48. Glöckler, B.; Kolios, G.; Eigenberger, G., Analysis of a novel reverse-flow reactor concept for autothermal methane steam reforming. *Chem. Eng. Sci.* 2003, *58* (3-6), 593-601.

49. Kolios, G.; Eigenberger, G., Styrene synthesis in a reverse-flow reactor. *Chem. Eng. Sci.* 1999, *54* (13-14), 2637-2646.

50. van Sint Annaland, M.; Nijssen, R., A novel reverse flow reactor coupling endothermic and exothermic reactions: an experimental study. *Chem. Eng. Sci.* 2002, *57* (22-23), 4967-4985.

51. Ma, L.; Trimm, D., Alternative catalyst bed configurations for the autothermic conversion of methane to hydrogen. *Appl. Catal., A* 1996, *138* (2), 265-273.

52. Hickman, D.; Schmidt, L., Production of syngas by direct catalytic oxidation of methane. *SCIEAS* 1993, *259* (5093), 343-346.

53. Ramaswamy, R.; Ramachandran, P.; Duduković, M., Coupling exothermic and endothermic reactions in adiabatic reactors. *Chem. Eng. Sci.* 2008, *63* (6), 1654-1667.

54. Ramaswamy, R.; Ramachandran, P.; Duduković, M., Recuperative coupling of exothermic and endothermic reactions. *Chem. Eng. Sci.* 2006, *61* (2), 459-472.

55. Buchanan, J.; Sundaresan, S., Optimal catalyst distribution and dilution in nonisothermal packed bed reactors. *Chem. Eng. Commun.* 1987, *52* (1-3), 33-51.

56. Zanfir, M.; Baldea, M.; Daoutidis, P., Optimizing the catalyst distribution for countercurrent methane steam reforming in plate reactors. *AIChE J.* 2011, *57* (9), 2518-2528.

57. Zanfir, M.; Gavriilidis, A., Influence of flow arrangement in catalytic plate reactors for methane steam reforming. *Chem. Eng. Res. Des.* 2004, *82* (2), 252-258.

58. Jeon, S. W.; Yoon, W. J.; Baek, C.; Kim, Y., Minimization of hot spot in a microchannel reactor for steam reforming of methane with the stripe combustion catalyst layer. *Int. J. Hydrogen Energ.* 2013, *38* (32), 13982-13990.

59. Kolios, G.; Frauhammer, J.; Eigenberger, G., A simplified procedure for the optimal design of autothermal reactors for endothermic high-temperature reactions. *Chemical Engineering Science* 2001, *56* (2), 351-357.

60. Venkataraman, K.; Redenius, J.; Schmidt, L., Millisecond catalytic wall reactors: dehydrogenation of ethane. *Chemical engineering science* 2002, *57* (13), 2335-2343.

61. Ding, S. X., *Model-based fault diagnosis techniques: design schemes, algorithms, and tools*. Springer Science & Business Media: 2008.

62. Frank, P. M.; Ding, X., Survey of robust residual generation and evaluation methods in observer-based fault detection systems. *Journal of process control* 1997, *7* (6), 403-424.

63. Frank, M. P.; Ding, X. S.; Koppen-Seliger, B., Current developments in the theory of FDI. *IFAC Proceedings Volumes* 2000, *33* (11), 17-28.

64. Gertler, J., Analytical redundancy methods in fault detection and isolation-survey and synthesis. *IFAC Proceedings Volumes* 1991, *24* (6), 9-21.

65. Frank, P. M., Advanced fault detection and isolation schemes using nonlinear and robust observers. *IFAC Proceedings Volumes* 1987, *20* (5), 63-68.

66. Frank, P. M., Fault diagnosis in dynamic systems via state estimation-a survey. In *System fault diagnostics, reliability and related knowledge-based approaches*, Springer: 1987; pp 35-98.

67. Frank, P. M., Fault diagnosis in dynamic systems using analytical and knowledge-based redundancy: A survey and some new results. *automatica* 1990, *26* (3), 459-474.

68. Luenberger, D., An introduction to observers. *IEEE Transactions on automatic control* 1971, *16* (6), 596-602.

69. Luenberger, D., Observers for multivariable systems. *IEEE Transactions on Automatic Control* 1966, *11* (2), 190-197.

70. Kravaris, C., Functional observers for nonlinear systems. *IFAC-PapersOnLine* 2016, *49* (18), 505-510.

71. Darouach, M., Existence and design of functional observers for linear systems. *IEEE Transactions on Automatic Control* 2000, *45* (5), 940-943.

72. Moore, J.; Ledwich, G., Minimal order observers for estimating linear functions of a state vector. *IEEE Transactions on Automatic Control* 1975, *20* (5), 623-632.

73. Fairman, F.; Gupta, R., Design of multifunctional reduced order observers. *International Journal of Systems Science* 1980, *11* (9), 1083-1094.

74. Tsui, C.-C., On the order reduction of linear function observers. *IEEE transactions on automatic control* 1986, *31* (5), 447-449.

75. Trinh, H.; Fernando, T., *Functional observers for dynamical systems*. Springer Science & Business Media: 2011; Vol. 420.

76. Trinh, H.; Tran, T.; Nahavandi, S., Design of scalar functional observers of order less than (ν− 1). *International journal of control* 2006, *79* (12), 1654-1659.

77. Trinh, H.; Nahavandi, S.; Tran, T. D., Algorithms for designing reduced-order functional observers of linear systems. *International journal of innovative computing, information and control* 2008, *4* (2), 321-333.

78. Trinh, H.; Fernando, T.; Nahavandi, S., Design of reduced-order functional observers for linear systems with unknown inputs. *Asian Journal of Control* 2004, *6* (4), 514-520.

79. Trinh, H.; Teh, P. S.; Ha, Q. P., A common disturbance decoupled observer for linear systems with unknown inputs. *International journal of automation and control* 2008, *2* (2-3), 286-297.

80. Xiong, Y.; Saif, M., Unknown disturbance inputs estimation based on a state functional observer design. *Automatica* 2003, *39* (8), 1389-1398.

81. Trinh, H., Linear functional state observer for time-delay systems. *International Journal of Control* 1999, *72* (18), 1642-1658.

82. Trinh, H. M.; Teh, P. S.; Fernando, T. L., Time-delay systems: Design of delay-free and low-order observers. *IEEE Transactions on Automatic control* 2010, *55* (10), 2434-2438.

83. Beard, R. V. Failure accomodation in linear systems through self-reorganization. Massachusetts Institute of Technology, 1971.

84. Jones, H. L. Failure detection in linear systems. Massachusetts Institute of Technology, 1973.

85. Clark, R. N.; Fosth, D. C.; Walton, V. M., Detecting instrument malfunctions in control systems. *IEEE Transactions on Aerospace and Electronic Systems* 1975, (4), 465-473.

86. Clark, R. N., A simplified instrument failure detection scheme. *IEEE Transactions on Aerospace and Electronic Systems* 1978, (4), 558-563.

87. Clark, R. N., Instrument fault detection. *IEEE Transactions on Aerospace and electronic systems* 1978, (3), 456-465.

88. Mehra, R. K.; Peschon, J., An innovations approach to fault detection and diagnosis in dynamic systems. *Automatica* 1971, *7* (5), 637-640.

89. Frank, P.; Keller, L., Sensitivity discriminating observer design for instrument failure detection. *IEEE Transactions on Aerospace and Electronic Systems* 1980, (4), 460-467.

90. Patton, R.; Willcox, S.; Winter, J., Parameter-insensitive technique for aircraft sensor fault analysis. *Journal of Guidance, Control, and Dynamics* 1987, *10* (4), 359-367.

91. Watanabe, K.; Himmelblau, D., Instrument fault detection in systems with uncertainties. *International Journal of Systems Science* 1982, *13* (2), 137-158.

92. Wüunnenberg, J.; Frank, P., Sensor fault using detection via robust observer. *System fault diagnosis, reliability and related knowledge-based approaches'(Reidel Press, Dordrecht, 1987)* 1987, 147-160.

93. Magni, J.-F.; Mouyon, P., On residual generation by observer and parity space approaches. *IEEE Transactions on Automatic Control* 1994, *39* (2), 441-447.

94. Ding, S.; Ding, E.; Jeinsch, T., An approach to analysis and design of observer and parity relation based FDI systems. *IFAC Proceedings Volumes* 1999, *32* (2), 7718-7723.

95. De Persis, C.; Isidori, A., A geometric approach to nonlinear fault detection and isolation. *IEEE transactions on automatic control* 2001, *46* (6), 853-865.

96. Rajamani*, R.; Ganguli, A., Sensor fault diagnostics for a class of non-linear systems using linear matrix inequalities. *International Journal of Control* 2004, *77* (10), 920-930.

97. Seliger, R.; Frank, P. M. In *Fault-diagnosis by disturbance decoupled nonlinear observers*, [1991] Proceedings of the 30th IEEE Conference on Decision and Control, IEEE: 1991; pp 2248-2253.

98. Gertler, J., All linear methods are equal-and extendible to nonlinearities. *IFAC Proceedings Volumes* 2000, *33* (11), 53-64.

99. Kinnaert, M., Robust fault detection based on observers for bilinear systems. *Automatica* 1999, *35* (11), 1829-1842.

100. Hammouri, H.; Kinnaert, M.; El Yaagoubi, E., Observer-based approach to fault detection and isolation for nonlinear systems. *IEEE transactions on automatic control* 1999, *44* (10), 1879-1884.

101. Kazantzis, N.; Kravaris, C., Nonlinear observer design using Lyapunov's auxiliary theorem. *Systems & Control Letters* 1998, *34* (5), 241-247.

102. Zhu, F.; Han, Z., A note on observers for Lipschitz nonlinear systems. *IEEE Transactions on automatic control* 2002, *47* (10), 1751-1754.

103. Thau, F., Observing the state of non-linear dynamic systems. *International journal of control* 1973, *17* (3), 471-479.

104. Venkateswaran, S.; Liu, Q.; Wilhite, B. A.; Kravaris, C., Design of linear residual generators for fault detection and isolation in nonlinear systems. *International Journal of Control* 2020, 1-17.

105. Ko, D. Y.; Stevens, W. F., Studies of singular solutions in dynamic optimization: II. Optimal singular design of a plug-flow tubular reactor. *AIChE Journal* 1971, *17* (1), 160-166.

106. Smets, I. Y.; Dochain, D.; Van Impe, J. F., Optimal temperature control of a steady-state exothermic plug-flow reactor. *AIChE Journal* 2002, *48* (2), 279-286.

107. Logist, F.; Smets, I.; Van Impe, J., Derivation of generic optimal reference temperature profiles for steady-state exothermic jacketed tubular reactors. *Journal of Process Control* 2008, *18* (1), 92-104.

108. Logist, F.; Van Erdeghem, P.; Smets, I.; Van Impe, J., Optimal design of dispersive tubular reactors at steady-state using optimal control theory. *Journal of Process Control* 2009, *19* (7), 1191-1198.

109. Ni, Z.; Seebauer, E.; Masel, R. I., Effects of microreactor geometry on performance: differences between posted reactors and channel reactors. *Industrial & engineering chemistry research* 2005, *44* (12), 4267-4271.

110. Deen, W. M., *Analysis of Transport Phenomena, Topics in Chemical Engineering*. Oxford University Press, New York: 1998; Vol. 3.

111. Kirby, B. J., *Micro-and nanoscale fluid mechanics: transport in microfluidic devices*. Cambridge university press: 2010.

112. Bravo, J.; Karim, A.; Conant, T.; Lopez, G. P.; Datye, A., Wall coating of a CuO/ZnO/Al2O3 methanol steam reforming catalyst for micro-channel reformers. *Chemical Engineering Journal* 2004, *101* (1-3), 113-121.

113. Venkateswaran, S.; Wilhite, B.; Kravaris, C., Optimal heating profiles in tubular reactors with solid-phase axial wall conduction for isothermal operation. *AIChE Journal* 2019, *65* (11), e16742.

114. Bryson, A.; Ho, Y.-C., *Applied Optimal Control: Optimization, Estimation, and Control*. Taylor & Francis, Abingdon.1975.

115. Wächter, A.; Biegler, L. T., On the implementation of an interior-point filter line-search algorithm for large-scale nonlinear programming. *Math. Program.* 2006, *106* (1), 25-57.

116. Van Welsenaere, R.; Froment, G., Parametric sensitivity and runaway in fixed bed catalytic reactors. *Chemical Engineering Science* 1970, *25* (10), 1503-1516.

117. Varma, A.; Morbidelli, M.; Wu, H., *Parametric sensitivity in chemical systems*. Cambridge University Press: 2005.

118. Morbidelli, M.; Varma, A., Parametric sensitivity and runaway in tubular reactors. *AIChE Journal* 1982, *28* (5), 705-713.

119. Boddington, T.; Gray, P.; Kordylewski, W.; Scott, S. K., Thermal explosions with extensive reactant consumption: a new criterion for criticality. *Proc. R. Soc. Lond. A* 1983, *390* (1798), 13-30.

120. Morbidelli, M.; Varma, A., Parametric sensitivity and runaway in fixed-bed catalytic reactors. *Chemical engineering science* 1986, *41* (4), 1063-1071.

121. Morbidelli, M.; Varma, A., A generalized criterion for parametric sensitivity: application to thermal explosion theory. *Chemical Engineering Science* 1988, *43* (1), 91-102.

122. Shampine, L. F.; Reichelt, M. W., The matlab ode suite. *SIAM journal on scientific computing* 1997, *18* (1), 1-22.

123. Venkateswaran, S.; Wilhite, B.; Kravaris, C., Identification of Optimal Catalyst Distributions in Heat-Exchanger Reactors. *Industrial & Engineering Chemistry Research* 2020, *59* (13), 5699-5711.

124. Srinivasan, B.; Palanki, S.; Bonvin, D., Dynamic optimization of batch processes: I. Characterization of the nominal solution. *Comput. Chem. Eng.* 2003, *27* (1), 1-26.

125. Kravaris, C.; Venkateswaran, S., Functional Observers with Linear Error Dynamics for Nonlinear Systems. *arXiv preprint arXiv:2101.11148* 2021.

126. Kravaris, C. In *Functional observers for nonlinear systems*, 2011 9th IEEE International Conference on Control and Automation (ICCA), IEEE: 2011; pp 501-506.

127. Chow, E.; Willsky, A., Analytical redundancy and the design of robust failure detection systems. *IEEE Transactions on automatic control* 1984, *29* (7), 603-614.

128. Boutayeb, M.; Darouach, M., A reduced-order observer for non-linear discrete-time systems. *Systems & control letters* 2000, *39* (2), 141-151.

129. Smajdor, W., Local analytic solutions of the functional equationϕ (z)= h (z, ϕ [f (z)]) in multidimensional spaces. *aequationes mathematicae* 1968, *1* (1-2), 20-36.

130. Kazantzis, N.; Kravaris, C., Discrete-time nonlinear observer design using functional equations. *Systems & Control Letters* 2001, *42* (2), 81-94.

131. Cui, X.; Mannan, M. S.; Wilhite, B. A., Towards efficient and inherently safer continuous reactor alternatives to batch-wise processing of fine chemicals: CSTR nonlinear dynamics analysis of alkylpyridines N-oxidation. *Chemical Engineering Science* 2015, *137*, 487-503.

132. Zhang, Q.; Basseville, M.; Benveniste, A., Early warning of slight changes in systems. *Automatica* 1994, *30* (1), 95-113.

133. Gustafsson, F., Stochastic fault diagnosability in parity spaces. *IFAC Proceedings Volumes* 2002, *35* (1), 41-46.

134. Reynolds Jr, M. R.; Lou, J., An evaluation of a GLR control chart for monitoring the process mean. *Journal of quality technology* 2010, *42* (3), 287-310.

135. Benosman, M.; Lum, K. Y., Application of passivity and cascade structure to robust control against loss of actuator effectiveness. *International Journal of Robust and Nonlinear Control: IFAC-Affiliated Journal* 2010, *20* (6), 673-693.

136. Bolduc, L. P., X-33 redundancy management system. *IEEE Aerospace and Electronic Systems Magazine* 2001, *16* (5), 23-28.

137. Davis, G. J., An analysis of redundancy management algorithms for asynchronous fault tolerant control systems. 1987.

138. Fujita, M.; Shimemura, E., Integrity against arbitrary feedback-loop failure in linear multivariable control systems. *Automatica* 1988, *24* (6), 765-772.

139. Hsieh, C.-S., Performance gain margins of the two-stage LQ reliable control. *Automatica* 2002, *38* (11), 1985-1990.

140. Jiang, J.; Yu, X., Fault-tolerant control systems: A comparative study between active and passive approaches. *Annual Reviews in control* 2012, *36* (1), 60-72.

141. Jiang, J.; Zhao, Q., Design of reliable control systems possessing actuator redundancies. *Journal of Guidance, control, and dynamics* 2000, *23* (4), 709-718.

142. Liang, Y.-W.; Xu, S.-D., Reliable control of nonlinear systems via variable structure scheme. *IEEE Transactions on Automatic Control* 2006, *51* (10), 1721-1726.

143. Liao, F.; Wang, J. L.; Yang, G.-H., Reliable robust flight tracking control: an LMI approach. *IEEE Transactions on Control Systems Technology* 2002, *10* (1), 76-89.

144. Mahmoud, M. S.; Saif, A.-W. A., Robust quantized approach to fuzzy networked control systems. *IEEE Journal on emerging and selected topics in circuits and systems* 2012, *2* (1), 71-81.

145. Osder, S., Practical view of redundancy management application and theory. *Journal of Guidance, Control, and Dynamics* 1999, *22* (1), 12-21.

146. Seo, C.-J.; Kim, B. K., Robust and reliable H∞ control for linear systems with parameter uncertainty and actuator failure. *Automatica* 1996, *32* (3), 465-467.

147. SHIMEMURA, E.; FUJITA, M., A design method for linear state feedback systems possessing integrity based on a solution of a Riccati-type equation. *International Journal of Control* 1985, *42* (4), 887-899.

148. Sijak, D., Parameter Spacemethods forrobust control design: A guide tour. *IEEE TranSactions on Automatic Control* 1989, *34* (7), 674-688.

149. Šiljak, D. D., Reliable control using multiple control systems. *International Journal of Control* 1980, *31* (2), 303-329.

150. Veillette, R. J., Reliable linear-quadratic state-feedback control. *Automatica* 1995, *31* (1), 137-143.

151. Vidyasagar, M.; Viswanadham, N., Reliable stabilization using a multi-controller configuration. *Automatica* 1985, *21* (5), 599-602.

152. Wang, R.; Wang, J., Passive actuator fault-tolerant control for a class of overactuated nonlinear systems and applications to electric vehicles. *IEEE Transactions on Vehicular Technology* 2012, *62* (3), 972-985.

153. Wu, H.-N., Reliable LQ fuzzy control for continuous-time nonlinear systems with actuator faults. *IEEE Transactions on Systems, Man, and Cybernetics, Part B (Cybernetics)* 2004, *34* (4), 1743-1752.

154. Yang, G.-H.; Lam, J.; Wang, J., Reliable H/sub/spl infin//control for affine nonlinear systems. *IEEE Transactions on Automatic Control* 1998, *43* (8), 1112-1117.

155. Yang, G.-H.; Wang, J. L.; Soh, Y. C., Reliable guaranteed cost control for uncertain nonlinear systems. *IEEE Transactions on Automatic Control* 2000, *45* (11), 2188-2192.

156. Zhang, Y.; Jiang, J., Bibliographical review on reconfigurable fault-tolerant control systems. *Annual reviews in control* 2008, *32* (2), 229-252.

157. Moerder, D. D.; Halyo, N.; Broussard, J. R.; Caglayan, A. K., Application of precomputed control laws in a reconfigurable aircraftflight control system. *Journal of Guidance, Control, and Dynamics* 1989, *12* (3), 325-333.

158. Kanev, S.; Verhaegen, M., Controller reconfiguration for non-linear systems. *Control Engineering Practice* 2000, *8* (11), 1223-1235.

159. Maybeck, P. S.; Stevens, R. D. In *Reconfigurable flight control via multiple model adaptive control methods*, 29th IEEE Conference on Decision and Control, IEEE: 1990; pp 3351-3356.

160. Theilliol, D.; Noura, H.; Ponsart, J.-C., Fault diagnosis and accommodation of a three-tank system based on analytical redundancy. *ISA transactions* 2002, *41* (3), 365-382.

161. Hess, R.; Wells, S., Sliding mode control applied to reconfigurable flight control design. *Journal of Guidance, Control, and Dynamics* 2003, *26* (3), 452-462.

162. Shtessel, Y.; Buffington, J.; Banda, S., Tailless aircraft flight control using multiple time scale reconfigurable sliding modes. *IEEE Transactions on Control Systems Technology* 2002, *10* (2), 288-296.

163. Ochi, Y., Application of feedback linearization method in a digital restructurable flight control system. *Journal of guidance, control, and dynamics* 1993, *16* (1), 111-117.

164. Ochi, Y.; Kanai, K., Design of restructurable flight control systems using feedback linearization. *Journal of Guidance, Control, and Dynamics* 1991, *14* (5), 903-911.

165. Bacon, B. J.; Ostroff, A. J.; Joshi, S. M., Reconfigurable NDI controller using inertial sensor failure detection & isolation. *IEEE Transactions on Aerospace and Electronic Systems* 2001, *37* (4), 1373-1383.

166. Zhang, X.; Polycarpou, M. M.; Parisini, T. In *Integrated design of fault diagnosis and accommodation schemes for a class of nonlinear systems*, Proceedings of the 40th IEEE Conference on Decision and Control (Cat. No. 01CH37228), IEEE: 2001; pp 1448-1453.

167. Polycarpou, M. M., Fault accommodation of a class of multivariable nonlinear dynamical systems using a learning approach. *IEEE transactions on automatic control* 2001, *46* (5), 736-742.

168. Napolitano, M. R.; An, Y.; Seanor, B. A., A fault tolerant flight control system for sensor and actuator failures using neural networks. *Aircraft Design* 2000, *3* (2), 103-128.

169. Napolitano, M. R.; Neppach, C.; Casdorph, V.; Naylor, S.; Innocenti, M.; Silvestri, G., Neural-network-based scheme for sensor failure detection, identification, and accommodation. *Journal of Guidance, Control, and Dynamics* 1995, *18* (6), 1280-1286.

170. Wang, H.; Wang, Y., Neural-network-based fault-tolerant control of unknown nonlinear systems. *IEE Proceedings-Control Theory and Applications* 1999, *146* (5), 389-398.

171. Venkidasalapathy, J. A.; Kravaris, C., Safety-centered process control design based on dynamic safe set. *Journal of Loss Prevention in the Process Industries* 2020, 104126.